Towards an improved representation of building occupant's thermal interaction: integrating detailed occupant thermal models within building simulation

PhD Thesis

Mohamad Rida

Energy Systems Research Unit

Mechanical and Aerospace Engineering Department

University of Strathclyde, Glasgow

July, 2020

Abstract

This thesis is concerned with advancing the modelling of the building occupant thermal interaction in building simulation tools. A detailed multi-segment human thermal model has been implemented within the building simulation tool ESP-r and its integrated computational fluid dynamic CFD module.

The improvement of ESP-r's building occupant representation in building simulation has been done in three stages. With the complexity of the integration increasing in each stage.

In the first stage, a responsive occupant heat load model has been developed and implemented in ESP-r. In this model, the sensible and latent heat loads are regression equations derived from the literature and are a function of operative temperature and metabolic rate.
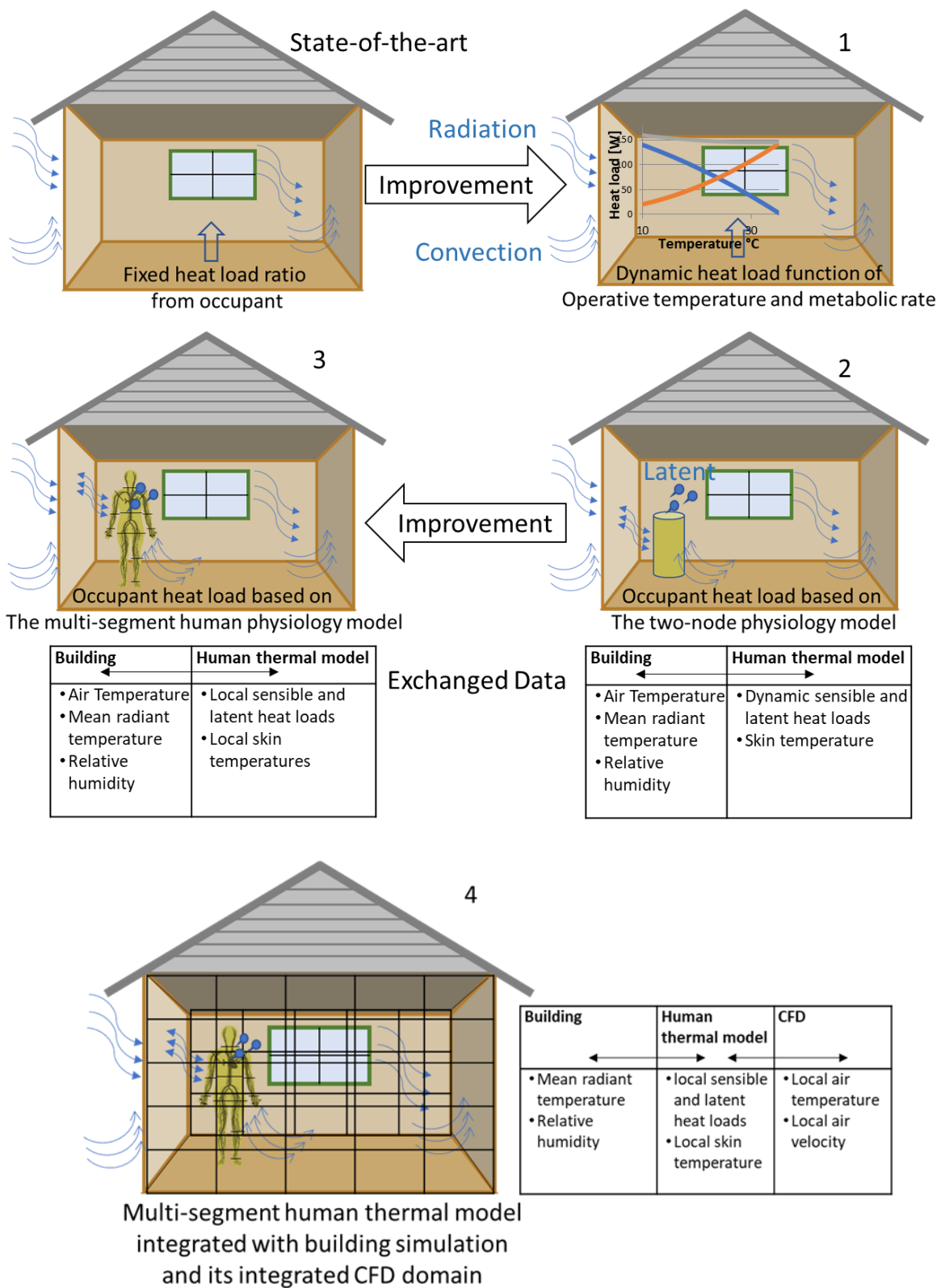
In the second stage, a two-node thermo-physiology model has been developed and implemented that dynamically simulate with the thermal building model. This ensures that occupant thermal models are responsive to the prevailing conditions and secondly, improves the resolution modelling of occupants and their environment. In addition, clothing adaptation has been considered by implementing a dynamic clothing algorithm.

The third stage involved implementing a multi-segment human thermal model within ESP-r and its integrated CFD module.

The integration of all three levels of occupant model has been validated with published experimental data. Moreover, each of the three approaches has been demonstrated using example applications.

It is hoped that these fully-integrated models of occupant thermo-physiology help advance the modelling of the indoor environment, occupant thermal comfort and building performance prediction within a whole-building simulation.

Graphical abstract

State-of-the-art

1

Radiation

Improvement

Convection

Fixed heat load ratio from occupant

Dynamic heat load function of
Operative temperature and metabolic rate

Heat load [W]

Temperature °C

3

Improvement

2

Latent

Occupant heat load based on
The multi-segment human physiology model

Occupant heat load based on
The two-node physiology model

Exchanged Data

Building	Human thermal model
• Air Temperature • Mean radiant temperature • Relative humidity	• Local sensible and latent heat loads • Local skin temperatures

Building	Human thermal model
• Air Temperature • Mean radiant temperature • Relative humidity	• Dynamic sensible and latent heat loads • Skin temperature

4

Building	Human thermal model	CFD
• Mean radiant temperature • Relative humidity	• local sensible and latent heat loads • Local skin temperature	• Local air temperature • Local air velocity

Multi-segment human thermal model
integrated with building simulation
and its integrated CFD domain

Preface/Acknowledgements

I would like to express my special appreciation and thanks to my research supervisor, Dr Nick Kelly for his marvellous guidance, support and for the unlimited freedom he offered me during the preparation of this thesis.

My thanks are extended to the following members of the Energy System Research Unit ESRU, Dr Andrew Cowie and Dr Jon Hand for their advice, the numerous useful discussions and for the assistance in tackling the technical software obstacles.

I wish to express the sincerest gratitude to Prof. Dr.-ING. Sabine Hoffman head of the department of the Built Environment at TU Kaiserslautern for her belief in me, her vision to support my studies and for her constant encouragement. My colleagues in the Built Environment Group at TU Kaiserslautern have been an incredible support to me and source of encouragement.

My gratitude is expressed to Professor Joe Clarke and Dr Paul Strachan for providing their expert knowledge and advice during my meeting with them.

Finally, thanks to my extended family and friends for the continuous encouragement, and inspiration. Especially to Dr Lina Akil for being a great assistant and supporter for the time I spend in Glasgow.

A very special thanks to my wife and my son for their continuous support and patience through the period of this work. My sincere thanks go to my parents for their lifetime help and support.

This thesis is dedicated to my parents and family.

Contents

Contents

Contents

Contents

Contents

List of Figures

List of Figures

List of Figures

List of Figures

List of Tables

Chapter 1: Thesis Introduction

1.1 Introduction

The global building sector accounted for 36% of total final energy consumption in 2018 and 39% of the energy-related CO_2 emissions as stated in the United Nations Environment Programme UNEP Global Status Report 2019 (IEA and UNEP, 2019). The majority of this energy is consumed in heating, cooling and ventilation of spaces (IEA, 2019 a). Worldwide, there is a massive demand to reduce the energy consumed in buildings. According to the International Energy Agency (IEA) the global building sector energy demand is growing fast and could reach 50% of total final energy consumption in 2050, where the major growth comes from developing countries (IEA, 2016; IEA, 2019 b)

People spend the majority of their time around 90% in buildings (Klepeis, 2001); consequently, occupant comfort is one of the main performance metrics to evaluate during the design stage. However, in the era of sustainable buildings, building designers (building physicists) must balance comfort with minimising energy consumption. This is a complex issue, particularly in low carbon buildings with natural ventilation or mixed-mode ventilation. Such sustainable ventilation designs often feature a fluctuating indoor thermal environment; there may also be a non-uniform thermal environment such as radiant surfaces, or solar gain from large windows, and allowance of temperature drift by using control strategies which allow ambient temperatures to drift in the acceptable thermal comfort zone which is considered a way of reducing energy (Hensen, 1990; De Dear, 2002; Zmeureanu et al., 1992; Karmann et al., 2017). In such cases achieving acceptable comfort requires the use of appropriate models and tools.

1.2 Building simulation tools

A building simulation is the process of creating a virtual building where the designer has the ability to specify in detail all parameters that have an impact on

the building performance. The designer always tries to bring the simulation results as possible as closer to reality (Hensen, 2012; Clarke & Hensen, 2015).

Building simulation has been developed to provide an immediate and dynamic solution of thermal and mass flow in buildings. Moreover, a building simulation can give a projection of what environment the occupants is likely will be exposed to.

The use of building simulation tools has increased rapidly over the last five decades (Crawley et al., 2008). This was due to the improvement of the computers, the energy crisis that led to an increase in the interest in sustainability and the rise of various ideas such as Zero Carbon Buildings and Net-Zero Energy Buildings. Moreover, more building regulation is relying on building simulation to show compliance (Coakley et al., 2014). Therefore, there are a wide variety of energy simulation engines available today like (ESP-r, TRNSYS, DOE-2, BLAST, Energy Plus, IDA ICE, Virtual Environment, etc.). Every simulation tool has some advantages and limitations (Crawley et al., 2008). The complexity of these programs ranges from steady-state calculation to high resolution of calculation including (computational fluid dynamic) CFD simulation.

1.2.1 Building simulation limitation

With all the advancement and developments on these pieces of software, there are still a number of simplifications. Further, simulations in these tools are a theoretical representation of the building of both status and operation. Therefore, it is not possible to reach exact similarity in the energy use prediction with the real-life one (Coakley et al., 2014; de Wilde, 2014), as internal loads may be different (Hoes et al., 2009), weather data may not match the real climate and many other reasons. Designers usually make assumptions, especially the one regarding building usage once the building is established the building may be used differently. That will change the actual energy use compared to what originally planned (Dodoo et al., 2017; Daly, et al., 2014).

Building simulation tools are only as reliable as the accuracy of their input. One of the important and influential inputs is the occupant internal loads. Traditionally occupant internal loads are represented in building simulation tool as a fixed amount of heat flux or time-varying profile, representing the contribution of the occupant heat gains to the thermal energy balance of a building. However, such approach is problematic, when considering buildings with varying indoor conditions as occupant heat gains are affected by the thermal environment like air temperature, mean radiant temperature, humidity, and air velocity (ASHRAE standard 55, 2017), along with some personal factors like metabolic heat production and clothing. Assuming a static occupant heat load, therefore, could lead to inaccuracies, both when assessing comfort and when calculating heating and cooling loads. In general, the predictions of cooling and heating demand of a building are one of the determinants in successful measures of energy-saving (Crawley et al., 2008). With all that in hand still these tools are the best approach to simulate the energy use and occupant comfort in buildings. The contribution of this thesis is therefore to advance the state-of-the-art in how occupant internal gains are represented and integrated into building simulation tools, intending to improve predictions of thermal comfort and heating/cooling loads.

1.2.2 Occupant heat loads

The human body produces heat mainly from the oxidisation of food in the body, through the process of metabolism. The main objective of burning food and generating heat is to keep our body warm and have a nearly constant body core temperature. The body surface area; body mass, age and sex in addition to the physical activity all affect the heat generation rate. The human body loses the heat generated to the environment by the different means of heat exchange (Parsons, 2014).

The metabolic rate is one of the major factors that determine the total heat transfer from the human body, but the metabolic rate alone does not dictate which form the heat is transferred. Heat is dissipated from the human body

through convection, radiation, evaporation and conduction where a higher metabolic rate leads to greater heat loss to the environment (Höppe, 1993).

Clothing is another factor as clothing plays the role of the insulation layer that preserves heat from being dissipated to the outer environment. Clothing reduces the amount of both latent and sensible heat load. The higher the clothing insulation the less heat is dissipated to the environment (Arens et al., 2006).

Both air temperature and air velocity affect the amount of heat dissipated by convection. In a naturally ventilated zone, higher temperature fluctuation and higher air velocity are noticed compared to conditioned tight buildings. The human body will always try to regulate its temperature through physiological phenomena like shivering, sweating and blood circulation control. From all above one can approximately determine whether the human body feels thermally comfort or not (Arens et al., 2006).

1.3 Occupant thermal comfort

ASHRAE defines thermal comfort, as the state of mind that expresses satisfaction with its environment (ASHRAE standard 55 2013; ISO 7730, 2005). Multiple factors can influence occupant thermal comfort it could be physical, physiological or psychological. In fact, people sitting in the same thermal environment could have different thermal sensations, even though they are from the same age group and a similar cultural background (ASHRAE standard 55 2013; De Dear et al., 1998).

During the design stage of new and retrofit building, the comfort of its occupants is typically evaluated by doing a simulation using building performance tools. Many models to calculate comfort are available and adopted in standards, are based on correlations of thermal comfort criteria. The most widely used is the mathematical model developed by Fanger (Fanger, 1970), which is based on results from climate-controlled chamber experiments. This model is appropriate for static and uniformly thermal conditions since it considers that all people

achieve thermal comfort in a narrow, well-defined range of thermal conditions irrespective of race, age and gender.

During steady-state, the rate of the metabolic heat generated is equal to the rate of heat loss from the body (Djongyang et al., 2010). However, in cases such as natural ventilation or when allowing a large temperature fluctuation, the Fanger model could lead to unreliable results (Jones, 2002). In addition, many cases exist in buildings where occupants have different activity levels, that can be seen in hospitals and care homes for the elderly when nurses have higher metabolic rates compared to patients (Van Hoof et al., 2006; Wang et al., 2008). Each group could have different thermal comfort.

1.3.1 Accurate environmental prediction for better thermal comfort assessment

Accurate modelling of the thermal environment is required to predict the thermal comfort level of the occupant during the design stage. It is very important to consider the building envelope and the systems used to thermally condition the space when assessing thermal comfort. Therefore, it is essential to have accurately predicted information on local air temperature, mean radiant temperature, air velocity and relative humidity in a room in order to predict occupant comfort. The occupant comfort level does change over time and that is due to the transient nature of the environmental parameters.

The building simulation tool classically represents a room as one single control volume since it is easier for the modeller to conceptualise, and it is computationally efficient and simple. On the other hand, in the solution, the whole air volume is represented as one node as if the air is well-mixed resulting in a single value of air temperature and no information on air movement within the room. The well-mixed air assumption in building simulation tools ignores temperature stratification, stagnant areas, thermal plumes and cold draughts that usually exist in rooms (Cook, 1998; Bartak et al., 2002). As previously explained the local thermal environment of the human is essential to predict its comfort.

When the local environment of the human body is necessary, such as local air velocity and air temperature the use of computational fluid dynamic CFD approach should be considered to resolve local intra-zone air flows.

The internal loads such as occupant thermal loads also have a significant impact on the energy use and consequently the comfort level. The loads are considerable especially in non-domestic buildings, where a large number of occupants are usually present in the same zone such as in hospitals, schools, theatres and offices. Consequently, it is very important to identify these loads as accurately as possible, as well as the differentiating between the heat and moisture emissions in a zone. Since occupant heat loads are sensitive to the variation of the thermal environment conditions, using a dynamic occupant heat load model, which is responsive to changing environmental conditions is crucial. Additionally, the variation provided in a predefined prescription like the change in occupant number, activity level and clothing level should be defined as accurate as possible to achieve greater realism in simulation prediction.

1.3.2 Designing for Thermal Comfort

For many years, engineers and designers have used building simulation tools to predict the comfort and the energy performance for new and retrofit buildings, assessing different options (de-Wilde, 2018; Hong et al., 2000). In building simulation, there are two general thermal comfort modelling approaches.

- First, the models used in standards which consider the average of the whole body like the Fanger (Fanger, 1970) Gagges two-node model (Gagge et al., 1986).

- Second, the adaptive models, de-Dear (De Dear et al., 1998) summarised the adaptive approach into three categories: behaviour adaptation, physiological adaptation and psychological adaptation (IEA EBC Annex 66, 2017; Jones, 2002; Nicol et al., 2002).

The strength of adaptive models tends to increase with the capability of the occupants to regulate their thermal comfort; personal fans, for example, operable windows, or a relaxed dress code (ASHRAE, 2017). A human thermal comfort model can contribute to the adaptive model by providing detailed thermal comfort analysis, the model can be used as an adaptive controller to adapt all thermal comfort influencer as window opening, clothing adaptation or even applying personal cooling or heating devices.

1.4 Continuing the evolution

Building occupant heat loads ratio is significantly dependent on the environmental parameters, consequently, internal heat gain from the occupant affect the prediction of the thermal environment, both predictions rely on each other. To predict internal heat gain from occupants more precisely and evaluate the occupant thermal comfort in a dynamic way integration of detailed occupant thermal model in the whole building simulation is desirable. A building simulation which able to predict the thermal environment may predict a more accurate and dynamic thermal environment when the occupant heat loads are well defined. Without doubt, a complete integration of the two models building and detailed thermal occupant could simulate and predict more realistically.

ESP-r is an integrated modelling tool for building simulation it is capable of simulating the thermal (heat, air, moisture, light and electrical power flow), visual and acoustic performance of buildings (ESRU, 2002). It has a worldwide development community, and the source code is available under an open-source license. Still, ESP-r lack of detailed documentation has a primitive interface and require a steep learning curve. The tool is, therefore, a useful platform on which to test new developments in building simulation, consequently, ESP-r has been selected to improve the occupant building representation and to study its influence on the energy performance and thermodynamic and airflow behaviour prediction.

1.5 Aims and objectives

The basic aim of this work is to improve the thermal interaction of space and occupants in building simulation tools through developing a more realistic building occupant thermal model and fully integrating this with a building simulation tool. Specifically, this will be achieved through developing and integrating a detailed multi-segmented human thermal physiology model in the building simulation tool, in order to have a fully-coupled representation of occupant thermal loads, which is responsive to dynamically change conditions, facilitating better evaluate local and overall thermal comfort of building occupants.

The specific objectives of this study were therefore as follows:

1. Explore the effect of the occupant heat load on the indoor thermal condition by the developing and integrating the simple polynomial equations of sensible and latent loads for the occupant in ESP-r, which are functions of indoor conditions and occupant activity.
2. Advance the first approach by integrating a two-node model (core and skin) building occupant model with ESP-r. This model accounts for physiological parameters as blood flow, sweating and shivering in addition to the effect of clothing insulation.
3. Further integrating the dynamic two-node model with ESP-r's CFD representation of indoor air, which is in turn fully couples to ESP-r's building model.
4. Integrate a multi-segmented human thermal model with ESP-r and its CFD capability, and providing a new, detailed and fully coupled modelling capability for the assessment of the interaction between building occupants and indoor spaces.
5. Evaluate the capability of such integration in multiple simulation case scenario.

Climate change especially the increase in temperature of the air layer close to the ground surface affect the human thermal perception. Outdoor thermal comfort can be directly affected by the changes in air temperatures and the changes of short and longwave radiation. Moreover, climate change will lead to high energy consumption in building spend on cooling aiming to provide acceptable thermal comfort for building occupant. Figure 1.1 shows the inter-relation between the different aspects already highlighted where the aim of this research stand.
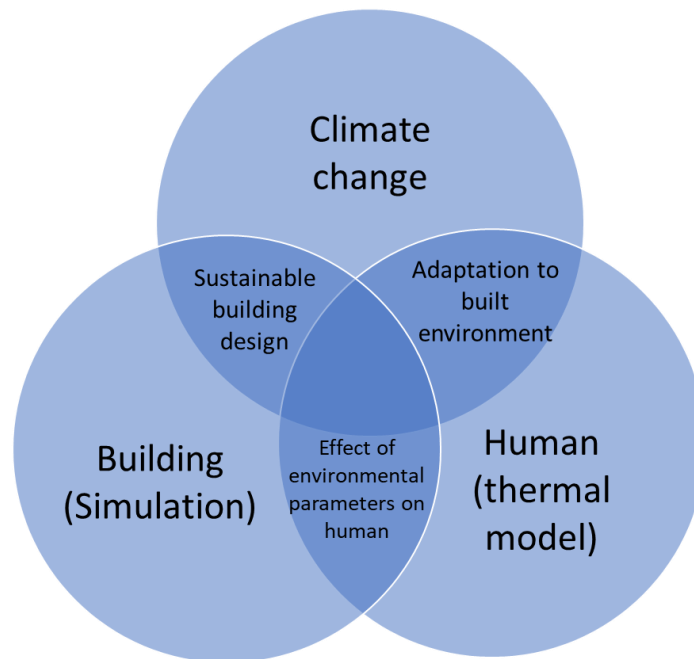
Figure 1.1 Inter-relation between the major aspects of this research.

1.6 Contribution

Although multiple works have been done in the area of integrating detailed human thermal model within CFD tools non within building simulation tool and CFD. To the Author's knowledge, there are no other examples in the literature where a detailed, multi-segment occupant model has been fully integrated with a building simulation tools and CFD for use in such activities as detailed comfort assessment and modelling of passive ventilation systems. Where a full-integration means, two-way thermal interaction, both building and human

exchange heat dynamically. It also contributes to building simulation tools by applying a dynamic sensible and latent heat ratio from the occupant.

1.7 Outline of the Dissertation

The work required to achieve the aim and objectives is structured in 8 chapters, which are outlined below.

Chapter one: Introduction

> This chapter sets the context for the work and outlines the aims, objectives and contribution.

Chapter two: State-of-the-art

> This chapter reviews the literature related to the work, it includes parts on thermal comfort and human thermal modelling; building simulation and building simulation tools and the current state of occupant representation; CFD studies with thermal manikin and human thermal model presence.

Chapter three: ESP-r and modelling approach

> This chapter briefly describes the ESP-r energy building simulation tool chosen for this study and its underpinning modelling approach.

Chapter four: Simple dynamic linear model of occupant thermal loads

> This chapter describes the integration of a dynamic occupant model into ESP-r, changing internal heat load from a fixed value to dynamic heat fluxes by representing occupant heat loads by a polynomial equations function of operative temperature and metabolic rate. The impact of this change is quantified.

Chapter five: Two-node model toward better occupant thermal load representation in ESP-r

In this chapter, the two-node thermal occupant model is presented and its implementation in ESP-r is described. The benefit of applying the model over simpler representations is described and quantified. The integration of the model with ESP-rs CFD domain is also described.

Chapter six: A multi-segmented human thermal model for a better thermal comfort prediction

The process of developing a multi-segmented human thermal model is described in this chapter along with its integration within ESP-r.

Chapter seven: CFD modelling of multi-segment human thermal model in ESP-r

In this chapter the coupling of the multi-segmented human model in ESP-r and its CFD solver has described it shows our approach in representing the human body in CFD domain. This chapter also includes case studies for different scenarios showing the outcomes of the linking in regards to thermal comfort and the environmental changes.

Chapter eight: Conclusion and further research

This chapter discusses the whole work and presents the outcomes of this research, the benefit of using this integration also gives a conclusion drawn from this research work. This chapter shows how this research can be used in practice for design and future case study.

Chapter 2: State-of-the-art

2.1 Overview

This chapter will go through the different areas of research concerning human thermal modelling, their comfort in buildings and the linking of such models in building simulation tools and CFD models.

Section 2.2 presents a description of the human thermal environment and the environmental parameters, a brief description of the different types of heat exchange between the human body and its environment.

Section 2.3 has a general description of the human thermoregulatory system and the human physiology system. Section 2.4 addresses the occupant behaviours.

The most important human thermal models available in the literature have been described and their applications in section 2.5. Thermal comfort models have been listed in section 2.6. And finally, section 2.7 and section 2.8 present the use of such models in combining with CFD and building simulation tools and section 2.9 describe the state of the art of the integration of CFD models in building simulation. Section 2.10 highlights research gaps, particularly those addressed by this thesis.

2.2 Human Thermal Environment

The human body responds to the environment in dynamic interaction. It is exposed to different levels of environmental conditions; in extreme cold and hot environments the body uses its resources to maintain its optimum operating

temperature (the average core temperature is 37°C with an acceptable variation of ±0.5°C) (Parsons, 2014). In the case of the thermal environment, this will determine whether a person is too hot, too cold or in thermal comfort (Parsons, 2014; Hensen, 1990).

The four basic environmental variables that affect human comfort and the body's response to thermal environments are - air temperature, radiant temperature, humidity and air movement. The factors that define human thermal comfort are the combination of these four basic environmental variables, along with the metabolic heat production and type of clothing worn by a person (ASHRAE Standard 55, 2013; Clarke, 2001).

Often, the environmental limits are defined through the air temperature for example in a thermally controlled building. But, in many situations, this is insufficient, because all other five factors are relevant. For example, when the human body is exposed to direct solar radiation by sitting near a fenestration in offices or vehicles this could significantly affect the thermal comfort, in this case, air temperature alone will be inadequate to specify comfort limits (Parsons, 2014). The heat loss by the evaporation of sweat is essential to a person exposed to heat stress. Where the two influencing factors of evaporative heat loss are the environmental humidity and clothing levels.

In particular situations, other factors will be dominant; for example, when a person is exposed to asymmetric wall temperatures the heat exchange between the person's posture and the environment is greatly affected. Therefore, the six fundamental factors form the basis for which a human thermal comfort and environment can be assessed.

The human body follows the laws of thermodynamics. When heat energy lost at the surface of the human body, its temperature falls and when heat flows into the body its temperature rises. The human body temperature is an indicator of its thermal condition. Human beings are homeotherms therefore the body tries to maintain an internal temperature around 37°C. The effort required to maintain

this core temperature will be significantly affected by the temperature of the surrounding environment (fluid and surfaces).

2.2.1 Environmental parameters

This section starts with the definitions of the environmental parameters that affect human thermal comfort.

Air temperature, defined as the temperature of the air point (ISO standard 7730, 2005) ASHRAE standard 55 (ASHRAE 55, 2013) recommend using the average air temperature which represents the average of the air temperatures at the ankle, the waist and the head level. The three levels were defined for a sitting person as 0.1, 0.6 and 1.1 m and for a standing person at 0.1, 1.1 and 1.7 m (ASHRAE Standard-55, 2013). Heat exchange between the human body and air is a continuous process because air temperature varies. ASHRAE standard 55 recommended for the air temperature average a time averaging between three and 15 minutes.

Air velocity around the human body can influence the amount of convective heat transfer from the body surface to the air and vice-versa, it can also change and accelerate the evaporation process of the sweat at the skin surfaces. Air can move at a point in any direction; therefore, its velocity intensity can be defined for a variation in time in an orthogonal three axes space, and airspeed is considered to be the mean air velocity intensity of a defined time for all directions. ISO 7730 (2005) and ASHRAE standard 55 (2013) stated the importance of the effect of air velocity on the human body and have shown that variation in air velocity may affect human comfort due to draught.

Besides, there is also the radiant temperature that has a large influence on the human body temperature. The construction and geometry of a zone play a large role in the radiant temperature, for example, the amount of fenestration, and its orientation affects the radiant temperature. Further, the occupant location inside a zone can vary the experienced radiant temperature, since every location in a zone has a unique radiant environment. The radiant temperature could be

represented by the mean radiant temperature or the plane radiant temperature. The mean radiant temperature is defined as "the temperature of a uniform enclosure with which a small black sphere at the test point would have the same radiation exchange as it does with the real environment."(Parsons, 2014). Furthermore, the plane radiant temperature defines as "the uniform temperature of an enclosure where the radiance on one side of a small plane element is the same as in the non-uniform actual environment."(Parsons, 2014).

The final parameter of the environment affecting thermal comfort is humidity. In high-temperature environments, the human body regulates its temperature by sweating, and the sweat at the skin layer will be evaporated and lost to the environment. The 'driving force' for heat loss by evaporation is considered to be the difference in partial vapour pressures between that at the skin layer and that in the environment. So, the humidity of the environment is an influencing parameter. The relative humidity is one of the commonly used expression to reflect the humidity in the air and it is the ratio of the pressure of the water vapour in the air to the saturation pressure of water vapour at the same temperature and total pressure (Parsons, 2014).

2.2.2 Heat transfer between the occupant and the environment

It is necessary that all the excess heat produced by the body to dissipate to the surrounding environment to keep the body in thermal neutrality and prevent the core body temperature from increasing. This happens through the processes of conduction, convection, radiation and evaporation. The heat transfer rate is dependent on the environmental parameters mentioned in section 2.1, in addition to the skin surface, skin temperature and skin wettedness. The heat losses from the human body to the environment was described in Fanger (1973) and Du Bois (1939).

2.2.2.1 Conductive heat transfer

Conductive heat transfer happens when the human body is in contact with another surface at a temperature different from the skin temperature. The magnitude of heat being transferred by conduction is dictated by the contact surface area, the temperature difference and the thermal conductivity of both skin, intervening clothing and the solid surface (Parsons, 2014; Djongyang et al., 2010).

The conductive heat transfer between the human body and the environment is usually neglected because of the small area of the body being affected, e.g. when the bottom of the feet are in contact with the floor when standing. More examples of this are when holding a cup filled with hot or cold liquid or when lying on a couch or chair. In some cases, conduction can't be neglected. For example, in different cultural behaviour when occupant tends to sit on the ground for a longer period while having underfloor heating or cooling systems.

2.2.2.2 Convective heat transfer

The convective heat exchange between an occupant body and the environment, could be either natural or forced and is greatly dependent on the temperature gradient between the skin and air, gravity, surface geometry, air density and viscosity. The convective heat transfer increases when air velocity increase and in that case, it will be considered as forced convection. in addition to the airflow pattern as air velocity and its physical properties (ASHRAE Fundamental, 2017; Parsons, 2014; Djongyang et al., 2010).

$$Q_c = Ah_c f_{cl}(t_{cl} - t_a) \qquad (2.1)$$

The convective heat transfers Q_c [W] is defined by the difference between t_{cl} the clothed body's mean surface temperature (°C) and t_a the ambient air temperature (°C). where f_{cl} is the clothing area factor, representing the ratio of clothed body surface area to nude body surface area ($\frac{A_{cl}}{A_D}$) and A is the total exposed surface area in [m^2]

The convective heat transfer coefficient hc of the unit [W/m2 °C] from both skin or clothing develop from airstream disturbing the insulating boundary layer of air attached to the surface of the body (de_Dear et al. 1997). Typically, when it has a fast flow of air around the body, the boundary layer of air on the body's surface becomes thinner, causing a lower the thermal insulation sustains the subject. The convective heat transfer process from the human body surfaces can be categorized into three different modes:

1. Natural convection, which is driven purely by thermally induced buoyancy and generally confined to ambient airspeeds lower than $V_{air} < 0.2 \, \text{m/s}$. In this case, the air around the warm body surface starts to move up by buoyancy forces as its temperature increases this called buoyant convection. For example, for a standing person, the flow starts at the foot level as a laminar flow, however, while moving up there will be a transition occurs and the flow becomes turbulent around the upper body parts (Cook, 1998). The buoyancy-driven flow from the head and the shoulders will be mixed producing the human thermal plume.

2. Forced convection at speeds generally higher than $V_{air} > 1.5 m/s$ (Danielsson, 1993).

3. Mixed-mode convection prevailing at airspeeds between these two limits.

The local convective heat transfer coefficient method from de-Dear et al. (1997) is described in chapter 6 section 6.2.3.

2.2.2.3 Radiative heat transfer

The heat exchanged by radiation takes place between the occupant external surface where it could be skin or clothes and the surrounding zone surfaces like windows, walls, radiative panels etc. (ASHRAE Fundamental,2017; Parsons, 2014; Djongyang et al., 2010). The radiative heat exchange is given by the following equation:

$$Q_r = A_r \varepsilon_{sk} \sigma (\bar{T}_{sk}^4 - \bar{T}_r^4) \tag{2.2}$$

Where Qr is the radiative heat transfer in [W] Ar is the effective radiation area of the body in [m^2], ε is the skin emissivity σ is the Stefan-Boltzmann constant, 5.67*10^{-8} [W/m^{2}K^4], Tsk and Tr are the mean skin and the mean radiant temperature, respectively.

The radiation area is termed "effective" because not all the body surface area is exchanging radiation heat with the environment, some of the areas are obscured, so the effective area is always smaller than the total body surface area and it depends on the posture of the occupant. The emissivity value relates to the capacity of an object to radiate heat. The emissivity for indoor calculations without considering the shortwave radiation can be considered as 0.97 (ASHRAE fundamental chapter 9, 2017) for both clothing and skin as independent of the colour, but when considering the shortwave radiation colour will influence the emittance value (Balzejczyk et al., 1993).

The mean radiant temperature is defined as the area-weighted average temperature of the surrounding surfaces. The radiative heat transfer will be affected by the difference between the external body surface temperature and the mean radiant temperature which is influenced by the view factor. When the difference value of the temperatures is negative there is heat gain by radiation.

2.2.2.4 Evaporative heat transfer

The evaporative heat loss at the skin layer is a result of the diffusion of water vapour through the skin and the evaporation of sweat on the skin. The phase-change of the state of water from liquid to vapour requires heat, that heat is taken from the skin.

The evaporative heat loss by diffusion is a function of the difference between the water vapour pressure in the ambient air and the saturated water vapour pressure at the skin temperature. This part of the evaporative heat loss from the human body is happening all the time and it is not subject to thermoregulatory control (ASHRAE Fundamental,2017; Parsons, 2014; Djongyang et al., 2010).

The evaporation of sweat generated by the body is crucial as it can reduce any potential increase in the body temperature even during a hard exercising or high temperatures. The sweating evaporation heat loss can go from 0 [W/m2] at rest to 400 [W/m2] at an elevated activity level in a hot and dry environment.

For office and residential building occupants practising a moderate activity, the evaporative heat loss will be around 25% of the total heat loss (Viessman, 1966). In the case of moderate sweat secretion and an environment is at a comfortable level, all sweat is assumed to be evaporated. In some situation not all sweat gets evaporated and it starts to accumulate on the skin layer at that point the occupant will not be thermally satisfied and the level of discomfort will increase.

2.2.2.4 Heat losses due to respiration

The heat loss from respiration is constituted of a dry convective heat transfer because of the colder air temperature inhaled. Where air enters into the lungs at the ambient temperature and exhaled at a temperature near the core inner temperature. In addition to the evaporative heat loss due to respiration, where air enters into the lungs and exit saturated. ASHRAE fundamental (2017) gives the equation for the total heat loss by respiration as:

$$C_{res} + E_{res} = [0.0014\,M(34 - t_a) + 0.0173\,M(5.87 - P_a)] \qquad (2.3)$$

Where M is the metabolic rate in [W/m^2] and t_a is the air temperature in [°C] and P_a is the water vapour pressure in the ambient air in [kPa].

2.3 Human thermal physiology and thermoregulation

Human beings are homeotherms, warm-blood is circulated through the whole body, where heat generated through metabolism and heat loss were regulated to maintain an internal body temperature of around 37 °C, over a wide range of fluctuations in environmental conditions. The human thermoregulation balances heat production and heat loss. In case the body lost more heat than it produced its body temperature drop. Contrary, if the heat production was higher than heat

lost the body temperature raise. A deviation from the neutral body temperature of more than 2 °C can lead to severe consequences, e.g. a fall in body temperature can cause hypothermia, and an increase of 3 °C in core temperature can lead to hyperthermia (Höppe, 1999; Hensen, 1990).

The heat production and heat loss from the human body are boosted or prevented through the thermoregulatory system which is responsible for keeping the core temperature at the normal level.

The control of the heat balance or thermoregulation can be efficiently accomplished by modulating behaviour (like changing clothes or change activity) and physiologically through shivering, sweating and controlling blood flow).
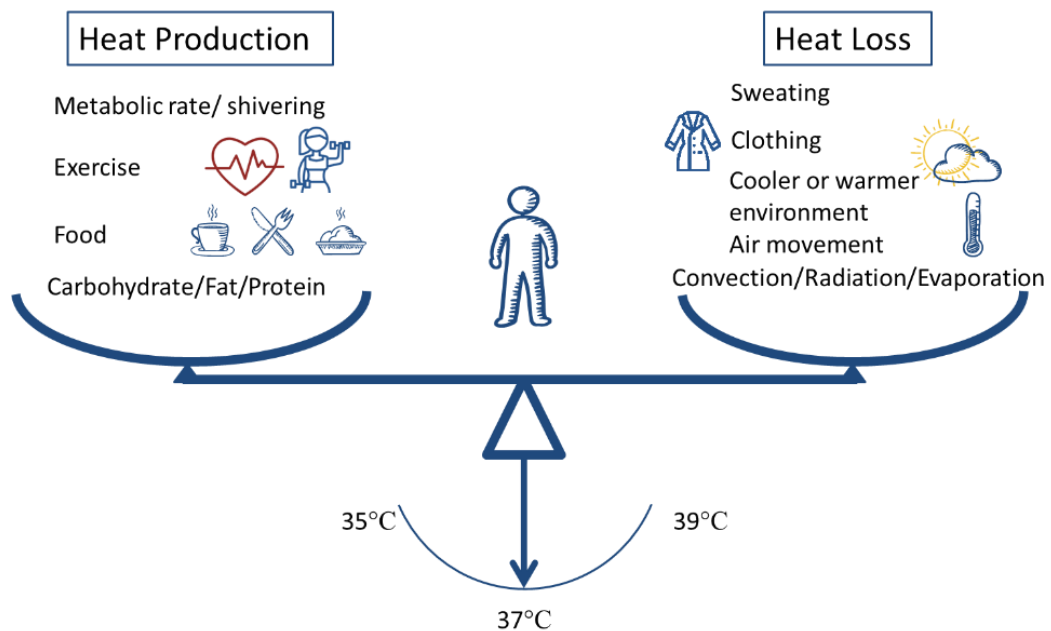
Figure 2.1 Heat balance, factors that affect heat production and heat loss. Adapted from (Du Bois, 1939).

The diagram in figure 2.1 adapted from Du Bois (1939) indicates the multiple factors that can affect the energy balance of a human body. The heat production is on one side of the balance and the heat loss is on the other side, where, in an equilibrium state, the neutral body temperature is achieved. Starting from an equilibrium state, for example, a human is sitting relaxed in a warm room the heat produced in this case it is called the basal metabolic rate and it is equal to the heat

loss. In case of any change in the heat production parameters, for example, greater metabolic rate requires the heat loss side to be also altered to go back to a neutral equilibrium state. That could happen for example by decreasing the room temperature, less clothing or sweating to increase the heat loss by convection radiation and evaporation.

The hypothalamus in the brain receives signals of local temperatures and temperature changes from the thermoreceptors, sensors located in the skin and other parts of the body. The hypothalamus analyses the signals received and appropriates effector commands aiming to thermally regulate the body for example by sweating shivering and blood circulation (vaso-motor) (Havenith, 2002; Hammel et al., 1963). The thermoregulatory systems respond to environmental change in three different ways: vasomotor, sudomotor and metabolic. When the body is exposed to a high environment thermal loads or when exercising its temperature rises, reaching a point above the neutral level, the skin blood flow increases due to vessel dilation. This phenomenon increases the heat transferred by convection from the core to the skin. The temperature gradient between the skin and the environment is responsible for the volume of heat losses from the body, a higher gradient temperature lead to an increase in the convective and radiative heat losses, however, a decrease in the gradient temperature leads to minimizing the heat losses. The blood circulated at the skin surface, its temperature will be decreased and consequently will lower the core temperature. On the other hand, when the body is exposed to a cold environment, its core temperature starts to fall, when the core temperature reaches a point below the neutral level, the skin blood vessels constrict, which reduce the warm blood flow to the skin. When less blood is flowing to the skin, the gradient temperature between the skin and the surrounding temperature decreases that lead to a reduction in the sensible heat losses. So the vasomotor response is the response of blood vessels constriction and dilation.

In conjunction with vasodilation when the core temperature continues to rise, a sweating response occurs. The sudomotor response, or sweating, will enhance

heat loss at the skin surface by latent loss when moisture evaporates to the environment.

Similarly, in conjunction with vasoconstriction, shivering may occur to help the body temperature to reach the normal level again. Shivering is a metabolic response where an involuntary muscle contraction begins to increase the metabolic rate.

In summary, the body regulates its temperature through the thermoregulatory systems, vasodilation, vasoconstriction, sweating and shivering by using feedback temperature sensed by thermoreceptors located throughout the body.

2.4 Occupant behaviours

Human behaviour also affects thermoregulation through actions performed to reduce thermal discomfort. For example, by altering the clothing level, shelter from the sun or cold wind, moving towards the heat source to increase the heat transfer, in addition to controlling the building thermal environment by using heating or air conditioning systems.

Occupant thermostat use has a significant effect on building energy performance. Occupants of commercial buildings have less control over their thermostats compared to residential occupant (Andrews et al., 2013). Multiple research stated that giving the occupant the control over its thermal environment will not only increase the occupant thermal comfort but will also increase productivity and satisfaction (Fountain et al., 1996, Wyon, 2000).

The occupant behaviours studied in the literature varies from the window opening, light use, clothing level adjustment and even the occupant presence inside the building. There are multiple approaches to modelling human behaviour in the literature. Some used classical statistical models and others used the time dependant data like Markov and Hidden Markov chains approach (De Dear et al., 1998; Yan et al. 2017; Haldi et al., 2008; Flett et al.,2014).

2.5 Human thermal models

The process of body temperature regulation requires the body to balance between the heat generated from the metabolic and the heat losses from evaporation, radiation, convection and conduction with the environment. The fundamental laws of thermodynamics apply to the human body.

The history of the human thermal modelling started in 1911 with the first attempt by Lefevre where the human body modelled as a sphere that exchanges heat with the environment. Since then several human thermal models have been developed. And as a result, the first human thermoregulation model developed in 1970. The development of the computer helped in the developing of more detailed and more complex thermal models by using more powerful computers. The most commonly used and well-known models are the Gagge (Gagge et al., 1986), Stolwijk (Stolwijk, 1971) and Wissler (Wissler, 1985) models. All models developed after the three mentioned models and found in the literature were a modified form of them (Havenith et al., 2011).

Human thermophysiology models can be classified from simple to more complex models. In the literature, there are plenty of thermophysiological models from the single segment or the whole body represented as one segment to the multi-segment model representing more than one body part. Additionally, these models can also be classified from one node models to two-node models and multi-node models, where an energy balance equation is set to every node (Katić et al., 2016; Havenith et al., 2011).

The one-node models are usually derived from experimental data. The model represents the human body as one unit so usually, the thermoregulatory system is not included in a one-node model. The two-node model usually represents the whole body as one segment, but it divides the body into two concentric shells the core body layer and a skin layer. One of the well-recognized two-nodes models is the Gagge's model developed in 1971 and improved in 1986 (Gagge et al., 1971; Gagge et al., 1986). The model can predict the skin and core temperature under

the steady-state and the transient environment with a moderate activity level. The model also considers a uniform temperature in the body compartment as one temperature of the skin and one temperature for the core. The model considers the heat flow between the two nodes and between the skin and the environment, it also considers the physiological phenomena, where the model includes the shivering the sweating in addition to the blood flow regulation as vasodilatation and vasoconstriction. Multiple two-node models were found in the literature all based on the Gagge model (Gagge et al., 1986) and Pennes equation (Pennes et al., 1948) like Foda and Zolfaghari (Foda et al., 2011; Zolfaghari et al., 2010 a; Zolfaghari et al., 2010 b). Zolfaghari et al. (2010 b) based on the Gagge's model developed a simplified three nodal thermal sensation model. Where the human body was divided into three lumped compartments: core, bare skin and bare skin.

The two-node model was extended and the first influential multi-node model was developed by Stolwijk (1971) this model is considered as a foundation for the different multi-node models available these days. The model first developed for The National Aeronautics and Space Administration NASA to predict the thermal responses of astronauts in their missions. The model divides the body into six body segments, including the head, trunk, arms, legs and each body part has four layers the core, fat, muscle and skin in addition to a central blood flow compartment which is connected to all the other nodes. The control system in the Stolwijk model is based on the two temperature signals cold/warm which reflect the change in the temperature of each node. The model proves accountability in results for simulating persons of low activity level, also it is still limited to constant environment conditions (Cheng et al., 2012). The active system of this model is still widely used in the advanced and modern models. Some of the multi-node models based on Stalwijk model (Stalwijk, 1971) like Tanabe model (Tanabe et al., 2002), Fiala model (Fiala, 1998), Berkeley model (Huizenga et al.,2001), Karaki model (Karaki et al., 2013) and Salloum model (Salloum et al. 2007).

In 1991 Smith (Smith, 1991) developed a detailed three-dimensional multi-element human thermal model. The model is comprised of fifteen cylindrical

body parts, it is also known as KSU (Kansas State University) model. The Smith model includes a detailed control system for the thermoregulation. She used the finite element techniques to solve the heat transfer equations. Although it is considered as one of the most advanced and detailed models due to its three-dimensional calculation, the model didn't consider the blood perfusion that occurs in the capillary beds, Furthur, it didn't consider the accumulation of sweat. Fu 1995 improved the Smith model by including a detailed clothing model. The model introduced a new solution for the blood perfusion, sweat accumulation between the clothing and the skin layers, clothing moisture absorption and radiation in the clothing (Fu, 1995).

Another multi-segmented model was developed by Fiala, the model is able to predict the body state well in both steady-state and transient conditions (Fiala et al. 2001). The model consists of two interacting systems, 1. The controlled passive system and 2. The controlling active system. The Fiala model has been made to predict in a wider temperature environment. Like most of the human thermal models, it is considered for a typical adult person of 1.85 m2 body surface area and 73.4 kg of weight. It decomposed the human subject into 15 spherical or body cylindrical elements: head, face, neck, shoulders, arms, hands, thorax, abdomen, legs, and feet. Each element is constituted of tissue layers where for example the leg has bone, muscle, fat and skin distributed in the radial direction to reduce the numerical error due to temperature gradient at the outer regions. The passive system of Fiala's model responsible for all the thermo-physical and basal physiological properties. The system calculates all the heat exchanged between the tissues in the body, in addition to the heat exchange of the body with the environment (Fiala, 1998). The active system represents the thermoregulatory system of the human body, it simulates shivering, sweating and the vasomotor response of the human body. The model was validated with independent experiments where it covered an environmental temperature range between 5 and 50°C with a metabolic rate between 0.8 and 10 met (Fiala et al., 2001). To create a new Universal Thermal Climate Index (UTCI), the original Fiala's model was adapted and expanded to form a new model the UCTI-Fiala

model. They developed this model for the combined simulation of outdoor and indoor thermal environment where an adaptive clothing model has been included to fit the outdoor environmental factors as clothing permeability and behavioural adaptation of the clothing insulation (Fiala et al., 2012).

Tanabe et al., 2002 developed a multi-segmented, multi-node model based on the Stolwijk model the model has 16 body segments, each segment four concentric layers and a total of 65 nodes by considering a central blood compartment as one node exchanges convective heat with all other nodes through blood flows.

Huizenga et al., 2001 based on Stolwijk model and Tanabe model, developed the Berkeley comfort model. The model allows an unlimited body segment with four concentric body layers in each segment. The model is capable of predicting under transient, non-uniform thermal environments. They also included a clothing node to model both heat and moisture capacitance of clothing and to model evaporative heat loss correctly from the body through clothing (Huizenga et al., 2004). They declared that the model is useful for evaluating innovative HVAC systems that provide a stratified or non-uniform environment. Although, they stated that the input structure of their model allows it to be connected to building simulation programs, but to the extent of the author knowledge there was no further publication found on that topic later. Zhang et al. 2001 included the body builder in the UC Berkley model to have the capability to change the physiological characteristic input (height, weight, body fat, gender, skin colour, and body type) of the model, where all other models are considered for a typical average aged man (Zhang et al., 2001).

The AUB (American University of Beirut) model is a highly sophisticated human thermo-physiology model developed by Salloum et al. 2007 the model initially divided the human body into 15 body segments, head, Upper Chest, Lower Chest, Upper arms, Lower arms, hands, thighs, legs, and feet each segment is composed of four nodes core, skin, artery and vein. The model applies to an average young person. They used a multi-branched blood flow model of Avolio, it starts from the heart to the rest of the body parts, it also includes a blood flow pulsation in the

main arteries. The model updates arterial blood flow every time step and capable of handle changes in cardiac output triggered by metabolic rate and thermoregulation during the heat and cold stress period. Al-Othmani et al., 2008 improved the model to account for the asymmetric radiation by dividing the outer skin layer of each body part to six equal angular sectors. Karaki et al., 2013 improved the model to accurately predict the blood flow in the hands and fingers where they added the ten digits to the other body parts and modified to the number of the artery branch of Avolio to represent the ten fingers. The model introduced an innovative control model for the AVA arterio-venous anastomoses to have a better blood flow prediction in the fingers. Rida et al., (2013 a) used the whole-body physiology model and developed a model to predict the physiological phenomena of CIVD cold-induced vasodilation for hands exposed to extreme cold weather. The model was later modified by (Rida et al., 2014 b) to account for elderly people. The AUB model has been selected to be a reference model for the physiology model developed and implemented in ESP-r. And that is because the model is in an advanced level of details it accounts for detailed blood flow calculation and it showed robustness compared to other simplified models.

2.5.1 Coupling of human thermal model and sensation and comfort models

Schellen et al., 2013 discussed the use of a thermo-physiological model to support and improve comfort assessment compared to existing more simplified, thermal comfort models. To show the importance of the local thermal comfort, they combined the ThermoSEM, a human thermal model developed by van Marken Lichtenbelt et al. 2004 with three different sensation model, the PMV model, the UC Berkeley model and the EN-ISO 14505 standard. They used the CFD to simulate and analyse the thermal environmental conditions around the human body. They determined that combining with the UC Berkeley model or the EN-ISO 14505 standard gives better results comparing to PMV model which it is not capable of predicting the whole-body thermal sensation when local effects took place. In this study, they simulated the physiological responses using the

environmental conditions calculated by CFD where a manual coupling was applied.

Foda et al. in (Foda et al., 2011 b) compared the skin temperature of three different human thermoregulation models the Fiala model, the University of California, Berkeley (UCB) thermoregulation model and a multi-segmental (MS) Pierce model were compared to recent experimental studies (measured data from literature). They found that MS-Pierce had the best predictability in steady-state.

Cheng et al. (2012) coupled two typical thermal comfort models, the UC Berkeley model and the ISO 14505 standard in a CFD numerical simulation to assess the thermal environment of a small office for the non-uniform environment. Their study concluded that the ISO 14505 standard, even though it is public and easy to implement in a CFD, needs more validation of its reliability. They also concluded that for an asymmetric environment, a complete human thermal model with physiological and psychological factors is required. They also stated that connecting the UC Berkley in a CFD simulation is complex and such coupling needs to be done (Cheng et al., 2012). To study the effect of solar radiation on the thermal environment around the human body, Yamane et al. 2013 reported a comparison between experimental results of a man sitting in a room exposed to solar radiation with a CFD model. Results of a particular time of the day have been compared with a CFD study after coupling the thermoregulatory model of Tanabe et al. 2002. This study helped them to understand the effect of localised solar radiation on the function of thermoregulation.

Conceição (2003) worked on two numerical models to study human thermal comfort in a building where they simulated the building thermal response and evaluated the internal air quality, and the results were used as input data in the second one to simulate the human with clothing thermal system. Katić et al. (2016) reviewed some thermal models and compared them in a thorough review.

VTT Technical Research Centre of Finland worked on developing a human thermal comfort model. This model was firstly introduced by Holopainen et al. (2010). Holopainen in her dissertation 2012 (Holopainen, 2012) presented her human thermal model implemented in a building simulation environment. She defined the importance of applying the two models because that Fanger's Predicted Mean Vote PMV based on a heat balance model which referred to as a static model, and it does not take the human thermoregulatory system, also that it is only valid under restricted conditions (Holopainen, 2012). This implementation enables defining the external boundary conditions for the human thermal model as surface temperatures and radiation heat transfer more correctly compared to previous human thermal models. The human thermal model (HTM) takes into consideration the physiological behaviour of the human body and models the physical interactions between the human body and the surrounding space. For calculation, she used the finite-difference method. The model divides the human body into 16 body parts as cylindrical shape each consisted of four layers bone, muscle, fat and skin. To calculate thermal sensation and thermal comfort of the human body they used Zhang's method, and then the overall thermal sensation was calculated with a purpose to calculate the Predicted Percentage of Dissatisfaction. The HTM was implemented with the non-commercial building simulation environment VTT House. The VTT House simulates air infiltration, ventilation and heat transfer processes. The VTT House program is designed for simulation experts because it requires a good understanding of the simulation case and principles knowledge of the nodal network creation. The number of nodes in the HTM was adjusted depending on the simulation situation (Holopainen et al. 2010).

The HTM was validated with previous published examined data and other human simulation models at different conditions. For the implementation, Holopainen studied the effect of building structures on thermal sensation and comfort. The case study was on changing the envelope construction with more energy-efficient windows and wall insulation for an old built apartment located in Finland during winter to explore the impact on thermal comfort. The human located in the

middle of the living room floor, with light activity. For simplicity and to have a rapid model the HTM uses constant basal blood flows stating that the use of residential and offices usually for light work with a low metabolic rate. The model was standing up in the middle of the room with no contact with the floor or any other objects. The Convective heat transfer coefficients used was calculated for naked skin surface temperature (Holopainen, 2012), and it used the same for clothing temperature. That HTM study showed the differences in thermal response between different ages (Holopainen et al., 2010).

A human thermal model could have multiple applications, but the focus of this review section of the dissertation was on their ability to predict the human thermal response which can be utilized to evaluate the comfort of building occupants in different environments. These models can be used to optimize the environmental parameters, clothing and metabolic rate variation studies aiming to reduce the need for pilot studies. There are some other usages for the physiology models which are out of the scope of this research like the prediction of the human physiological limits, physiological abnormality and medical treatments on human thermal response.

2.6 Human thermal comfort models

The thermal state of the human body is the key factor in stating the human sensation and the perception of thermal comfort (Fanger et al., 1985; Stolwijk, 1971; Gagge et al., 1967). To ensure a suitable indoor thermal environment a mechanical or natural ventilation system may be required. A system that is capable to provide the indoor design parameters directly such as indoor air temperature, air movement and relative humidity. One of the bases of design criteria for the indoor parameters is the occupant thermal comfort.

One of the widely used comfort models is the Predictive Mean Vote's (PMV) model developed by Fanger and based on an equation for the human body heat exchange. The PMV model was reviewed and described in (Van Hoof et al., 2008). In the PMV model, the thermal satisfaction or dissatisfaction of occupants is a

function of the six variables the activity level, thermal resistance of the clothing, air temperature, mean radiant temperature, relative air velocity and the water vapour pressure in ambient air. An empirically comfort equation was obtained, it assumes a linear relationship between the activity level and the sweat rate in addition to the relation between the activity level and the mean skin temperature, where these relationships formulate the human energy balance equation. The six variables used in the model will determine whether the building occupant is in thermal comfort or not.

The PMV model was expressed by Fanger (1970) and adopted by CIBSE and ASHRAE (CIBSE, 2018; ASHRAE Standard 55-2013) on a 7-point scale for thermal sensation and it is widely accepted and used in the design process as an index of maintaining indoor thermal comfort. The deficiencies of the PMV model were that the body is considered as a whole and the mean skin temperature is used. Moreover, the body responses predicted are at steady-state conditions environment. Since then, more research was done on the development of human thermo-physiological modelling. A PMV range of ±0.5 corresponds to 10% of predicted percent dissatisfied (PPD). Based on the adaptive model a percentage of dissatisfaction of 80% to 90% can be accepted. Table 2.1, shows the PMV thermal sensation scale.

Table 2.1: ASHRAE Thermal Sensation Scale.

Index	Thermal sensation
3	Hot
2	Warm
1	Slightly warm
0	Neutral
-1	Slightly cool
-2	Cool
-3	Cold

Fiala in 1998, developed the DTS model (dynamic thermal sensation) to predict the human thermal sensation based on core temperature, mean skin temperature and rate of change in mean skin temperature. The model is based on a regression analysis between the predicted physiological responses and thermal comfort measurements from the database of comfort experiments.

Another study conducted by Zhang et al. (Zhang et al., 2010 a, b & c) related physiological responses to local thermal sensation. The model is based on differences between local skin temperature and the setpoint of skin temperature for a specific body part, the rate of change in local skin temperature and rate of change in core temperature. The setpoint temperatures are the neutral body part skin and core temperature at a neutral temperature. Since neutral temperature is variable when a change happens to clothing insulation or activity level, Zhang suggested an interpolation for neutral temperatures to account for a wider range of neutral conditions. The model is based on experimental results it can be linked with a physiological model it predicts local sensation, local comfort, overall sensation and overall comfort. Although these models show promising results, one could argue whether setpoints are a good representation of the physiology behind thermoregulation or thermal sensation.

The sensation scale in Zhang's model has limits between -4 and +4 table 2.2 shows the sensation scale. The local comfort model is based on the local sensation and overall sensation calculation and it is given in a scale of -4 +4 scale provided in table 2.3.

Table 2.2: Zhang model thermal sensation scale.

Index	Thermal sensation
4	Very hot
3	Hot
2	Warm
1	Slightly warm

0	Neutral
-1	Slightly cool
-2	Cool
-3	Cold
-4	Very cold

Table 2.3: Zhang model thermal comfort scale.

Index	Thermal comfort
4	Very comfortable
2	Comfortable
+0	Just comfortable
-0	Just uncomfortable
-2	Uncomfortable
-4	Very uncomfortable

2.7 Hygrothermal Interaction of Occupant and Building

As comfort prediction is a very important factor at the detailed design stage, for that purpose thermal comfort models have been connected to building simulation.

For comfort analysis, the use of the two-node model or Pierce model is used as a physiology model in many building simulation tools but only as a post-processing simulation, none of the available building simulation tools has used the two-node model to predict the occupant heat loads and none has implemented it in the energy equations of building thermal balance.

The Energy Plus has used a regression line model of the available steady-state heat loss values from the human body, to predict the sensible and latent heat loads from the occupant at the different metabolic rate and operative

temperature (Crawley et al. 2001; DoE, 2020). This approach considered steady-state and is a good approach toward applying variable internal heat loads from occupants. The Energy Plus occupant heat load model has some limitations first it considers the summation of sensible and latent heat load always equal to metabolic rate as if the body is at thermal equilibrium it simplifies the dynamic nature of the human thermo-physiology.

To the knowledge of the author Holopainen (2012) developed a human thermal model based on the model of Fiala and she integrated it in VTT a building simulation tool. Holopainen in her studies considered the effect of the building on the occupant where she studied the effect of the building envelop structure and the effect of heating distribution on thermal sensation and comfort. The model was used in the building simulation to control HVAC system but does not consider the occupant thermal load dynamically. Similarly, Baudier et al. (2016) used a multi-segmented model based on the 25 node model of Tanabi (Tanabi et al., 2002) the thermo-physiology model is coupled with a thermal sensation and comfort model of Zhang (Zhang, 2003) in ESP-r that approach was used as a controller and has been demonstrated in the use of local cooling and heating systems inside building, for example, a radiant panel made from thermocouples (Baudier et al. 2019). All the preceding improvement needs to be expanded and improved.

2.8 CFD and its integration in building simulation

The computational fluid dynamics (CFD) discrete a building zone into a large number of control volumes. The CFD simulation can provide a detailed description of the airflow by solving the Navier–Stokes equations (Versteeg et al., 2007). The parameters solved in CFD are air velocity, air temperature, contaminant concentrations, relative humidity, and turbulence quantities. As human comfort is influenced by environmental variables at the local or micro-scale level, the use of CFD tools becomes crucial for designing a comfortable indoor environment (Nilsen et al., 2007; Srebric and Chen 2002)

Over the last 50 years, CFD has been considered effectively as a tool for evaluating the indoor environment of buildings and heat and mass transfer between the indoor environment and the building envelope (e.g. Nielsen, 2004, Awbi 1991, Chen et al. 1995, Heiselberg 1996, Chen, 2009, Srebric et al. 1999, Bartak et al. 2002, Beausoleil-Morrison 2002, Sorensen and Nielsen 2003, Djunaedy et al. 2005). One of the earlier CFD studies on indoor airflow was Nielsen (1974).

Normally, CFD has a high computational cost, in addition, CFD simulation similar to any other simulation tools are sensitive to the boundary conditions. Engineering judgment and knowledge is essential to decide whether the use of CFD is appropriate in solving a specific problem. Moreover, an accurate and effective simulation is a joint initiative of the CFD code and the CFD user. Misuse of a CFD model could lead to inaccurate results and along with poor interpretation could lead to weak designs. Based on that the accuracy relies on a solid understanding of flow physics and requires considerable user expertise (CIBSE Guide A, 2018).

CFD has limitations, with the ability to model turbulent flow and the high computational resources required being two of the most important ones. Especially in the case of time-dependent flows and advanced turbulence models such as large eddy simulation (CIBSE, 2008).

Most of the current CFD programs usually, do not have embedded models to determine the dynamic boundary conditions in buildings (Tian et al., 2018). Because of that, the users of CFD tools lose the transient nature of the boundary for example when using fixed supply airflow rate and temperature, fixed wall temperature or heat flux through the envelopes. Thus, coupled building energy simulation with CFD is very attractive, since it increases the potential of an accurate analysis of building energy.

The coupling of building energy simulation and CFD simulation has been considered in several publications (Negrao, 1995; Srebric et al., 2000; Beausoleil-Morrison, 2002; Zhai et al., 2002; Djunaedy et al., 2005). A building energy simulation can provide dynamic boundary conditions to CFD. On the other hand,

the CFD can provide the local airflow information to building energy simulation aiming to improve the HVAC control system and the thermal load calculation inside a building.

2.9 CFD and human body simulation

CFD modelling is usually used to evaluate the indoor airflows and to study temperature distribution when applicable, induced by a specific heating, ventilation and air conditioning system. The effect of the presence of occupants inside a domain on the surrounding airflow in CFD is influence. Evaluating both thermal comfort and the indoor environment in CFD, it requires to model occupants inside the domain as well as their thermal boundary conditions.

To get an accurate prediction of thermal state one needs accurate environmental data as input to the physiological model. Hence, it is convenient to integrate the thermo-physiology model with environmental modelling tools (such as building simulation tools) and computational fluid dynamics (CFD). These can provide the physiological model with dynamic boundary conditions, and also reflect the thermal state of the occupant in the simulation. In this way, the complex interaction between the human body and its thermal environment can be characterised (Dixit et al., 2015).

Buildings can be ventilated in different ways, and this can strongly affect both thermal comfort and the energy consumption of space. With the assistance of the CFD simulator and building simulation tool, it can predict the airflow in the occupied spaces and the ventilation system more realistically than with building simulation alone.

The simple shape of the human body can be represented as a block shape where it is often used in CFD in design practice, and the boundary conditions are set as fixed values and the predicted mean vote (PMV) and predicted percentage of the dissatisfied person (PPD) has been used to predict the thermal comfort parameters. It has been found that in naturally ventilated spaces, the human body

has a significant effect on the local environment compared to that in other environments. For that reason, the consideration of two-way interactive simulation systems integrating detailed environmental CFD simulation with a human thermo-physiological model is preferred. Recent developments in computing technology have heightened the need for using computer-simulated manikin or human thermoregulatory models to study thermal comfort and thermal environment.

In the past years, there has been an increasing interest in evaluating thermal comfort of building occupant using CFD it was usually done in stages where first a CFD simulation conducted for the proposed domain and the results used as input in the thermal comfort model. This approach of evaluating thermal comfort can be taken as a primary evaluation because the linking between thermal environment and thermal comfort is not fully addressed and there should be a combined simulation which bridges analysis of the indoor air environment and thermal comfort (Gao et al., 2005).

In 1995 Gan published a study using a CFD model to predict room air distribution, with Fanger's comfort model equations incorporated in the CFD model (Gan, 1995). Sørensen et al. (2003) modelled in detail the shape of a seated manikin and used it in a CFD study to calculate the radiative heat transfer coefficient and the natural convection flow around the manikin. They compared simulated and experimental results, though a constant skin temperature was used in the simulation.

Murakami et al. (2000) used Gagge's two-node model as a thermo-physiological model in a CFD study to predict the heat released from a human body. The shape of the human body was represented using a curvilinear coordinate system. Murakami stated that even though the rectangular shape was very popular to represent the shape of a human body, they believed that the physical shape of the human body could have an impact on the indoor climate.

Nielsen et al. (2003) set a CFD benchmark exercise, to validate CFD models specifically for modelling airflow around an occupant. The experimental data of

the benchmark was presented in Kato and Yang 2006. This benchmark was used by multiple researchers (Srebric et al., 2008; Deevy et al., 2008; Cropper et al., 2010).

Gao et al. (2004) studied the micro-environment around a computational thermal manikin with a real geometry of the human body shape in two cases one with personalized ventilation and the other without. Showing through experimental and simulation that personalized air system plays a major role in reducing pollutants in the respiratory zone. The integration of the clothing human body has been studied by Takada et al. 2016 They studied the airflow ventilation in the air layer of a clothed person using CFD where a 3D laser scanner was used to get the geometrical shape of the thermal manikin, and fixed skin surface temperature was used at the boundaries.

Deevy et al (2008) modelled the benchmark of the displacement ventilation room where they used the geometry of the experimental manikin in the CFD model, arguing that using the detailed body shape will minimise potential errors comparing to a simplified form. They also included the thermal radiation from the manikin where they used the discrete transfer radiation model. Also, the total heat transfer from the manikin considered 76 W a constant value and the convective part was 38 W. They have also compared two different turbulence models, but differences in results were minor.

Srebric et. al (2008) studied the effects of three boundary condition elements in a CFD study; the contaminant source, the size of the body area, and the shape of the human body. They found that the fraction of convective to radiative heat flux affects the accuracy of predictions of the thermal environment around the occupant. Also, they found that using a simplified shape of the human simulator will still give accurate results for the domain environment, but not when studying the local environment of the occupant, where the shape plays a major role in predicting airflow near the body. Srebric also noted that in a typical CFD approach, only the convective heat transfer is taken into account, which is insufficient where thermal radiation plays a major role in heat transfer from any

heat sources (Srebric et al., 2008). Additionally, Yang et al. (2007) included a computational thermal manikin in a CFD simulation. CFD is used by researchers to study the building occupancy factor. The complexity of the geometry of the thermal manikin is used from the simplest one to more detailed 3D scanned real manikins. In their research, they intend to use a detailed human geometry, where they used a 3D graphic design package to model the detailed human body and they used a manikin of 1.8m height and a DuBois area of $1.83m^2$. In this study, they validated their work with the experimental benchmark of displacement ventilation. The human thermos-physiological model exchange data using files with the CFD model. Also, Cropper et al. (2010) published a paper on the methods used in coupling a thermo-physiology model with a commercial CFD program. In their approach, they used the shared files method to exchange data between CFD and a thermo-physiology model. For that, they used the Fiala model as a multi-segmented human thermal model which is able to predict the response of the human body to changes in the environment. They coupled it with the ANSYS CFX commercial CFD solver.

In a more recent study Angelova et al. 2015, integrated a thermo-physiological model with the Fluent CFD software. They studied the effect of clothing and the metabolic rate on the human body and the environment (Pichurov et al., 2014; Angelova et al., 2015).

To study the transient and local effects of thermal sensation and comfort perception, van Treeck et al., 2009 have developed a parametric multi-segment manikin model. The model is an interface between the Fiala's thermoregulatory model and other computational models. They used the iFluids CFD solver to get the environmental parameters, this method requires a high-performance computer in addition the manikin was placed within the flow as a passive obstacle.

Literature did not show any application of using an internal coupled Building Energy simulation and CFD together with a detailed human thermo-physiology

model. multiple studies have linked a thermo-physiological model with a stand-alone CFD simulation, some utilising advanced meshing tools and detailed manikin geometry. However, none of the research has studied the effect of a thermal manikin on building performance.

2.10 Conclusion and Research Gap

The large differences between people in both psychological and physiological make it difficult to thermally satisfy everyone placed in the same environment (Schellen et al., 2013). Moreover, the occupant thermal state is very sensitive to the environmental conditions surrounding it. So, the environment has a critical influence on its thermal comfort, productivity and the living environment.

In real life occupant dynamically exchanges heat with its surrounding, which is based on multiple environmental parameters. The two-way interaction of heat exchange is not well addressed in building simulation tools. Internal loads input such as occupant heat loads has an important impact on the building simulation results. As well as, the surrounding environmental changes have an impact on human thermal comfort. Consequently, the representation of the occupant in building simulation needs improvement and that could be done by the mean of combining a dynamic thermal occupant model with the building simulation tool.

To design a new ventilation system or to test an existing one a CFD study could provide a wealth of data on the details of the flow in the domain, it is useful for the domain visualisation and obviously, it will reduce the experimental costs. CFD results will be susceptible to boundary conditions and the most accurate the boundary conditions the better the results. Correspondingly, a human thermoregulatory model could predict better the thermal boundary conditions from an occupant in addition to that such a model is dynamic which means that boundary conditions will change every time-step. Further, A human thermal model is a valuable tool to understand the human thermal behaviour when exposed to different environmental conditions for different activity levels, clothing type also plays a major role in predicting the thermal status of the human

body as it acts as a resistance layer next to the skin layer. It is very important to use a multi-segmented human thermal model to predict local skin and core temperature in order to assess local thermal discomfort, especially in cases of asymmetry situation and non-uniform radiant temperature.

However, the transient nature of the occupant heat load is not fully addressed and implemented in a building simulation tool. Most previous studies are limited to the influence of the transient environment on occupant thermal comfort. As both sensible and latent heat load emitted from occupant affected by its environment, and in situations where building allows zone temperature fluctuation as in naturally ventilated building, therefore it is essential to consider the dynamic occupant heat loads in building simulation.

Summary of the gap found based on our literature:

- Building simulation usually does not consider the transient nature of the building occupant heat loads.
- There were a few attempts to use detailed physiology models in building simulations to check for thermal comfort, but none of them has considered the transient nature of heat losses in building simulation. (The effect of the occupant heat loads on the building environment have-not been fully addressed).
- None of the CFD approaches has considered both building and occupant in one dynamic simulation. Therefore, the approach (building simulation-physiology model-CFD) has never been considered in a previous study.

This thesis contributes to the state of the art by developing a method for coupling an explicit thermal representation of building occupants within in CFD-coupled building simulation tools in order to have a reliable and more detailed prediction of their thermal comfort and their thermal interaction with the building in greater detail than has been done before.

Chapter 3: Building Energy simulation tool ESP-r

3.1 Chapter overview

In this research, the author chooses to use ESP-r a reliable and widely known energy simulation tool. The reason behind this choice was because ESP-r is an open-source, a researcher attractive tool, and the help and support that can be delivered from the developers. Although ESP-r lack of detailed documentation and it has a primitive interface, but one of the keys to choosing ESP-r is to integrate our dynamic occupant is its flexibility. Moreover, the adaptive coupling functionality in esp-r between the dynamic thermal model with computational fluid dynamic was the most valuable motivation of the selection. The integrated CFD tool was profoundly used in this research.

This chapter briefly describes the ESP-r software and the main energy balance equation and method and solution used. In addition to a brief methodology of improving the occupant representation.

3.2 ESP-r Energy Building Simulation Tool

ESP-r a dynamic building simulation tool which stands for Environmental System Performance and the r for research it is a computing environment for building and/or plant energy simulation as defined in (ESRU 2002). The first numerical engine of ESP was introduced in 1977. Clarke (2002) investigated and compared the different energy modelling techniques and in order to represent all building heat flux exchanges and dynamic interactions, he developed a set of coupled state-space equations and a numerical processing approach.

In ESP-r, a simulation model consists of a setting with one or more building. A building model in ESP-r can be consist of one or more polyhedral zones. To set up a zone, one needs to define its geometry, its construction materials and its usage profiles. By increasing the number of zones ESP-r also uses networks to define energy subsystems in the building such as airflow, HVAC systems and electrical systems.

The building and its subsystems can be decomposed into a coupled set of differential equations that when solved yield the energy and mass exchanges occurring throughout the building. To solve these energy and mass balances in buildings an advanced numerical method was adopted in ESP-r to integrate the different equation types of algebraic, ordinary differential and partial differential.

ESP-r is a helpful design tool for studying energy and environmental performance. It contains a number of interdependent program modules. The integrated simulator in ESP-r is constituted of multiple numerical solvers which can be considered separately or in various combinations. Solvers were optimised for the building, network or computational fluid dynamic CFD based flow, plant and electrical power domain. The solvers have the ability to pass information so they can pass results from one solver to another and vice versa depending on its order in the calculation. The next section will briefly explain the modelling process adopted when using ESP-r.

3.3 Structure of ESP-r
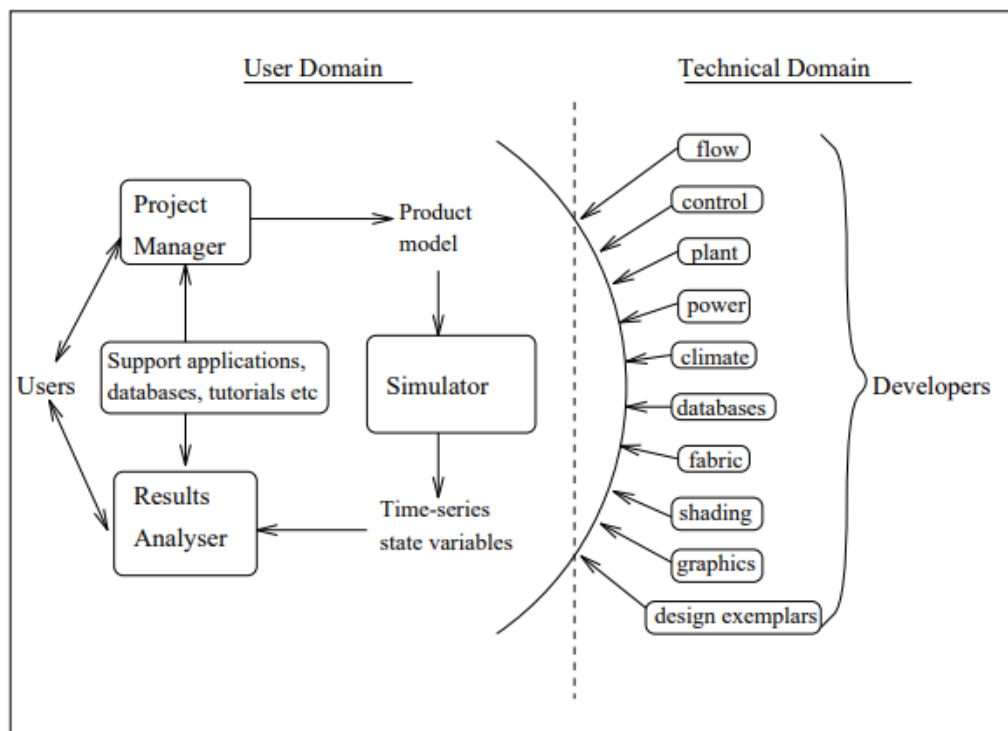
Figure 3.1: ESP-r structure (ESRU, 2002)

Figure 3.1 shows the relationship between the different part of the ESP-r program. Following is a description of a number of the modules of ESP-r.

The *Project Manager* is the place where the building and plant configuration are defined, and the complete description is called a product model. Since a building model is subjected to weather impact and it is simulated over time, then those weather file and time needs have to be set here (ESRU 2002). Through *the project manager,* user can access multiple modules like the Event Profiles *Database Management Module*, which is responsible for defining profiles of the time-dependent variations in zone occupants, lighting, plant control and appliance usage. The *Construction Data Management Module* manages (creates, modifies, edits and lists) primitive and composite constructions databases. (ESRU 2002) The *Plant Components Database Management Module*, which manages a *plant components database*, and a *Climate Database Management Module* to manage and analyse climatic data collections. The *Simulator* is the building and plant

simulation engine which grabs all the defined information through the other modules, especially the construction and weather data in order to do a simulation which able to predict building and plant energy and fluid flows by a rigorous numerical method.'

To present the results obtained from the simulator to the user in a variety of output options. Like a perspective visualisation, results interrogation, statistical analysis, graphical display, tabulations, frequency binning and 3D plotting (ESRU 2002; Hand, 2018).

Another important module that will be used in this research is the *computational fluid dynamic module, the* function of which is to set the CFD domain the boundary conditions, the openings and sources. A CFD domain is composed of a number of cells that represents the air volumes within a thermal zone. For a CFD domain, it needs to define the gridding of the domain, the boundary conditions applicable, groups of cells at the boundary which represent inlets or outlets, blockages within the domain representing solid objects, in addition to the sources of heat and/or contaminants.

The cells within a domain in ESP-r are rectilinear in the X and Y axis and normally rectilinear in the Z-axis. The CFD domain solver is implemented with the building solver Building-plant solver (bps) supporting coupled solution with the zone solver and the mass flow solver (Hand, 2018). Further details about the CFD domain in ESP-r is discussed in Chapter 7 section 7.2.1.

3.4 ESP-r Thermal Model

The model of a building in ESP-r is constituted of multiple small control volumes, each control volume, which represents a region or category of space is represented by a node, the conservation of mass, energy and momentum between the nodes is then applied. Each control volume equation can be derived from the law governing the conservation of mass, energy and momentum. These equations describe all the physical action that could apply in a volume like heat conduction, convection airflow and moisture flow, etc (Clarke, 2002). Setting the

boundary conditions and choosing real climate data in order to solve the set of equations which allows the assessment of the transient energy and fluid flow process happening within the building (Kelly, 1998).

Based on the conservation equations of energy, mass and momentum the characteristic equations are defined for each control volume. Where these characteristic equations enclose the physical characteristics and changes related to the control volume and also implicitly link the volume to its neighbours. The linkage to the adjacent volumes can be as heat or mass exchange.

For each node has an energy balance considering the relevant energy flow paths. The energy balance of the thermal interaction between each two-neighbour node is called inter-node heat flows and a resulting equation set links all inter-nodes equation over time and space (Clarke, 2001; Kelly, 1998; Beausoleil-Morrison, 2000; Negrao, 1995).

3.4.1 Heat balance for building fabric nodes

The heat exchange within opaque constructions is complex, it usually involves different modes of heat transfer like solid conduction, gaseous convection, radiation and sometimes moisture transfer. In ESP-r the building fabrics are represented as multi-layered construction by adding a series of solid elements. The construction layers defined in a model provide the physical boundaries to the zones. The building construction layer is normally represented by three control volumes (nodes). A homogeneous material volume in the middle of a layer, and two surface volume at the boundaries of the layer (Kelly, 1998; Beausoleil-Morrison, 2000; Negrao, 1995).
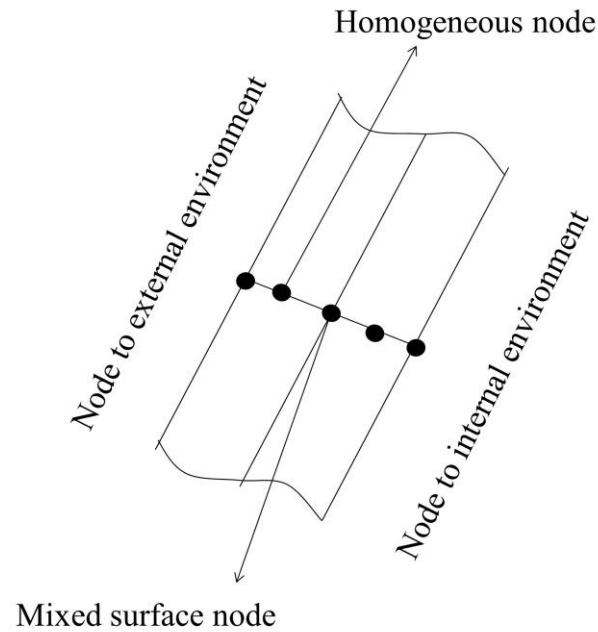
Figure 3.2: nodal discretization for a typical building construction component.

In the case of multiple layers, every two neighbours' layers they share the surface volume defined as mixed property volume.

A multi-layered construction is represented in figure 3.2 it shows the different layers and the different nodes forming the final construction.

3.4.2 Energy balance at the homogeneous node

The heat balance for the homogeneous control volume can be described with the following three terms,

$$Storage\ of\ heat\ in\ CV = net\ conduction\ into\ CV +$$
$$Source\ of\ heat\ within\ CV \quad (3.1)$$

The relation state that the defined homogeneous node will store or release energy in a proportion of heat transferred by conduction from the neighbouring

node and to the amount of heat generated. the storage term is characterised by the rate of change in temperature of the control volume. The heat source can be an embedded heating system as underfloor heating (Kelly, 1998; Beausoleil-Morrison, 2000; Negrao, 1995).

The mathematical form of this energy balance in the x-direction is given as

$$\rho c_p \frac{\partial T}{\partial t} = -\frac{\partial q_x''}{\partial x} + q_{plant}'''$$ (3.2)

Where c_p is the specific heat [J/kgK] and ρ the density [kg/m3] of the material; T is temperature [K]; t is time [s]; q''x is the conductive heat flux in the x-direction [W/m2]; and q_{plant}''' is the heat injection from the embedded plant component [W/m3]. For the sake of clarity, the nodal thermophysical properties ρ, k and c are shown as time-invariant.

3.4.3 Energy balance at an internal surface node

The internal surface node of a construction layer exchange heat with its neighbour node the homogeneous node in the middle of the layer and the air zone node from the other side. Figure 3.3 shows a representation of an internal surface node in a construction section and the heat exchange with the other nodes. The energy balance at this node is similar to the previous one with an addition of two means of heat transfer radiation and convection (Kelly, 1998; Beausoleil-Morrison, 2000; Negrao, 1995). The heat balance than can be described as:

Storage of heat in CV
= net conduction into CV + source of heat within CV
+ net longwave radiation into CV
+ net convection into CV
(3.3)

The conduction happens at the boundary of the control volume with the next-to surface node which is the homogeneous node of the construction. The source of heat can be in addition to plant injection it can be from solar gains and long-wave radiation and sources of heat in the zone like radiation from occupant, lighting and equipment.
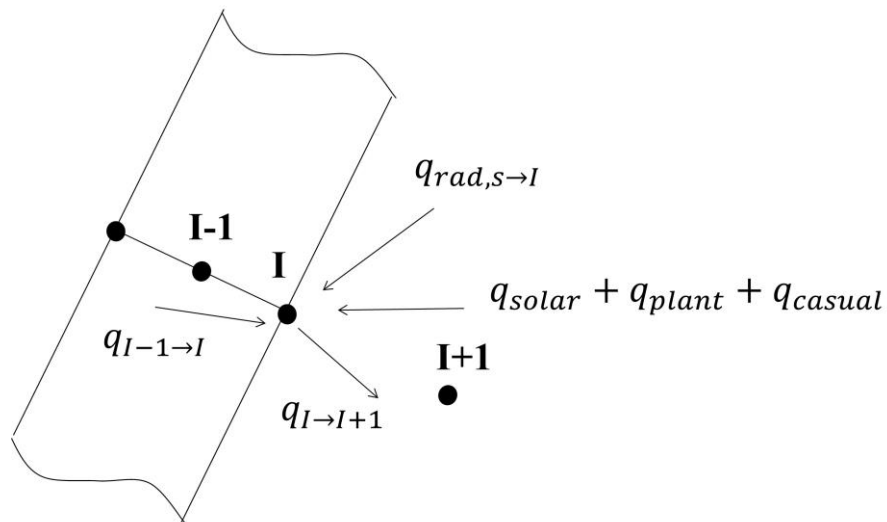
Figure 3.3: Heat balance at the internal surface node.

The net long-wave radiation represents the radiation heat exchange with the other surrounding surfaces. And finally, the convection heat exchange term represents the heat exchanged by convection between the zone air node and the wall construction internal surface node. In this approach, the zone air temperature is considered uniform. This term is affected by the difference in temperature between the two nodes and the

heat transfer coefficient (Kelly, 1998; Beausoleil-Morrison, 2000; Negrao, 1995).

After considering the storage as a backward difference scheme, Adding the implicit and explicit expressions and grouping future time step terms the final form of the energy balance equation is given as

$$\left[\frac{2\cdot(\rho c_p)_I}{\Delta t} + \frac{k_{I-1}}{\Delta x \Delta x_{I-1}} + \frac{h_{c,I}^{t+\Delta t}}{\Delta x} + \frac{\sum_{s=1}^{N} h_{r,s\to I}^{t+\Delta t}}{\Delta x}\right] T_I^{t+\Delta t} - \left[\frac{k_{I-1}}{\Delta x \Delta x_{I-1}}\right] T_{I-1}^{t+\Delta t} -$$

$$\left[\frac{h_{c,I}^{t+\Delta t}}{\Delta x}\right] T_{I+1}^{t+\Delta t} - \frac{\sum_{s=1}^{N} h_{r,s\to I}^{t+\Delta t} T_s^{t+\Delta t}}{\Delta x} - \frac{q_{solar,I}^{t+\Delta t}}{\Delta x \Delta y \Delta z} - \frac{q_{cas-rad,I}^{t+\Delta t}}{\Delta x \Delta y \Delta z} - \frac{q_{plant,I}^{t+\Delta t}}{\Delta x \Delta y \Delta z} =$$

$$\left[\frac{2\cdot(\rho c_p)_I}{\Delta t} + \frac{k_{I-1}}{\Delta x \Delta x_{I-1}} + \frac{h_{c,I}^{t}}{\Delta x} + \frac{\sum_{s=1}^{N} h_{r,s\to I}^{t}}{\Delta x}\right] T_I^{t} - \left[\frac{k_{I-1}}{\Delta x \Delta x_{I-1}}\right] T_{I-1}^{t} +$$

$$\left[\frac{h_{c,I}^{t}}{\Delta x}\right] T_{I+1}^{t} - \frac{\sum_{s=1}^{N} h_{r,s\to I}^{t} T_s^{t}}{\Delta x} - \frac{q_{solar,I}^{t}}{\Delta x \Delta y \Delta z} - \frac{q_{cas-rad,I}^{t}}{\Delta x \Delta y \Delta z} \tag{3.4}$$

The I node is located at the internal surface of the construction. I-1 is the preceding node in the construction and it represents the homogeneous node and I+1 is the zone's air node.

Where $h_{c,I}^{t+\Delta t}$ is the convection heat transfer coefficient [W/m²K] between the surface at node I and the zone air node, evaluated at the future time-step. N is the number of surrounding surfaces in longwave contact. $h_{r,s\to I}^{t+\Delta t}$ is a linearized radiation heat transfer coefficient [W/m²K].

$q_{solar,I}^{t+\Delta t}$ is the solar radiation absorbed at node I at the future time-step. $q_{cas-rad,I}^{t+\Delta t}$ represents, the radiant energy absorbed from casual sources (such as occupants, lights, office equipment) at the future time step. $q_{plant,I}^{t+\Delta t}$ represents, a radiant plant input to node I, that can be from a radiant heater located within the room at the future time step.

That is the basic discretised equation used in ESP-r to characterise the energy balance at the internal surface node of a construction. As the equation shows it considers he heat storage, the conduction with the inner layer of the fabric layer the convection with the air node, the long-wave radiation exchange with surrounding surfaces and the absorption of solar radiation, radiant casual gains (eg. Occupant) and radiant plant injection (Kelly, 1998; Beausoleil-Morrison, 2000; Negrao, 1995).

3.4.4 Air point node energy balance

This section will deal with the most important element of building model which is the enclosed air volumes that form the thermal zones of the building.

The simple and basic representation of the volume of fluid that constitutes a zone is by considering it as a single volume which can be represented as a single node. Where this volume is surrounded by solid constructions in addition to heat transfer by convection, the fluid exchange with its neighbour fluid volumes, external infiltration, the occupants' heat and vapour gains, plant interaction etc.

The boundaries of the control volume of the air inside a zone are the solid constructions internal surfaces. Looking to the air node in the following the node I will represent the air node. J will represent an air node in an adjacent zone and S represents the surface nodes, Node o will represent the outdoor air node (Kelly, 1998; Beausoleil-Morrison, 2000; Negrao, 1995). Figure 3.4 sketches an example representing the air node and the interaction with the other surfaces, external and neighbour air nodes.
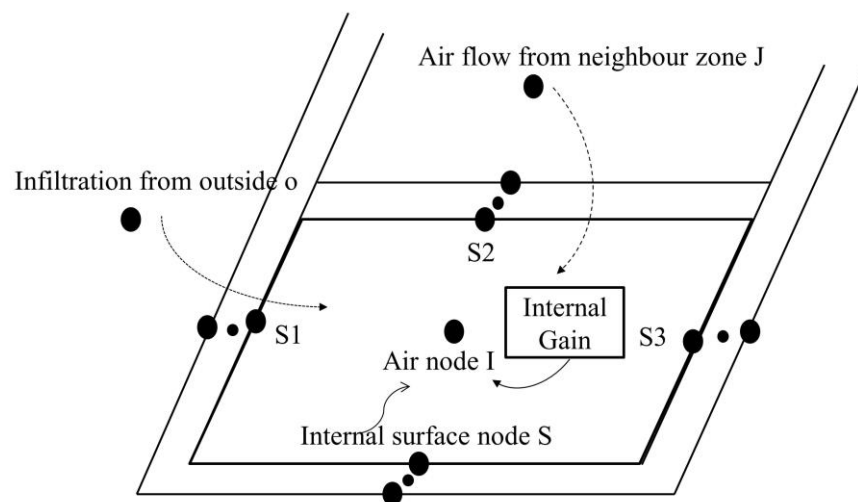
Figure 3.4: Energy balance at air node of zone.

51

As shown in the previous section the internal surface node and the air node exchange heat by convection, the convection term in the air node energy balance represents the total heat transfer from all surrounding surfaces to the zone air node. In addition, the energy balance of an air node considers the airflow from adjacent zones and outdoors and convective and latent sources of heat. The energy balance at the air node can be described as:

$$
\begin{aligned}
Storage\ of\ heat\ in\ CV \\
= net\ convection\ into\ CV + advection\ into\ CV\ by\ inter \\
- zone\ air\ flow + advection\ into\ CV\ by\ infiltration \\
+ source\ of\ heat\ within\ CV
\end{aligned}
$$

(3.5)

The energy balance equation governing these exchanges is of the form:

$$
\rho_i V_i c_i \frac{\partial \theta_i}{\partial t} = \sum_{j=1}^{n} q_{ij}
$$

(3.6)

Where, ρ_i; V_i; c_i; θ_i are the fluid volume average density [kg/m³], volume V [m³], average specific heat [J/kgk] and the average temperature [ºC] consecutively. They represent the thermal capacitance of the fluid volume. The right-hand side of the equation represents the summation of the energy fluxes [W] interacting with the control volume.

The final form of the energy balance equation at the air node after adding the explicit and implicit forms and dividing by the zone volume V_{zone}. The equation is arranged with the future time step on the left and the present to the right the final form of the mathematical equation is given as

$$\left[\frac{2 \cdot (\rho c_p)_I}{\Delta t} + \frac{\sum_{s=1}^{N} h_{c,s \to I}^{t+\Delta t} A_s}{V_{zone}} + \frac{\sum_{J=1}^{M} \dot{m}_{J \to I}^{t+\Delta t} c_p}{V_{zone}} + \frac{\dot{m}_{o \to I}^{t+\Delta t} c_p}{V_{zone}}\right] T_I^{t+\Delta t}$$

$$-\left[\frac{\sum_{s=1}^{N} h_{c,s \to I}^{t+\Delta t} A_s T_s^{t+\Delta t}}{V_{zone}}\right] - \left[\frac{\sum_{J=1}^{M} \dot{m}_{J \to I}^{t+\Delta t} c_p T_J^{t+\Delta t}}{V_{zone}}\right] - \left[\frac{\dot{m}_{o \to I}^{t+\Delta t} c_p T_o^{t+\Delta t}}{V_{zone}}\right]$$

$$- -\frac{q_{cas-conv,I}^{t+\Delta t}}{V_{zone}} - \frac{q_{plant,I}^{t+\Delta t}}{V_{zone}}$$

$$= \left[\frac{2 \cdot (\rho c_p)_I}{\Delta t} + \frac{\sum_{s=1}^{N} h_{c,s \to I}^{t} A_s}{V_{zone}} + \frac{\sum_{J=1}^{M} \dot{m}_{J \to I}^{t} c_p}{V_{zone}} + \frac{\dot{m}_{o \to I}^{t} c_p}{V_{zone}}\right] T_I^{t}$$

$$- \left[\frac{\sum_{s=1}^{N} h_{c,s \to I}^{t} A_s T_s^{t}}{V_{zone}}\right] - \left[\frac{\sum_{J=1}^{M} \dot{m}_{J \to I}^{t} c_p T_J^{t}}{V_{zone}}\right] - \left[\frac{\dot{m}_{o \to I}^{t+\Delta t} c_p T_o^{t}}{V_{zone}}\right]$$

$$- \frac{q_{cas-conv,I}^{t}}{V_{zone}} - \frac{q_{plant,I}^{t}}{V_{zone}}$$

$$(3.7)$$

where N is the number of bounding surfaces. A_s is the area of the surrounding surfaces [m2], and $h_{c,s \to I}^{t+\Delta t}$ the future time-step convective heat transfer coefficient, for surface S. M is the number of zones supplying air to the control volume. $\dot{m}_{J \to I}^{t+\Delta t}$ is the mass airflow from zone J to the zone I [kg/s] at the future time step and $\dot{m}_{o \to I}^{t+\Delta t}$ is, the infiltration rate from the outdoors [kg/s] for the future time step. $T_J^{t+\Delta t}$ and $T_o^{t+\Delta t}$ are, the future time step temperatures of the air node in zone J and the outdoor air, respectively.

And as defined previously, $q_{cas-conv,I}^{t+\Delta t}$ is the heat transferred from casual sources, but only the convective part goes directly to air node (such as occupants, lights, office equipment) at the future time. $q_{plant,I}^{t+\Delta t}$ represents a convective plant input to node I at the future time, that could be from a convective heater located within the room or from an air-based mechanical system delivering a supply of conditioned air to the room (Kelly, 1998; Beausoleil-Morrison, 2000; Negrao, 1995).

The above equation describes the one-dimensional heat flow associated with air volume ESP-r deals with three-dimensional heat and mass flow in the air volume using integrated computational fluid dynamic (CFD), this will be discussed in chapter 7.

3.4.5 Solution of finite volume equations

The previous sections show the energy balance equation using the control volume to different aspects of the building, similarly for other building components, the energy balance equation is defined for example for the plant, external fabric surface, window surface etc. All will have the same equation structure but with different coefficients. Each equation has expressions representing the future temperature of nodes in thermal contact and corresponding present time step expression.

After defining the set of energy balance equations of all nodes in the model, a large matrix of equations is formed. The equations are arranged in the form where the future time-row nodal temperatures, plant injections, source terms, and external environment excitations grouped to the left and the corresponding present time-row quantities to the right. The coefficients of the future time-step cannot be evaluated until the future timestep temperatures are evaluated for that the system of equation is not linear. In order to linearize this system of equations, the coefficients are evaluated one time-step in arrears. That means the future time coefficients are calculated using present temperatures, while present coefficients are calculated with the immediate past temperature. Similarly, the same technique has been adapted for the dynamic occupant heat load where the current environmental parameters are used to calculate the future internal heat loads. This technique of linearization is very efficient, especially for small time-step of less than one hour (Kelly, 1998; Beausoleil-Morrison, 2000; Negrao, 1995). Since the outdoor environmental parameters are predefined by the user and by using the linearization approach, this allows the future time-step data to be moved to the right side of the equation.

The set of zonal equations can be written in matrix form as:

$$AT_n^{t+\Delta t} = BT_n^t + C = Z \qquad (3.8)$$

Where A is the matrix holding the coefficients corresponds to the future time-step, B is the matrix holding the coefficients corresponds to the current time step, and matrix C contains known boundary interactions such as heat exchange with the sky and ground. $T_n^{t+\Delta t}$ and T_n^t are column matrices that hold the nodal temperatures and heat injections for the future and present time-steps respectively.

Since the right side of the equation (present time-step) are known it can be combined and represented as Z matrix.

The solution of the equation can be achieved by multiplying both sides by the inverse of A, to get the unknown temperatures and heat injections.

$$T_n^{t+\Delta t} = A^{-1}Z \qquad (3.9)$$

ESP-r employs a simultaneous direct solution approach based on matrix partitioning and Gaussian elimination. A full explanation and details are given in chapter 4 of Clarke (2002).

The solution method intends to deduce the boundary conditions to the rest of the model, and hence calculate the performance of the modelled zone taking into account the interaction of other factors such as the plant injection and the control system. The control system is very important for the processing of the equation sets. The control system in ESP-r based on sensing a specified nodal parameter, which is linked to an actuator which takes action appropriately at the same or different node. The objective of the actuator is to bring the sensed nodal parameter to its desired value.

3.5 Methodology and Linking approach

As stated earlier in chapter 2 (section 2.10) research gap, building simulation considers internal heat gains from people as fixed numbers based on a defined schedule. ESP-r also follows the same approach by allowing users to define internal heat gains from occupants as fixed ratio numbers distributed over an hourly-weakly schedule. It is also clear from section 3.4.4 how the internal heat gain from occupant has been represented in the air node energy balance equation. The equation showed that the user-defined heat flux is always used as a fixed ratio number. Since the amount of sensible/latent heat flux are not a fixed number and heavily dependent on the environmental conditions, and the human physiology. The dynamic behaviours of sensible and latent heat loads using three degrees of detailed human representation have been addressed.

3. 5.1 Occupant heat node system

As it has been stated before in this thesis the occupants are always described as fixed rate of heat load injected into the air node. Moreover, the occupant/human body has not been described in any building simulation tool as a thermal node having mass and interacting with the other nodes of the building system. In this section the author trying to propose an approach of describing the building occupant in more detail.

The occupant heat node inside the building simulation system can be described as:

$$Storage\ of\ heat\ in\ CV = net\ convection\ into\ CV + net\ radiation\ into\ CV + \\ net\ conduction\ into\ CV - net\ convection\ from\ CV - \\ net\ radiation\ from\ CV - net\ latent\ from\ CV + source\ of\ heat\ within\ CV$$

$$(3.10)$$

The human body exchange heat with air node in addition to all surrounding construction nodes. Radiative heating and cooling systems can be applied directly

as radiation into the control volume. The mathematical equation of the occupant node in the building is described in detail in chapter 5 using the two-node thermo-physiology model and chapter 6 when using the multi-segmented thermo-physiology model. Where all heat transfer between the human body and its surroundings has been addressed.

The dynamic occupant model requires some user-defined parameters as occupant presence, number of occupants, metabolic rate and clothing insulation. These data are user predefined and stored in the operation file. The operation file is hourly based, that means each defined hour has its inputs.

The dynamic occupant models are subroutines in the building-plant solver (bps) and will be called each time step from the routine which handles the internal heat gains exchange with the surrounding nodes in a zone. That is to assign the future occupant internal loads. It uses the present environmental parameters with the corresponding individual input parameters from the operation file which describe the occupant schedule in each zone.

The progress of improving the occupant representation in building simulation will be in three stages:

1.   **A simple responsive model predicting sensible and latent heat loads directly**

In this approach, the sensible and latent heat load from occupants has been modified to be calculated as a function of operative temperature and metabolic rate, instead of the fixed values. Figure 3.5, is a representation of this approach.
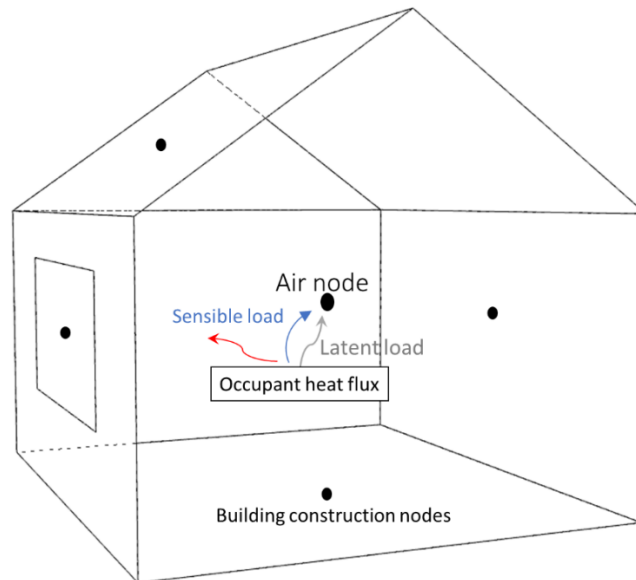
Figure 3.5 Representation of the interaction of the first approach the responsive internal occupant heat fluxes with the building.

2. A two-node physiology model

The two-nodes model is a physiological model account for sweating, shivering, and blood flow the core node is an internal node and interact with the skin node, both represent the human and the interaction with the building parts happens through the skin node. Clothing is also considered as an insulation layer. The energy balance equations for the two-node accounts for the heat exchange within a time step.

Figure 3.6 is a representation of this approach in the building. The model predicts heat fluxes and responds to the environmental changes; the prediction of the skin temperatures allows for comfort assessment.
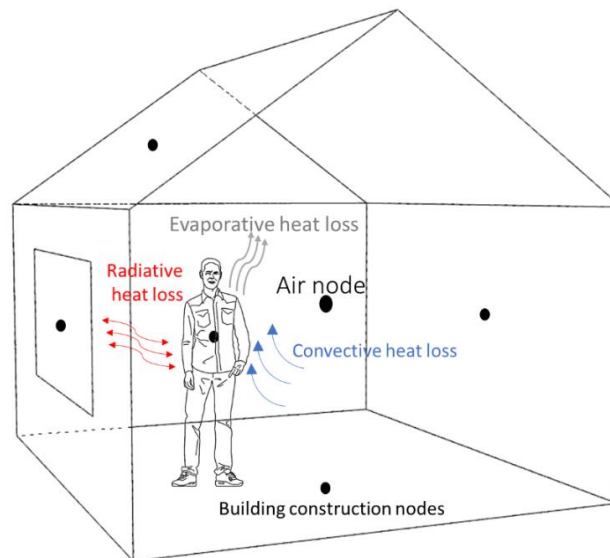
Figure 3.6 Representation of the interaction of the second approach the two-nodes model skin/core with the building.

3.   A multisegmented physiology model

As the name suggests a multisegmented occupant model, the model segments the human body into multiple body parts. Each segment of the body interacts thermally with the environment and the other body parts. Blood flow circulates in the body parts through arteries and veins where each represents an internal node. Energy balance equation is set for each node. The model predicts the temperature of the current node based on the previous time steps values and the heat exchanges within a defined time step and for that it is dynamic. Figure 3.7 is a representation of this approach.
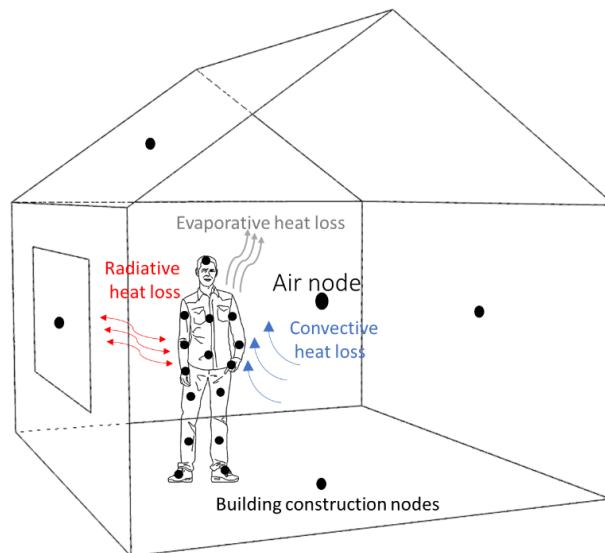
Figure 3.7 Representation of the interaction of the third detailed multi-segmented physiology model with the building.

In building simulation, the preceding approach multisegmented occupant will be interacting with one air node, the dry bulb temperature distribution over the body is not considered, also air velocity is considered as a fixed number. For that, to increase the level of details the multisegmented model has been applied to CFD in order to study detailed airflow inside the room and around the human body. Figure 3.8 is a representation of the segmented human thermal model inside a CFD domain.
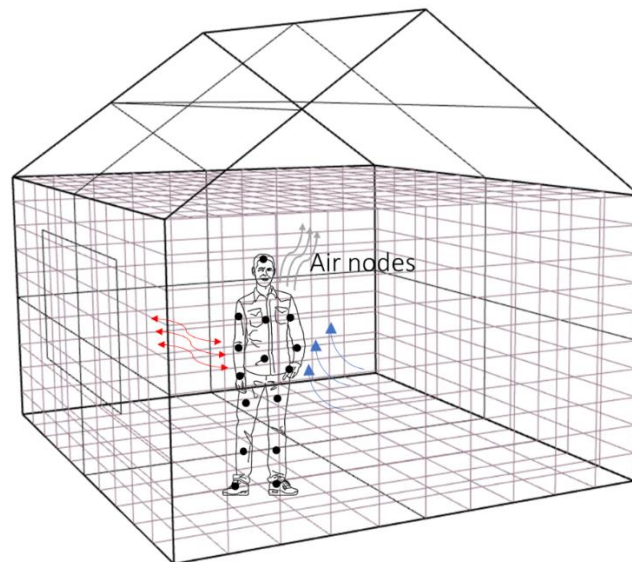
Figure 3.8 Representation of the interaction of the multisegmented model with CFD domain.

3.6 Summary

As ESP-r was the selected building simulation tools to improve the occupant heat loads integration in the energy balance system. This chapter has presented a brief description of the ESP-r's energy balance equations and especially the current state of occupant internal heat gain representation in this equation system. Later the proposed approach was discussed and different steps of implementation were defined. Where a dynamic internal heat gain from occupants is proposed in three approaches by using a simplified regression equation second by using a two-node thermo-physiological model and third by using a detailed multi-segment human thermo-physiology model in a detailed building simulation including CFD.

Chapter 4: Simple dynamic linear model of occupant thermal loads

4.1 Chapter overview

Most building simulation tools use a predefined fixed occupant sensible/latent heat load ratio. This approach simplifies the dynamic nature of heat losses from the human. This chapter will introduce the first responsive approach to modelling the occupant heat loads. This will be the first step toward the detailed dynamic occupant model. For this reason, two dynamic polynomial equations were developed based on published data for both sensible and latent heat loads emitted from building occupant under different operative temperature and for different activity level.

4.2 Internal heat gain from Occupant

When it comes to defining the occupant's heat loads in a building for energy performance simulation, there are some recommendations for the designers and building simulation tools users to follow. Recommendations were usually based on experimental data for people in thermal equilibrium, usually provided in CIBSE (2008), ASHRAE Standard 55-2013, also in ISO 7730 2005 and ISO 8996 (2004). The data provided describes the latent and sensible loads emitted from people at steady-state once they achieve thermal equilibrium for specific room temperature and metabolic rate. The designer needs to decide beforehand on the operative temperature and the metabolic rate with regard the selection of heat loads.

The common practice of defining the occupant heat loads for a building simulation in a predefined schedule does not allow for the dynamic nature of heat loads. The ratio of sensible to latent loads is fixed over the periods based on a design indoor temperature (ASHRAE_Standard 2015). This is not always the case, especially when it comes to design natural ventilated buildings where zone temperature is variable during the day. Moreover, new building designs allow a range of temperature variation to reduce energy consumption. Furthermore, the fixed occupant heat loads approach leads to prediction error, especially when allowing the temperature to vary in a specific range (draft in temperature) and high density occupied buildings.

As it has been discussed in the literature review chapter 2 section 2.2.2, occupant heat loads are affected by its environmental conditions. This approach will take into consideration the first two major parameters that affect the occupant heat loads which are the operative temperature and the metabolic rate. From a physiological point of view, thermal equilibrium will be achieved in a human body when the production of heat is equal to the heat losses (ISO 7730, 2005; Choudhury et al., 2011).

The body is working at maximum efficiency only at comfort condition so when the environmental temperature increases or decreases, heat losses will be changed and aim to achieve a new thermal equilibrium state, the body will try to acclimatise itself to the new conditions which might require a regulatory mechanism (shivering, sweating, vasomotor) to be functional. The normal body temperature for human beings is the 37°C with a tolerance of ±0.5 °C and any change in the body temperature will cause a variation in the heat losses or heat production which will bring the body temperature back to its normal value (DuBois, 1939). Heat production in a body is done through the metabolic activity/ oxidisation of foods. The metabolic heat production in a body is generated at different rates depending on the activity level. Consequently, at a higher activity level (high metabolic rate) the body will emit as much heat in which the latent heat loss plays a major role in order to keep the body temperature constant (Höppe, 1993).

Though the metabolic rate is the rate of heat emitted at equilibrium by the body per unit skin area, it has a unit of met where each 1met is equivalent to 58.2[W/m^2]. For a normal average body with 1.8 [m^2] body surface area, the heat generates for 1met will be around 104[W]. Even when the body is in an idle state, the body will be emitting around 100 [W]. Different factors could affect the basal metabolic rate value, like age and gender. For example, older people have a lower metabolic rate compared to young people because of less body muscle. Further, the metabolic rate will increase when the body weight and surface area increase (Höppe, 1993).

4.3 Methodology

To investigate the effect of making the occupant loads variable in the energy building simulation, we have made our first approach by changing the way heat gain from people was represented in ESP-r, by moving from defining the internal loads based on the design operative temperature and specified metabolic rate to specifying only the activity level and using the dynamically predicted operative temperature from the building simulation. With that changes the sensible and latent heat load ratio from occupant becomes a variable function of the dynamically predicted operative temperature in building simulation. Additionally, for the final load calculation, the number of people and gender/age were considered.

After analysing the available data of building occupant heat loads in the literature, the author was able to produce a simple regression model to predict the overall sensible and latent occupant heat loads refer to section 4.3.2.

As ASHRAE published some data of occupant loads for selected activity level and different room temperature (ASHRAE Fundamental, 2017). Humphreys et al. (1966) published a study of heat loads emitted from occupants of a survival shelter, in that study, they measured the skin temperature of the occupants and used a model to calculate the latent and sensible loads. The data of sensible and latent heat from people for the different metabolic rate and different surrounding

temperatures has been adopted. A regression model was developed for occupant heat gain as a function of the two variables metabolic rate and operative temperature.

4.3.1 Categorized metabolic rate model

A regression line is made for the three sets of data taken from (Humphreys et al., 1966). The three sets of data represent three activity levels 1 met (seated relaxed), 1.2 met (Sedentary activity) and 1.6 met (Standing, light activity). The regression lines are for both sensible and latent heat load from people wearing clothing insulation of 1 Clo and an air velocity of 0.2 m/s of an operative temperature ranged between 10 and 50°C (Humphreys et al., 1966). The fitted to data line has a polynomial equation of a second-degree function of zone operative temperature.

Figure 4.1 a,b and c shows the data lines of sensible and latent heat losses from the clothed person at three different activity levels. It can be seen from the graphs that the ratio between sensible and latent load from occupant heavily changed depending on the surrounding operative temperature. Sensible heat gain decreases and latent heat gain increases while the operative temperature increases. In addition, the latent heat gain increases when the metabolic rate increases, the aggregation point between the latent and sensible load happens at a lower operative temperature compared to a lower metabolic rate. Relative humidity inside a zone plays a major role on the evaporative latent load due to sweating evaporation where higher evaporation occurred during low relative humidity. On the other hand, during higher relative humidity an accumulation of sweating happens at the skin.
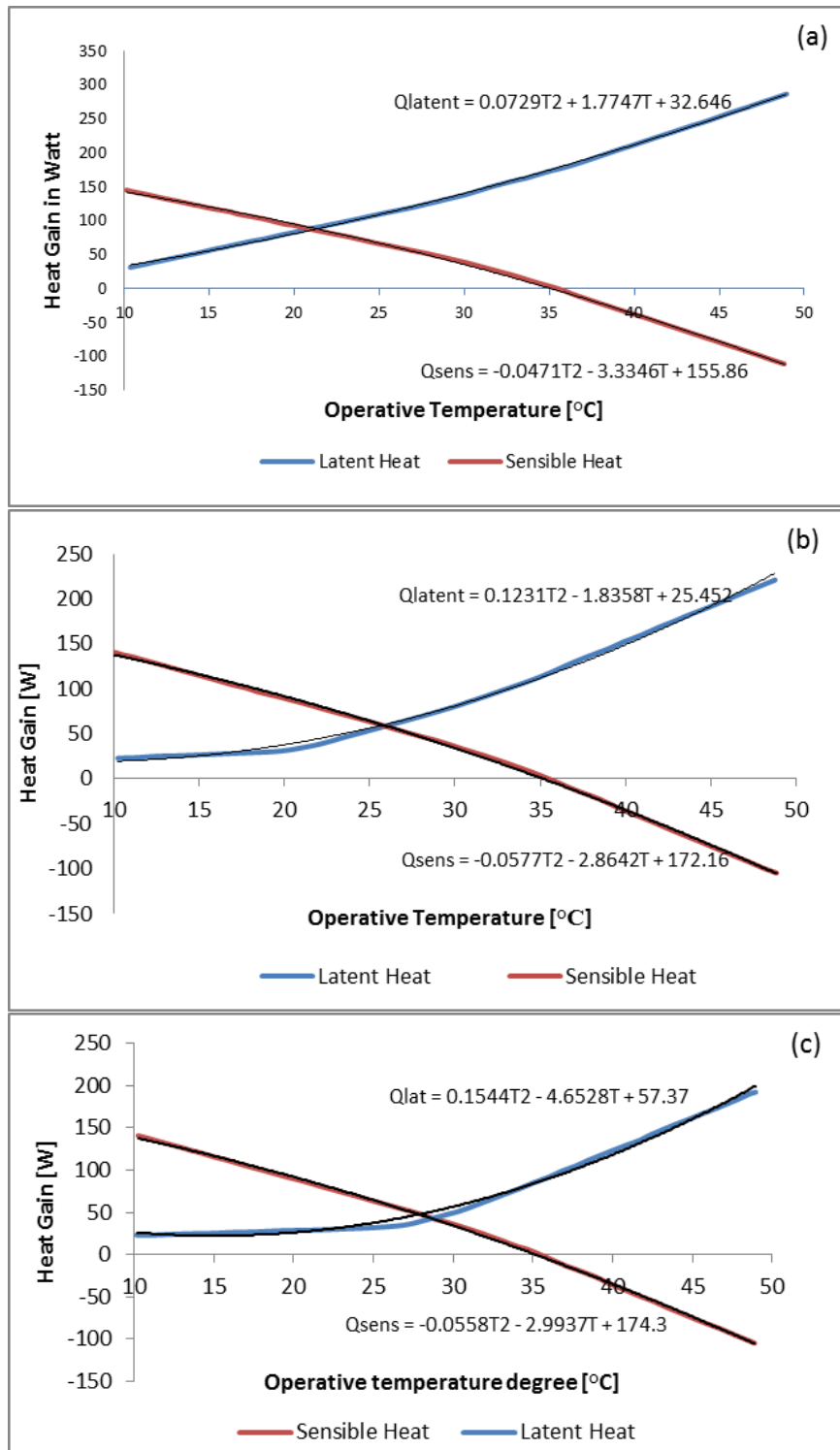
Figure 4.1: Sensible and latent heat dissipated from an average body weighted person at the activity level of a) 1.6 met b) 1.2 met c) 1.0 met.

The intersection point between the latent and sensible heat load from occupant varies for the different activity levels. At a higher activity level, skin temperature of the human body will rise, and more sweating will be generated at a lower temperature, which explains why the sensible and latent load will be equal at about 21°C for 1.6 met compared to 29 °C for the activity of 1 met. The equations below are the three set regression lines for the different activity levels.

$$\begin{cases} Q_{sens} = -0.0558T^2 - 2.9937T + 174.3 \\ Q_{lat} = 0.1544T^2 - 4.6528T + 57.37 \end{cases} \quad At\ 1\ met \quad (4.1)$$

$$\begin{cases} Q_{sens} = -0.0577T^2 - 2.8642T + 172.16 \\ Q_{lat} = 0.1231T^2 - 1.8358T + 25.452 \end{cases} \quad At\ 1.3\ met \quad (4.2)$$

$$\begin{cases} Q_{sens} = -0.0471T^2 - 3.3346T + 155.86 \\ Q_{lat} = 0.0729T^2 + 1.7747T + 32.646 \end{cases} \quad At\ 1.6\ met \quad (4.3)$$

For a wider range of activity levels, the degree of complexity to the polynomial equation was increased to calculate the sensible load from occupant with both variable temperature and metabolic rate.

4.3.2 Simple dynamic occupant heat load model

The three models are then evaluated, and more detailed regression model developed with both operative temperature and metabolic rate as variables by analysing more data.

More data were taken from the tables provided by (ASHRAE Standard 55-2013; Carrier, 1965). Figure 4.2 and 4.3 are the extraction of the data table taken from the references previously mentioned. The data represented the average adjusted metabolic rate function of room air dry-bulb temperature.

Temperature range provided by Carrier is between 21 and 28 °C values which considered suitable for the indoor thermal conditions. ASHRAE table and data provided are set to the room air temperature of 24 °C and they added that an increase of 3 °C to the room air temperature will result in a 20% increase in the latent load and a similar decrease in the sensible load.

After analysing all data and grouped based on temperature and metabolic rates a new combined model for latent and sensible are provided below equation 4.4 and 4.5.

DEGREE OF ACTIVITY	TYPICAL APPLICATION	Metabolic Rate (Adult Male) Btu/hr	Average Adjusted Metabolic Rate* Btu/hr	ROOM DRY-BULB TEMPERATURE									
				82 F Btu/hr		80 F Btu/hr		78 F Btu/hr		75 F But/hr		70 F Btu/hr	
				Sensible	Latent	Sensible	Latent	Sensible	Latent	Sensible	Latent	Sensible	Latent
Seated at rest	Theater, Grade School	390	350	175	175	195	155	210	140	230	120	260	90
Seated, very light work	High School	450	400	180	220	195	205	215	185	240	160	275	125
Office worker	Offices, Hotels, Apts., College	475	450	180	270	200	250	215	235	245	205	285	165
Standing, walking slowly	Dept., Retail, or Variety Store	550											
Walking, seated	Drug Store	550	500	180	320	200	300	220	280	255	245	290	210
Standing, walking slowly	Bank	550											
Sedentary work	Restaurant†	500	550	190	360	220	330	240	310	280	270	320	230
Light bench work	Factory, light work	800	750	190	560	220	530	245	505	295	455	365	385
Moderate dancing	Dance Hall	900	850	220	630	245	605	275	575	325	525	400	450
Walking, 3 mph	Factory, fairly heavy work	1000	1000	270	730	300	700	330	670	380	620	460	540
Heavy work	Bowling Alley‡ Factory	1500	1450	450	1000	465	985	485	965	525	925	605	845

TABLE 48-HEAT GAIN FROM PEOPLE

Figure 4.2: The heat gain from people. The table is taken from Carrier Air Conditioning Company book (1965).

Table 1   Representative Rates at Which Heat and Moisture Are Given Off by Human Beings in Different States of Activity

Degree of Activity	Location	Total Heat, W		Sensible Heat, W	Latent Heat, W	% Sensible Heat that is Radiant[b]	
		Adult Male	Adjusted, M/F[a]			Low V	High V
Seated at theater	Theater, matinee	115	95	65	30		
Seated at theater, night	Theater, night	115	105	70	35	60	27
Seated, very light work	Offices, hotels, apartments	130	115	70	45		
Moderately active office work	Offices, hotels, apartments	140	130	75	55		
Standing, light work; walking	Department store; retail store	160	130	75	55	58	38
Walking, standing	Drug store, bank	160	145	75	70		
Sedentary work	Restaurant[c]	145	160	80	80		
Light bench work	Factory	235	220	80	140		
Moderate dancing	Dance hall	265	250	90	160	49	35
Walking 4.8 km/h; light machine work	Factory	295	295	110	185		
Bowling[d]	Bowling alley	440	425	170	255		
Heavy work	Factory	440	425	170	255	54	19
Heavy machine work; lifting	Factory	470	470	185	285		
Athletics	Gymnasium	585	525	210	315		

Notes:
1. Tabulated values are based on 24°C room dry-bulb temperature. For 27°C room dry bulb, total heat remains the same, but sensible heat values should be decreased by approximately 20%, and latent heat values increased accordingly.
2. Also see Table 4, Chapter 9, for additional rates of metabolic heat generation.
3. All values are rounded to nearest 5 W.

[a] Adjusted heat gain is based on normal percentage of men, women, and children for the application listed, and assumes that gain from an adult female is 85% of that for an adult male, and gain from a child is 75% of that for an adult male.
[b] Values approximated from data in Table 6, Chapter 9, where V is air velocity with limits shown in that table.
[c] Adjusted heat gain includes 18 W for food per individual (9 W sensible and 9 W latent).
[d] Figure one person per alley actually bowling, and all others as sitting (117 W) or standing or walking slowly (231 W).

Figure 4.3: Heat and moisture emitted by people for different activity taken from ASHRAE Standard 55 (2017).

Sensible heat load

$$= 198.42617 - 3.80901T - 0.05419T^2 - 0.42472Met$$
$$+ \ 0.00171Met^2 + 0.01287TMet - 0.00004TMet^2$$
$$+ 0.00002MetT^2 - \ 3.8516 \times 10^{-7} \ Met^2T^2$$

$$(4.4)$$

Latent Heat load

$$= 227.89011 - 14.95202T + 0.24884T^2 - \ 2.56734Met$$
$$+ \ 0.00715Met^2 + \ 0.132TMet - \ 0.00017TMet^2$$
$$- \ 0.00107MetT^2$$

$$(4.5)$$

The model shown in equations 4.4 and 4.5 is of the second degree with two variables dependent on the metabolic rate and operative temperature. The operative temperature is a dynamic parameter predicted and updated by the building simulation tool ESP-r and the metabolic rate is an input provided by the designer based on a schedule.

This model is valid for occupant wearing clothing insulation of 1 Clo and air velocity surrounding the occupant of 0.2 [m/s].

Energy plus has previously made a similar attempt modelling a variable occupant load. Their model based only on the data taken from the Carrier Air conditioning book (Carrier, 1965), The model considers occupant has already been in steady-state thermal condition. For that, they provide a model to describe the sensible heat load as a function of operative temperature and metabolic rate. Then, the latent heat load is simply the difference between the metabolic rate and the predicted sensible load. By doing that, they neglect any possibility of heat storage in the body saying that all metabolic heat generated is dissipated to the environment. The model does not consider any none steady-state situation.

Although the metabolic rate is a constant input in this model, but by providing two separate models for sensible and latent heat loads it got a slightly flexible result where the sum of the heat loss is not always equal to the metabolic rate. It showed more reasonable results compared to what it is achieved by considering all heat generated is lost to the environment.

4.3.3 Gender and Age differentiation

The heat dissipated from the people can be different from one to another due to the differences in body surface areas and weight.

In this approach, the age and gender have been considered as input for the model dividing the occupants into three category adult female, adult male, and children. In this case, the amount of heat load transferred from a female will be equal to 85% of that emitted from an adult male, and children are 75% of an adult male. As an approximation to what it is stated in ASHRAE standard 55 2017.

4.3.4 Model integration in ESP-r

Figure 4.4 shows a schematic flow chart for the integrated dynamic occupant heat load model in ESP-r. The chart shows all the input required for the model to predict the total sensible and latent heat loads at each time-step. The predicted

values are considered as part of the internal heat load for bps to predict the new internal environmental conditions.

4.3.5 ESP-r interface changes

The implementation of the new model in ESP-r required changes to the casual gain algorithm and the user interface. The following functionality was added.

Our model required new inputs to get the total occupant heat loads in ESP-r. The new model requires the metabolic rate, the metabolic rate is given based on an hourly schedule.
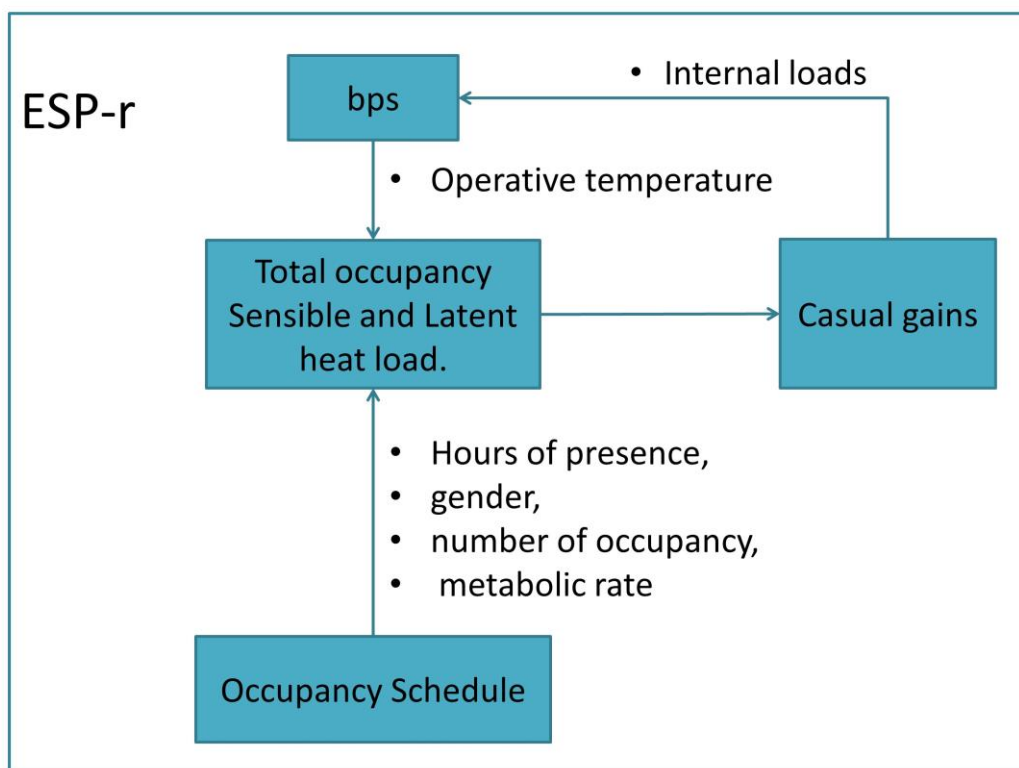
Figure 4.4: Flow chart shows the model integrated into ESP-r inputs and outputs. schedule.

The metabolic rate, describe the activity level of the occupant during the specific hours. ISO 8996 (2004) describes the ways of calculating it. The standard provided different levels of accuracy for estimating metabolic rate each level has different methods to characterise the mean workload for a given occupation. The

first level is screening and it is based on selecting the average metabolic rates based on tables provided. The second level is the observation, it reduces the error by increasing accuracy, but require more details of the occupational activity, it is based on observation of the body segments involved, the workload of the body segment, the body posture and work speed. Further, it counts for the rest duration during the period of work cycles (ISO 8996, 2004).

Once the schedule for the activity level is defined, the model requires also the number of people and gender. The number of people is set to be a real number so it can count for occupants who spent a partial time of an hour, for example, a room has one occupant for one full hour and another occupant for 15 min the number occupant would be 1.25 occupants.

While defining the type of casual gains in ESP-r the new feature of using dynamic people needs to be selected see figure 4.5. The selected feature allows the user to define the occupant casual gain based on metabolic rate and number occupant approach by using the developed dynamic model.

After selecting the needed number of periods for a day, the user will be asked to define:

    1.The number of men, number of women and number of children.

    2.The average metabolic rate for that period.

The final operation file will look as in figure 4.6 an example of an operation file.

```
Available types

a -            not yet defined W & W/m2
b people    basic occupant W & m2/p
c lighting basic lighting W & W/m2
d equipment basic small power W & W/m2
e other     non-specific gains W & W/m2
f dynamicpeople nb people & metabolic
g net_utilities as legacy icgtyp = 5
h ALOtherElectric H3K other appliances
i ALStoveNG H3K natural gas stoves
j ALStoveElectric H3K electrical stoves
k ALDryer H3K clothes dryers

--------------------------
* default is option `b`
? help
- exit this menu
```

Figure 4.5: Menu of internal gain type selection in ESP-r where (f) is the new function type.

```
17 *casual
18 no casual gain notes (yet)
19 # casual user-label type-key-word slot attributes
20 *type Occupant      dynamicpeople    1  1  0
21 *type Light          lighting         2  0  0
22 *type Equipment      equipment        3  0  0
23 *end_type
24     12   # number of casual gains in day type: weekdays
25 # slot, period, sensible, latent, rad_frac, conv_frac
26 # slot, period, nb men, nb women, nb child, metabolic clo, air vel, rad_frac, conv_frac
27   1,   0,   7,  0.00,  0.00,  0.00,  1.40,  0.00,  0.00,  0.600,  0.400
28   1,   7,   8,  1.00,  0.50,  0.00,  1.40,  0.00,  0.00,  0.600,  0.400
29   1,   8,   9,  0.00,  1.00,  0.00,  1.40,  0.00,  0.00,  0.600,  0.400
30   1,   9,  14,  0.50,  1.00,  0.00,  1.40,  0.00,  0.00,  0.600,  0.400
31   1,  14,  17,  1.00,  1.00,  0.00,  1.40,  0.00,  0.00,  0.600,  0.400
32   1,  17,  24,  0.00,  0.00,  0.00,  1.40,  0.00,  0.00,  0.600,  0.400
33  -2,   0,   8,      0.0,      0.0,  0.300,  0.700
34  -2,   8,  12,     10.0,      0.0,  0.300,  0.700
35  -2,  18,  24,      0.0,      0.0,  0.300,  0.700
36  -3,   0,   8,      0.0,      0.0,  0.400,  0.600
37  -3,   8,  18,      5.0,      0.0,  0.400,  0.600
38  -3,  18,  24,      0.0,      0.0,  0.400,  0.600
```

Figure 4.6: operation file including the new inputs required for the new approach.

4.3.6 Final model evaluation

The model can predict both sensible and latent heat loads emitted from an occupant at the different metabolic rate and a dynamically predicted operative temperature. Figure 4.7 a,b shows the predicted occupant heat loads for two

different metabolic rate of 1.1 and 1.6 met for a wide range of temperature [15 to 30°C] (a) and [18 to 25°C] (b). In naturally ventilated building it can be possible to give a wide range of indoor temperature aiming to reduce energy consumption. Based on the adaptive comfort model developed by De Dear et al. (2001) the acceptable indoor temperature in a naturally ventilated building can be between 17 to 31°C. The variation of occupant heat loads prediction is shown in figure 8. The graphs showed a decrease in sensible heat load and an increase in the latent heat load of around 40 [W] for an increase of 7 °C in the operative temperature.
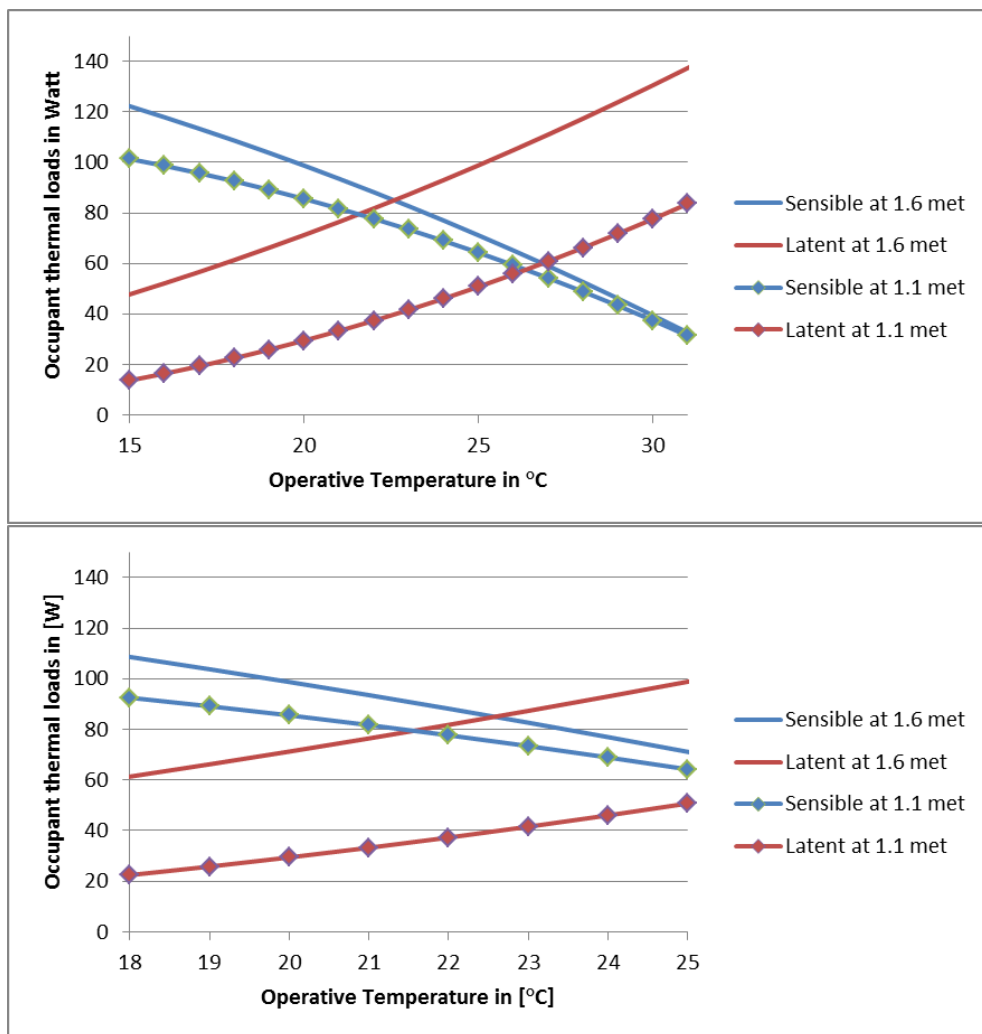
Figure 4.7: a,b sensible and latent heat load emitted from a person with 1.1 and 1.6 met at different operative temperature.

74
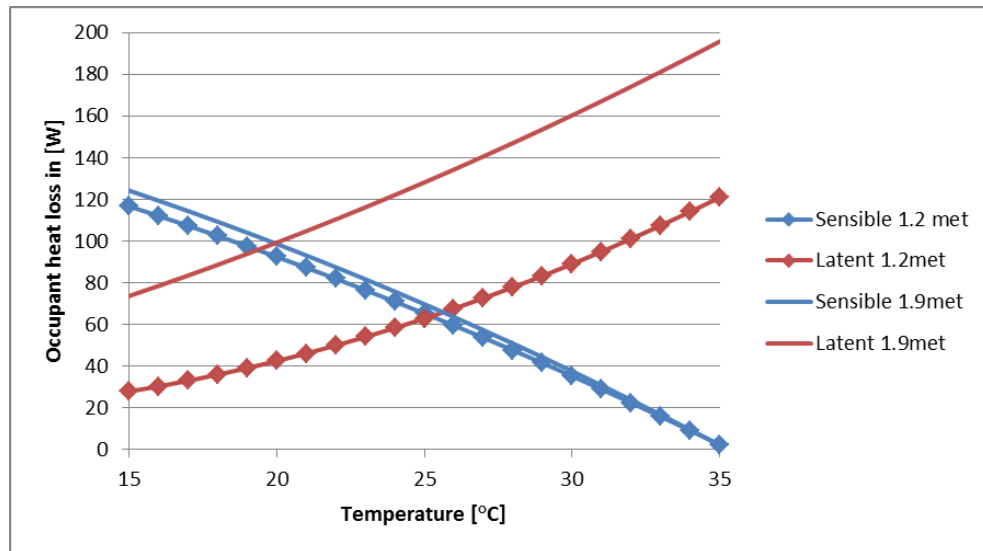
Figure 4.8: sensible and latent heat load emitted from a person with 1.2 and 1.9 met at different operative temperature.

Another set of model prediction sensible and latent heat emitted from a person with a metabolic rate of 1.2 and 1.9 met are presented in figure 4.8. Similar to the previous case sensible and latent heat loss reacts with respect to the operative temperature. A decrease in sensible heat loss accompanies with an increase latent when the temperature increases. The other fact is that increasing the metabolic rate does increase the latent heat loss considerably, conversely, the sensible heat loss has a very small increase. That can be explained as when metabolic rate increases, skin temperature also increases to a certain point since the parameters in the environment are constant as air temperature and air velocity the sensible heat loss stay nearly the same compared with a lower metabolic rate case. The body increases the sweating and consequently the latent heat losses.

4.4 Test case and simulation results

In this section, the effect of using a dynamic occupant heat load in building simulation is presented. For that, the three approaches of representing occupant heat load in ESP-r has been compared. The building model used in this section is

a predefined model from the examples model of ESP-r, the selected building model has been modified to account for the dynamic occupant load.

Internal load input using a fixed amount of heat, representing the occupant heat load can lead to some calculation deficiency in the calculation of building loads. In this example, the fixed input of occupant heat loads inside a domain for the same schedule has been compared with the dynamic approach also together with the model provided by the Energy plus.
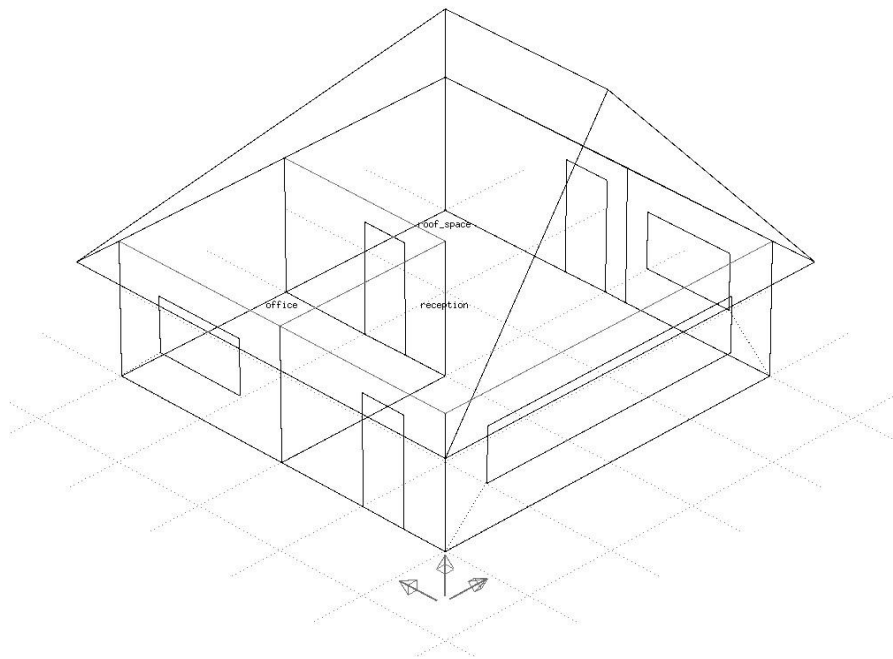
Figure 4.9: Zone geometry representation.

4.4.1 Model description

A basic and simple model has been selected from the example models provided with ESP-r. The basic model is constituted of three zones of two rooms and a roof. A small office room of 16m^2 floor area and floor dimension: 4m width x 4m depth x 2.8m height and a second zone represent the reception and it has a base area of 48 m^2 figure 4.9 shows the geometry of the model considered. The third zone represents the roof on top of the two previously described zones.

All the construction materials used in this model is briefly described in table 4.1.

Table 4.1: model construction and thermal specification.

Construction types	U value [W/m² K]
External walls	0.4
Internal walls (partition)	2.1
Floor	0.9
Ceiling	0.3
Door	3.3
Windows double glazed	2.8
Roof	2.1

Table 4.2: Occupancy internal gain schedule for Office zone

Time of day	Sensible heat load [W]	Latent heat load [W]
0:00 to 7:00	0.0	0.0
7:00 to 12:00	180	100
12:00 to 17:00	90	50
17:00 to 24:00	0.0	0.0

For such a model, the designer will probably choose a basic office schedule with the occupant heat load input presented in table 4.2 for the office zone and table 4.3 for the reception zone.

Table 4.3: Occupancy internal gain schedule for Reception.

Time of day	Sensible heat load [W]	Latent heat load [W]
0:00 to 7:00	0.0	0.0
7:00 to 12:00	360	200
12:00 to 17:00	180	100
17:00 to 24:00	0.0	0.0

On the other hand, for comparing with the dynamic model, the nearest approximated metabolic rate has to be selected. For that, the metabolic rate 1.4 met has been chosen as it represents a total heat at a steady state of 145 [W]. Table 4.4 below shows the input data required for the dynamic model for both zones office and reception.

A basic controller with a very wide dead band has been set, where heating starts at 16°C and cooling at 35°C from 7:00 to 17:00 hours. The weather file of Glasgow, UK in ESP-r has been used.

Table 4.4: Occupancy schedule for the dynamic model.

	Office zone		Reception zone	
Time of day	Number of occupants	Metabolic rate	Number of occupants	Metabolic rate
0:00 - 7:00	0	0.0	-	0.0
7:00 - 12:00	2	1.4	4	1.4
12:00 - 17:00	1	1.4	2	1.4
17:00 - 24:00	0	0.0	-	0.0

A repeated simulation with the three-occupant model approach has been conducted. The simulation period selected was one year with 15 min time step. But the results have been assessed in the following section choosing three different typical days of the year.

First, a typical winter day has been presented to show how is the prediction of sensible and latent loads was during the day. From the results in figure 4.10 it can be seen that the sensible heat prediction is higher compared to the fixed one and the latent heat load were lower, the great difference in these results was because of the low temperature where it reached 16 °C it is considered low for an indoor environment and it may lead to an uncomfortable environment but it serves the purpose of this comparison.

Figure 4.11 presents the occupant loads prediction using the dynamic models for a zone temperature around 21°C. At this temperature, the occupant heat load prediction was almost at the same level as the fixed heat load values.

To see the model prediction in a warm environment, figure 4.12 shows the dynamic heat load predictions for a summer day where the temperature goes up to a level of 31 °C. The graph shows how the predictive dynamic latent load exceeds the fixed latent load, and the sensible load was around 50 [W] lower than the fixed sensible load for one person when the operative temperature reached 30 °C.

From above, it can be evidently seen how the indoor thermal environment may influence the amount of the occupant heat load in building simulation. Where the distribution of sensible and latent load varies when the operative temperature deviates from the neutral or the design temperature.

The dynamic model predicts a higher sensible and lower latent values compared to the fixed ratio input at lower temperature and contrarily, a higher latent and lower sensible values at a higher temperature. That variation is stated in ASHRAE fundamental table (ASHRAE Fundamental 2017) and designers were given instructions on how to select the occupant load based on the design temperature,

but that was not fully studied and implemented to be dynamically calculated in a building simulation tool.
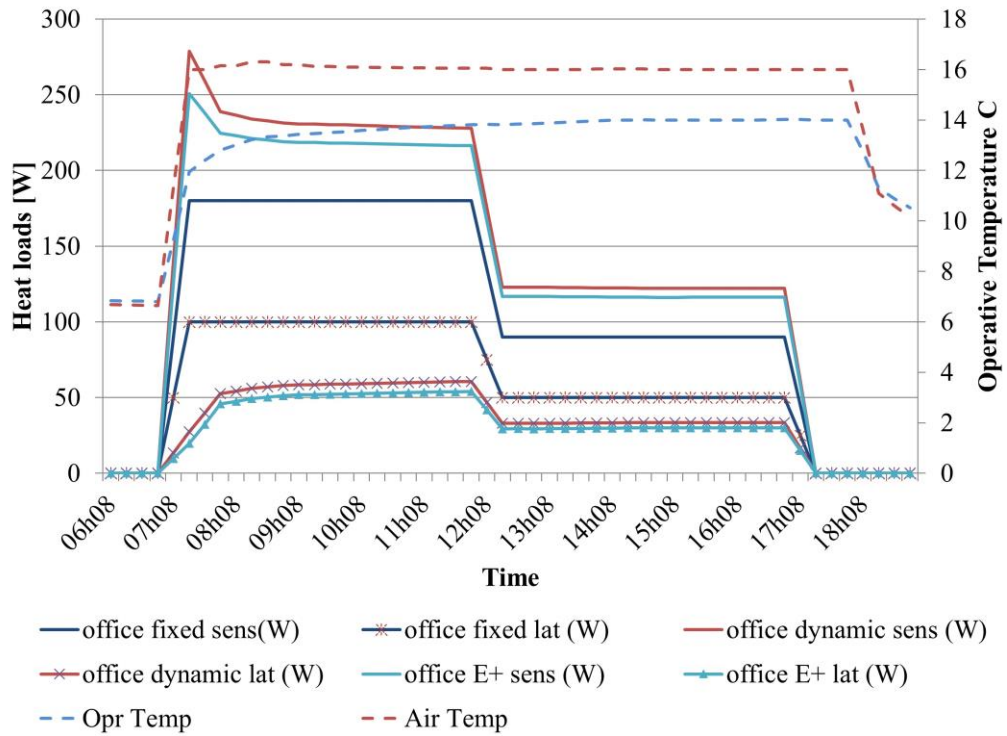
Figure 4.10: Sensible and latent heat loads predicted from the different models during one day in Winter.
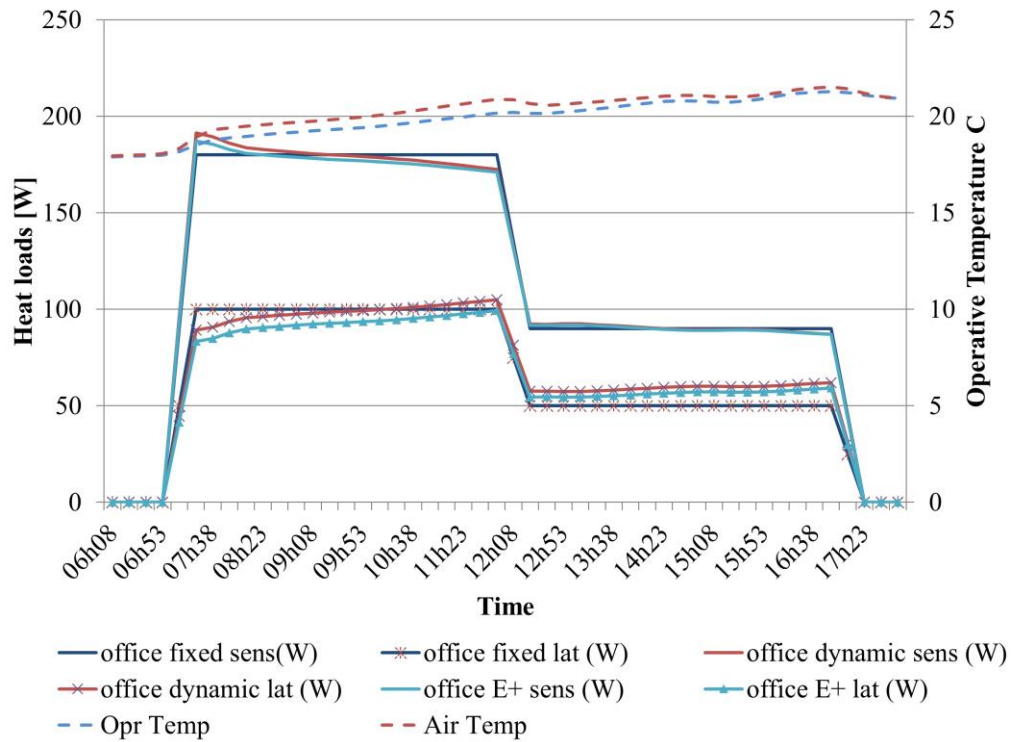
Figure 4.11: Sensible and latent heat loads predicted from the different models during one day of a Spring, moderate temperature.
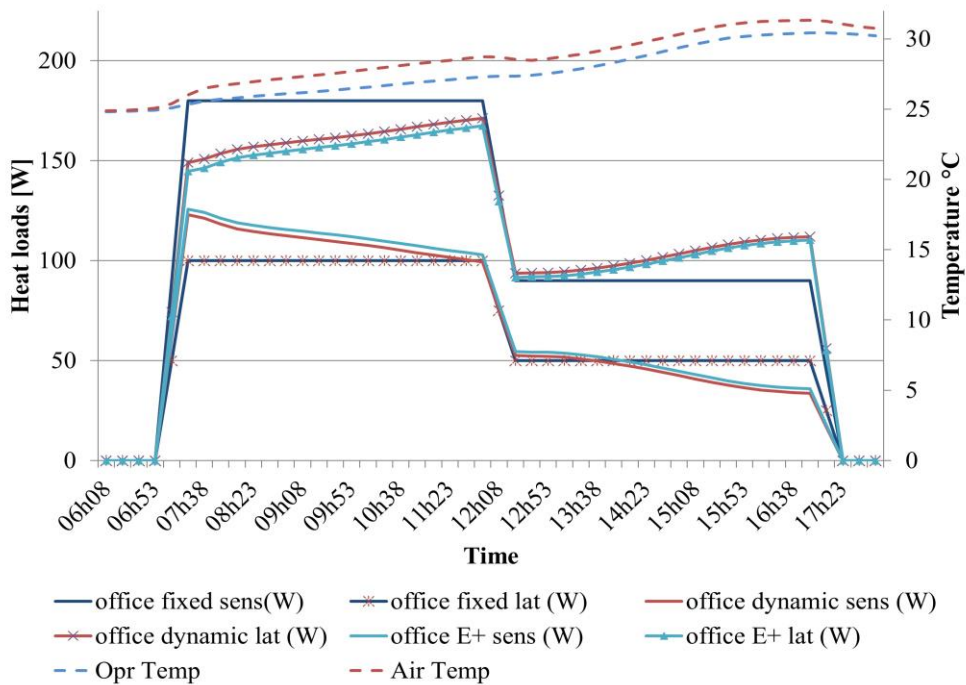
Figure 4.12: Sensible and latent heat loads predicted from the different models during one day in Summer.

How does this approach of building occupant heat loads influence the prediction of building performance?

Continuing the analysis of results from the same model, for the cold case and since the zone is controlled to be heated to a minimum temperature of 16°C. The heating loads required in this case has been compared. Figure 4.13 shows the heating load required to raise the office zone temperature to 16°C. As the predicted (dynamic) sensible load is higher than the fixed one. For both zones, reception and office, the reduction in heating load was around 4.3 [kWh] for that day during the working hours. Figure 4.14 shows the relative humidity for the different modelling approach. As it is expected with lower latent heat load prediction from the dynamic model the zone will have lower relative humidity compared to the fixed approach.

For the warm environment, in figure 4.15, the results show that temperature prediction of the office zone was slightly lower (around 0.95 °C) using the dynamic model and that was because the prediction of the sensible heat load was lower compared to the fixed load. Contrarily, relative humidity was higher as the dynamic prediction of the latent load was higher. Figure 4.16 shows the relative humidity in the office zone of the warm day, for the three different

Figure 4.13: Heating load prediction using the different model during a cold day.
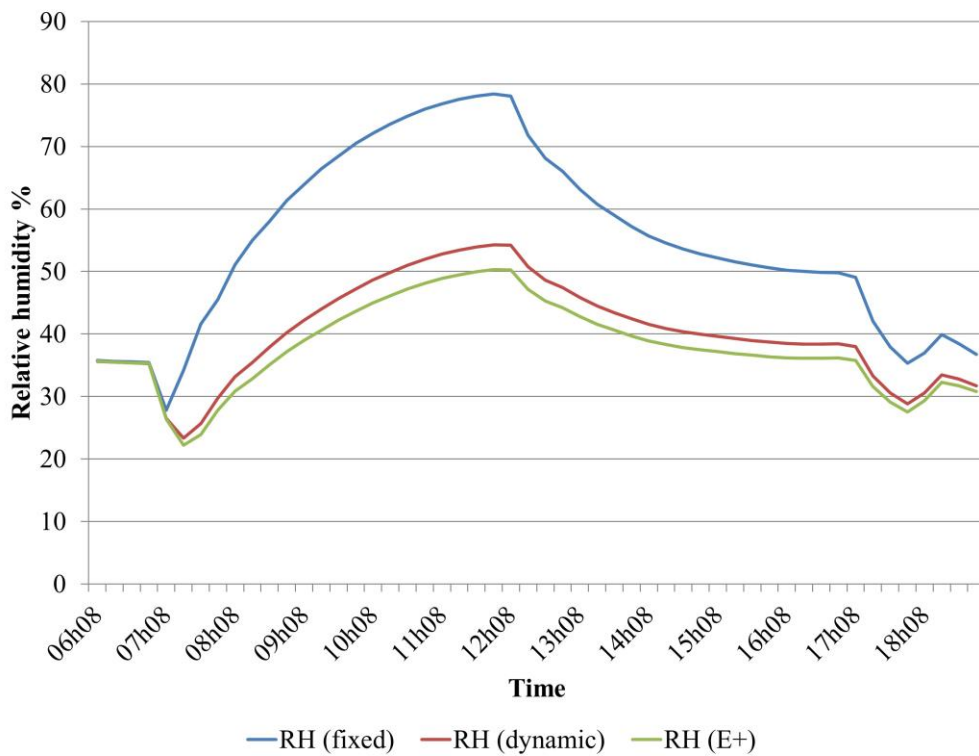
Figure 4.14: Relative humidity prediction using the different model during a cold day.
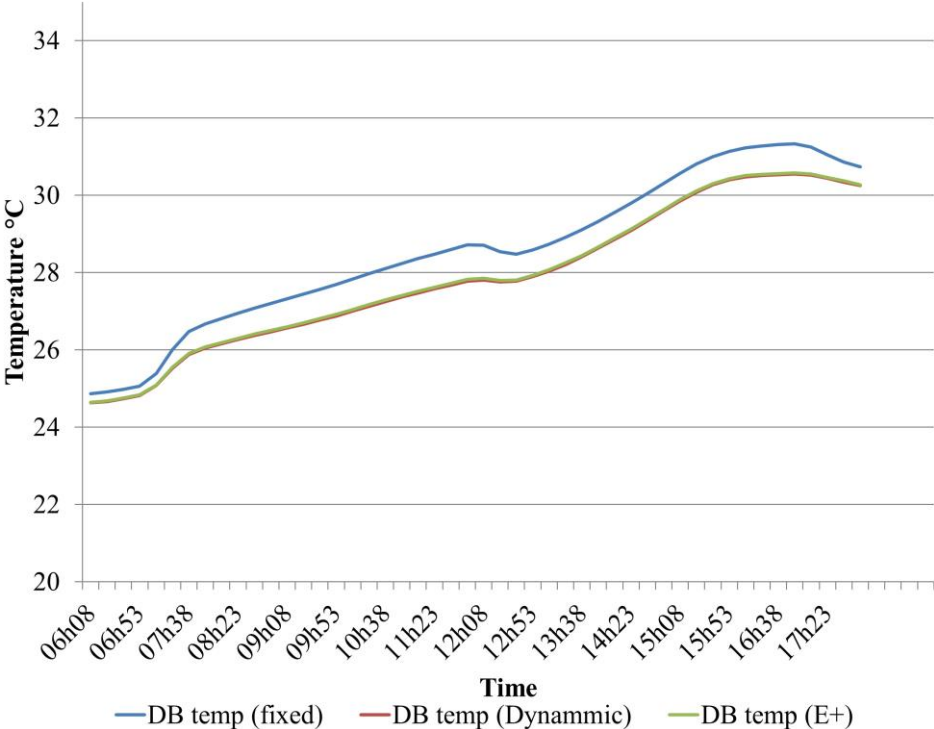
Figure 4.15: room air temperature prediction from the different models during a hot summer day.
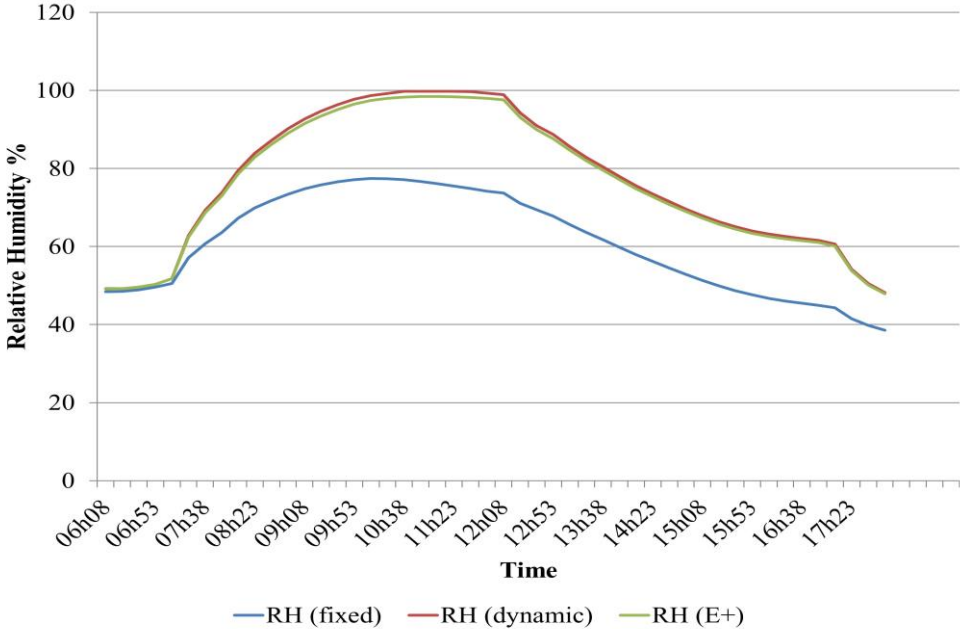
Figure 4.16: relative humidity prediction from the three models during a hot summer day.

What is the difference between the developed dynamic occupant heat load model and the Energy plus model?

As it has been mentioned previously that energy plus model predicts the sensible heat load based on the operative temperature and metabolic rate considering the occupant is always a steady-state, the latent load was calculated from the difference of the metabolic rate and the predicted sensible load. In the dynamic model approach presented in this chapter, two distinct components were used: one to predict the sensible load and a second one to predict the latent load.

Allowing both sensible and latent load to be a function of metabolic rate and operative temperature gives a freely fluctuating total heat emission (sum of sensible and latent loads). Figure 4.18 shows that in a cold environment the sum of sensible and latent heat load predicted using the dynamic model was slightly higher compared to the given metabolic rate with a maximum difference of 20[W]. As the Energy Plus model of occupant total heat losses is always equal to the metabolic rate. *The question that could be asked here if whether that variation in the total load injected to the zone is realistic?* The answer to this question is that in reality, the heat losses from the human body is not always equal to its metabolic rate, In the case when the heat losses are less than the metabolic rate that means the heat storage in the human body is higher than zero and consequently, the skin and core temperature are increasing, on the other hand, In the case when heat losses are greater then the metabolic rate skin and core temperature decreases. Figure 4.17 and 4.18, shows how our model predicts the total sensible and latent heat load for a given metabolic rate and a wide range of operative temperature 4.17 and the Energy Plus prediction 4.18. The differences in the total heat losses can be also seen in figure 4.19 taken from (Viessman, 1966), the figure shows in compliance to the dynamic model developed here that heat losses vary from the metabolic rate at high and low temperature and only at neutral temperature is equal to metabolic rate when storage is zero. In general comparing the dynamic model and the energy plus equation both showed similar results of building

performance which gives the model credibility, in addition, comparing the dynamic model to the fixed ratio results gives a clear statement that a fixed ratio can easily lead to roughly estimate the internal heat load from the occupant.
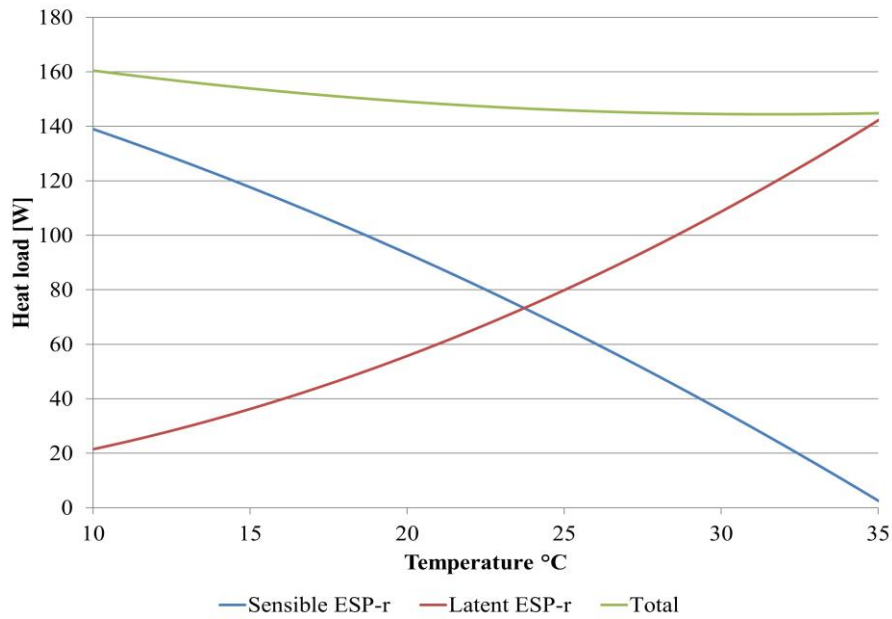
Figure 4.17: the heat load prediction from the dynamic model.
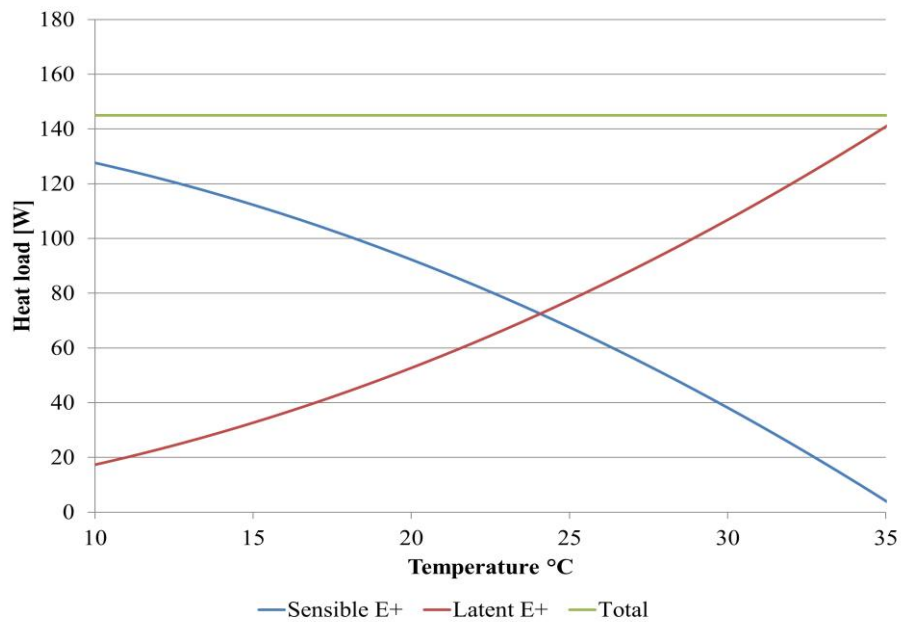
Figure 4.18: The heat load prediction from the Energy+ model.
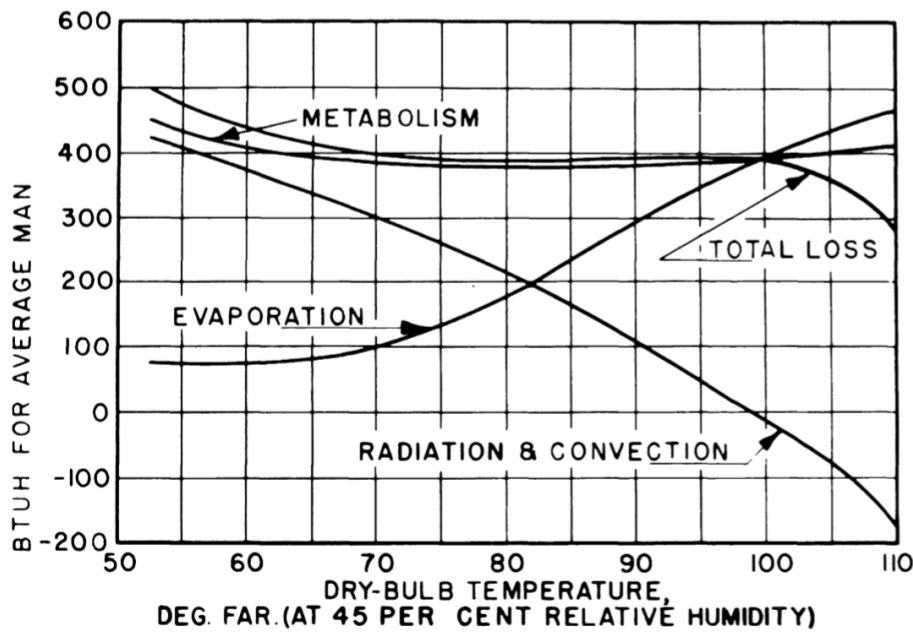
Figure 4.19: heat loss from a human body at rest taken from (Viessman, 1966).

4.5 Conclusion

The use of a dynamic human thermal model will be essential in the case of having a variable indoor temperature.

If there is temperature fluctuation inside a zone a variable occupant heat load demonstrated to be useful as results in this chapter showed. Where there is a significant difference between the results using static (profile) models and environment-responsive models on the building simulation results.
The approach described in this chapter presented a method of calculating the sensible and latent heat ratio from occupant based on the dynamically predicted operative temperature. Nevertheless, this approach did not consider the effect of the surrounding relative humidity, air velocity and even the clothing insulation.

For that, the need for a physiology model can be potential, not only for the internal load calculation, but also for studying and predicting the thermal state of the occupants, and the comfort level. For this reason, in the following chapter, the development, the use and the integration of physiology two-node model in ESP-r is discussed.

Chapter 5: Two-node occupant model integration with ESP-r

5.1 Chapter overview

Figure 5.1 shows the building energy flow path used from Clarke (2002), the figure shows the occupant as part of the energy flow as one of the internal heat loads. In the previous chapter, the effect of the dynamic calculation of building occupant thermal loads inside a zone by using a dynamic sensible and latent load prediction model has been presented. By having some user inputs like the metabolic rate, the number of occupants and the gender, along with the operative temperature as a dynamic input from the building simulation. However, the occupants were not represented as a mass or as a node in ESP-r's thermal balances. In this chapter, a two-node physiology model (core, skin) based on the Gagge model is developed and implemented in ESP-r (Gagge et al., 1973; Pennes, 1948; Foda et al., 2011; Shih et al., 2007) to increase the detail of occupant representation in the building. In addition, the use of dynamic clothing insulation model has been presented.
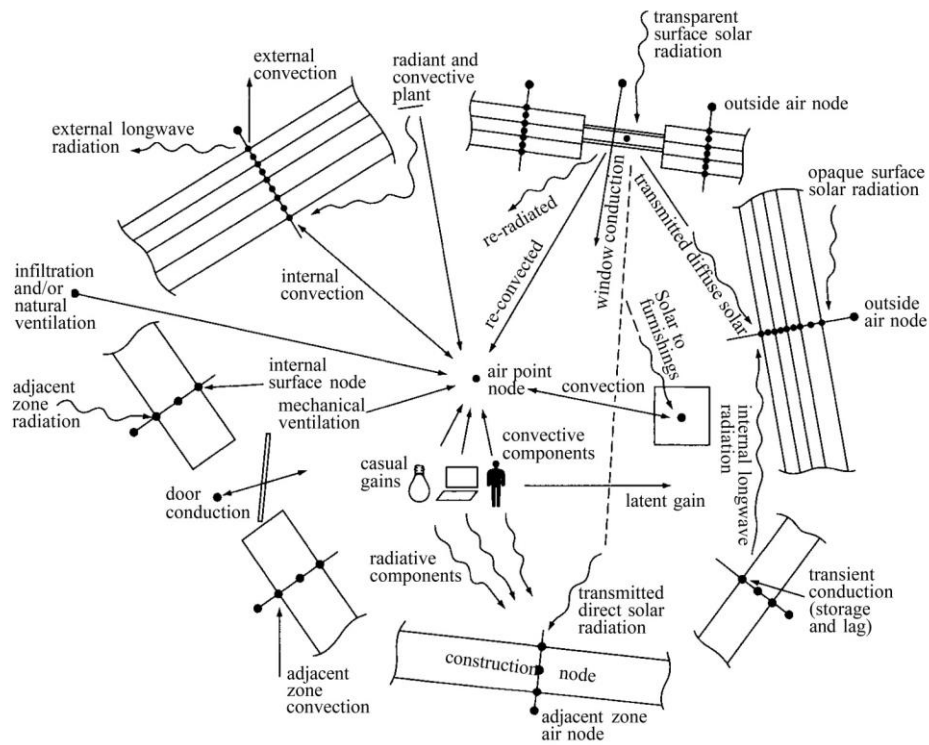
Figure 5.1: energy flow path in building (Clarke, 2002).

5.2 Two-node model Description

This section will discuss the heat energy balance equation describing the heat losses occurs between the skin layer and the environment and the core layer for the heat transfer between the core and the skin.
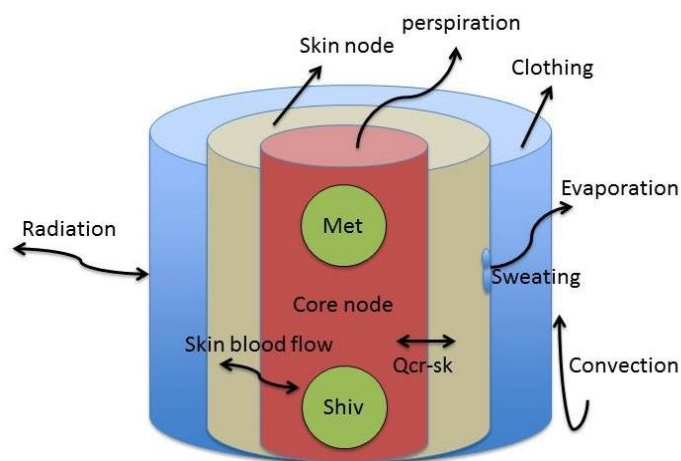
Figure 5.2: two-node model schematic representations of thermal interaction.

As it has been already discussed, for the human body core temperature to remain at a constant level, there should be a good energy balance between heat produced and the heat loss.

The general energy balance equation is defined as below:

$$S = M + W \pm R \pm C \pm K - E - RES \qquad (5.1)$$

Where S is the heat storage and it is equal to the sum of M the metabolic rate a positive number, W the external work, R the radiative heat exchange, C the convective heat exchange, K the conductive heat exchange, in addition to E the evaporative heat loss and the respiration heat exchange RES. W, R, C and K can be either heat loss or heat gain.

At the time when S is zero the energy balance is reached. Figure 5.2 shows the different means of heat transfer that are considered in the two-node model. The core and skin are the two nodes where metabolic heat generated in the core level also the respiration part a small amount of heat transfer from the core to the environment directly. Heat transfer to the skin node from the core throughout the conduction and blood flow. Based on the clothing insulation level the heat transfers from the skin to the environment by convection, radiation and evaporation.

5.2.1 Mathematical equations

The thermoregulatory model comprises a core and skin volume. Each of which can be subjected to energy and mass balance. The model accounts for the variation in the occupant surrounding environmental condition (zone temperature and relative humidity), occupant activity rate and clothing level.

The energy balance equation used to calculate the body core temperature is as follows.

$$C_{cr} \frac{dT_{cr}}{dt} = M_{cr} + M_{s\square iv} - W - Q_{res} - Q_{cr-sk} + \dot{m}_{bl,sk} c_{bl}(T_{sk} - T_{cr}) \quad (5.2)$$

The equation to calculate the skin temperature is:

$$C_{sk}\frac{dT_{sk}}{dt} = Q_{cr-sk} - A_{sk}\left[h_c(T_{sk} - T_{amb}) + h_r\left(T_{sk} - \overline{T}_{amb_{mrt}}\right) + h_e(P_{sk} - P_{amb})\right]$$
$$+\dot{m}_{bl,sk}c_p(T_{cr} - T_{sk})$$

$$(5.3)$$

Where, T_{cr}, T_{sk} are the core and skin temperature. C_{cr}, C_{sk} are the core and skin thermal capacitance of body. M_{cr} and M_{sk} are the basal core and skin metabolic rate. M_{Shiver} is the thermoregulatory shivering metabolic rate. W is the mechanical work done by the body. Q_{res} is the heat dissipated through respiration. Q_{cr-sk} is the heat exchange between the core and skin through contact resistance. $\dot{m}_{bl,sk}$ is the skin blood flow. C_{bl} is the specific heat constant of blood. hc is the external convection heat transfer coefficient between the skin and the surrounding. hr is the radiation transfer coefficient he is the evaporation coefficient deduced from hc by Lewis formula. T_{amb} is the surrounding air temperature, $\overline{T}_{amb_{mrt}}$ is the mean radiant temperature, P_{amb} is the ambient vapour pressure P_{sk} is the skin vapour pressure.

Skin blood flow $\dot{m}_{bl,sk}$ is variable and it depends on the body thermal state. The relation below defines the blood vessel constriction term from the cold thermal signal of the skin

$$Con = 0.5 \times (T_{sk} - 33.7) \tag{5.4}$$

While the blood vessel dilation factor is calculated, using the equation below related to warm core thermal signal.

$$Dil = 3.43 \times (T_{cr} - 36.8) \tag{5.5}$$

Skin blood is given by the relation addressed below taken from Foda et. al (2011)

$$\dot{m}_{bl,sk} = (6.3 + 60 \times Dil)/(1 + Con) \tag{5.6}$$

For the sweating rate, the correlation introduced by Smith (1993) was adopted, where sweating is sensitive to skin and core temperature.

First, the sweating threshold temperature T_{sweat} is calculated from the correlation below

$$T_{sweat} = \begin{cases} 42.084 - 0.15833T_{sk} & for\ T_{sk} < 33\,°C \\ 36.85 & for\ \ T_{sk} \geq 33\,°C \end{cases} \tag{5.7}$$

The sweat rate $\dot{m}_{sweat}$ is given by a relationship of the difference between sweat threshold and core temperature.

$$\dot{m}_{sweat} = 45.8 + 739.4(T_{cr} - T_{sweat}) \qquad T_{cr} > T_{sweat} \tag{5.8}$$

The heat exchange between the core and the skin is given by the equation:

$$Q_{cr-sk} = K(T_{cr} - T_{sk}) \tag{5.9}$$

Where K is the conductance between skin and core and is calculated based on two conductance the K_{muscle} muscle dependant and K_{fat} fat dependant based on the Havenith (2001) correlation.

$$K_{muscle} = \frac{A_{sk}}{0.5} \tag{5.10}$$

and $\qquad K_{fat} = \frac{A_{sk}}{0.0048(fat_{thick}-2)+0.0044} \tag{5.11}$

Q_{cr-sk} depends on the metabolic rate through the difference between the core and skin temperatures.

The heat dissipated through respiration Q_{res} is calculated through the correlation taken from ASHRAE Standard 55 (2017). The calculation is similar to the one used in the multi-segmented model chapter 6, section 6.2.2.

5.2.2 Initial conditions

The model needs initial conditions for the first time-step of calculation. The initial conditions, taken for Tskin and Tcore are the values of neutral conditions the model starts at:

- T_{cr}=37 °C

- T_{sk}=33 °C

The model body parameters were considered for an average adult human as in table 5.1.

Table 5.1: Body parameters

Variable name and unit	Value
Total body mass (kg)	m_{total}=75.3
Total body area (m2)	A_{sk}=1.85
Fat skin thickness (mm)	fat_{thick}=10
Blood specific heat (J/Kg°C)	C_{bl}=4000
Blood density (g/cm3)	ρ_{blood}=1.05
Mean body specific heat (J/Kg°C)	Cp_{body}=3100
Water heat of evaporation (J/Kg)	hfg=2.43$*$10^6
Air specific heat (J/Kg°C)	cp_{air}=1005.7

5.2.3 Clothing insulation and dynamic clothing model

Clothing insulation and moisture permeability are other factors affecting the sensible and latent heat losses from the skin. In the presence of clothing, it is convenient to combine the convective and radiation heat transfer through the

clothing into a single thermal resistance. And the sensible heat losses equation can be written as

$$C + R = (t_{sk} - t_{cl})/R_{cl} \tag{5.12}$$

Where R_{cl} is the clothing thermal resistance in $[(m^2.K)/W]$ and to exclude the clothing temperature from the equation (5.12) by using the operative temperature.

Further, the evaporative heat loss from the skin after considering clothing evaporative resistance and the skin temperature energy balance equation can be written in the form:

$$C_{sk}\frac{dT_{sk}}{dt} = Q_{cr-sk} - A_{sk}\left[(T_{sk} - T_{op})/(R_{cl} + \frac{1}{f_{cl(hc+hr)}}) + (P_{sk} - P_{amb})/(R_{e,cl} + \frac{1}{f_{cl(he)}})\right]$$
$$+\dot{m}_{bl,sk}C_p(T_{cr} - T_{sk})$$

$$\tag{5.13}$$

Where $R_{e,cl}$, is the clothing evaporative heat transfer resistance.

Selecting the intrinsic value of clothing Icl [clo] can be taken for example from figure 5.3 a table taken from ASHRAE fundamental chap9 2017 it allows to calculate the resistance of the clothing where Rcl=0.155Icl

Furthermore, the clothing surface area factor fcl can be estimated using the method provided in ASHRAE (ASHRAE Fundamental, 2017; ISO 9920, 2009) as in eq. 5.14.

$$f_{cl} = 1.0 + 0.3I_{cl} \tag{5.14}$$

Ensemble Description[a]	I_{cl}, clo	I_t,[b] clo	f_{cl}	i_{cl}	i_m[b]
Walking shorts, short-sleeved shirt	0.36	1.02	1.10	0.34	0.42
Trousers, short-sleeved shirt	0.57	1.20	1.15	0.36	0.43
Trousers, long-sleeved shirt	0.61	1.21	1.20	0.41	0.45
Same as above, plus suit jacket	0.96	1.54	1.23		
Same as above, plus vest and T-shirt	1.14	1.69	1.32	0.32	0.37
Trousers, long-sleeved shirt, long-sleeved sweater, T-shirt	1.01	1.56	1.28		
Same as above, plus suit jacket and long underwear bottoms	1.30	1.83	1.33		
Sweat pants, sweat shirt	0.74	1.35	1.19	0.41	0.45
Long-sleeved pajama top, long pajama trousers, short 3/4 sleeved robe, slippers (no socks)	0.96	1.50	1.32	0.37	0.41
Knee-length skirt, short-sleeved shirt, panty hose, sandals	0.54	1.10	1.26		
Knee-length skirt, long-sleeved shirt, full slip, panty hose	0.67	1.22	1.29		
Knee-length skirt, long-sleeved shirt, half slip, panty hose, long-sleeved sweater	1.10	1.59	1.46		
Same as above, replace sweater with suit jacket	1.04	1.60	1.30	0.35	0.40
Ankle-length skirt, long-sleeved shirt, suit jacket, panty hose	1.10	1.59	1.46		
Long-sleeved coveralls, T-shirt	0.72	1.30	1.23		
Overalls, long-sleeved shirt, T-shirt	0.89	1.46	1.27	0.35	0.40
Insulated coveralls, long-sleeved thermal underwear, long underwear bottoms	1.37	1.94	1.26	0.35	0.39

Source: From McCullough and Jones (1984) and McCullough et al. (1989).
[a]All ensembles include shoes and briefs or panties. All ensembles except those with panty hose include socks unless otherwise noted.
[b]For $t_r = t_a$ and air velocity less than 0.2 m/s ($I_a = 0.72$ clo and $i_m = 0.48$ when nude).
1 clo = 0.155 (m²·K/)W.

Figure 5.3 Clothing insulation values for a collection of clothing ensemble (ASHRAE 2017)

5.2.3.1 Dynamic clothing insulation model

Several pieces of research have been conducted, pointing out the significance of the variability of clothing insulation for thermal comfort. Dynamic clothing insulation models developed were based on either the current daily outdoor temperature or on the outdoor temperature of the previous day. (De Dear 1998; ASHRAE standard 55 2013; Schiavon and Lee 2013, Rida et al. 2019)

Schiavon and Lee (2013) developed a model to predict the clothing insulation dynamically. The model is based on 6333 selected observations taken from the ASHRAE RP-884 and RP-921 databases. They investigated multiple variables which can affect the clothing insulation selection and among those variables, they

found that the outdoor temperature at 6 o'clock and the indoor operative temperature were the two main variables that influence the insulation clothing prediction.

For that, the model of Schiavon (Schiavon and Lee 2013) to predict the total insulation value has been adopted.

$$DI_{cl} = 10^{(0.2134 - 0.0063 * t_{amb\ at\ 6} - 0.0165 * t_{op})}$$

DI_{cl} is the dynamic clothing insulation in clo, $t_{amb\ at\ 6}$ is the outdoor temperature of the day at 6 am in °C, and t_{op} is the zone operative temperature in °C.

The model predicts the clothing insulation value every time-step based on a daily fixed outdoor temperature. Which mean the model prediction varies during the day depending on the operative temperature, in case of a designed space with fixed indoor temperature the clothing insulation level will be fixed throughout the day, however, when the indoor temperature fluctuates the clothing insulation value will be variable during the day.

The previously described dynamic clothing model of Schiavon is implemented in ESP-r to give our occupancy modelling more reliability.

5.3 Methodology and coupling approach

Figure 5.4 shows an expansion in the flow path of ESP-r by adding the two nodes representing the core and the skin node of an occupant, as the metabolic heat production happens in the core node heat flows to the skin layer. From the skin node, all the heat flows to and from the environment is calculated after considering the clothing insulation. The heat from the skin node exchange with the air node through convection, and to surrounding construction and radiative heating/cooling through radiation.
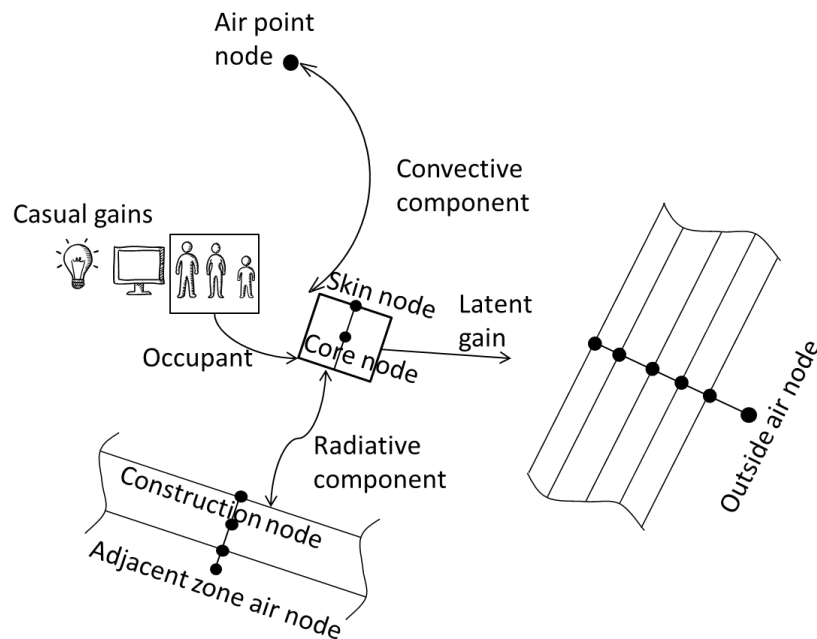
Figure 5.4: Two-node occupant representation in the energy flow path of ESP-r.

Figure 5.5 is a flow chart to summarize the process of calculation within ESP-r.

- For the corresponding zone, it reads the input data from the operation file which describe the occupancy schedule and other internal loads.

- In case when the dynamic clothing model is active, the clothing insulation value is calculated.

- The dynamic model is called from the ESP-r's algorithm that manages casual gains from occupants.

- The two-nodes human thermal model uses the latest calculated zone environmental parameters eg., air temperature, mean radiant temperature and relative humidity.

- It predicts skin and core temperature and the dissipated sensible and latent heat.

- After considering the number of occupant and age/gender, the final calculated internal loads from the occupants is passed back to the energy balance of zone in which the occupants are located.

- This process continues every time step of the simulation.
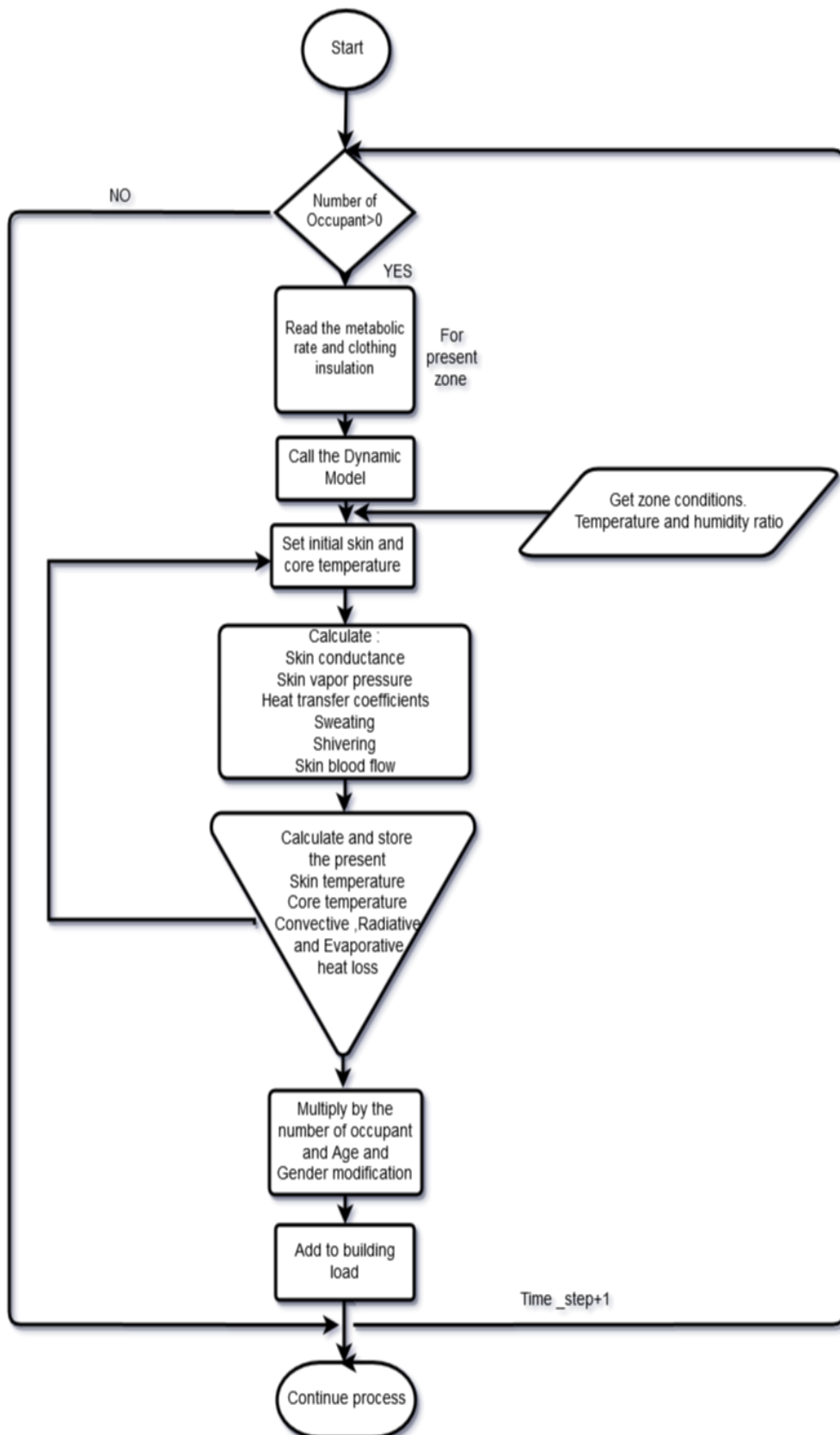
Figure 5.5: Flow chart shows the integration of the two-node model in ESP-r.

Note on time-step: the building simulation time-step can vary from one hour to one-minute time-step, on the other hand, the two-nodes model works on one-second time-step. By defining a smaller time-step for a building simulation can provide more detailed information on how the environmental parameters change within an hour, the environmental parameters which are inputs for the two-nodes model reduces the impact of sudden environmental changes when considering hourly simulation. For example, if the room temperature has two-degree kelvin change in one hour, the two-node model reacts differently when comparing a sudden change or a gradual of 0.5 [K] every 15 minutes. Even though the model input considers the hourly schedule (eg. Metabolic rate, number of people) and hourly weather file data but it is still recommended to use smaller time-steps. The reason behind the different time-steps between the building simulation and the two-nodes model is because the physiology seems to behave more accurately with one-second time-steps since it calculates blood flow and other physiology phenomena's every second.

In ESP-r there is a possibility to define an MRT sensor in a specific location inside a zone. The MRT calculated from the sensor can be used and linked to the two-node model. Where that helps in accounts for example to the effect of cold and hot surfaces on the occupant. But for generalizing in the following simulation the occupant (two-node model) was always set in the middle of the room.

5.3.1 Validation of model prediction

The two-node model implemented in ESP-r has been validated with some published experimental data.

To do the simulation using the coupled two-node in ESP-r a climatic chamber of dimensions 3m width x 3m length x 2.7m hight has been set up. All walls set to be

adiabatic and the room was controlled through a basic controller with a very high heating cooling capacity to ensure a fast temperature change. Time step used is 1 minute to ensure the required environmental conditions temperature and relative humidity reached in no more than three minutes.

The first comparison is for a person sitting in a room of 27°C air temperature and 55% relative humidity for 90 minutes, after that temperature changed to 20°C for two hours figure 5.6 shows the operative temperature over the simulation time. The data has been extracted from the published work of Severens et al. (2009). In the experiment subjects wearing cloth of 0.19 clo metabolic rate of 1 met. Figure 5.7 and 5.8 shows good agreement of the model results of skin and core temperature with the experimental data. Error bars considered as ±0.6°C for skin temperature and ±0.4°C core temperature sensor error.

The skin temperature, which is our interest, follows the experimental results with some differences of 0.5°C these degrees of error and differences are considered acceptable as the experimental skin temperature is a weighted average different local skin temperature. Core temperature stayed within the acceptable range near the 37°C, during the second phase of the simulation the core temperature showed a very fast response that is due to the thermoregulatory thresholds defined in our model in addition to the specific heat value considered in our model.
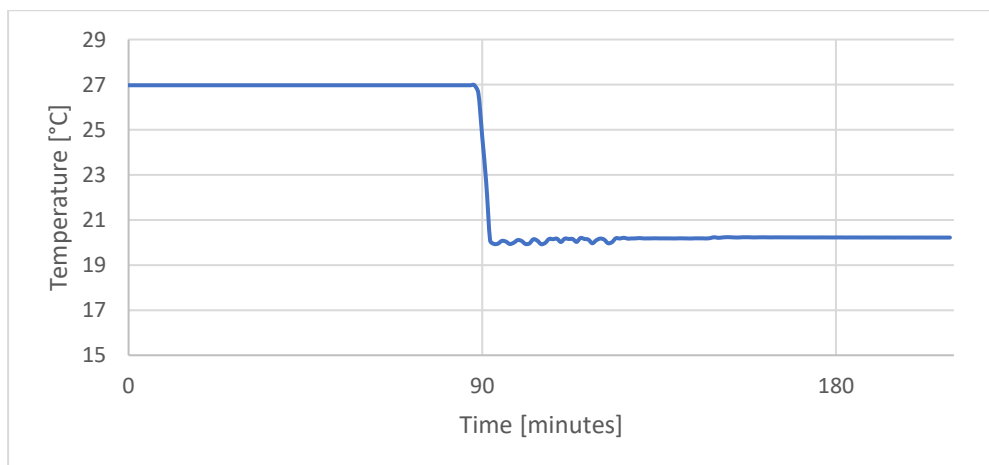
Figure 5.6: Operative temperature of the climatic chamber with respect to time.
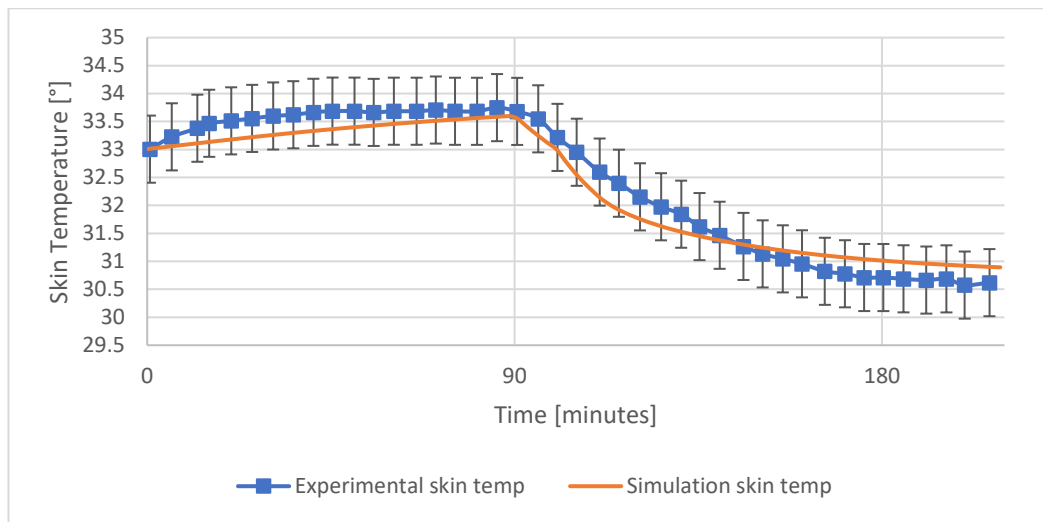
Figure 5.7: validation of simulated skin temperature vs. the experimental mean skin temperature published in (Severens et al., 2009)
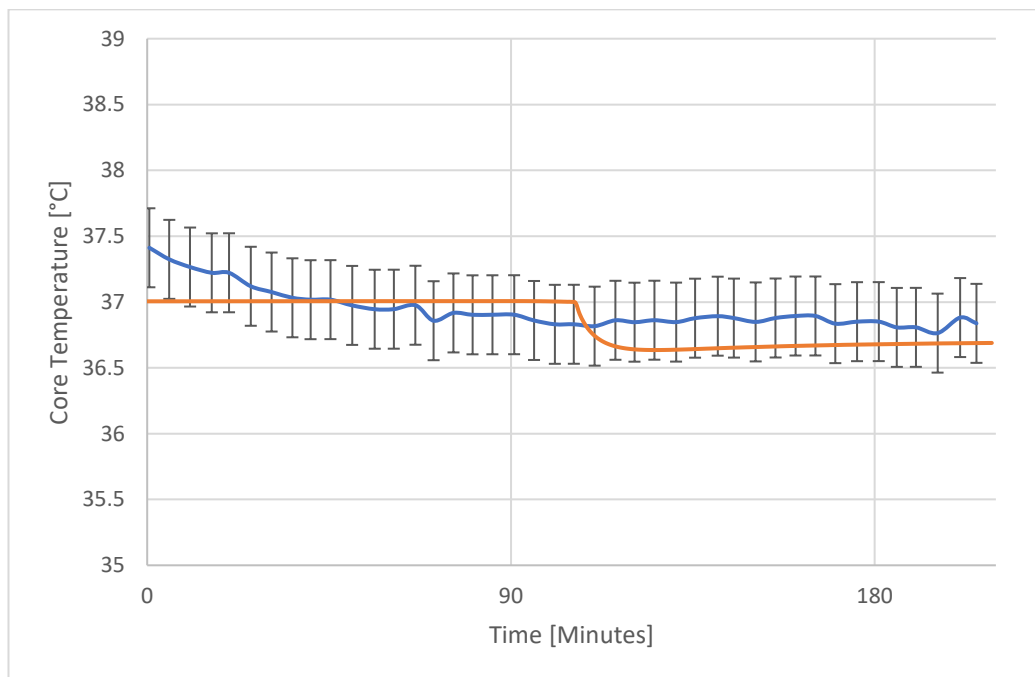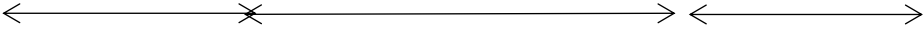
Figure 5.8: validation of simulated core temperature vs. the experimental core temperature published in (Severens et al., 2009)

The second comparison is with published experimental data of Hardy and Stolwjik (1996). The experiment was done in a step-change in the environment temperature, starting from a relatively neutral condition moving to a hot

environment of 37°C for two hours followed by one hour back to the initial starting environment.

The experimental and simulation setup is shown in table 5.2 below.

Table 5.2 simulation setup based on the experiment in [Hardy and Stolwijk, 1996]

	1 hour	2 hours	1 hour
Temperature [°C]	28.5	37.5	28.5
Relative humidity %	40	33	41

The comparison results are presented in figures 5.9, and 5.10. Figure 5.9, shows the skin temperature, in this case, the skin temperature showed a slightly slower response in the transition between the conditions, especially moving from the hot environment to the neutral conditions, that is due to the skin blood flow rate predicted. Although the environment temperature has dropped, but the vasodilation continues allowing more blood to circulate in the skin node. Figure 5.10, shows the core temperature comparison, where results demonstrate an acceptable agreement with the experimental results. The differences in all the comparison cases can be due to the model input parameters sensitivity like metabolic rate as a fixed number, the clothing value and the fact that the two-node model represents the human body as one whole part. Additionally, from the published experiment side like the experimental sensor's accuracy.
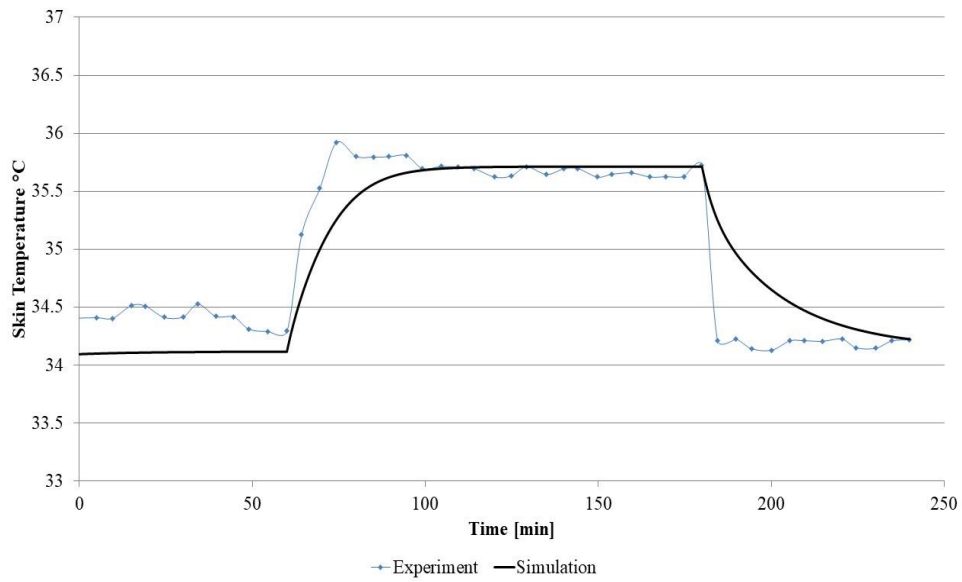
Figure 5.9: comparison of skin temperature with the experiment of (Hardy and Stolwijk, 1966).
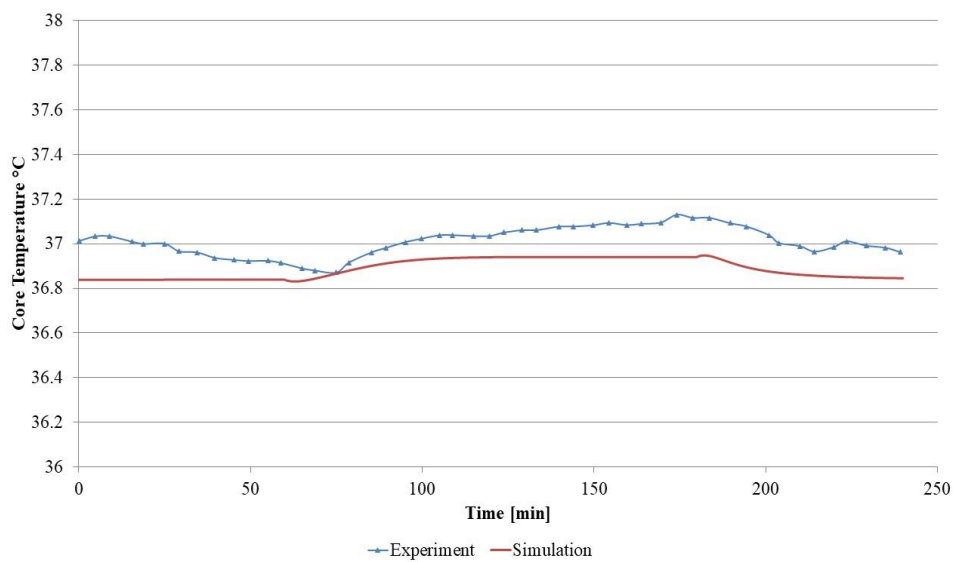
Figure 5.10: comparison of core temperature with the experiment of (Hardy and Stolwijk, 1966).

5.4 Model simulation results and discussion

In the following two subsections, applications of using the two-node model in building simulation were presented. In the first model, a multi-zone office building is considered with an occupancy capacity of 1 to 5 person and the second is a single zone model represents a classroom with 30 person capacity. In both simulation cases, a time-step of 15 min was selected for the building simulation.

5.4.1 Comparison with the previous approach

All three approaches, i.e. the scheduled sensible latent ratio, the polynomial model described in chapter 4 and the two-node model, have been applied to a test office (Figure 5.11) building. This comprises four main zones: a reception of 71 m^2 base area a general room of $77m^2$ a conference room of $62m^2$ and a manager office of $13.5m^2$. Figure 5.11 shows the model geometry.

The construction data are shown in Table 5.3 and the occupancy schedule is shown in Table 5.4.

For the occupant thermal model, clothing resistance is chosen to be 1 clo for all occupants.
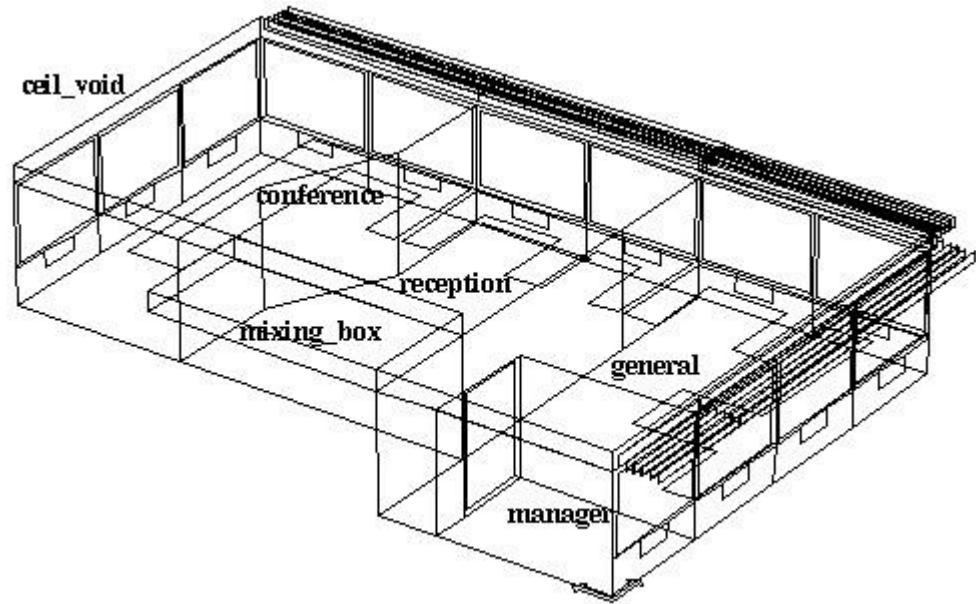
Figure 5.11: model geometry in ESP-r.

Table 5.3: Selected constructions used in the model

Construction	U-value (W/m2K)
Ceiling	0.323
Floor	1.32
External wall	0.21
Double glazed window	2.243

Table 5.4: occupancy loads schedule for zone general

Time (hrs)	No. of occupants	Sensible/Latent gain (W)	Metabolic rate (met)
00:00-07:00	0	0/0	0
07:00-08:00	1	100/60	1.54
08:00-09:00	3	300/180	1.54
09:00-12:00	5	500/300	1.54

12:00-14:00	3.25	325/195	1.54
14:00-17:00	5	500/300	1.54
17:00-00:00	0	0/0	0

The predictions of all three models were compared in a simulation of a typical summer week using climate data for London, UK.

Results in Figures 5.12 (a) and (b) show the input sensible and latent load from the occupants of the General room of the model as derived from the various modelling approaches. The figures show that there are substantial differences between the dynamic polynomial or two-node models and the commonly used fixed sensible latent ratio approach, with the sensible load was over-predicted when using fixed values and the latent load was under predicted in this particular case.

Figures 5.12 (c) and (d) show the latent cooling load and the sensible cooling load, when the air temperature of the general space is cooled to 25°C and the RH restricted to 50%. Both show appreciable differences between the fixed and dynamic modelling approach, which could have an impact if the results were being used to select plant size.
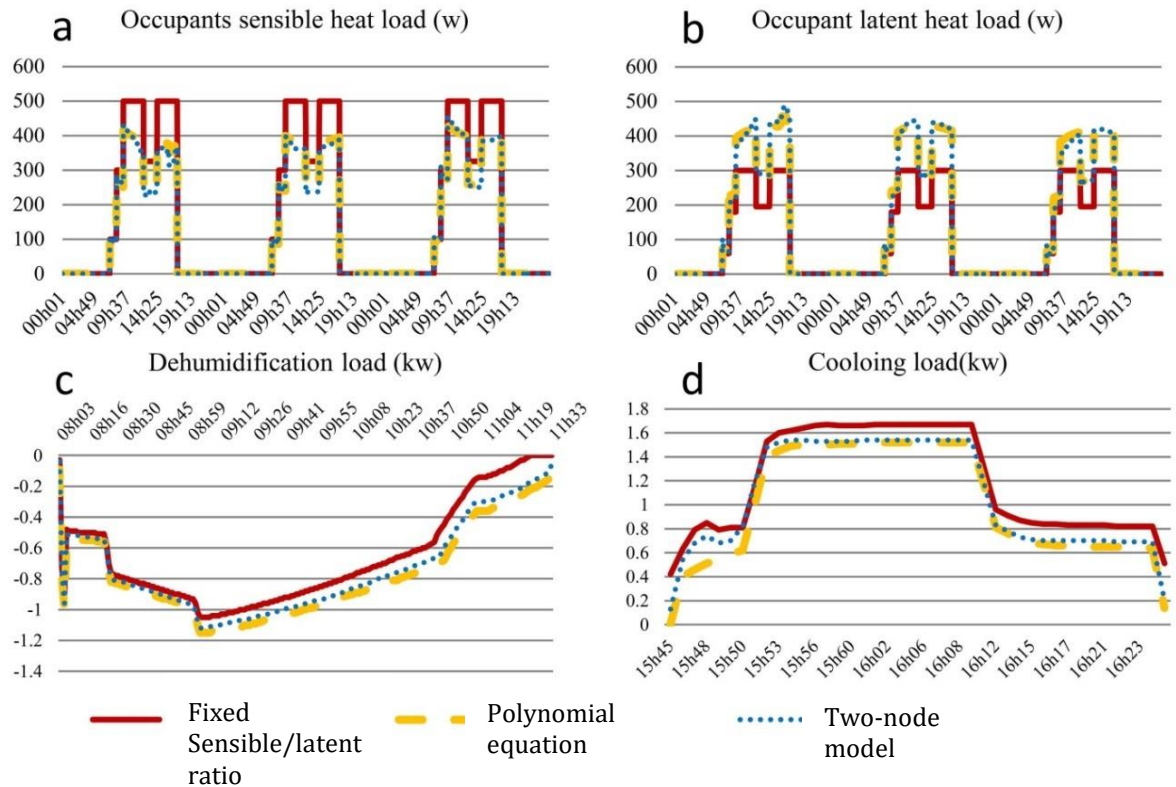
Figure 5.12: a,b, sensible and latent heat load from the different models c- Latent load typical day (-ve implies dehumidification) d- Sensible cooling load typical day.

5.4.2 densely occupied room

In the following study, the two-node model occupancy approach has been applied to a classroom. The classroom geometry is a general classroom with 8m length x 7m width and 2.8 m height. The floor area is 56m^2 with windows area of 6.75 m^2. This type of classroom has a student capacity of 30 students (Niemeyer, 2003; Daniels et al., 2017). Figure 5.13 shows the wireframe representation of the classroom modelled in ESP-r. The weather data used in this simulation is the default weather data of ESP-r of the city of Glasgow.

Table 5.5 construction characteristic of the classroom

Construction type	U-Value
External wall	0.2
Internal walls	1.36
Ceiling	0.14
Floor	1.32
Windows (double glazed)	2.24
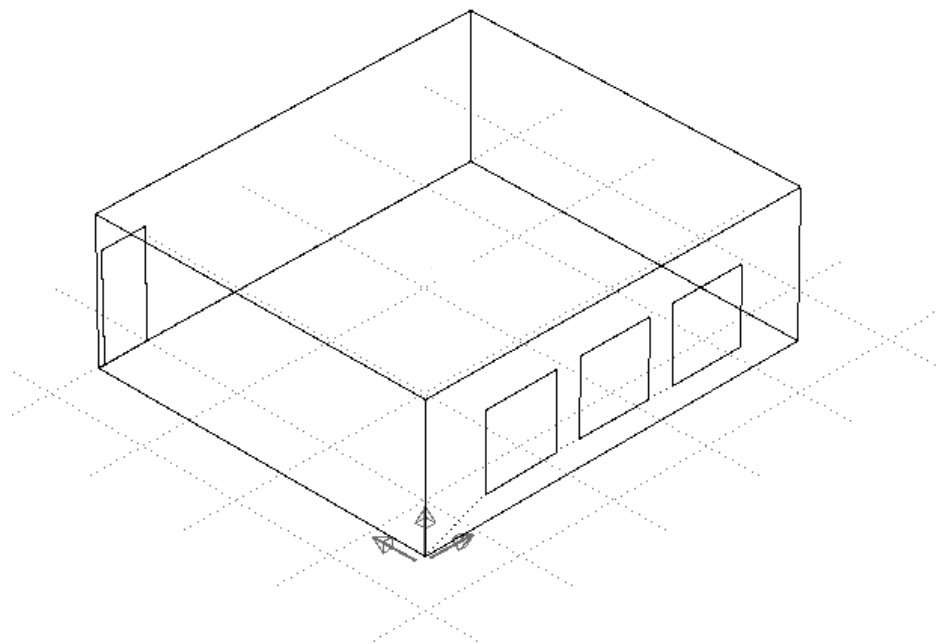
Figure 5.13 wireframe of the classroom modelled in ESP-r.

Table 5.5 presents the construction material thermal characteristic. To evaluate the results of the classroom using the two node-model occupancy approach, a comparison with the fixed sensible latent occupant load has been made. Table 5.6 present the schedule used in the simulation for a typical weekday occupant sensible/latent load. Table 5.7 presents the comparable inputs for the two-node model. The values in table 5.6 were calculated based on ASHRAE table presented

in section 4.3.2 as Figure 4.3 where data were chosen represent a person seated with a metabolic rate of 1 met (70 sensible 45 latent).

Table 5.6 Schedule with fixed occupant sensible/latent approach.

Time	Sensible heat load [W]	Latent [W]
00:00 to 08:00	0	0
08:00 to 12:00	2100	1350
12:00 to 13:00	700	450
13:00 to 17:00	2100	1350
17:00 to 24:00	0	0

Table 5.7 Schedule two-node model occupancy inputs.

Time	Number of occupants	Metabolic rate
00:00 to 08:00	0	0
08:00 to 12:00	15 men 15 women	1
12:00 to 13:00	5 men 5 women	1
13:00 to 17:00	15 men 15 women	1
17:00 to 24:00	0	0

A basic controller has been defined to control the indoor temperature between 20 and 25 °C and relative humidity between 50 and 60%. The controller active between 7:00 and 18:00. The ventilation rate used during the occupied hours is considered 2 ACH air change per hour of fresh air. The model is set to use the dynamic clothing approach which means clothing were dynamically calculated based on the outdoor temperature and the indoor operative temperature.

Figure 5.14 shows the indoor resultant temperature and the relative humidity from the two-node model simulation approach. Figure 5.15 presents the outdoor dry bulb temperature over the year and figure 5.16 shows the values of the

clothing insulation calculated and used during the simulation. Form figure 5.16 it is clear how the clothing insulation value is dynamically calculated and used where winter showed higher clothing insulation compared to summer.
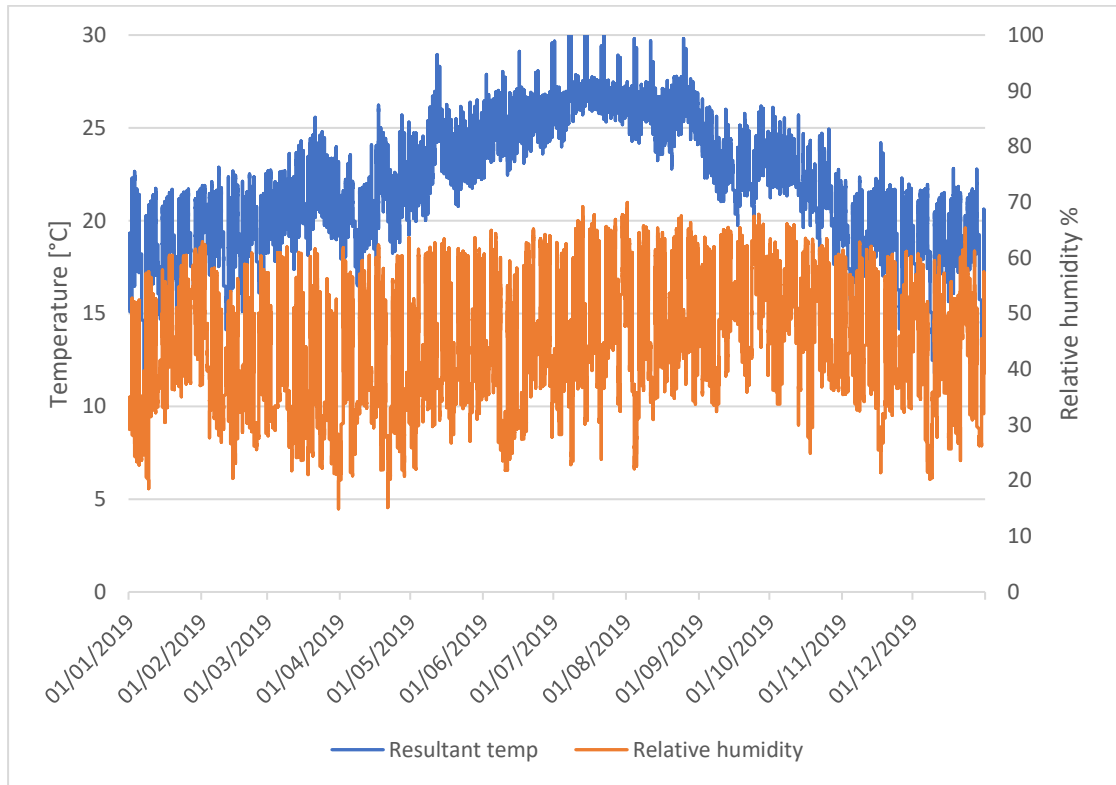
Figure 5.14: Resultant temperature and relative humidity prediction over a year.
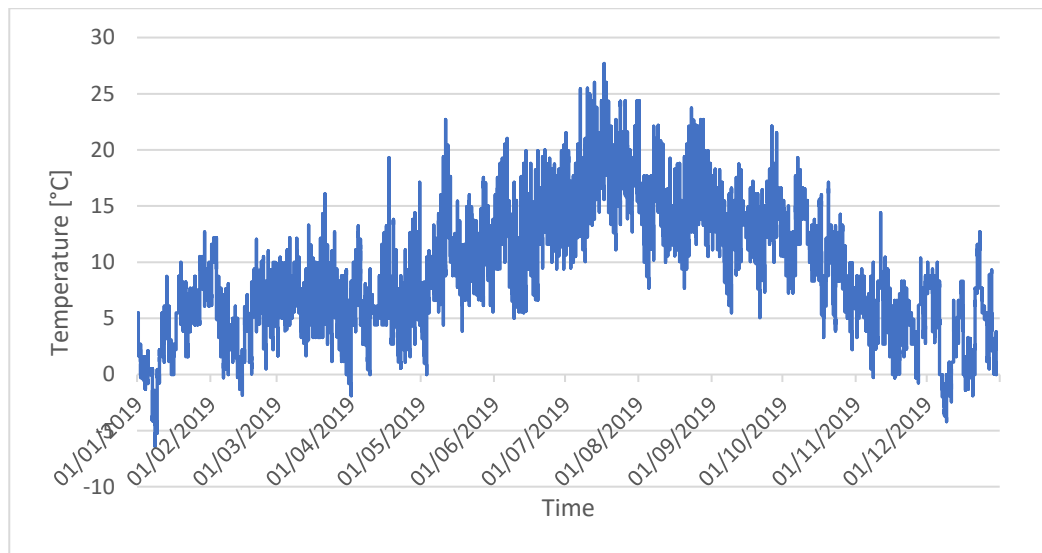
Figure 5.15: Outdoor dry bulb temperature over a year
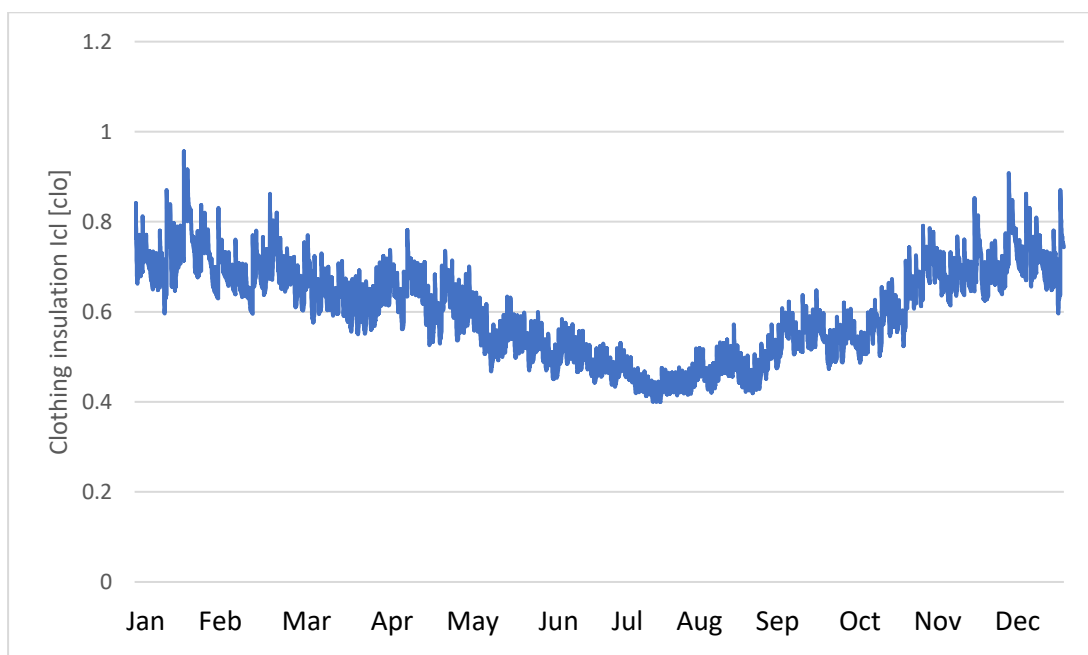
Figure 5.16: Dynamic clothing insulation value prediction for the full year.

The simulation results looked into the cooling and heating loads in addition to the dehumidification and the humidification demand over a year. The bar chart in figure 5.17 shows the simulated energy demand using both approaches the fixed

sensible latent ratio and the two nodes model. From the chart, it can be seen how the differences in demand are between the two approaches. Where the two-nodes model showed higher heating demand but much lower cooling demand comparing to the fixed sensible latent ratio. In addition, the two-nodes model simulation showed higher dehumidification and lower humidification demand compared to the fixed ratio approach.
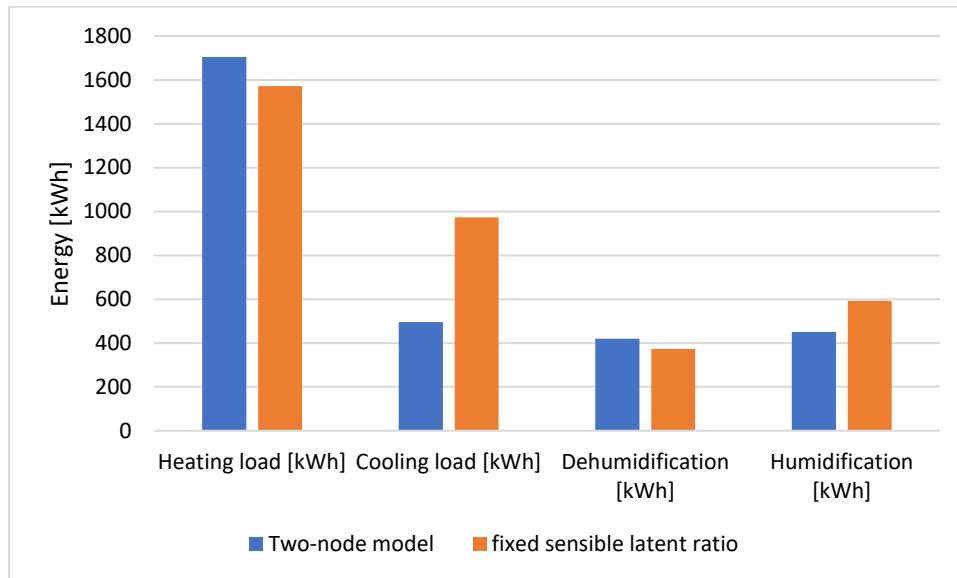
Figure 5.17: Comparisons of the different energy consumptions between the fixed ratio and two-node model approach.

These results of the cooling load can be explained by looking into one-day results. A random day in May has been selected. Figure 5.18 presents the predicted sensible and latent heat loads from occupants from the 2-nodes model and compared to the fixed ratio approach. From the results, it can be seen that latent load was much higher than the fixed latent and consequently the sensible load predicted was lower compared to fixed sensible load. Which explain the reason why the sensible cooling load was lower in the case of the dynamic 2-node model simulation. The correspondent temperature and relative humidity of the selected day are presented in Figure 5.19. From Figure 5.19 we can see the influence of sensible and latent heat load from occupant on temperature and relative humidity, as the latent load is higher the relative humidity was comparably higher

in the 2-node model simulation case. Contrarily, the sensible load was lower and that reflected in the temperature results.
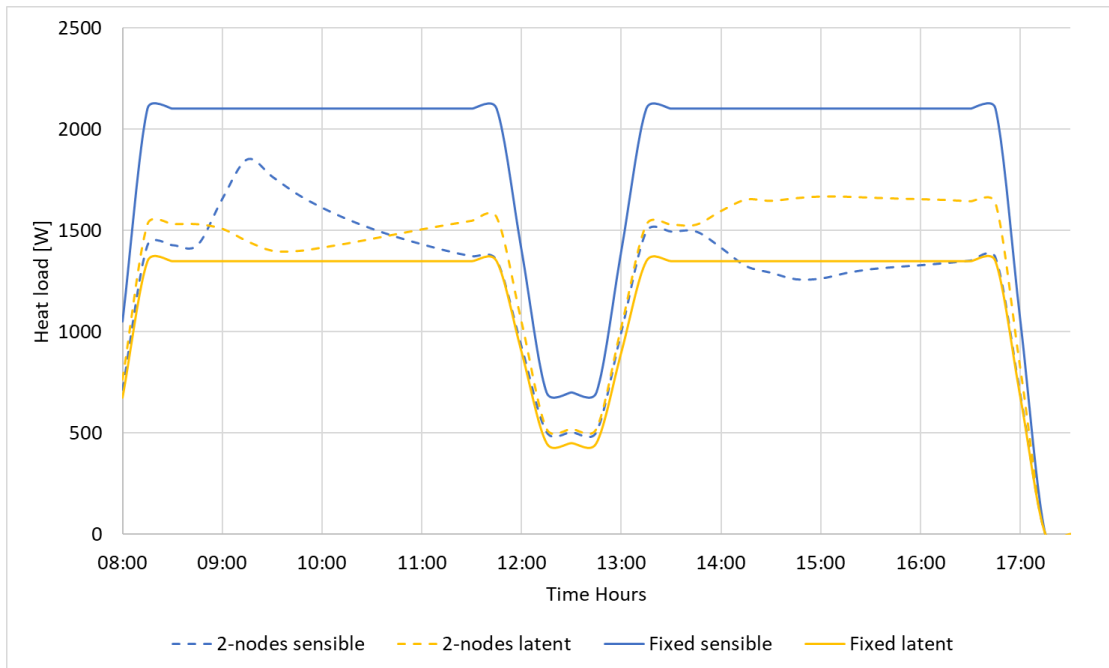
Figure 5.18: sensible and latent heat load comparison between 2-node and fixed ratio in one day of May.
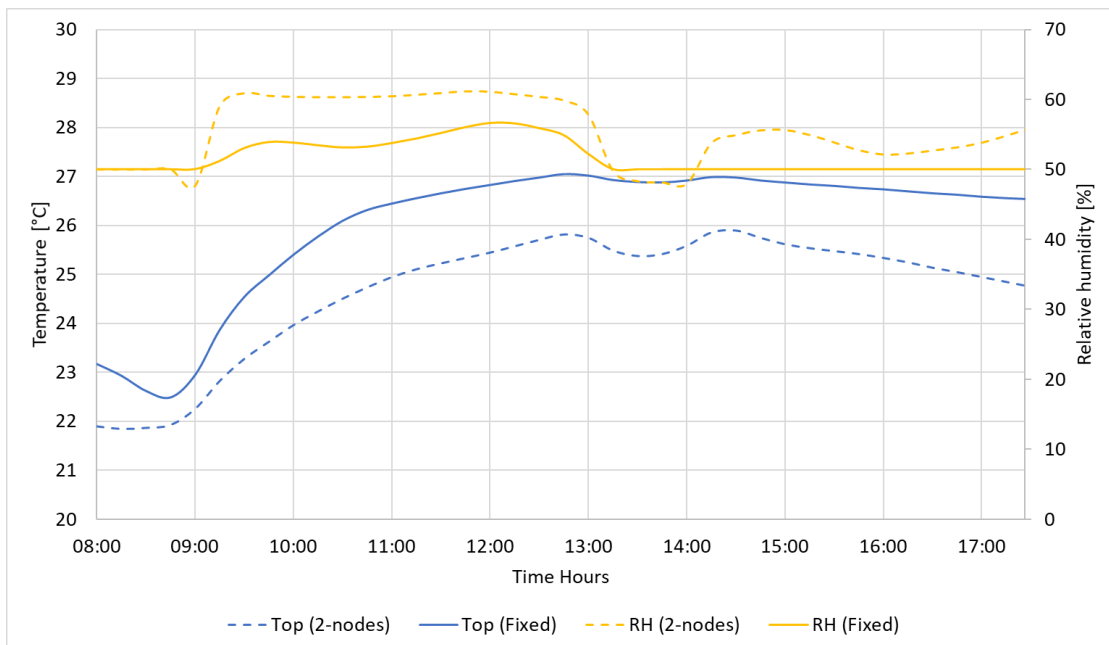
Figure 5.19: Operative temperature and Relative humidity for both simulation case 2-node model and fixed ratio.

To evaluate the clothing effect on the total energy demand since clothing insulation value affects the sensible and latent heating losses from the human body. The same building model has been selected using the two-node model approach but fixing the clothing insulation value to 0.7 [clo]. The bar-charts in Figure 5.20 shows the differences in energy demand of cooling, heating, humidification and dehumidification over a year for both simulation dynamic and fixed clothing. The graph shows how clothing can affect the energy demand values and that is because during summer an occupant might be wearing clothing of insulation 0.5 [clo] that mean higher sensible heat load from the human body to the zone compared to 0.7 [clo] case, that leads to higher cooling demand. Contrarily, during winter higher insulation will result in a lower sensible heat loss from the occupant and consequently, lower heating demand. Also, more sweating will be resultant in summer if higher clothing insulation is imposed, and that is why the dehumidification value was higher in the case of fixed clothing.
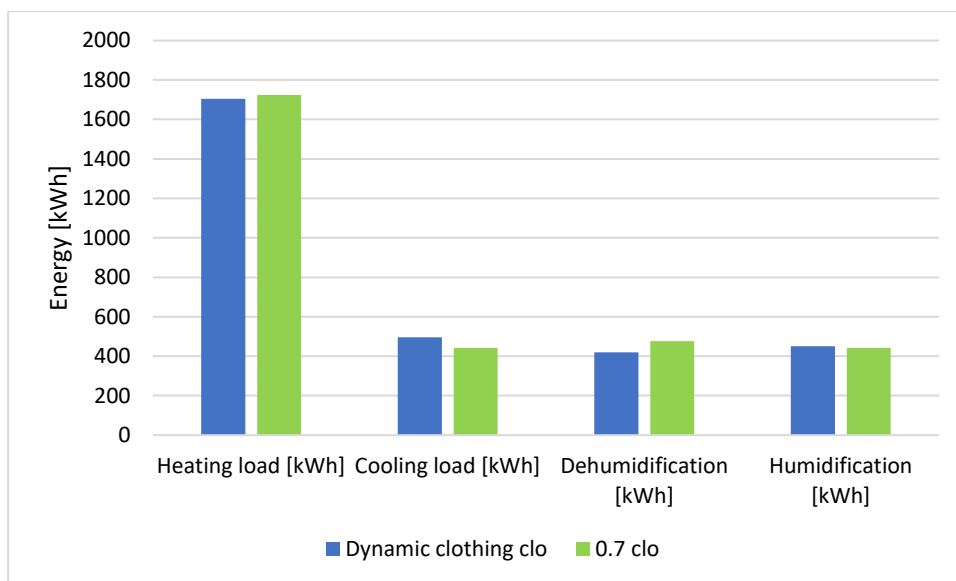
Figure 5.20: Comparisons of the different energy consumptions between the two-node model with dynamic and fixed clothing insulation.

114

5.5 Conclusion

This chapter showed the importance of using a dynamic physiology model in combination with building simulation. In order to size the cooling and heating plants correctly it is very important to provide as realistic as possible the internal heat loads and in our case the occupant heat loads. The latent heat load from occupant is another very important factor to simulate and size correctly a dehumidifier if needed. The two-node model can predict the required occupant heat loads, further, the model can predict the core and skin temperature of occupant which are the main factors to study thermal comfort. The core and skin temperature can be linked to any comfort model like the PMV method.

From above a two-node model is a good approach to predict the internal heat load from the occupant and to predict thermal comfort. The model can not predict the local body thermal comfort, for that a detailed human thermal model is needed. Keeping in mind that a multi-segment human model will require higher detail input as a local environmental condition. For simplicity, one can assume the uniform temperature, but to be more accurate and predict meaningful results a detailed environmental condition for each body part is needed. For that, a CFD simulation can be a solution. In the following chapter, a description of the detailed multi-segmented model has been presented and the use as integration in building simulation and CFD is discussed in chapter 7.

Chapter 6: Multi-segment Human Thermal Model

6.1 Chapter overview

Several simple transient human thermo-physiology models were developed before the sixties for example (Machle et al., 1947; Kerslake et al., 1958; Wyndham et al., 1968). Around 1970, more complex thermal models started to appear, that was because of the fast development of digital computers. The human thermal models were developed based on thermodynamics, mass transport and physiology theories to predict the thermal behaviour of the body or parts of it (Stolwijk, 1971; Rupp et al., 2015).

A detailed multi-segment describes the human thermal system is adequately detailed to provide valid thermal data from the different human body parts like local skin temperature local heat losses and sweating rates. In this chapter, the multi-segment physiology model has been described. All the equation related to the passive and active heat transfer is presented. The model has been implemented in ESP-r and made available open-source. The model implemented is based on the work of Salloum et al. (2007) and Karaki et al. (2013) with some modifications to fit the purpose and linkage to the building simulation like heat transfer coefficients. The multi-segment model thermally interacts with its surrounding space. The chapter is divided into multiple sections describing the blood circulation system, the energy balance equations and the thermoregulatory system.

6.2 The human thermal model: passive heat regulation

The Physiology model divides the human body into 25 body segments, Where Salloum et al. (2007) initially developed his model with 15 body segments and later development done by Karaki et al. (2013) including the ten fingers to the same physiology model. It is constituted of the head (representing both head and neck), upper and lower chest (representing the trunk), and symmetrically for left and right, it has the upper arm, lower arm, hand, five fingers in addition to the thigh, leg and foot. Each segment can be represented as a cylindrical form with a uniform temperature. All body parameters such as surface area, mass for each segment can be found in table 6.1. Each segment is divided into four nodes (Core, Artery, Vein, and Skin) representing the concentric layers of each body segment in the model, Forearms and fingers has an additional node the superficial vein. These nodes exchange heat between each other by convection, conduction and perfusion figure 6.1 clarify the proceeding also in figure 6.2 the body segment considered in the model is shown.
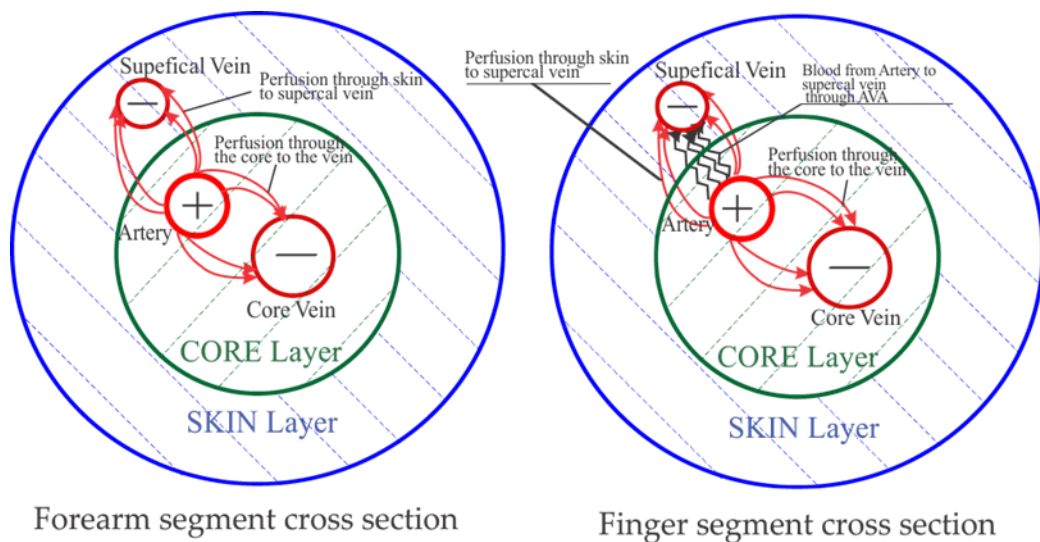
Figure 6.1: the representation of the node in the body segment, figure is taken from Rida et al. 2014.

Table 6.1: Body parameters mass, area and fat thickness (Salloum et al,. 2007).

Body segment	Mass [kg]	Area [m²]	Fat thickness [mm]
Upper Chest	16.1	0.40	19.12
Lower Chest	24.4	0.26	19.12
Head	5.0	0.14	8.5
Thigh x 2	5. 5	0.15	10.64
Calf x 2	2.44	0.10	10.64
Foot x 2	1.01	0.058	11.7
Upper arm x 2	2.5	0.01	4.51
Forearm x 2	1.4	0.068	4.51
Palm x 2	0.36	0.023	7.4
Fingers x 10	0.036	0.0043	3.3

The body segments are connected through the blood vessels. In each body segment, a number of arteries and veins are passing through and connecting other body segments representing a branch as described in the Avolios arteries branch (Avolio, 1980). The origin of the blood starts with the aorta from the heart located in the upper chest and ends in different locations as extremities and figure 6.1 shows the Avolio blood tree distribution.

The detailed blood flow will be explained in subsection 6.3.3 later in this chapter.
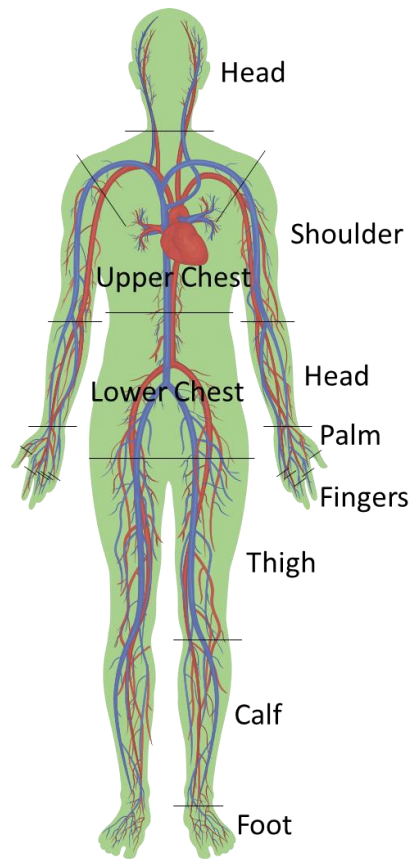
Figure 6.2: The human body representation with the 25 body segments.

6.2.1 Metabolic heat production

The metabolic heat production is an input to the model to represent the activity level of the human subject. The metabolic heat rate is expressed by the unit of MET as described earlier. In the multi-segmented model, the basal metabolic rate is distributed over all the body segments, table 6.2 shows the values considered for each segment with a total of 83.4 [W].

Table 6.2: Basal metabolic rate for each body segment (Salloum et al., 2007).

body segments	Basal metabolic [W]
Upper CHEST	6.56
Lower Chest	47.47
Head	18.65
Right/left THIGH	2.05

Right/left Calf	0.91
Right/left Foot	0.27
Right/left Upper-Arm	1.24
Right/left Forearm	0.73
Right/left Palm	0.11
Fingers x 10	0.009

6.2.2 Heat dissipated by respiration

The calculation of heat dissipated by respiration in the model is based on the equation provided in ASHRAE (ASHRAE Fundamental, 2017) where the respiration heat loss Qres is the sum of the Latent Eres and the sensible Cres compartment.

$$Q_{res} = C_{res} + E_{res} \qquad (6.1)$$

$$Q_{res} = \dot{m}_{res} C_{p,air}(T_{ex} - T_{amb}) + \dot{m}_{res} h_{fg}(w_{ex} - w_{amb}) \qquad (6.2)$$

Where, $\dot{m}_{res}$ Is the mass flow rate of air inhaled into the lung during the respiration and it is calculated through: $\dot{m}_{res} = K_{res}M$ ($K_{res} = 1.43 * 10^{-6}\ Kg/J$) and M is the metabolic rate in W.

The specific heat capacity of air is given as follows: $C_{p,air} = 1005.7\ (J/KgK)$

The exhaled air temperature is given by $T_{res} = 32.6 + 006T_{amb} + 32w_{amb}\ (°C)$

Tamb is the ambient temperature w_{amb} is the ambient humidity ratio.

The heat of vaporization of water is $h_{fg} = 2.43 * 10^6\ (j/Kg)$ and the exhaled humidity ratio is calculated $w_{ex} = 0.2w_{amb} + 0.0277 + 6.5 * 10^{-5}T_{amb}$

6.2.3 Heat transfer coefficients

The convection heat transfer at the body surface areas can be categorised into natural convection which is the process of air movement naturally at the border of the outer layer of the body, and it is driven by the thermally induced buoyancy. The other form is the forced convection when air velocity is higher than 1.5 [m/s], when air velocity is less than 1.5 [m/s] a combined of the mixed convection mode should be considered.

In the model, a default fixed value of the convective heat transfer coefficient for each body part is considered in the case of building simulation, where air velocity inside a zone is assumed constant and uniform. That approach neglects the effect of air velocity. In this research, when using the model in CFD (see Chapter 7), local air velocity is being updated and linked with the heat transfer coefficient calculation. The calculation of the local heat transfer coefficients is according to the empirical equation's correlation published by De-dear et al. (1997).

Values of local hc, used for the building occupant in building simulation and CFD are stated in table 6.3.

Table 6.3: convective heat transfer coefficient at each body segment [De-Dear et al. 1997].

Body segment	hc in building simulation $[W/m^2K]$	hc in CFD $hc = Bv^n[W/m^2K]$	
		B	n
Upper CHEST	3.1	7.5	0.66
Lower CHEST	3.1	7.5	0.66
HEAD	3.6	3.2	0.97
Right THIGH	4.1	10.1	0.52
Left THIGH	4.1	10.1	0.52

Right Calf	4.1	12.9	0.5
Left Calf	4.1	12.9	0.5
Right Foot	5.1	12	0.5
Left Foot	5.1	12	0.5
Right Upperarm	5.1	10	0.62
Left Upperarm	5.1	10	0.62
Right FOREARM	5.4	12.6	0.54
Left FOREARM	5.4	12.6	0.54
Right Palm	7.0	14.4	0.56
Left Palm	7.0	14.4	0.56
Fingers x 10	7.0	14.4	0.56

The evaporative heat transfer coefficient is given by the Lewis relation and it is calculated by the equation $h_e = LR * h_c$ where LR is the Lewis ratio and is equal to 16.5.

The radiative heat transfer coefficient hr is considered as the linear radiation heat transfer coefficient which is calculated from the equation taken from the ASHRAE Handbook of fundamental (2017).

$$hr = 4\varepsilon\sigma(A_r/A_D)[273.2 + (t_{sk} + \bar{t}_r)/2]^3 (W/m^2 per\ K) \qquad (6.3)$$

Where ε is the average body surface emissivity assumed to be equal 0.95, σ is the Stefan-Boltzmann constant, $5.67 * 10^{-8}$ W/m² per K; A_D is the DuBois body surface area (m2) and A_r is the effective radiation area of the human body (m²) t_{sk} is the skin body surface temperature (°C)

6.3 The active human thermal model: active heat regulation

6.3.1 Shivering model

The mathematical model describing the shivering metabolic rate used in the AUB model (Salloum, 2005) which is based on the experimental data. The model is represented as a set of correlations to predict the shivering metabolic rate. The model is described as follows, As soon as the skin temperature falls below the thermal neutrality the first body response will be the vasoconstriction by decreasing blood flows to the skin to reduce the heat losses when that is insufficient and if core temperature keeps decreasing the shivering phenomena starts to generate more heat. The higher setpoint temperature is the 37.1 °C core temperature where, above this temperature, no shivering will occur, and the lower set point is 35.8 °C where shivering will always occur. In between these two values, the threshold is being calculated and it decreases linearly based on the core temperature. Equation 6.4 showing the shivering threshold calculation.

Table 6.4: body segment shivering weighting factor (Salloum, 2005).

Body segments	Shivering
Upper CHEST	0.515
Lower CHEST	0.3875
HEAD	0.0775
THIGH x 2	0.0039
CALF x 2	0.0017
FOOT x 2	0.0004
UPPERARM x 2	0.0024
FOREARM x 2	0.0014
PALM x 2	0.0001
Fingers x 10	0.00002

$$T_{shiv}$$

$$= \begin{cases} 35.5°\text{C} & for\ T_{core} \leq 35.8°\text{C} \\ -1.0222 \times 10^4 + 570.97T_{core} - 7.9455T_{core}^2 & for\ 35.8°\text{C} < T_{core} < 37.1°\text{C} \end{cases}$$

(6.4)

The total shivering rate is calculated in [Joules/hour] and it is given by the following equation 6.5.

$$M_{shiv} = M_{max,shiv}\left[1 - \left(\frac{T_{skin} - 20}{T_{shiv} - 20}\right)^2\right]\ \ for\ \ (40 - T_{shiv}) < T_{skin} < T_{shiv}$$

(6.5)

The maximum shivering rate can be attained at mean skin temperature around 20°C and is calculated by the equation 6.6 in unit Watts according to the core temperature.

$$M_{max,shiv} = \frac{(-1.1861 \times 10^9 + 6.552 \times 10^7 T_{cr} - 9.0418 \times 10^5 T_{cr}^2)}{3600}\ \ for$$

$$T_{cr} < 37.1°\text{C}$$

(6.6)

All local shivering rates are calculated by multiplying the total shivering rate by the shivering weighting factor provided in table 6.4.

6.3.2 Sweating model

When the core temperature rises, the thermoregulatory system activates the first response which is the vasodilation if it is insufficient the sweating response takes place. The sweating system is modelled as when the core temperature reaches a threshold, it gets activated and gradually increase the sweat with respect to the increase of body temperature until the swearing reaches its maximum limit. This can be resumed as when the core temperature is below the threshold no sweating will occur and once the core temperature exceeds the threshold the body starts to sweat. In addition, the skin

temperature will have an impact on the sweating model by modifying the sweating threshold temperature. The sweating threshold temperature is varying between 36.85°C, below this value, no sweating will occur and 37.1°C above this core temperature sweating will always occur regardless of the skin temperature value. The sweating threshold temperature (eq. 6.7a) correlation and the sweating rate (eq. 6.7b) equation are taken from Salloum (2005) which are based on the work of Bezinger (Salloum, 2005) equation 6.7.

$$T_{sweat} = \begin{cases} 42.084 - 0.15833 * T_{skin} & for \quad T_{skin} < 33.0°C \\ 36.85°C & for \quad T_{skin} \geq 33.0°C \end{cases}$$

(6.7a)

$$m_{sweat} = \frac{45.8 + 739.4(T_{core} - T_{sweat})}{3600} \quad for \quad T_{core} > T_{sweat}$$

(6.7b)

The sweating value m_{sweat} is calculated in [gram/s] and it can reach 0.193[g/s] as the highest value of the sweat rate. The sweating is distributed over the whole body by multiplying the sweat rate by a weighting factor for each body part values stated in table 6.5.

Table 6.5: body segment sweating weighting factor.

Body segment	Sweat factor
Upper CHEST	0.275
Lower CHEST	0.206
HEAD	0.081
THIGH x 2	0.0645
CALF x 2	0.0445
FOOT x 2	0.0175

UPPERARM x 2	0.0444
FOREARM x 2	0.0326
PALM x 2	0.00775
Fingers x 10	0.00155

6.3.3 Blood flow system

The heat transfer is significantly influenced by the rate of blood perfusion. Contrary, to what was described in the two-node model Chapter 5 section 5.2.1 the blood flow is not distributed uniformly in all the body segments. That assumption was taken into consideration in the multisegmented physiology model.

Karaki et al., (2013) modified the arterial branch tree of Salloum et al., (2007) to include the palm and five fingers instead of one block for the hand. Where in multiple studies fingers showed significant importance in the thermoregulation of the human body (Karaki et al., 2013; Rida et al., 2014 a; Salloum, 2005).

The input impedance for each of the 138 arteries is calculated using the Avolio method (Avolio, 1980). Each arterial branch velocity is calculated recursively starting from the aorta using an input/output artery velocity ratio based on impedance. The input waveform of heartbeat with a Fourier series expansion describes the instantaneous periodic velocity of the aorta, with its mean was taken as the average blood velocity out of the heart. Figure 6.3 shows the blood circulatory system representation where the numbers represent the artery index from 1 to 138. The detailed blood flow calculation within the human physiology model showed improvement in the prediction of skin and core temperatures (Karaki et al. 2013, Kobayashi and Tanabi, 2013). This detailed blood flow calculation is not only useful for improving the prediction of skin temperature and consequently thermal comfort, but it can be also a useful

application in medical research. An example of such an application can be predicting blood flow at the extremities in operation rooms.
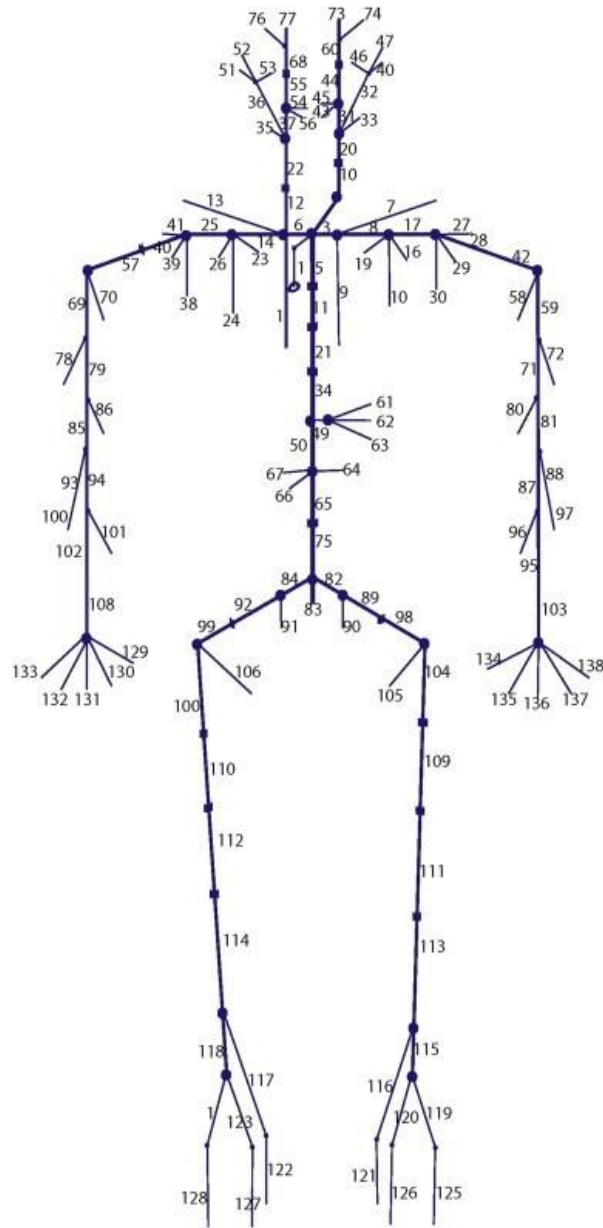
Figure 6.3: The modified Avolio tree as presented in (Karaki et al., 2013).

6.3.3.1 Input Impedance

The following are some assumptions in the blood circulatory model like:

1.The flow is incompressible.

2. The blood behaves as a Newtonian fluid.

3. The blood viscosity is constant.

4. The flow is laminar and fully developed.

5. The flow is axisymmetric.

After taking all the necessary assumption, for a given artery the Navier-stokes equation is 6.8,

$$\frac{\partial^2 w}{\partial r^2} + \frac{1}{r}\frac{\partial w}{\partial r} - \frac{\rho}{\mu}\frac{\partial w}{\partial t} = -\frac{1}{\mu}\frac{\partial P}{\partial z}$$

(6.8)

Where ρ is the density of blood, μ is its dynamic viscosity w is the blood velocity in the z-direction, P is the blood pressure. The pressure is pulsatile with an unknown amplitude A and a frequency defined by,

$$\frac{\partial P}{\partial z} = Ae^{j\omega t}$$

(6.9)

The angular frequency ω is given by

$$\omega = 2\pi\frac{heart\ rate}{60}$$

(6.10)

The analytical general solution of this equation then is:

$$w = \frac{AR^2}{j\mu\alpha^2}\left(1 - \frac{J_0(\alpha y j^{\frac{3}{2}})}{J_0(\alpha j^{\frac{3}{2}})}\right)e^{j\omega t}$$

(6.11)

$$\alpha = R\sqrt{\omega/v}$$ (6.12)

Where R is the radius of the artery, J_0 is a zero-order Bessel function of the first kind, $y = r/R$, and alpha is the Womersley number.

Integrating from $r=0$ to R, the mean axial velocity is obtained as.

$$\bar{w} = \frac{A}{j\mu\alpha}(1 - F_{10})e^{j\omega t} \qquad (6.13)$$

$$F_{10} = \frac{2J_1(\alpha j^{3/2})}{\alpha j^{3/2} J_0(\alpha j^{3/2})} \qquad (6.14)$$

Here the flow and solution are still dependent on an unknown pressure amplitude A.

To get rid of A, the longitudinal impedance is derived as:

$$Z_L = \frac{\partial P/\partial z}{\bar{w}} = \frac{e^{j\omega t}}{\bar{w}} = \frac{j\mu\alpha^2}{R^2}\frac{1}{1-F_{10}} \qquad (6.15)$$

Z_L can now be found with all the parameters known, independent of A.

The characteristic impedance is found and corrected for wall elasticity σ [92].

$$Z_0 = \frac{\rho c_0}{\sqrt{1-\sigma^2}}(1 - F_{10})^{-1/2}[\cos(\emptyset/2) + j\sin(\emptyset/2)]$$

$$(6.16)$$

$$\gamma = \frac{j\omega}{c_0}(1 - F_{10})^{-1/2}\sqrt{1-\sigma^2}[\cos(\emptyset/2)\,j\sin(\emptyset/2)]$$

$$(6.17)$$

$$c_0 = \sqrt{\frac{Eh}{2\rho R}}$$

$$(6.18)$$

$$\emptyset = \emptyset_0(1 - e^{-k\omega})$$

$$(6.19)$$

where k=2, and φ_0=15 deg.

Through equation 6.20, the wave reflection is evaluated at the level of each branch.

$$\Gamma = \frac{Z_T - Z_0}{Z_T + Z_0}$$

(6.20)

Where Z_T is the sum of all previous impedances starting from the terminal backwards (at terminal arteries, Z_T=0.8) summed in parallel is there is bifurcation or summed directly if all the arteries are in series. The input impedance is then expressed as,

$$Z = Z_0 \frac{1 + \Gamma e^{-2\gamma L}}{1 - \Gamma e^{-2\gamma L}}$$

(6.21)

At the terminals, γ assumed = 0.8. However, since additional branches at the hands would increase the impedance, γ is taken 0.975 at the fingers to counter this increase.

6.3.3.2 Blood flow circulation

Once the impedance in all the arteries is calculated, the blood flow is calculated starting from the ascending aorta. The periodic cardiac ejection waveform is expanded into a Fourier series. The flow ratio is the ratio of the mean axial velocity ω at the outlet of an artery to mean axial velocity at its inlet (Salloum, 2005). This ratio is a complex number defined by,

$$\frac{\overline{\omega}_{z=L}}{\overline{\omega}_{z=0}} = \frac{1 - \Gamma}{e^{-\gamma L} - \Gamma e^{-\gamma L}}$$

(6.22)

This ratio is multiplied by the Fourier expansion, and thus the velocity v(t) is found. The flow ratio in each consecutive artery is found by multiplying the preceding flow ratios of the previous arteries all the way to the ascending aorta (artery index 1). Therefore, when this flow ratio is multiplied by the Fourier

expansion, the velocity of the flow with time can be found in each artery. The blood velocity in the vein, unlike the artery, is steady rather than periodic and is taken as the mean velocity of the blood in the corresponding artery.

6.3.3.3 Blood flow regulation

6.3.3.3.1 Cardiac output

The cardiac output does not remain constant at different core body temperatures (Smith, 1991). The cardiac output model (Fu, 1995) only changed within a narrow margin of core temperatures before and after which it plateaued. This was adjusted to account for the variability observed experimentally (Smith,1991) where the cardiac output changes if the core temperature decreases or increases beyond this margin.

The constricted cardiac output is found by eq 6.23,

$$
\begin{cases}
CO_{con} = 290000 & T_{sk} \geq 33.7 \\
CO_{con} = \dfrac{(T_{sk} - 10.7)(290000 - 270000)}{(33.7 - 10.7)} + 270000 & T_{sk} > 10.7 \ and \ T_{sk} < 33.7 \\
CO_{con} = 270000 & T_{sk} \leq 10.7
\end{cases}
$$

$$(6.23)$$

The dilated cardiac output is found by,

$$
\begin{cases}
\qquad CO_{dil} = 427500 \ \ if \ \ T_{cr} \geq 41 \\
CO_{dil} = (T_{cr} - 37.2) * \dfrac{508000.0 - 400000.0}{41 - 37.2} + 400000.0 \ if \ \ 37.2 \leq T_{cr} < 41 \\
CO_{dil} = (T_{cr} - 36.8) * \dfrac{427500.0 - 290000.0}{37.2 - 36.8} + 290000.0 \ \ if \ \ 36.8 < T_{cr} < 37.2 \\
\qquad CO_{dil} = 290000.0 \ \ if \ \ T_{cr} \leq 36.8
\end{cases}
$$

$$(6.24)$$

The total cardiac output is finally determined by,

$$
CO = CO_{dil} \times CO_{con}/290000.0
$$

$$(6.28)$$

The cardiac output calculated using this model is used to find the cardiac index.

6.3.3.3.2 Vaso-constriction and vaso-dilation

The radius of the arteries in the limbs and neck change in correspondence with the change in cardiac output (Smith, 1993), dilating with higher core temperatures and constricting with lower ones. This change becomes important in modelling situations where the body's core temperature changes significantly, and thus should be accounted for. The previous model (Salloum, 2005) which used constant artery radii, which imposed constant blood into each body segment no matter the conditions, was unable to simulate certain situations where the body temperature changed enough to cause a significant increase in skin perfusion such that is exceeded the maximum possible blood flow into the body segment. For this reason, a model was introduced to simulate the dilation and constriction of the arteries in the neck, upper arms, forearms, palms, fingers, thighs, calves, and feet based on the cardiac output.

$$R_a = \sqrt{\frac{(R_{a,max}^2 - R_{a,min}^2) * (CO - 270000)}{(427500 - 270000)} + R_{a,min}^2}$$

(6.29)

R_a is the radius of the artery, $R_{a,min}$ is the maximum constricted radius of the artery, and $R_{a,max}$ is the maximum dilated radius of the artery. The impedance and blood flow calculations were then repeated at each time step in the model.

6.3.3.4 Skin blood perfusion

The skin perfusion is calculated using the method outlined in (Salloum, 2005). The mass blood flow rate in the skin is described by,

$$\dot{m}_{bl_{skin}} = \frac{\dot{m}_{bl_{skin_{Dil}}} \times \dot{m}_{bl_{skin_{Con}}}}{\dot{m}_{bl_{skin_{Bas}}}}$$

$$(6.30)$$

$$\dot{m}_{bl_{skin_{Dil}}}$$

$$= \begin{cases} \dot{m}_{bl_{skin_{Bas}}} & for \quad T_{cr} \leq 36.8°C \\ \dfrac{T_{cr} - 36.8}{37.2 - 36.8}\left(\dot{m}_{bl_{skin_{Max}}} - \dot{m}_{bl_{skin_{Bas}}}\right) + \dot{m}_{bl_{skin_{Bas}}} & for\ 36.8°C < T_{cr} < 37.2°C \\ \dot{m}_{bl_{skin_{Max}}} & for \quad T_{cr} \geq 37.2°C \end{cases}$$

$$(6.31)$$

$$\dot{m}_{bl_{skin_{Con}}}$$

$$= \begin{cases} \dot{m}_{bl_{skin_{min}}} & for \quad T_{skin} \leq 10.7°C \\ \dfrac{T_{skin} - 10.7}{33.7 - 10.7}\left(\dot{m}_{bl_{skin_{Bas}}} - \dot{m}_{bl_{skin_{min}}}\right) + \dot{m}_{bl_{skin_{min}}} & for\ 10.7°C < T_{skin} < 33.7°C \\ \dot{m}_{bl_{skin_{Bas}}} & for \quad T_{skin} \geq 33.7°C \end{cases}$$

$$(6.32)$$

Basal, maximum, and minimum skin blood flow rates are calculated from Fu (1995) based on the volumetric cardiac output blood flow.

6.3.3.5 AVA modelling

In the peripheral body segments (forearms, palms, fingers, calves, and feet), some veins run close to the skin, which is called the superficial veins, as well as direct connections or shunts between the arteries and veins these veins known as arteriovenous anastomoses or AVA. This physiological phenomenon is most likely to be seen in a very hot and very cold environment. The thermo-physiological reaction to a cold environment is to preserve the body from losing heat, and in a hot environment, it increases heat loss from the body. In the limbs, the heat loss is increased because of the AVA blood flows in the superficial veins. But in the cold environment, the body reduces heat losses and that due to the vasoconstriction of arteries and the closure of AVA (Arens et al., 2006; Daanen, 1991; Takemori, 1995). Although this theses concerns about the indoor building occupant where the thermal environmental conditions are usually neutral. Including the AVA in the multi-segmented model allows it to be used either for indoor or outdoor simulations.

The AVA model was developed by (Takemori et al., 1996). The skin blood flow which includes both the skin perfusion and the AVA blood flow is calculated by,

$$\dot{V}_{bl,sk} = \dot{V}_{bl,sk,max} AVA \tag{6.33}$$

where $V_{bl,sk,max}$ is the maximum skin blood flow rate [ml/min], and AVA is a coefficient from 0 to 1 that depends on the extent that the AVA's are open.

$$\dot{V}_{bl,sk,max} = V_{limb} \cdot \frac{f_{skin,ave}}{100}$$

$$\tag{6.34}$$

V_{limb} is the volume of the limb (hand, foot, lower arm, etc.) in cm^3, and $f_{skin,ave}$ is the maximum skin blood flow in limb in [ml/min] per 100ml tissue, and is usually 30 [ml/min] in 100[ml] tissue.

The AVA coefficient to core and skin temperature relationship is,

for the hands

$$AVA = 0.265(T_{sk} - 34) + 0.953(T_{cr} - 36.8) + 0.9126$$

$$\tag{6.35}$$

for the feet

$$AVA = 0.265(T_{sk} - 35.4) + 0.953(T_{cr} - 37) + 0.9126$$

$$\tag{6.36}$$

if   AVA $\geq$ 1,   AVA=1

if   AVA $\leq$ 0,   AVA=0
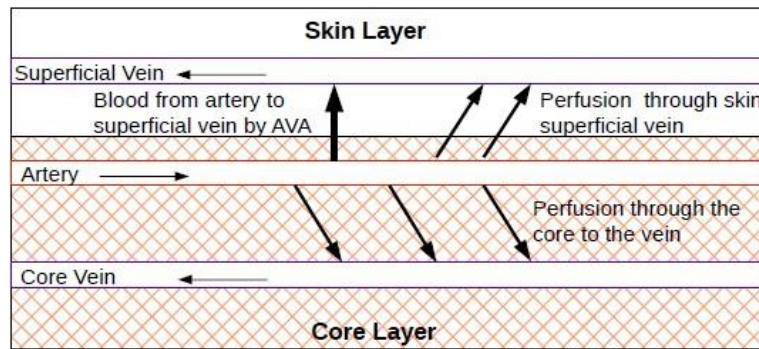
Figure 6.4: Flow of blood through a peripheral body segment (Karaki et al., 2013)

6.3.3.6 Blood flow in the body segments

Blood comes in through the artery to the body segment. The blood returning through core vein is assumed to be the combination of blood from the previous vein and the blood coming in through perfusion from the core. In terminal body segments where there are superficial veins, the blood returning through the superficial vein is the blood from the previous superficial vein and from the artery by blood perfusion through the skin and also through direct connection with the AVA.

The body segments which contain the superficial vein node are:

- All 10 digits of the hand

- Palms

- Forearms

The flow in the veins in these peripheral body segments are calculated as follows,

1.The total perfusion is found in a segment by subtracting the mean inlet and the outlet blood flow rate in the arteries.

2.Skin perfusion is found through Smith's model using equation 6.31 (6.28). AVA model is used to find the total blood flow to the skin layer which includes skin perfusion and blood through the AVA.

3.Core perfusion is calculated by subtracting the total skin perfusion, including AVA from the total perfusion.

4.The flow in the regular core vein and the superficial vein are defined respectively

as,

$$\dot{m}_{vein} = \dot{m}_{prev,vein} + \dot{m}_{perf,cr}$$

(6.37)

$$\dot{m}_{s,vein} = \dot{m}_{prev,s,vein} + \dot{m}_{perf,sk} + \dot{m}_{AVA}$$

(6.38)

5.Blood flow of the previous vein (both core and superficial) for the terminal body segments (fingers and feet), and is considered zero.

6.4 Heat transfer model (Energy Balance Equations)

6.4.1 Core node

Using lumped capacitance, there are five nodes for the energy balance in each segment. The nodes are: core, skin, artery, core vein, superficial vein.

$$C_{cr}\frac{dT_{cr}}{dt} = M_{cr} + M_{shiv} - W - \alpha Q_{res} - Q_{cr-sk} - \sum_{arteries} h_{artery}A_{artery}(T_{cr} - T_{bl,a})$$
$$- \sum_{veins} h_{vein}A_{vein}(T_{cr} - T_{bl,v}) + \dot{m}_{perf,total}c_{bl}(T_{bl,a} - T_{cr})$$

(6.39)

C_{cr} is the thermal capacitance for each body segment M_{cr} and M_{shiv} are the basal and segmental thermoregulatory shivering metabolic rate respectively. W is

136

the mechanical work done by the body. α is a coefficient which is 1 for the chest and zero for all other body parts, and Q$_{res}$ is the heat dissipated through respiration. Q$_{cr-sk}$ is the heat exchange between the core and skin through contact resistance. $Q_{cr-sk} = K\ (T_{cr} - T_{sk})$ h$_{artery}$ and h$_{vein}$ are the convection coefficients of the blood in the artery and core vein respectively.

A$_{artery}$ and A$_{vein}$ are the cross-sectional area of the artery and core vein respectively. T$_{bl,a}$ and T$_{bl,v}$ are the temperatures of the blood in the artery and core vein respectively. $m_{perf,cr}$ is the blood perfusion in the core only (i.e. total perfusion skin perfusion) c$_{bl}$ is the specific heat constant of blood.

6.4.2 Skin node

Despite the assumption of lumped capacitance, there is a difference between the temperature of the skin at the surface exposed to the surroundings and the temperature which is in the middle of the skin node. For this reason, and to increase accuracy in the skin temperatures calculated the following correction to find the surface skin temperature is used.

$$T_{sk,sur} = 2\mathrm{T}_{sk} - T_{cr}$$

$$(6.40)$$

$$C_{sk}\frac{dT_{sk}}{dt} = M_{sk} + Q_{cr-sk} - A_{sk,\exp}[h_c(T_{sk,sur} - T_{amb}) + h_r(T_{sk,sur} - \bar{T}_{amb}) +$$
$$h_e(P_{sk} - P_{amb})]$$
$$+\dot{m}_{perf,sk}c_p(T_{cr} - T_{sk}) + \sum_{veins} h_{vein,s}A_{vein,s}(T_{bl,v,s} - T_{sk})$$

$$(6.41)$$

C$_{sk}$ is the skin thermal capacitance for each body segment. M$_{sk}$ is the metabolic rate in the skin h$_c$ is the external convection heat transfer coefficient between the skin and the atmosphere h$_r$ is the radiation transfer coefficient h$_e$ is the evaporation coefficient deducted from h$_c$ by Lewis formula. T$_{sur}$ is the surroundings radiant temperature, P$_{amb}$ is the ambient vapour pressure P$_{sk}$ is the skin vapour pressure $h_{vein,s}$ is the convection heat transfer coefficient of

blood in the superficial vein $A_{vein,s}$ is the cross-sectional area of the superficial vein $\dot{m}_{perf,sk}$ is the blood perfusion in the skin layer

6.4.3 Artery node

$$C_{bl,a} \frac{dT_{bl,a}}{dt} = -\sum_{arteries} h_{artery} A_{artery}(T_{bl,a} - T_{cr}) + \dot{m}_a c_{bl}(T_{a,adjacent} - T_{bl,a})$$

(6.42)

$\dot{m}_a$ is the blood flow rate through the artery $T_{a,adjacent}$ is the temperature of the blood in the adjacent artery of the previous body segment.

6.4.4 Vein node

$$C_{bl,v} \frac{dT_{bl,v}}{dt} = -\sum_{veins} h_{vein} A_{vein}(T_{bl,v} - T_{cr}) + \dot{m}_v c_{bl}(T_{v,adjacent} - T_v)$$
$$+ \dot{m}_{perf,cr} c_{bl}(T_{cr} - T_v)$$

(6.43)

$\dot{m}_v$ is the blood flow rate through the vein, $T_{v,adjacent}$ is the temperature of the blood in the adjacent core vein of the previous body segment.

6.4.5 Superficial vein node

$$C_{bl,v,s} \frac{dT_{bl,v,s}}{dt} = -\sum_{veins} h_{vein,s} A_{vein,s}(T_{bl,v,s} - T_{sk}) + \dot{m}_{v,s} c_{bl}(T_{v,s,adjacent} - T_{v,s})$$
$$+ \dot{m}_{perf,sk} c_{bl}(T_{sk} - T_{v,s}) + \dot{m}_{AVA} c_{bl}(T_{bl,a} - T_{v,s})$$

(6.44)

$\dot{m}_{perf,sk}$ is the blood perfusion in the skin layer without AVA.

$\dot{m}_{AVA}$ is the blood flow due to AVA, i.e. skin blood perfusion calculated by Takemori minus $\dot{m}_{perf,sk}$.

6.5 Code structure and algorithm

The multi-segment human thermal model was implemented with ESP-r. All the data required for the model like body parameters, all sweating shivering and blood coefficients were stored in a database file. The model needs inputs defined by the user like the metabolic rate and the clothing insulation level. Clothing ensemble predefined in the model as databases are either summer or winter clothing distribution with total values of 0.5 and 0.9 clo respectively.
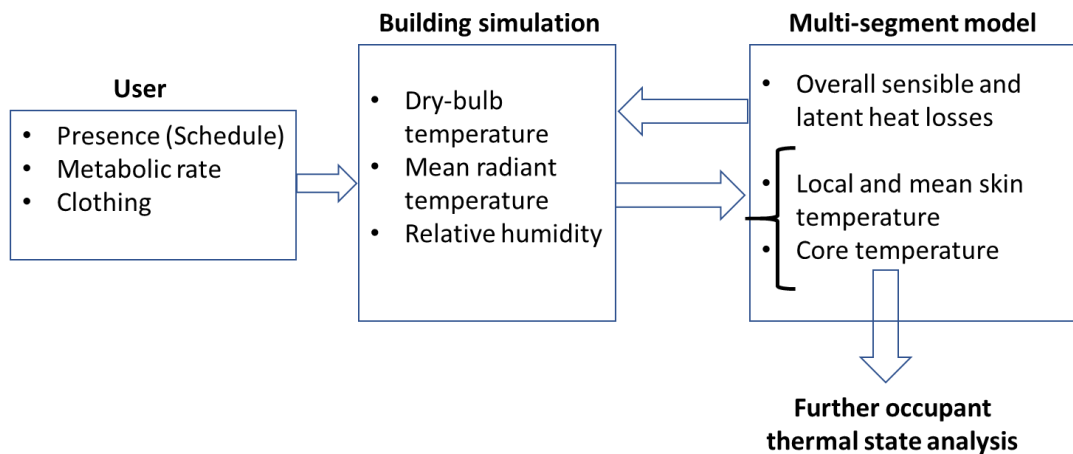
Figure 6.5 Data exchange between building simulation and the multi-segment model

The environmental parameters required are passed from the ESP-r building simulation or from the integrated ESP-r CFD calculation which will be described in Chapter 7. Figure 6.5 presents the data exchange between the building simulation and the multisegmented model. Air dry bulb temperature, mean radiant temperature (in the middle of the room, unless a sensor location is defined /place of the occupant in CFD simulations) relative humidity are passed every time step.

For the stability of the model, especially for accurate blood flow calculation the multi-segmented physiology model run on a smaller time step compared to the building simulation time step. The physiology model runs on the same environmental parameters for the period of the building simulation time step. For example, if the time

step in building simulation is set to 15 minutes, the physiology model will run for a duration of 15 minutes on the same environmental condition. The smaller time-step in the physiology model is required for an accurate blood flow calculation since it is based on the cardiac-outputs. This has seen to be computational time consumer, especially when assessing yearly simulation. As an example, the time required for a one year-simulation has been increased around 15-20 times compared to a simulation without calling the physiology model.

Figure 6.5 is a flow chart summarizing the logical steps of the mathematical model and all the inputs. The model has two loops every time the subroutine is called, the first loop is over the body segments and the second one is over the simulation phase time which is same as the building simulation time step. After the model finished the calculation, the final nodes temperatures are stored to be used in the next time the subroutine is called. Later the predicted skin and core temperatures can be linked to a detailed thermal sensation and comfort analysis such as Zhang (2003) model to describe the occupant thermal perception.

The model is written in Fortran language although it is fully merged with ESP-r, the model can be easily transferred and used in different building simulation tools.
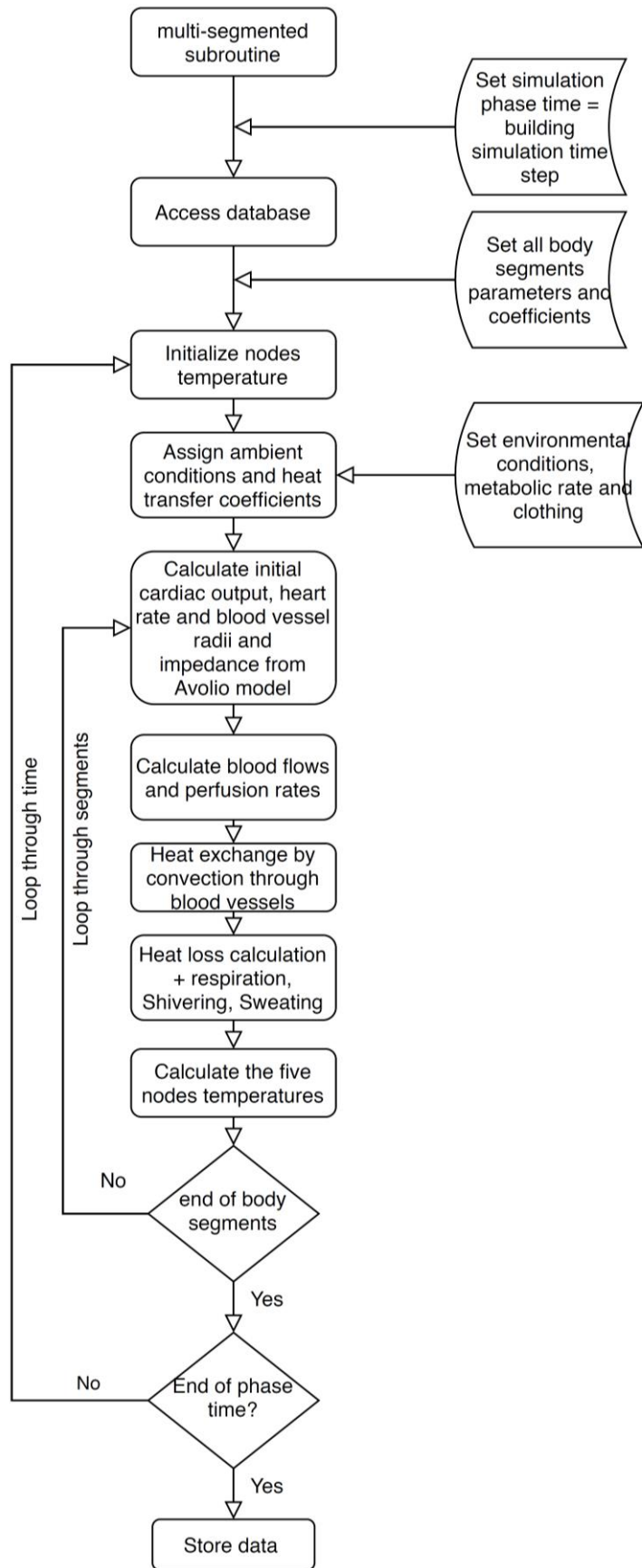
Figure 6.5 Flow chart of the multi-segmented human thermo-physiology model.

6.6 Conclusion

The main equations used in the multi-segmented human thermo-physiology was presented in this chapter. The model is very detailed, it segments the body into 25 segments and it accounts for a detailed calculation of the blood flow. The model subroutine is already submitted to the final release of ESP-r. the model is linked to the building simulation similar to the two-node human thermal model, the multi-segmented model gives a detailed projection of how local comfort is likely to be to a certain thermal environment. To that extent, the environmental parameters around the human body should be set to be at an equal level of details and information exchange. For that reason, in the following chapter, the linking and the use of the multi-segmented model with ESP-r's integrated CFD calculation is presented.

Chapter 7: Multi-segmented Model Integrated with CFD

7.1 Chapter overview

As previously discussed, using the well-mixed air node temperature predicted in ESP-r's simulator with an airflow network (Hensen, 1991) with a multi-segmented physiology model does not give the full functionality of the detailed human thermo-physiology model. Even though, it can provide more detail about each segment of the human body.

The nodal network approach has some limitations with regards to indoor thermal comfort and air quality. Since it neglects the momentum effect, the air movement within a space cannot be studied. With such low-resolution, local surface heat transfer is usually accounted for by empirically-derived coefficients. Further, assigning the local environment for each body parts is not possible as there is only a single air temperature.

The integrated computational fluid dynamics (CFD) solver within ESP-r can give detailed information about the local environment inside a zone, and consequently around the human body. The CFD tool calculates the intra-zone airflow, convective heat transfers and temperature variation, whilst ESP-r's building-plant solver (BPS) computes surface temperatures, radiant exchanges, etc. Figure 7.1 a schematic of the integration and the information passed from each model.
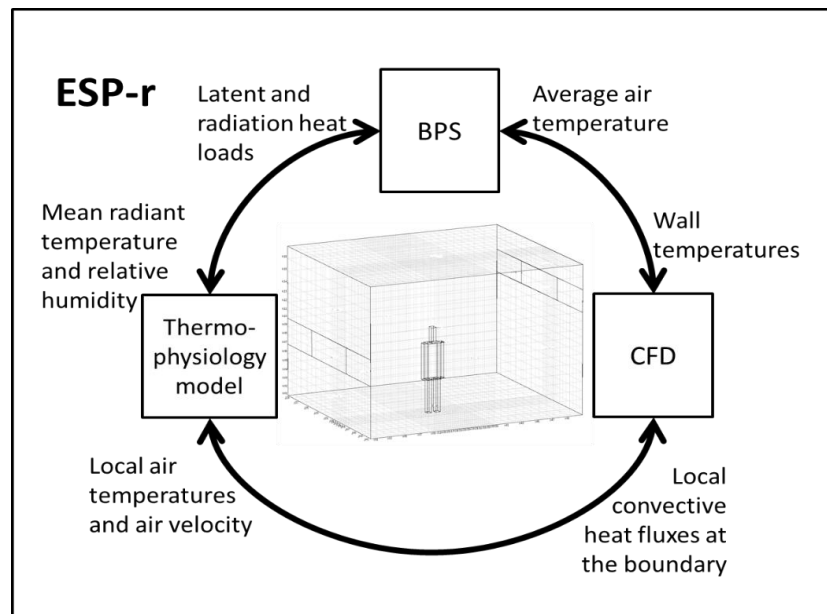
Figure 7.1: BPS-multisegmented-CFD representation and data passed.

This chapter describes the method of integrating the detailed multi-segmented model described in chapter 6 with the ESP-r's BPS and its integrated CFD domain.

The capability of the integration of the detailed occupant model is demonstrated using examples of natural and displacement ventilation.

7.2 Methodology

7.2.1 CFD in ESP-r

CFD has been widely and effectively applied in the prediction of room air motion. It usually demands high computational requirements, which has generally restricted simulations to single rooms and domains within buildings. The boundary conditions supplied by the user play a major role in the accuracy of prediction results in a simulation. With the advances of computational power, these issues started to end gradually.

Negrao (1995) integrated a CFD code into ESP-r, by using the handshaking (a term in ESP-r describe the method of data exchange between the two solvers

multi-segmented model integration with ESP-r's CFD domain energy simulation and CFD) which allows the two modelling domains to interact on a time-step basis. That approach in ESP-r eliminates the requirement of explicitly define the boundary conditions as the boundary conditions are determined dynamically by the building thermal simulation. The approach was expanded by Beausoleil-Morrison (2000), who implemented the adaptive conflation controller (ACC). The controller automated the process of passing the boundary conditions from the building simulation to the CFD on a time-step basis and sending back the resultant heat flux to building simulation. The handshaking mechanism can be defined as "one-way" or "conditional two-way". The one-way mechanism is appropriate when the objective of the study is to predict the flow and temperature field within the room, visualising the flow inside the room, evaluating thermal comfort of the occupant or studying the dispersion of contaminants. In addition to the tasks performed with the one-way mechanism, the two-way mechanism can enhance the thermal simulation by providing surface convection estimates for the thermal domain (Beausoleil-Morrison, 2002).

The combined building simulation/CFD simulation develops a clear prediction and detailed temperature and airflow distribution within a defined zone of a building. The outcomes of such integrated simulations are normally used to show a detailed flow visualisation, to study pollutant spreading, for detailed thermal comfort assessments or to improve ventilation systems by looking at the heat transfer within the internal building surfaces.

ESP-r's CFD model shares much in common with other CFD codes that have been used for modelling room airflow. Flow inside a room is characterized by a set of time-averaged conservation equations for the three-dimensional velocities (U, V, W), temperature and concentration. It contains seven coupled partial differential equations. The velocity distribution of the room flow is obtained from the three momentum equations conforming to the three spatial axes. It uses the SIMPLEC (Semi-Implicit Method for Pressure Linked Equations) pressure-correction solution approach. It is finite-volume based and employs a three-dimensional, Cartesian grid. The turbulent diffusion of heat and momentum is estimated with

the widely applied standard $k - \varepsilon$ model, while log-law wall functions are used to account for viscous effects in the near-wall regions (Beausoleil-Morrison 2000; Clarke 2001; Clarke et al. 2011). To model the complex motion some advanced techniques with various level of complexity and computational capacity have been developed. Methods like the direct numerical simulation and the large-eddy-simulation, attempt to model with little or no assumptions the details of the turbulent fluctuations. But that requires finer grids, and it increases the computational costs dramatically (Blocken et al., 2010).

The CFD solver in ESP-r can be defined to be undertaken at every time step where the boundary conditions are updated dynamically. An advantage of this simulation technique in ESP-r has been taken to link the detailed human physiology model. The reason behind the selection of the CFD solver in ESP-r to implement the detailed human thermal model was because the CFD solver with ESP-r provides dynamic boundary conditions, it is tested and validated, also it is acceptable in solving most indoor simulation problems.

7.2.2 Integration of Multi-segment Occupant Model Into ESP-r

A flow domain in CFD is the volume in which the flow takes place. The walls of a room define the boundaries of the CFD domain.

Defining a blockage in ESP-r is a way to represent an object that blocks the airflow inside the domain. In addition, in ESP-r, blockages in a CFD domain can have heat fluxes defined at its boundaries, that can represent an object with a source of heat like a computer, machine or even an occupant. The convective heat fluxes are fixed values defined by the user.

For the approach described in this chapter, the blockages method has been adapted to represent the human body physically inside the CFD domain. Alongside the conflation method, the boundary conditions around the human body representation surfaces are dynamically updated. The two models CFD and

multi-segmented model integration with ESP-r's CFD domain Human physiology communicate every time step and exchange data. The human physiology model receives from the CFD solver the average air temperature and velocity around each block (body part) and update the convective heat fluxes at the boundaries of blockages in the CFD domain. Figure 7.1 shows the data passed between the three

7.2.3 A Method of integrating the dynamic human thermal model with CFD

As described in chapter 6, the multi-segmented model can run with BPS by having a uniform dry bulb and radiant temperature around the human body (around the 25 segments). First the number of occupants in addition to their metabolic rates and clothing level needs to be defined in the specified zone schedule file, BPS calls the multi-segmented occupant model by sending the environmental parameters dry bulb temperature radiant temperature and relative humidity considering air velocity constant and equal to 0.1 [m/s] in order to get an updated convective radiative and latent heat loads from the occupant.

As it has been described before a multisegmented occupant model can be more suitable with a CFD simulation aiming to increase the resolution of the simulation. Where a CFD solution provides details as

The occupant geometry needs to be defined in the domain, for simplicity the 25-body segment in the physiology model has been simplified and grouped into six body parts in the CFD domain. We found that applying this simplification is acceptable since it accounts for the environmental distribution.

The boundary conditions at the occupant body surfaces are linked to the heat fluxes calculated from the multi-segment dynamic model. Every block defined as a human body part the average air temperature and air velocity around it is being calculated from the adjacent non-blockage cells. Figure 7.2 a schematic of a block in the CFD domain and the considered surrounding cells.

$$if\ (i,j,k)\ is\ a\ blockage$$

$$read\begin{cases}Ta_{(i-1,j,k)}\\va_{(i-1,j,k)}\end{cases}$$

$$read\begin{cases}Ta_{(i,j-1,k)}\\va_{(i,j-1,k)}\end{cases}$$
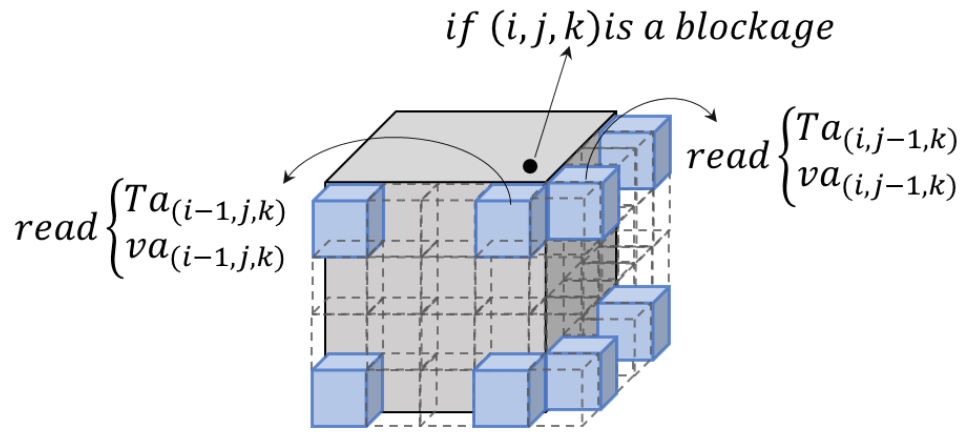
Figure 7.2 Average local temperature and air velocity calculation.

$$T_{a,body\ seg} = \sum_{i=1}^{i=n}\frac{Ta_{i,j,k}}{n} \tag{7.1}$$

The dynamic human thermal model is being run with the building simulation bps where the environmental conditions are the room well-mixed air temperature, mean radiant temperature and relative humidity. Those results considered as initialization boundary conditions at the first CFD simulation iteration.

When CFD start for the first time step the human body boundary conditions are taken from the previous time step, once the CFD reaches a converged solution, an average temperature around each body part is passed back to each corresponding body part in the human thermal model. The average local temperature and air velocity were calculated, see figure 7.2. Where for every block representing a body part the temperatures and velocities of the immediate cells around it are averaged. For the rest of the CFD model, heat fluxes are updated each time step considering the variation in temperature near each body part.

When specifying a reasonable small time-step, this approach is acceptable in indoor conditions where it is very rare to have a sudden change in room temperature in such case there will be a short delay in assigning the real boundary conditions from the body.

Such a linking technique allows to model multiple occupants inside a domain, each with different body mass, body surface area, clothing and activity level.

7.2.4 Body parts representation in CFD

As previously explained, the blockage in a CFD domain can be used to represent the human body. Although the cuboid shape has limitation particularly when studying the flow in detailed level around the skin as near the face and very close to the skin, but based on the literature it is considered acceptable especially for airflow calculations inside a CFD domain [Villi et al. 2014; Zelenský et al. 2013].

As previously mentioned, the 25-body segment physiology model presented in chapter 6 has been grouped into six groups. Each group was represented in a cuboid block inside the CFD domain. the body parts were grouped as follow:

- head: represent the head body segment.
- chest: represent the upper and lower chest body segments.
- left arm: represent the left upper and lower arm, palm and the 5 fingers.
- right arm: represent the right upper and lower arm, palm and the 5 fingers.
- left leg: represent the left thigh, calf and foot.
- right leg: represent the right thigh, calf and foot.

The area of the defined blockages needed to be in consistence with the human body surface area defined in the physiology model with a total of around $1.8m^2$. That requires a discreet complex grid structure at the location of the human inside the domain.

Figure 7.3 describes the grouped body part representation in the CFD domain and shows the parameters passed from each solver. The averaged environmental parameters calculated around each body segment is passed and considered the same for all the body segments in the corresponding group.

Receives
• Average local
  air temperature

• Average local
  air velocity

Receives
• heat fluxes
  from each
  body group

Multi-segmented model

Representation in CFD
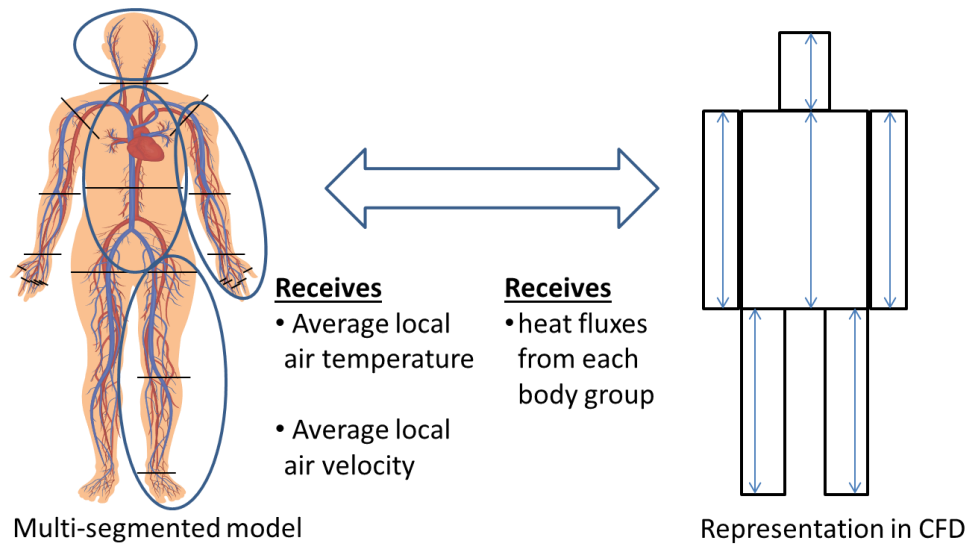
Figure 7.3: the cuboid human body in CFD

7.2.5 Updating boundary conditions around the blockages

Figure 7.1 presented earlier shows the parameters passed between the three solvers building simulation- physiology model-CFD. From the CFD simulation six averaged air temperatures and air velocity around the represented human surfaces are passed to the physiology model, the multisegmented human thermal model receives the mean radiant and relative humidity from BPS. The convective heat fluxes calculated from the multisegmented model are distributed around the blockages.

Figure 7.3 shows the flow chart of the integrated multi-segment model within ESP-r. The flow of the model can be described as follow:

- Starting from the file that holds information about the occupant schedules and internal load description, the model check whether there are occupants in the room or not. It also checks if the dynamic occupant is activated by sending the corresponding flag.
- The multisegmented model is being called at each time step if the occupant number is greater than zero, just before accounting for the internal loads in the energy balance equation in the energy simulation in BPS.

- All the current required environmental parameters sent to the multisegmented human model in order to get the heat fluxes.

- The multi-segmented model reads the body data from the database (body segments mass, area, basal metabolic and blood flow, etc.) which currently correspond to an average adult aged person. The metabolic rate and clothing insulation level are updated every time step (hour/ sub-hour) from the operation file.

- Another flag is set for the CFD simulation, if the human is physically defined in the CFD domain, the multisegmented model receives the local environmental conditions from the CFD solution, if not, it takes the environmental parameters from the building simulation as well mixed air for all body parts.

- Results from the multi-segmented model later considered as internal loads from occupant for the next step or updating convective heat flux around the blockages in the CFD domain.

- The radiation heat exchange is considered in the energy building simulation part between the human and the surrounding surfaces. In ESP-r the mean radiant temperature MRT can be calculated from a defined MRT sensor by defining a location inside the room, but to generalize, the human was always defined in the middle of the room. The latent heat load is always linked to the building simulation unless a source of (contamination) vapour is defined in the CFD domain.
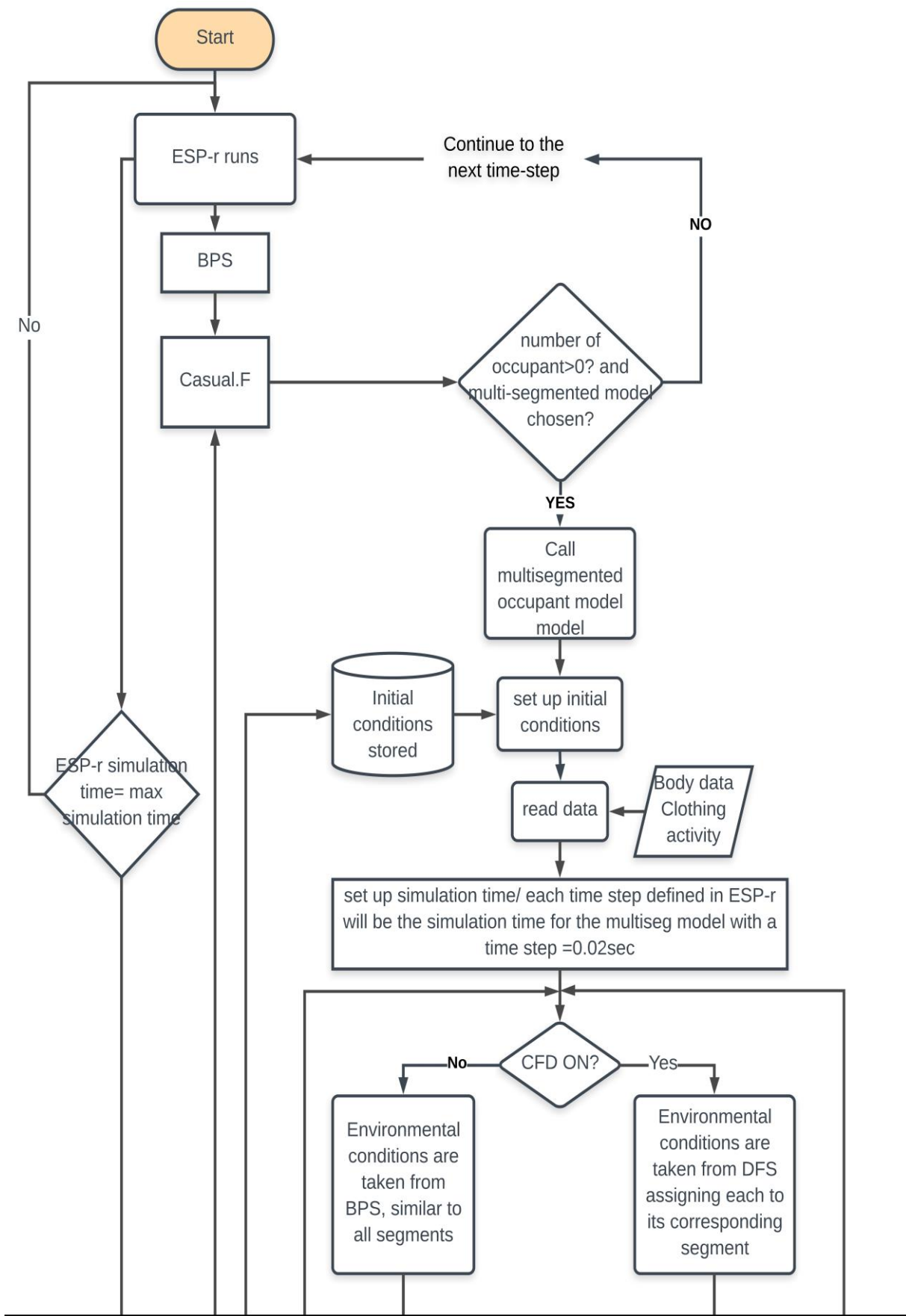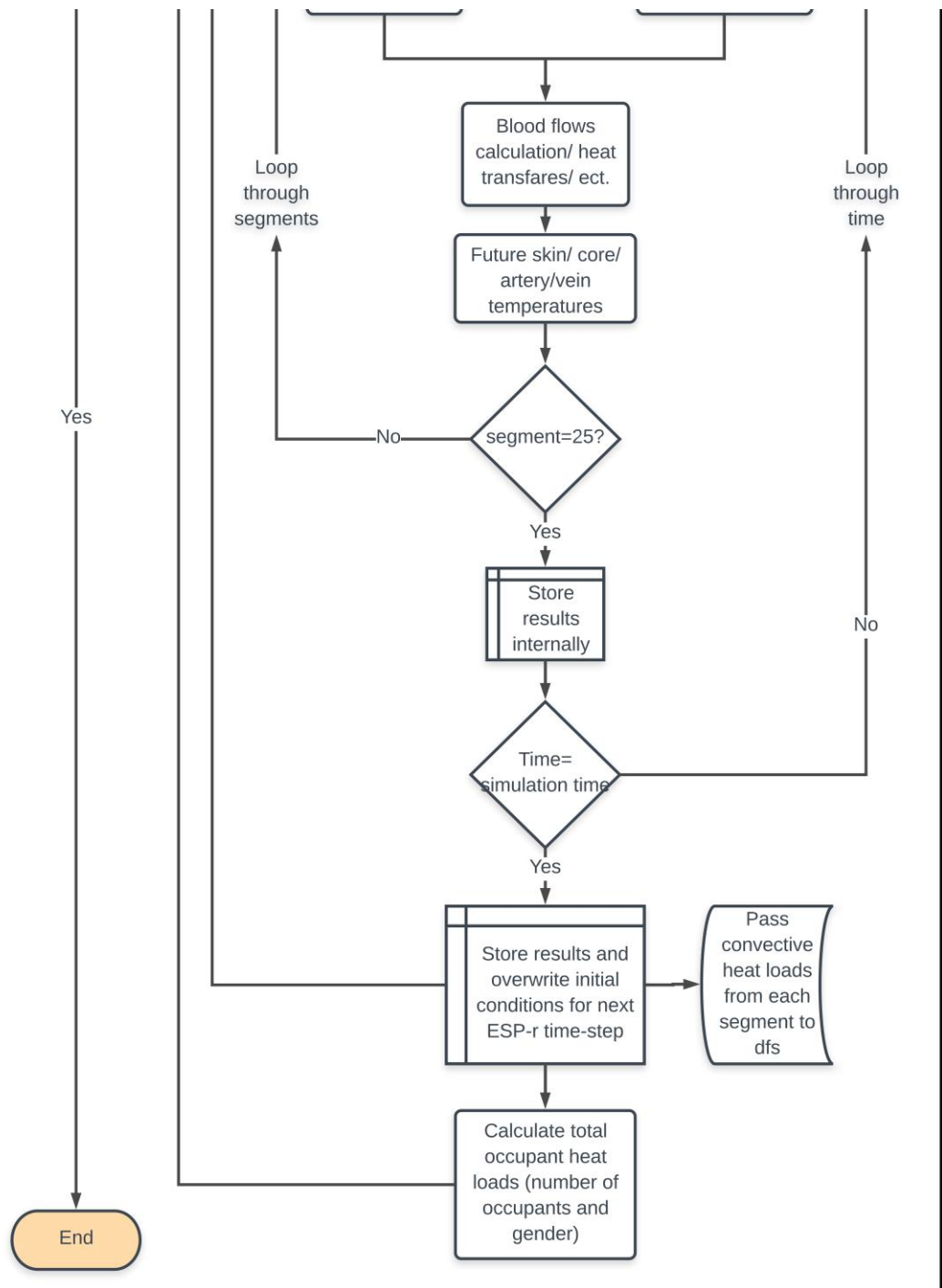
Figure 7.3: Flowchart of the integrated multi-segment within ESP-r

7.3 Simulation and Results

7.3.1 Validation with the manikin benchmark experiment

A benchmark test was set by Nielsen et al., (2003) for a CFD simulation with a manikin standing in the middle of the room. The benchmark came after the experiment conducted by Kato and Yang (2006) to study the fluid flow around the manikin. This simulation case attempts to reproduce the benchmark described by Nielsen et al. (2003). The room has dimensions 3m width x 3.5m depth x 2.5m height. The room has an inlet in the bottom of the east wall with dimension 0.2m x 0.4m and an outlet in the top of the opposite wall of 0.3m x0.3m. The boundary conditions of air entering the room were 21.8°C inlet temperature and average velocity of 0.182[m/s]. The measurements of air velocity and temperature were made at various locations; four vertical poles were set two in front of the manikin and two behind it, the temperature is measured at seven different heights while velocity was taken at six different heights. The velocity above the head was also monitored by using the particle image velocity (PIV). Figure 7.4 illustrates the computational domain of the benchmark described in (Nielsen et al., 2003). The figure shows the representation and the dimension of the room with the supply and exhaust openings, the room dimensions where manikin was placed in the middle of the room. Figure 7.5 shows the location of the four poles in the room, two poles are in front of the manikin, one close to the manikin the second close to the wall and the inlet opening, the other two were behind the manikin one immediately behind the manikin the second was near the wall which consisted the outlet opening. There were a slightly different between the experimental and the benchmark set up especially for the supply air velocity and temperature. For the purpose of comparison, the values from the experiment of air velocity and temperature at the supply opening have been considered.
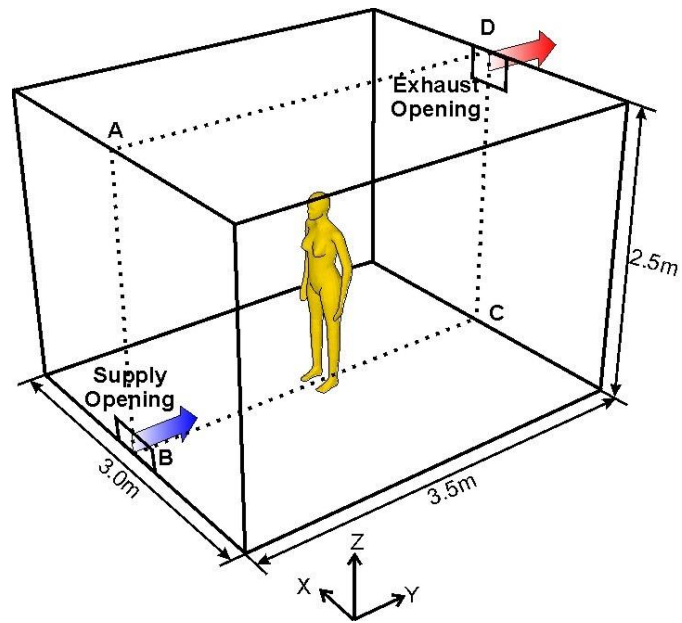
Figure 7.4: Sketch of the benchmark displacement ventilation case (Nielsen et al., 2003)

The benchmark set a total heat loss from the manikin to the surrounding of 76 [W] of sensible load without mentioning the ratio or the portion of what is convection and radiation. Walls were considered adiabatic in the benchmark which could have some implication on results, as heat transfer from wall typically has a significant effect on room airflow.
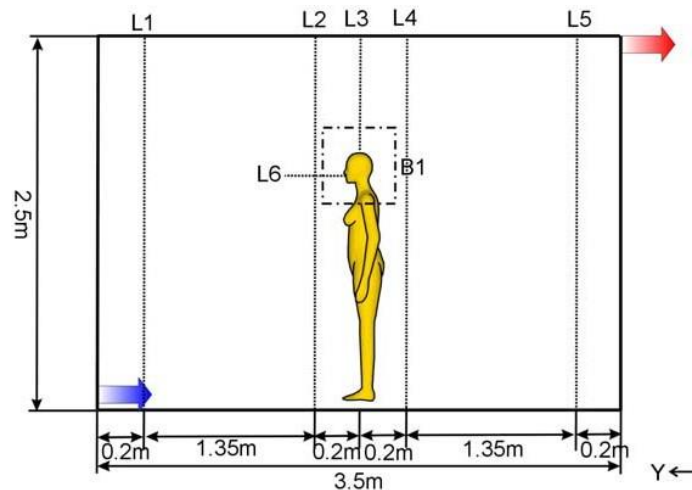
Figure 7.5: Sketch of the benchmark vertical measuring pole (Nielsen et al., 2003)

155

7.3.1.1 Integrated BPS-Physiology-CFD Simulation

The CFD domain grid consisted of rectangular structured mesh with cell dimensions approximately 0.03m around the human body and about 0.1m in other regions of the room. As described in section 7.2 ESP-r CFD uses an orthogonal grid it is necessary to represent the occupant body shape in a rectangular form. As described in subsection 7.2.4 The level of complexity of the body geometry has been considered by representing the human body by six blockages cuboids representing the head, torso, left and right arms and legs. The total number of cells was 81,000. To study the effect of increasing the meshing number on the results, another simulation case with 135,252 of a total number of cells has been conducted. Figure 7.6 shows the CFD domain in ESP-r first (a) with the low resolution the second (b) with a higher resolution. The defacto standard k-ε mode turbulence model was used in the simulations. Buoyancy was modelled using the Boussinesq approximation with a reference temperature of 24°C. The convergence criterion was of a maximum residual value of 10^{-3}. Simulations were performed with two-time steps per hour, on a computer with the Ubuntu operating system with a 6 GB RAM Memory and 3.60 GHz CPU. The human body represented in the room using the six blockages approaches the body surface area used in the simulation are given in table 7.1.

(a) 81,000 cells   (b) 135,252 cells
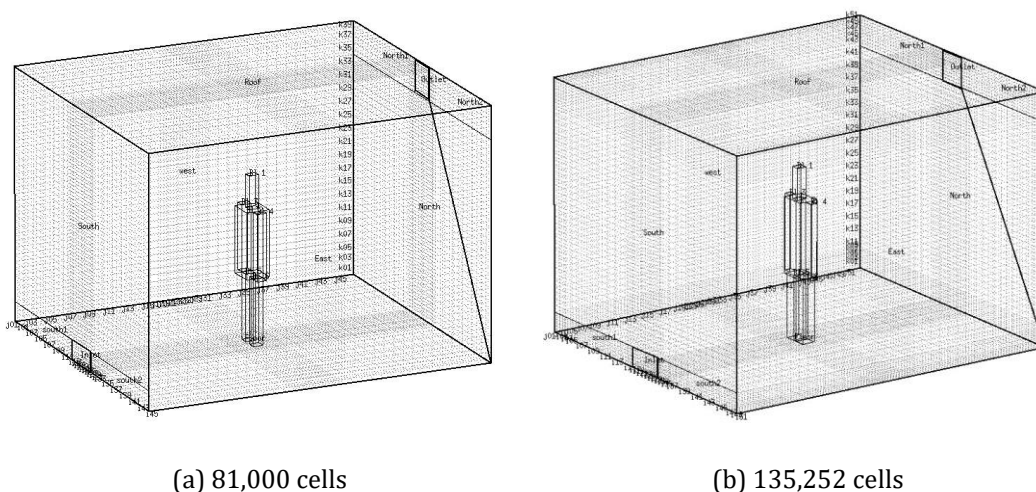
Figure 7.6: CFD domain setup with the occupant geometry.

Table 7.1: Body part surface area used in the simulation

Body Part	area [m^2]
Head	0.123
Trunk	0.6
One Arm	0.245
One Leg	0.31
Total	1.833

7.3.1.2 Results

The published experimental data and its description did not provide any accuracy or measurement error to be considered. For this reason, a qualitative comparison between the experimental and simulated results of both air velocity and temperature of the four poles has been done. The graphs 7.7 to 7.14 shows the comparison of the result between the measured data from Kato's published experiment and the simulated ones of the two meshing cases.

Figures 7.7, 7.8, 7.9 and 7.10 has the comparison of air velocity distribution over the poles one, two, four and five consecutively. Where the first two pols were in front of the manikin and two behind as figure 7.5 shows. The two sets of data represent the model prediction at low (a) and higher (b) meshing resolution where (a) has meshing discretized into 81,000 cells and (b) has 135,252 cells. Figures 7.11, 7.12, 7.13 and 7.14 shows the air distribution over the four poles and for the two-simulation resolution.
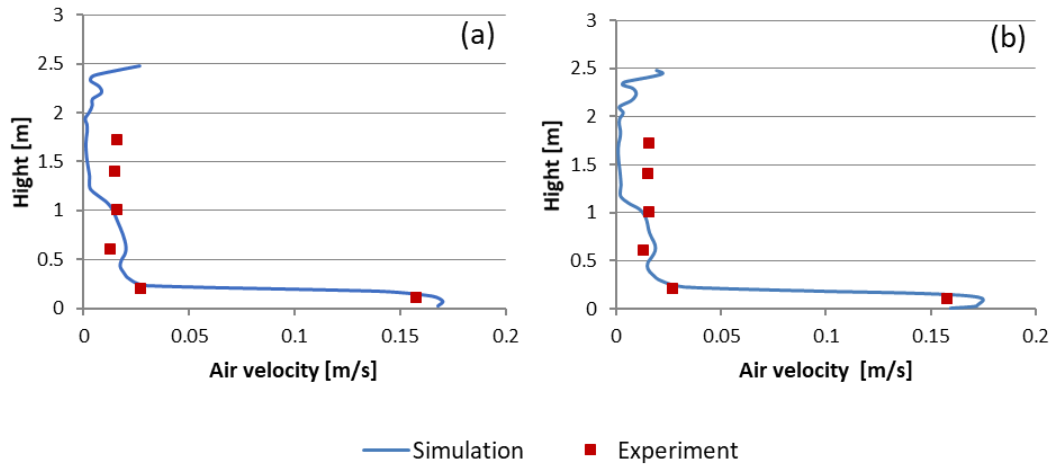
Figure 7.7: air velocity at Pole 1 (a) 81,000 cells; (b) 135,252 cells
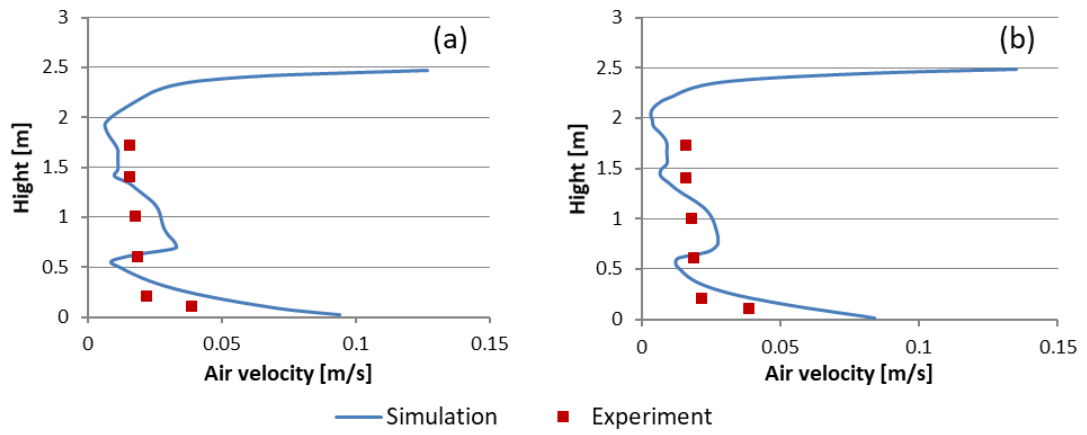
Figure 7.8: air velocity at Pole 2 (a) 81,000 cells , (b) 135,252 cells
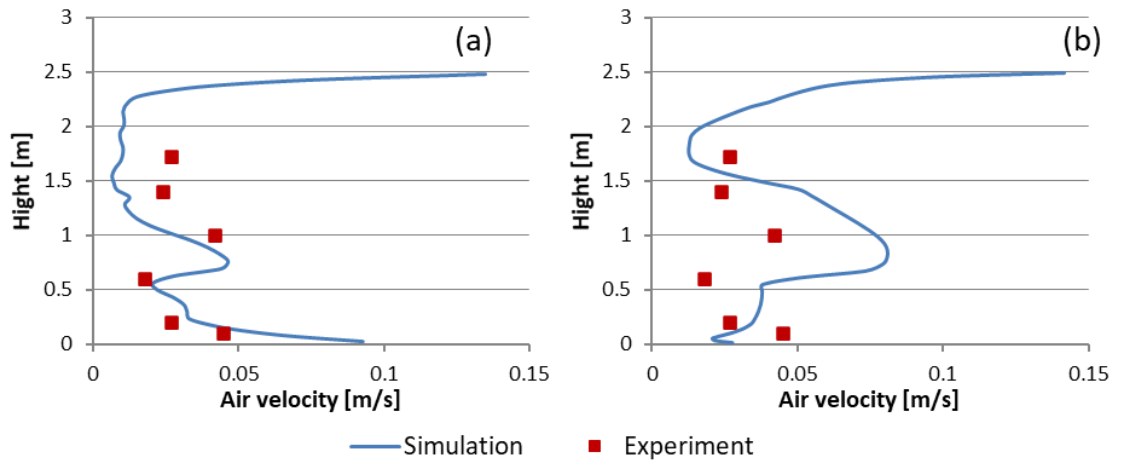
Figure 7.9: air velocity at Pole 4 (a) 81,000 cells, (b) 135,252 cells
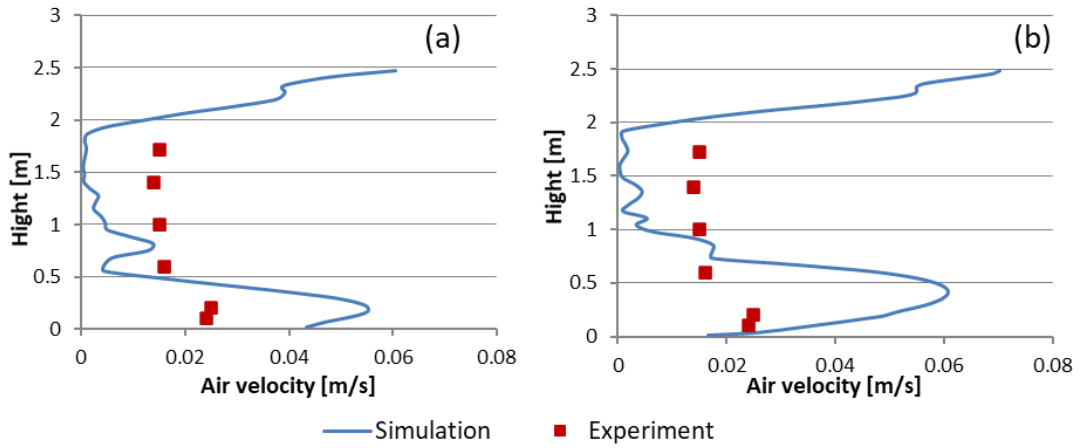
Figure 7.10: air velocity at Pole 5 (a) 81,000 cells, (b) 135,252 cells
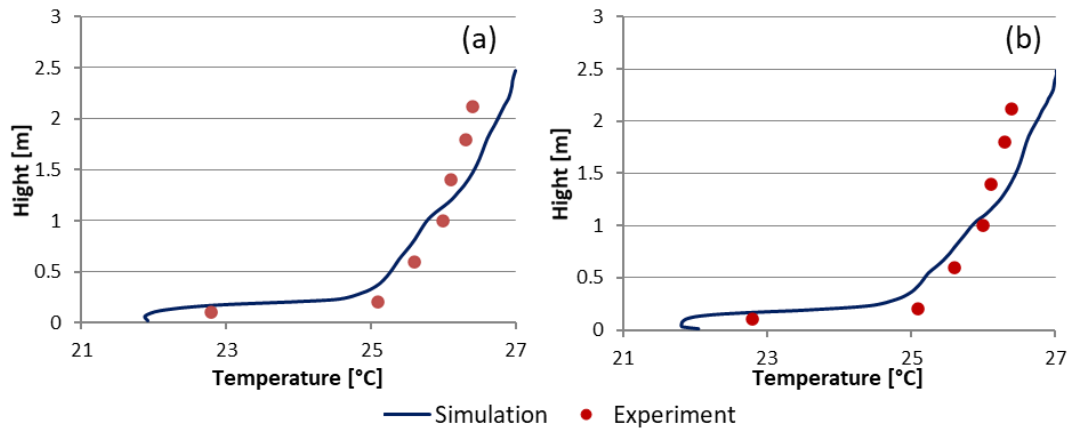
Figure 7.11: Temperature distribution at Pole 1, (a) 81,000 cells, (b) 135,252 cells
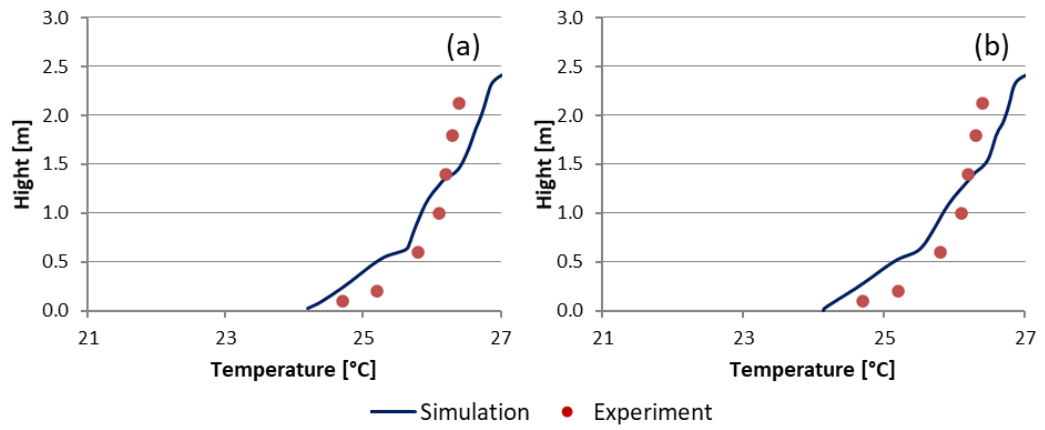
Figure 7.12: Temperature distribution at Pole 2, (a) 81,000 cells, (b) 135,252 cells
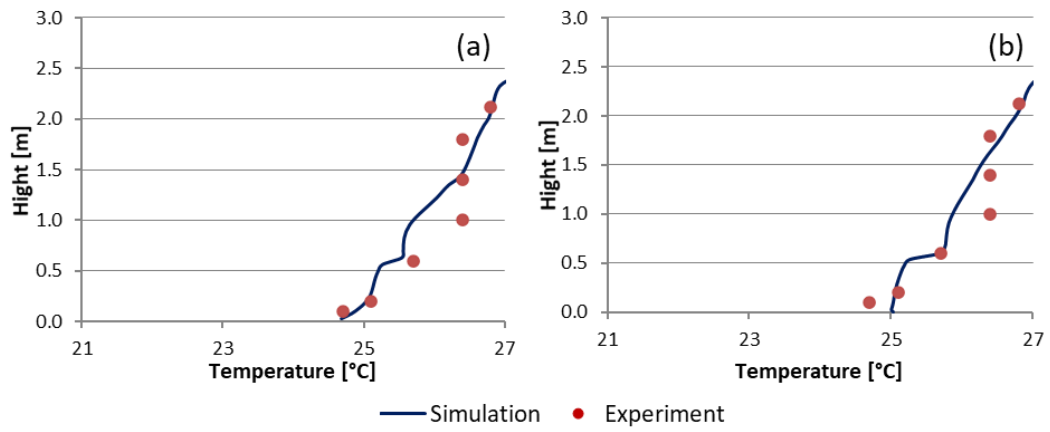
Figure 7.13: Temperature distribution at Pole 4, (a) 81,000 cells, (b) 135,252 cells
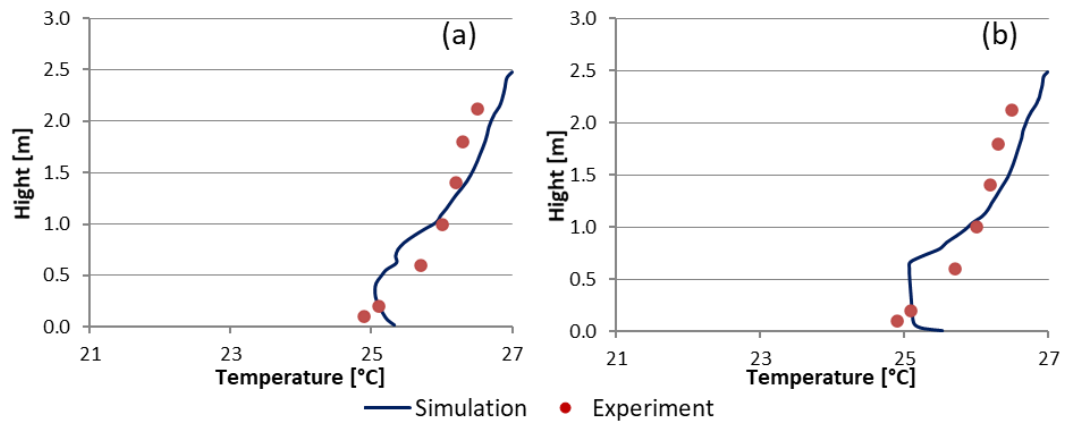
Figure 7.14: Temperature distribution at Pole 5, (a) 81,000 cells, (b) 135,252 cells

The qualitative comparison between the simulation and the experiment showed that results follow the experimental line with some discrepancy. The differences Error between the experimental and simulation results are shown in Table 7.2.

In order to evaluate the accuracy of the results, the root-mean-square (RMS) residuals and the mean absolute error (MAE) were used. RMS is a measure of the variability of the data it has been used as a standard statistical metric to measure model performance in meteorology, air quality, and climate research studies

multi-segmented model integration with ESP-r's CFD domain (Chai and Draxler, 2014). The difference in pairs data is calculated and squared for each pole, the sum of squared error is then added for the different heights and then divided by the respective number of measured points in a pole, according to equation 7.2, where Y is the considered data air temperature or velocity and n is the number of data. The mean absolute error (MAE) is another useful measure widely used in model evaluations (Chai and Draxler, 2014). The difference in pairs data is calculated and the sum of absolute values of the different hight for each pole is then divided by the respective number of measured points in a pole. MAE is calculated as in equation 7.3.

Table 7.2 shows the temperature and velocity RMS and MAE values for each pole. Maximum RMS was 0.68 °C for temperature and 0.025 [m/s] for velocity whereas MAE was 0.534 °C and 0.017 [m/s]. It can be also noticed from the table that the higher RMS and MAE in both temperature and velocity was at pole 1 and 5 the ones far from the manikin also the differences are acceptable but that could be due to the discretisation and meshing shape near the walls.

$$RMS = \sqrt{\frac{\sum_{i=1}^{n}(Y_{exp,i}-Y_{sim,i})^2}{n}} \qquad (7.2)$$

$$MAE = \frac{\sum_{i=1}^{n}|Y_{exp,i}-Y_{sim,i}|}{n} \qquad (7.3)$$

Table 7.2: Temperature and velocity RMS and MAE values for each pole

	RMS Temperature	RMS Velocity	MAE Temperature	MAE Velocity
Pole1	0.683	0.025	0.534	0.017
Pole2	0.342	0.016	0.312	0.013
Pole4	0.313	0.012	0.229	0.012
Pole5	0.50	0.018	0.38	0.017

Comparing the two simulation cases of the different resolutions, it can be seen that increasing the resolution didn't improve the results much at the four poles. Figure 7.15 shows the air velocity comparison of experimental and simulated air velocity above the head. particle image velocimetry (PIV) was used to take detailed measurements above the head. The differences between the simulation and experimental results in the air velocity above the head are because of the rectangular shape of the head. Moreover, that can also due to the turbulence model used in this study. As the buoyancy produced turbulence in the plume above the head is difficult to precisely model and for that, a large eddy simulation might be needed.
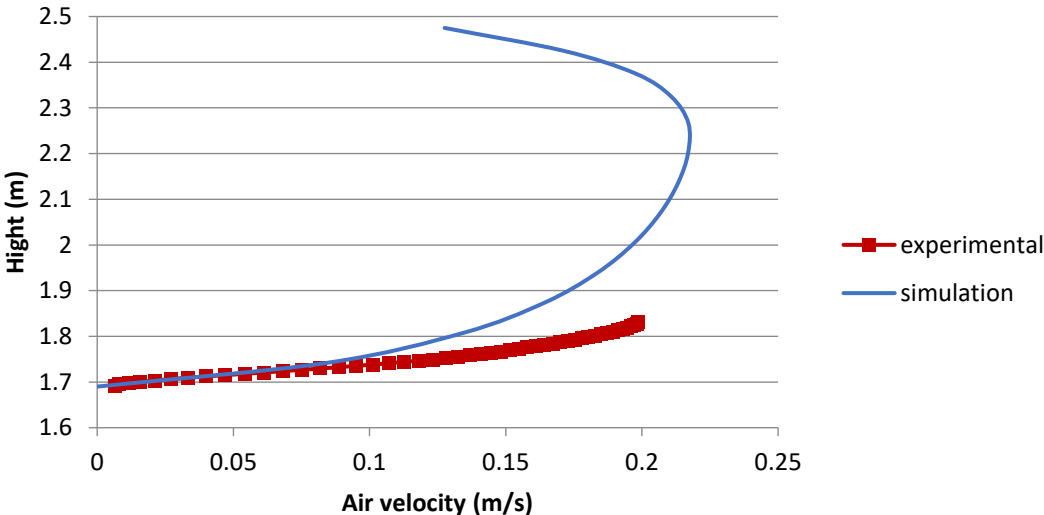
Figure 7.15: air velocity comparison above the head
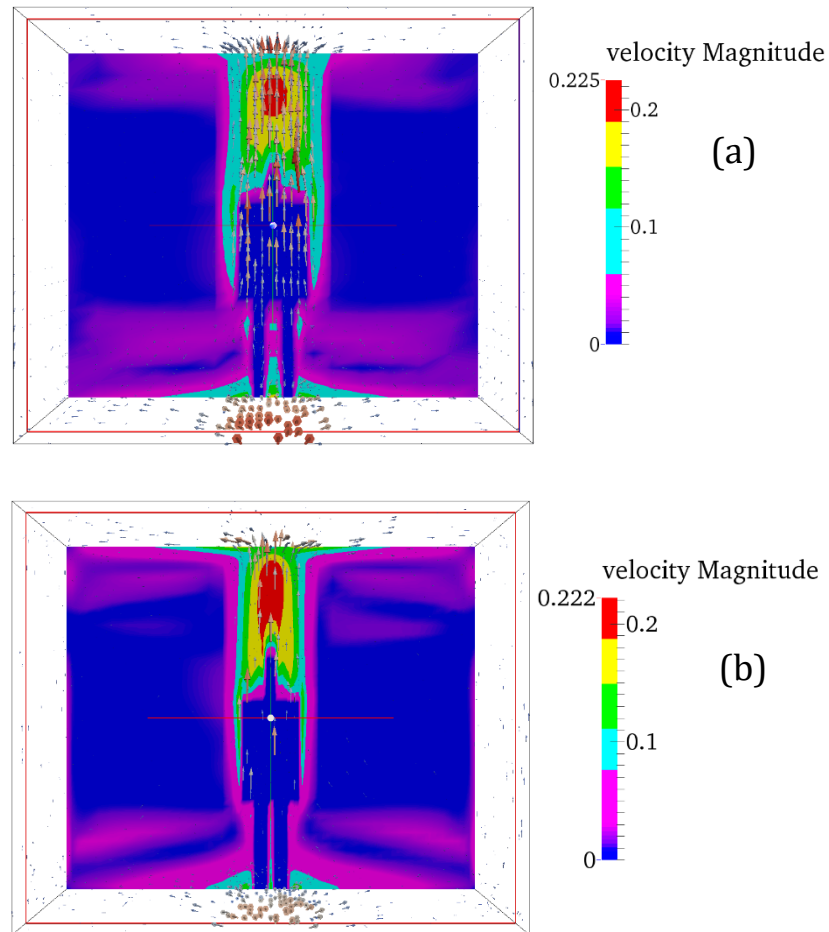
Figure 7.16: (a) low-resolution meshes, air velocity distribution in the domain (b) high resolution meshes air velocity distribution in the domain

Figure 7.16 (a) and (b) show the air velocity magnitude of a cross-sectional in the middle of the domain for a low and high resolution consecutively. Table 7.2 shows the skin temperature prediction from the two resolution cases in addition to the local air temperature predicted from CFD. The results in table 7.2 show some small differences in the local air temperature, and consequently has a small influence on the physiology model. Figure 7.17 shows the differences in skin temperature between the two meshing cases. From that, it can be concluded that increasing the meshing resolution can improve the simulation results a little bit especially the plume generated above the human body. On the other hand, the simulation time increases massively so it has a more computational cost.

Table 7.2: local body skin temperature and air temperature from a high and low resolution.

	Hres Tskin	Lres Tskin	T_air from Hres CFD	T_air from Lres CFD
Finger_L	31.63	31.56	24.66	24.496
finger_R	31.62	31.56	24.64	24.491
palm_L	33.06	33.02	24.66	24.496
palm_R	33.06	33.02	24.64	24.492
Forarm_L	32.28	32.23	24.66	24.496
Forarm_R	32.28	32.23	24.64	24.492
Upperarm_L	32.08	32.03	24.66	24.496
Upperarm_R	32.07	32.02	24.64	24.492
Foot_L	32.77	32.67	23.61	23.20
Foot_R	32.75	32.67	23.51	23.20
Calf_L	32.58	32.48	23.61	23.20
Calf_R	32.56	32.48	23.51	23.20
Thigh_L	33.44	33.37	23.61	23.20
Thigh_R	33.42	33.37	23.51	23.20
Head	35.49	35.42	26.23	25.64
Lower Chest	33.57	33.58	24.74	24.76
Upper chest	33.18	33.19	24.74	24.76

The experiment modelled here in this section was using a thermal manikin. Thermal manikins are usually used in such experiments studying the flow around the body. It usually uses a built-in thermoregulation model but the one used in the experiment had a fixed sensible heat loss. Based on that an experiment with real human body would suits better the validation purpose, but since there are lacking in such experiments this experiment is considered acceptable and it was widely adopted.
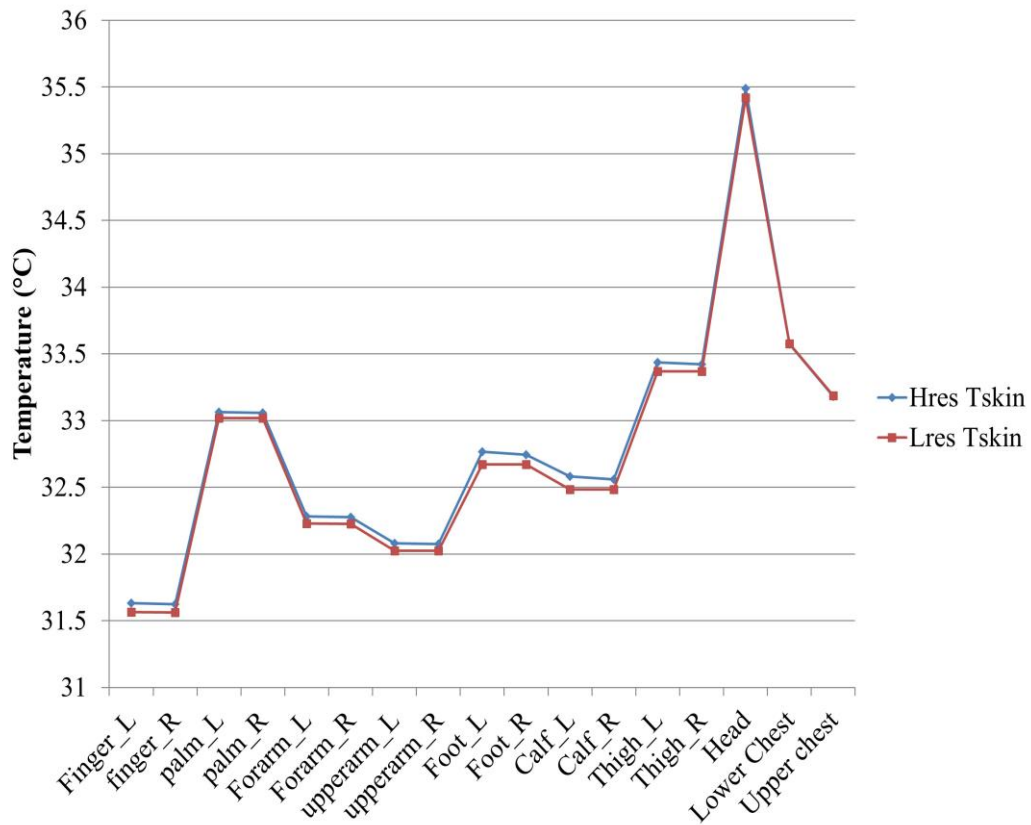
Figure 7.17: Skin temperature distribution over the different body part of the two-meshing resolution.

7.3.2 Plume development with respect to cell dimension size

In order to better understand the effect of the simulation resolution on the results, the same simulation with the same setup has been run for an additional lower resolution. The simulation with the smaller resolution it discretised the room into 13,824 cells. Figures 7.18, 7.19, and 7.20 present the streamlines of the flow inside the zone for the three different resolutions, figures also show the temperature scale on the glyph and the stream tracers. The resolution of the meshing plays a role in the definition of the flow results. In terms of simulation time, the lower resolution has significantly reduced the convergence time. In general, it can be concluded that a medium resolution can be also acceptable since its computational time and results are acceptable.
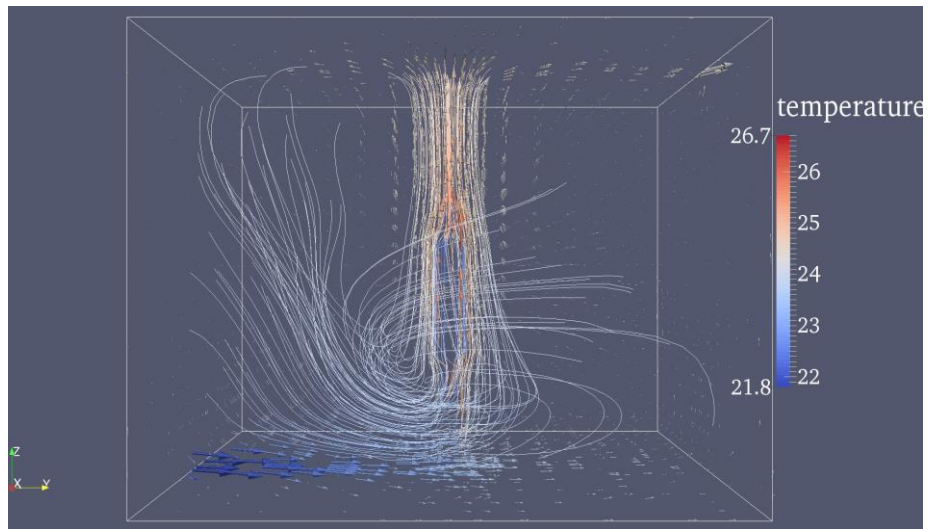
Figure 7.18: streamline of the flow in the room with low resolution.
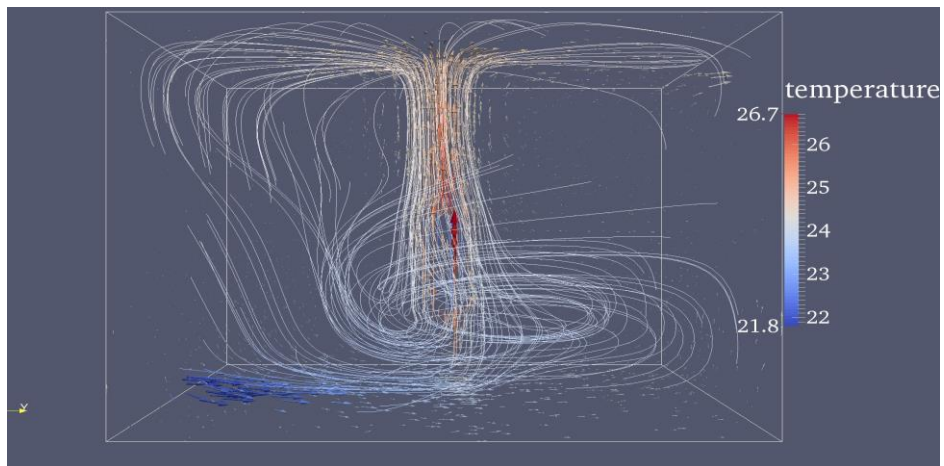
Figure 7.19: streamline of the flow in the room with medium resolution.
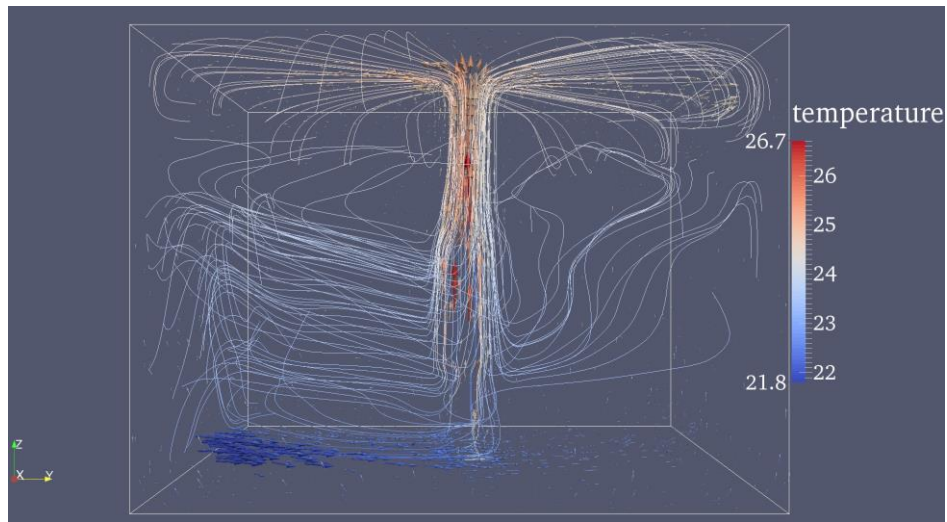
Figure 7.20: streamline of the flow in the room with high resolution.

To show the temperature distribution inside the room the temperature colour map has been extracted for two cross-sectional one on the X direction and the second on the Y direction. Figure 7.21 shows a cross-section on the middle of X-axes the human in the middle doesn't have the temperature representation for the inner and outer area since heat fluxes are only linked to the CFD domain.

Figure 7.22 shows the temperature distribution over a cross-section on the Y-axis of the room. It can very clearly demonstrate the temperature gradient from the ground to the head of a standing person.
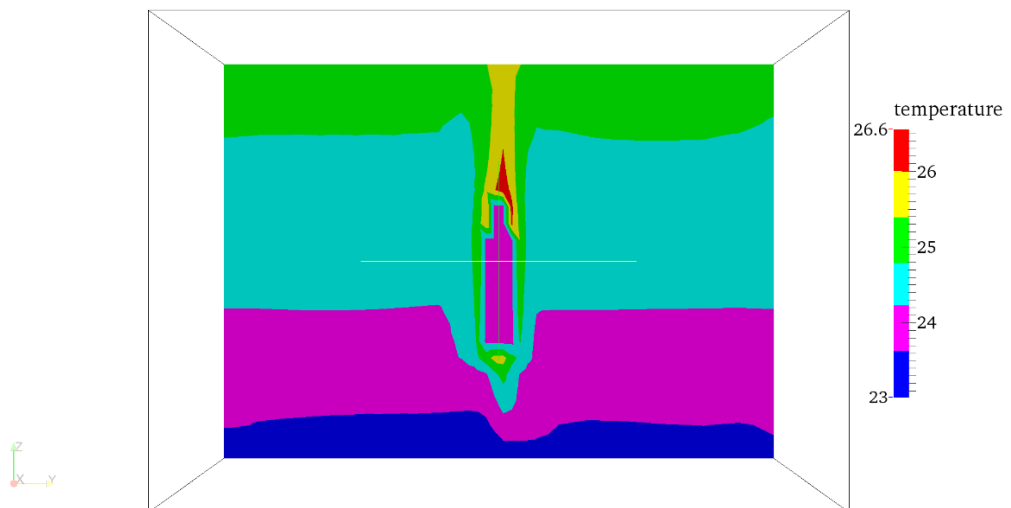
Figure 7.21: temperature distribution over a cross-section in the middle of the X-axes.

168
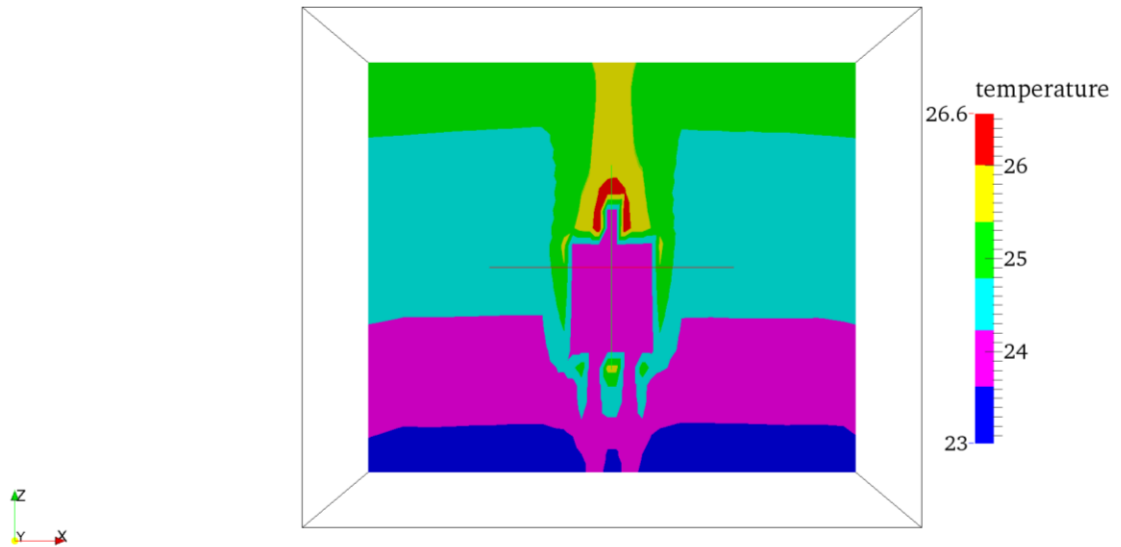
Figure 7.22: temperature distribution over a cross-section in the middle of the Y-axes.

7.3.3 The natural ventilated case

7.3.3.1 CFD domain description

The naturally ventilated case highlights the advantages of linking the BPS model, CFD and the occupant model for typical but complex thermal comfort scenarios.

The description of the simulation setup is as follow; the room has $15.12m^2$ base area dimension: 4.2m width x 3.6m depth x 3m height. It constitutes of three external walls: East wall with an opening in the top to the external environment, external walls in the south, and north. The west wall is an internal partition and has an opening in the bottom. Figure 7.23 shows the CFD domain of a cross naturally ventilated room geometry. A warm weather was chosen and table 7.3 shows the weather data of the chosen simulation day and corresponding hours. A flow network has been defined and linked to the CFD domain using the two-way handshaking method. Which means that at each time-step the thermal domain handshakes with CFD, Since the thermal and CFD solution domains operate independently, but exchange information at the internal surfaces at the begin- beginning of each simulation time-step (Beausoleil-Morrison, 2002). The

multi-segmented model integration with ESP-r's CFD domain thermal domain provides boundary conditions for CFD (temperatures or heat fluxes), while the CFD model calculates hc coefficients for the thermal domain.

The flow network connections setup is given in figure 7.24, where it shows the outdoor boundary at the outlet opening and from the opposite wall the inlet has boundary similar to the room conditions.
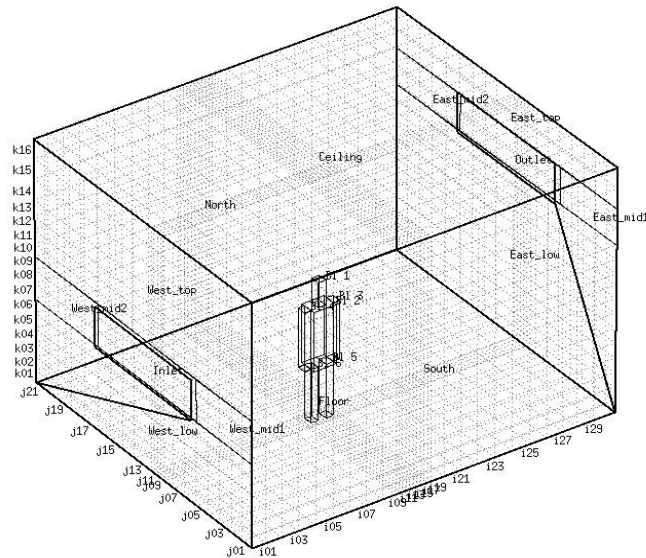
Figure 7.23: The CFD domain used in this section with two openings.
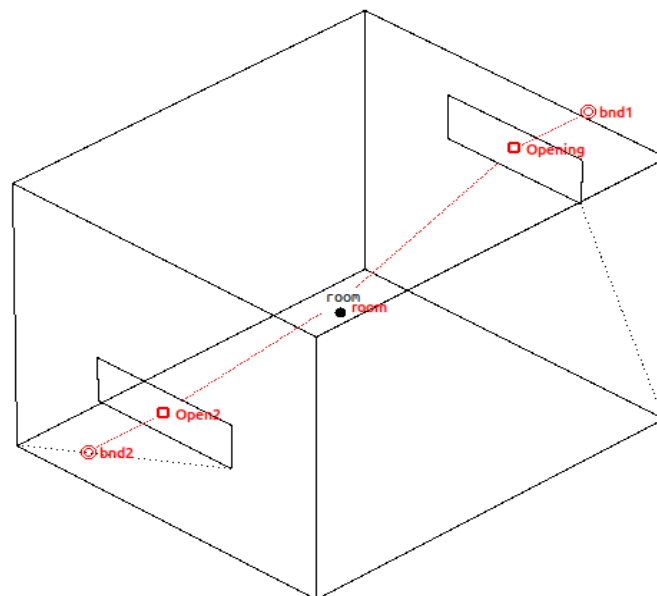
Figure 7.24: flow network connection representation.

The human representation was again the same approach used in the previous simulation by using the six blockages representing the six body parts, the head the trunk, two arms and two legs. The occupant model is linked to the multi-segmented model where heat fluxes are updated each time steps dynamically depending on the thermal environmental changes.

7.3.3.2 Changing metabolic rate with time.

Table 7.3: weather data for each hour of the simulation time for the simulation date.

Hour	Temperature	wind velocity m/s	wind direction	relative humidity
12	25	2.1	10	39
13	25.7	4.1	70	35
14	26.4	5.1	10	38

The occupant was given an initial metabolic rate of 1.4 met (standing doing light industrial work), changing to 2.4 met between 12:00 and 13:00 and then back to 1.4 met until the end of the simulation day. This approach demonstrated the effect of variable metabolic rate during a transient simulation. Clothing level was chosen as a summer clothes ensemble with insulation 0.45 clo (clothing layers covering thighs, chest and upper arms).

Figure 7.29 a, b and c gives results visualisations for temperature distribution at times 12:00 13:00 and 14:00. The temperature on a plane bisecting the occupant and the airflow openings, and arrow representations of the flow field (scaled by velocity), are shown. It can be seen how the air velocity change at the inlet opening with corresponding to the weather data.
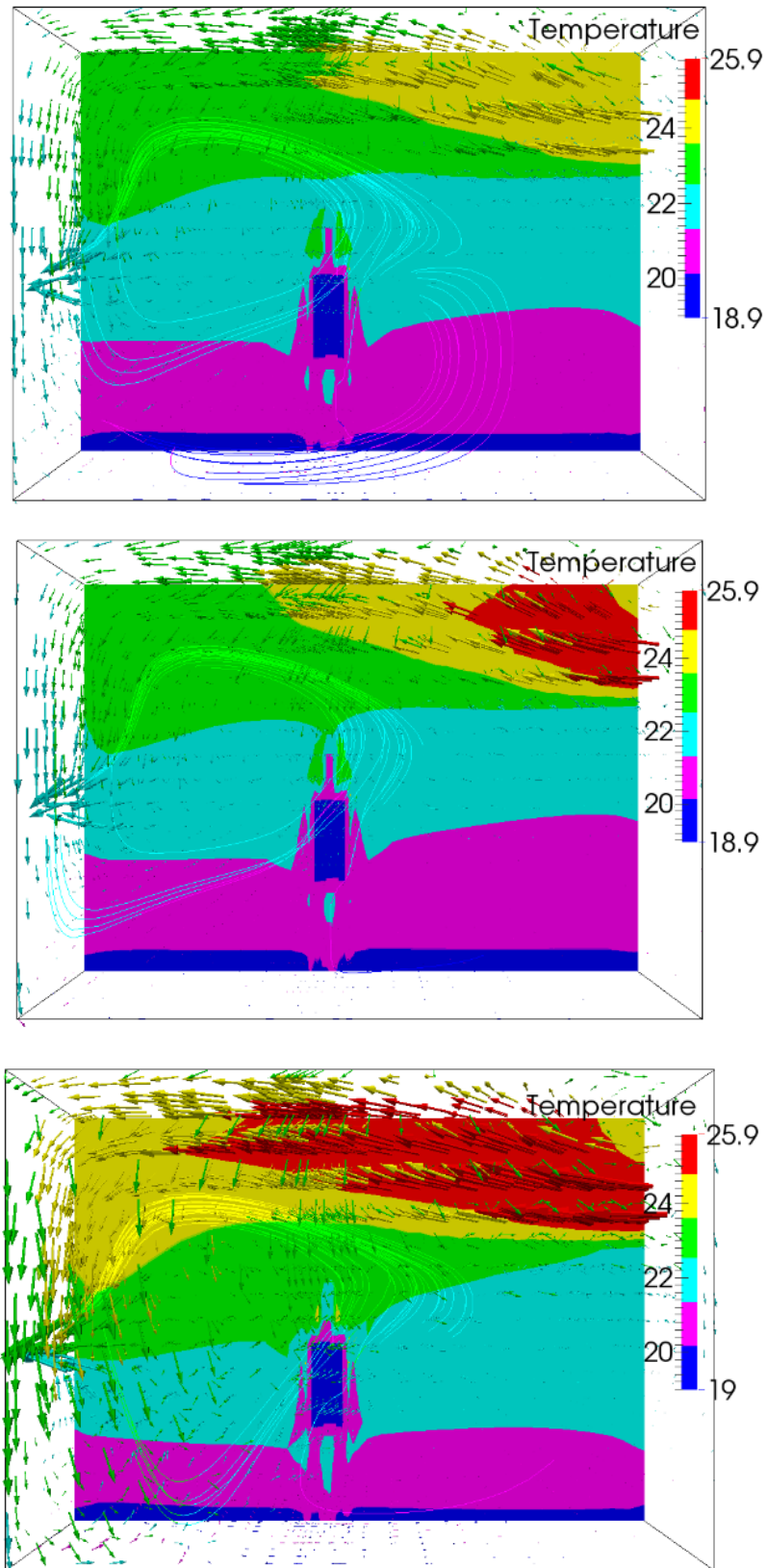
Figure 7.30 a, b, c temperature distribution around the manikin at a) 12:00 b) 13:00 c) 14:00

Figure 7.31 shows the variation in heat loss from the dynamic occupant over the simulation period. Although the change in metabolic rate has more influence on the occupant heat loads, it can be clearly seen that the transient nature of sensible and latent loads connected to the environmental conditions. In addition, figure 7.32 shows the skin temperature of the occupant body parts and the overall temperature. From the graph it can be seen the variation of the skin temperature over the simulation time, these temperatures influence the occupant thermal state and it can be connected later to a thermal sensation and comfort model.
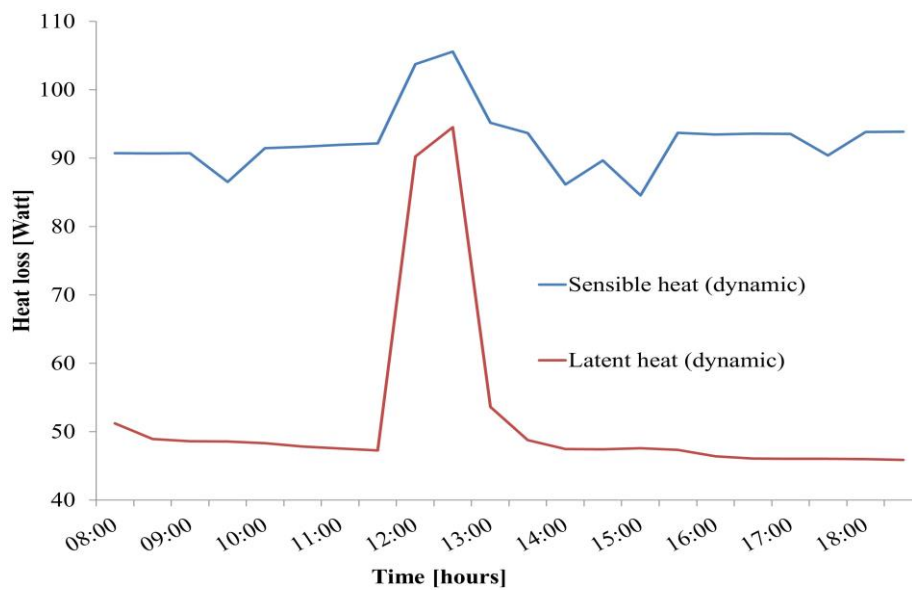
Figure 7.31: Variation of total sensible and latent heat during the simulation time.
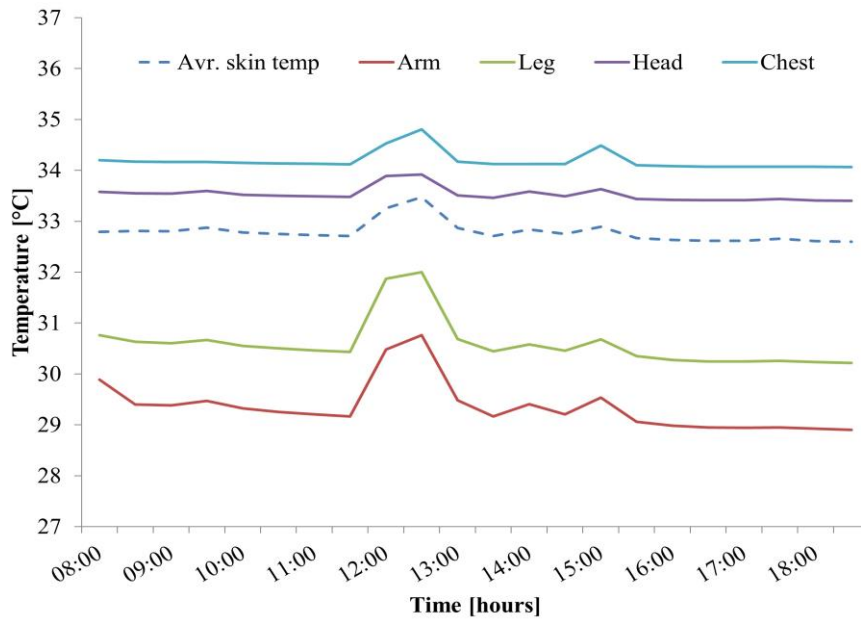
Figure 7.32: Skin surface temperature of each body part.

7.3.4 Two occupants in one domain with different metabolic rate

This modelling approach has the capability to model multiple occupants inside the room with different input characteristics. In the following simulation, two occupants in one domain with different metabolic rate were set. The CFD domain has the same boundary conditions as in the case described in section 7.3.1 with same room dimensions. A displacement ventilation case with two occupants standing in the room. In this approach, the two occupants were set to have two different metabolic rates. One occupant was at rest with 1met and the second occupant has higher activity with a metabolic rate of 1.8 met. Figure 7.33 shows the CFD domain with the discretised meshing and the location of the two occupants inside the room. The results from this simulation show the difference in heat loads emitted from the occupant body to the domain. Figure 7.34 shows the temperature distribution over a cross-section bisecting the location of the two occupants in the middle of the room of Y-axis. Similarly, figure 7.35 shows

multi-segmented model integration with ESP-r's CFD domain the air velocity magnitude distribution over a cross-sectional bisecting the two occupants. The temperature distribution shows higher values compared to the case with only one occupant, in addition, the occupant with a higher metabolic rate has a stronger plume over the head with higher temperature and velocity.

The model can be used in different cases, mainly to study the thermal environment surrounding occupants and their thermal comfort in cases where people have different activity level like in hospitals, school etc.
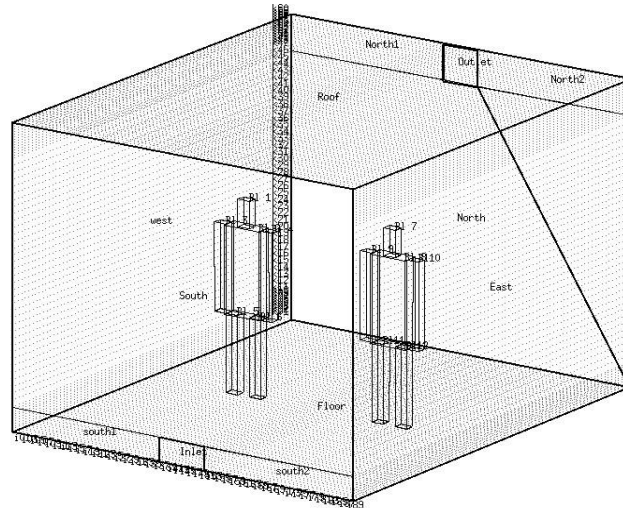
Figure 7.33: CFD domain with two human body inside the room.
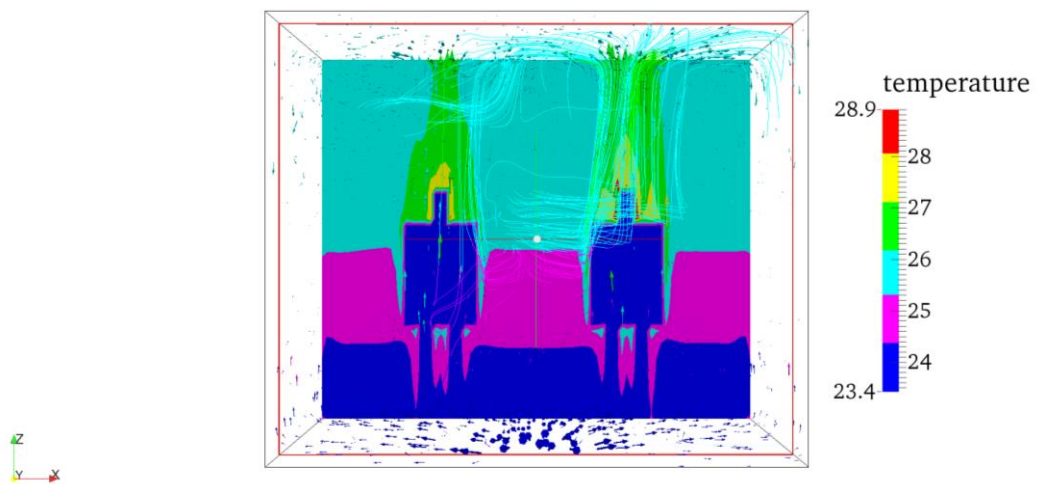
Figure 7.34: Temperature distribution over a cross-section bisecting the human.

175
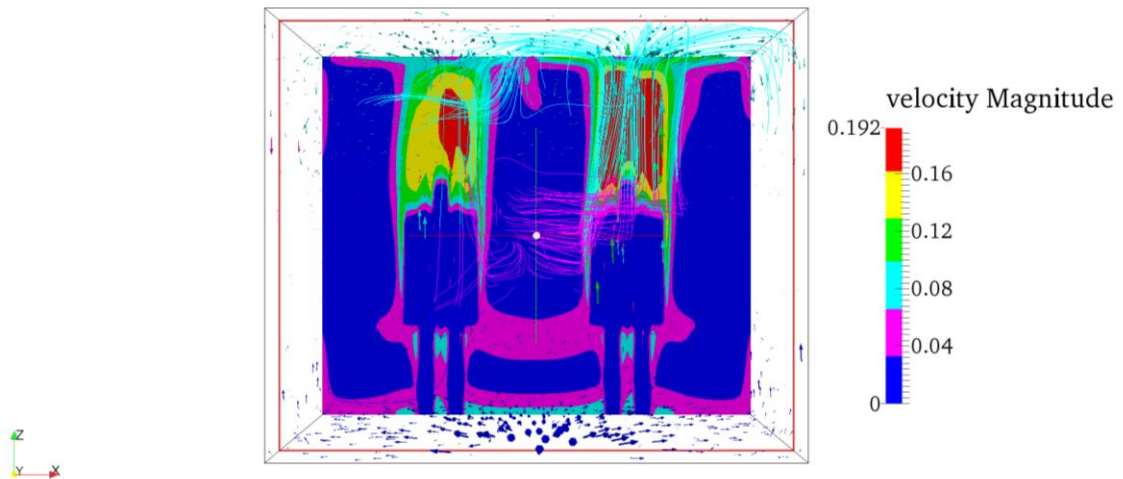
Figure 7.35: Air velocity distribution over a cross-section bisecting the human.

7.4 Conclusion

In this study, the coupling method of a multi-segmented thermo-physiology model with ESP-r and its integrated CFD solver has been presented. The coupling method was validated a benchmark study of displacement ventilation and our results were in a good agreement with the published data.

The detailed occupant representation of our coupling also applied in a natural ventilation case to show its transient capability. In addition, we applied this approach to simulate multiple occupants with different metabolic rates.

The coupling approach has the capability to present multiple occupants in one domain and allows the user to set a schedule for the building occupant activities over the simulation time. But on the CFD side, when assessing multiple occupants, the computational resources required to simulate requires longer.

By developing this model and the linkage associated, it increases the reliability of simulation for the flow and system.

The results presented here may facilitate improvements in the building simulation. Further investigation on the coupling method and studies on thermal comfort adaptation for multiple occupants with different thermal behaviour in the same domain will be presented in further studies.

Chapter 8: Conclusions and further development

8.1 Chapter overview

This chapter summarises what has been achieved throughout this thesis and connected it back with the aims and objectives. Also, it looks ahead to how the work presented in this thesis may be improved upon. In addition, opportunities for future work has been discussed.

8.2 Satisfaction of project aims and objectives

The stated aim of this research was to improve the representation of occupants in building simulation tools. Throughout this thesis, the author tried to show how the building occupants and the building thermal environment are coupled. And gradually the occupant representation has been improved from a simple dynamic sensible and latent heat load, to full integration of a detailed multi-segment human thermal model with the integrated CFD within the building simulation tool ESP-r.

Multiple objectives have been stated for this thesis, were:

1. To investigate the effect of the dynamic occupant heat load on the indoor thermal condition.
2. To integrate a two-node model (core and skin) building occupant model with ESP-r.
3. To integrate a multi-segmented human thermal model with ESP-r.
4. To integrated the multi-segmented model with ESP-r's integrated CFD.
5. To clarify the capability of such integration in multiple simulation case scenario.

These objectives have been realized within the framework of ESP-r's integrated and partitioned solution approach. First, the dynamic nature of the occupant heat loads (sensible and latent heat loads) was approached by developing and integrating a simple regression line for each sensible and latent heat load. The regression lines generated in chapter 4 were based on the data available in the literature of people at steady-state and in a dynamic environment. The regression lines model were basically a function of the indoor operative temperature and the occupant metabolic rate only. This integration demonstrated the needs of implementing a more detailed human thermal model which accounts for the physiological phenomena in addition of considering other environmental parameters like relative humidity, air temperature and radiant temperature and air velocity alongside to personal parameters like the clothing insulation and metabolic rate. So secondly the two-nodes model has been developed and implemented in ESP-r. That has been explained in chapter 5 where the energy balance equations of both skin and core of the human body have increased the level of representation of the building occupant thermally within the building performance simulation system.

A dynamic clothing insulation model has been adopted and implemented together with the two-node physiology model to account for the human behaviour of clothing adaptation. This integration provided in chapter 5 has given more robustness to the model, in general, knowing that clothing insulation level affects the heat transfer from the human body and consequently its thermal comfort. This integration model has been tested in chapter 5 in a couple of application where a model of a classroom has been presented showing the differences that may arise compared to the simplified method.

Third, The level of details of representing the building occupant has been augmented and that is by developing and integrating a multi-segmented thermal comfort model in ESP-r. Chapter 6 showed a description of the multi-segmented model which consider the human body as 26 body segment and accounted for the different thermoregulation phenomena as sweating, shivering and blood flow regulation. The model uses a realistic blood flow calculation and distribution over

the body parts. This increase of details in the occupant representation in building simulation missed the same level of details from the building simulation as chapter 5 stated. Finally, to cope with this issue of the level of details of representing the human body with multiple nodes compared to air and surfaces as one node each, the multi-segmented model has been integrated with the coupled CFD domain in ESP-r. That coupling approach has given the simulations more robustness it also opens a bigger possibility and usability for such integration.

The coupling approach in chapter 7 has been validated with published experimental results done on a thermal manikin in a chamber with a displacement ventilation system.

Also, chapter 7 presented a couple of simulation case where both displacement ventilation and natural ventilation has been applied. Besides, the application of having two human body inside a room with different metabolic rates has been presented where the possibility of showing differences in thermal perception can be valid.

8.3 General discussion

The thesis covered three approaches of occupant representation in building simulation, starting from a simple dynamic approach and ending by a more detailed including detailed human body and CFD.

The simple occupant heat loads model is good for a fast calculation to consider the transient occupant heat loads, but this approach does not account for the physiological/thermoregulatory behaviour of the human body. It is very useful for the occupant heat loads calculation at each time step considering the influence of operative temperature on the ratio of sensible/latent load.

The two-node model is another a quiet fast approach which accounts for the physiological phenomena and variable clothing insulations. As it does not require lots of inputs from the building simulation tool user. It is more accurate compared

to the previous approach it predicts skin and core temperature dynamically so it can be linked to a PMV scale model to predict thermal comfort. The model was linked to a dynamic clothing model that changes insulation values based on the outdoor weather of each simulation day. That provides an additional degree of dynamical prediction. This approach considered dynamic it does a quick calculation it is very useful if one needs to consider the dynamic thermal interaction between the human body and its thermal environment as surfaces and air temperature, relative humidity and clothing. The metabolic rate is considered as predefined input in a schedule.

The multi-segmented model requires more computational time and it is best suitable for local environmental and asymmetric studies. This model can be best used in a CFD domain where local environmental conditions give a greater degree of modelling detail. Further, it requires more information from the user as location and requires time to set up the human body (blockages) inside the CFD domain. This coupled simulation of multi-segmented physiology model and the integrated CFD in building simulation will be best used for studying HVAC system, asymmetric environment, radiant surfaces and local heating cooling devices.

8.4 Contributions to the State-of-the-Art

To the Author's knowledge, there were no other examples in the literature where a very detailed, multi-segment human physiology model has been fully integrated with a building simulation tools and CFD for use in such activities as detailed comfort assessment and modelling of passive ventilation systems. Additionally, previous to this research the occupant heat load was defined as a fixed ratio of sensible and latent heat loads.

This thesis contributes to the state of the art by developing a method for coupling an explicit thermal representation of building occupants within the CFD-coupled with building simulation tools in order to have a reliable and more detailed prediction of their thermal comfort and their thermal interaction with the building in greater detail than has been done before. The models have been

included in the final release of ESP-r and have been made available as open-source with a tutorial and examples.

Furthermore, this thesis showed how an occupant can be modelled as a thermal node in the building simulation system and being a connected part of the building simulation system. With the modification presented in this thesis the occupant heat loads become dynamic accounting for the effect of changes in the thermal environmental parameters.

8.5 Further development

 Although the work documented in this thesis represents a contribution towards integrating a detailed human thermal comfort model with building simulation and its integrated CFD domain, much work remains.

Here are some prospects for improvements in the code to be done in the future:

1. All the simulations presented in this thesis had considered the human body with a standing posture, different posture can be applied for the human body in a simulation and that requires some manual modifications in order to account for example for a sitting or even a lying human body.

2. Improving MRT calculation, the mean radiant temperature is considered as the average MRT calculated by ESP-r at the centre of the zone or the one calculated from a sensor located in a specific location and it is considered uniform for the whole body. In future local MRT sensor for each body segment can be considered to account for the local radiant heat exchange.

3. The direct solar radiation load on the human body is not considered in this thesis only longwave radiation exchange between the body and the building surfaces is considered. The detailed human thermal model is a valuable tool to study the direct solar radiation hitting the human body and that is for example to study thermal comfort of occupants sitting close to fenestration and transparent surfaces which allow the solar

radiation to penetrate the zone. In addition, it will be very useful in modelling the shading system like in complex fenestration systems.

8.6 Future research

The human behaviours of building occupant are greatly correlated with human thermo-physiology. Using the detailed multi-segmented model with other human behavioural models can lead to a better projection of the occupant thermal comfort and building performance.   Here are some examples for future consideration:

1. Developing a dynamic HVAC controller, the model can be further used as a controller (dynamic sensor) to control air conditioning or even considering the thermal state of the occupant for windows openings in a naturally ventilated building.

2. Improving and developing a detailed dynamic clothing model for the multi-segmented model and link it to the multi-segmented model. People change their clothing to adapt to their thermal environment.

3. Occupants move between the different building zones and between outdoors and indoors. With that in mind, a human behaviour model of building occupant movement and presence can be linked with the physiology model to account for the corresponding changes in the environmental conditions.

4. Thermal comfort of senior people becomes an interesting research topic with the increasing of the mortality age. Older people thermoregulation showed differences compared to young people, for that developing an adapted thermophysiology model for the elderly is important. With such a model, it would be easier to project and understand the thermal comfort of individuals with different age groups sitting in the same thermal environment.
5. Studying the effect of local heating and cooling devices on improving local thermal comfort and reducing the building energy consumption.

Devices such as foot warmer, heating/cooling chair and personalized ventilation.

6. The role of ventilation in increasing or reducing the infection rate of viruses becomes a big research question, especially during the COVID-19 era. More recommendation toward natural ventilation and personal ventilation with fresh air is another option.

Although in this thesis some application has been presented as in chapter 7. A further application is needed with respect to test the robustness of the modelling approaches. Most of the research questions mentioned in this section can be evolved with the advantage of the detailed human thermal model linked with building simulation presented in this dissertation.

Appendix A: Regression line statistics

The following statistical data presents the sensible and latent heat load regression line. It also shows the R-value, R-square and the residuals.

Linear Regression

Regression Statistics

R	0.99975
R-square	0.9995
Adjusted R-square	0.99946
S	1.79442
N	141

Sensible Heat = 198.42617 - 3.80901 * Temperature in Degree C - 0.05419 * Temp^2 - 0.42472 * Met + 0.00171 * Met^2 + 0.01287 * Temp*MET - 0.00004 * Temp*MET^2 + 0.00002 * MET*TEMP^2 - 3.8516E-7 * Met^2*Temp^2

ANOVA

	d.f.	SS	MS	F	p-level
Regression	8.	841,629.15799	105,203.64475	32,672.56111	0.
Residual	132.	425.03191	3.21994		
Total	140.	842,054.1899			

	Coefficient	Standard Error	LCL	UCL	t Stat	p-level	H0 (5%)
Intercept	198.42617	21.6898	155.52159	241.33074	9.14836	0.	rejected
Temperature in Degree C	-3.80901	1.63755	-7.04824	-0.56978	-2.32605	0.02154	rejected
Temp^2	-0.05419	0.02756	-0.10871	0.00034	-1.96583	0.05142	accepted
Met	-0.42472	0.34801	-1.11311	0.26367	-1.22043	0.22448	accepted
Met^2	0.00171	0.0013	-0.00085	0.00428	1.31928	0.18936	accepted
Temp*MET	0.01287	0.02629	-0.03913	0.06488	0.48973	0.62514	accepted
Temp*MET^2	-0.00004	0.0001	-0.00024	0.00015	-0.41822	0.67646	accepted
MET*TEMP^2	0.00002	0.00044	-0.00086	0.00089	0.03469	0.97238	accepted
Met^2*Temp^2	-3.8516E-7	1.65171E-6	-3.6524E-6	2.88208E-6	-0.23319	0.81598	accepted

T (5%) 1.9781
LCL - Lower value of a reliable interval (LCL)
UCL - Upper value of a reliable interval (UCL)

Residuals

Observation	Sensible Heat	Predicted Y	Residual	Standardized	Studentized	Deleted t	Leverage	Cook's D	DFIT	PRESS
1	145.21291	141.57615	3.63675	2.08721	2.16833	2.19963	0.12636	0.07556	0.83656	4.16278
2	143.73319	140.83963	2.89356	1.66068	1.7205	1.73351	0.12156	0.04551	0.64487	3.29399
3	141.25	138.95614	2.29386	1.3165	1.35516	1.35951	0.11017	0.02526	0.47838	2.57788
4	138.54026	136.57091	1.96935	1.13026	1.15522	1.1567	0.09746	0.01601	0.3801	2.18201
5	134.51786	133.68144	0.83642	0.48004	0.48711	0.4857	0.08433	0.00243	0.1474	0.91345
6	131.11355	130.92572	0.18783	0.1078	0.10877	0.10836	0.07386	0.0001	0.0306	0.20281
7	128.90819	128.90844	-0.00025	-0.00015	-0.00015	-0.00015	0.06732	1.7079E-10	-0.00004	-0.00027
8	123.71526	124.55597	-0.8407	-0.4825	-0.48221	-0.4808	0.056	0.00153	-0.11711	-0.89058
9	121.98321	122.93677	-0.95356	-0.54727	-0.54597	-0.54451	0.05265	0.00184	-0.12837	-1.00655
10	118.0461	119.63318	-1.58709	-0.91087	-0.90603	-0.90541	0.04705	0.0045	-0.20118	-1.65544
11	113.32912	114.53113	-1.20201	-0.68986	-0.68408	-0.6827	0.04115	0.00223	-0.14143	-1.25359
12	109.83688	112.09174	-2.25485	-1.29411	-1.28204	-1.2852	0.03931	0.00747	-0.25996	-2.34711
13	106.12367	108.18678	-2.06311	-1.18407	-1.17187	-1.17355	0.03742	0.00593	-0.2314	-2.14332
14	102.69093	104.40557	-1.71464	-0.98407	-0.97354	-0.97334	0.03663	0.004	-0.1898	-1.77984
15	97.18911	99.97136	-2.78225	-1.5968	-1.57977	-1.58887	0.03671	0.01057	-0.31016	-2.88828
16	94.48201	97.41417	-2.93216	-1.68283	-1.66526	-1.67664	0.03714	0.01188	-0.32928	-3.04525
17	93.4756	95.38179	-1.90619	-1.09401	-1.08286	-1.08358	0.03764	0.0051	-0.2143	-1.98075
18	89.53849	91.80083	-2.26234	-1.29841	-1.28596	-1.28918	0.03881	0.00742	-0.25903	-2.35367
19	86.02076	88.2951	-2.27435	-1.3053	-1.29373	-1.29707	0.0402	0.00779	-0.26546	-2.36961
20	80.10218	81.73652	-1.63433	-0.93798	-0.93113	-0.93065	0.04321	0.00435	-0.19778	-1.70814
21	75.32571	76.24616	-0.92045	-0.52827	-0.52513	-0.52369	0.04587	0.00147	-0.11482	-0.96469
22	69.43557	70.50122	-1.06565	-0.6116	-0.60883	-0.60737	0.04855	0.0021	-0.1372	-1.12002
23	64.21422	64.58329	-0.36908	-0.21182	-0.21114	-0.21037	0.05104	0.00027	-0.04879	-0.38892
24	58.04331	57.3121	0.73121	0.41966	0.41886	0.41755	0.05353	0.0011	0.0993	0.77257
25	51.11834	48.92862	2.18971	1.25673	1.25561	1.25839	0.05547	0.01029	0.30496	2.31831
26	42.46131	39.29989	3.16142	1.81441	1.81364	1.8297	0.05635	0.02182	0.4471	3.35018
27	36.57117	32.88724	3.68393	2.11429	2.11317	2.14168	0.05614	0.02951	0.52232	3.90304
28	27.88864	24.10018	3.78846	2.17428	2.17173	2.20321	0.05493	0.03046	0.53116	4.00865
29	18.70174	14.84933	3.85242	2.21099	2.20579	2.23907	0.05269	0.03007	0.52806	4.06669
30	8.45188	5.59778	2.8541	1.63803	1.63165	1.6421	0.04975	0.01549	0.37571	3.00351
31	0.24296	-2.8794	3.12236	1.79199	1.78218	1.79717	0.04673	0.0173	0.39791	3.27542
32	-10.39523	-11.26171	0.86648	0.49729	0.4938	0.49238	0.04375	0.00124	0.10532	0.90613
33	-17.87851	-17.93916	0.06065	0.03481	0.03452	0.03439	0.04159	5.74711E-6	0.00716	0.06328
34	-24.60801	-24.13333	-0.47467	-0.27242	-0.26997	-0.26902	0.03991	0.00034	-0.05485	-0.4944
35	-33.32159	-32.36527	-0.95633	-0.54886	-0.54348	-0.54202	0.03839	0.00131	-0.10831	-0.99451
36	-37.28714	-36.45426	-0.83288	-0.47801	-0.47324	-0.47184	0.03804	0.00098	-0.09383	-0.86582
37	-42.92524	-42.25894	-0.6663	-0.3824	-0.3786	-0.37737	0.03809	0.00063	-0.0751	-0.69268
38	-49.03929	-48.13181	-0.90748	-0.52083	-0.51586	-0.51442	0.03892	0.0012	-0.10352	-0.94423
39	-55.04314	-53.94169	-1.10145	-0.63215	-0.62668	-0.62523	0.04062	0.00185	-0.12865	-1.14809
40	-60.45998	-59.39172	-1.06825	-0.61309	-0.60859	-0.60713	0.04312	0.00185	-0.12889	-1.11639
41	-65.14823	-64.0032	-1.14503	-0.65716	-0.65331	-0.65189	0.046	0.00229	-0.14315	-1.20024
42	-70.45751	-69.35635	-1.10116	-0.63198	-0.6297	-0.62825	0.0503	0.00233	-0.14458	-1.15948
43	-76.1806	-75.33522	-0.84538	-0.48518	-0.485	-0.48359	0.05643	0.00156	-0.11826	-0.89593
44	-81.96319	-81.1403	-0.82289	-0.47228	-0.47396	-0.47256	0.06383	0.0017	-0.1234	-0.879
45	-88.6074	-88.18127	-0.42613	-0.24457	-0.2469	-0.24602	0.07491	0.00055	-0.07001	-0.46064
46	-94.7783	-94.63583	-0.14247	-0.08177	-0.08311	-0.08279	0.08727	0.00007	-0.0256	-0.15609
47	-99.21745	-99.29586	0.07841	0.045	0.046	0.04583	0.09758	0.00003	0.01507	0.08689
48	-104.91212	-104.98437	0.07226	0.04147	0.04273	0.04257	0.11185	0.00003	0.01511	0.08136
49	-108.3475	-108.75764	0.41015	0.23539	0.24399	0.24312	0.1224	0.00092	0.09079	0.46735
50	-111.05459	-111.61868	0.56408	0.32374	0.33721	0.33608	0.13098	0.0019	0.13048	0.6491
51	140.76262	137.46872	3.2939	1.89044	2.01191	2.03573	0.16756	0.09053	0.91333	3.95691
52	138.23781	135.75873	2.47908	1.4228	1.50174	1.50899	0.15366	0.0455	0.64298	2.92919
53	135.69161	133.21279	2.47882	1.42265	1.48551	1.4924	0.13524	0.03835	0.59019	2.8665
54	130.91661	129.46559	1.45101	0.83277	0.85835	0.85749	0.1125	0.01038	0.3053	1.63495

55	125.88663	125.36274	0.52389	0.30067	0.3065	0.30545	0.09269	0.00107	0.09763	0.57741
56	120.06946	120.61303	-0.54358	-0.31197	-0.31501	-0.31393	0.07523	0.0009	-0.08954	-0.5878
57	115.50898	116.58297	-1.07399	-0.61639	-0.6187	-0.61725	0.06418	0.00292	-0.16165	-1.14765
58	109.55876	111.27579	-1.71704	-0.98545	-0.98372	-0.9836	0.05383	0.00612	-0.23461	-1.81473
59	104.81599	107.19018	-2.37419	-1.3626	-1.35637	-1.36074	0.04846	0.01041	-0.30707	-2.49509
60	101.41314	103.28721	-1.87407	-1.07557	-1.06871	-1.06929	0.04499	0.00598	-0.23208	-1.96236
61	96.7495	99.65137	-2.90187	-1.66545	-1.65304	-1.66408	0.04294	0.01362	-0.35248	-3.03206
62	92.83993	95.13944	-2.2995	-1.31974	-1.30902	-1.3126	0.04165	0.00827	-0.27362	-2.39943
63	87.26601	89.3393	-2.07328	-1.1899	-1.18014	-1.18192	0.04148	0.0067	-0.24588	-2.16301
64	82.80137	84.7198	-1.91843	-1.10103	-1.0924	-1.09321	0.04219	0.00584	-0.22943	-2.00293
65	77.77491	79.77962	-2.00471	-1.15055	-1.14229	-1.14362	0.04345	0.00659	-0.24375	-2.09578
66	72.71152	74.4528	-1.74128	-0.99936	-0.99306	-0.99301	0.04515	0.00518	-0.21592	-1.82361
67	68.7829	69.9428	-1.1599	-0.66569	-0.66202	-0.66061	0.04667	0.00238	-0.14616	-1.21668
68	63.15095	63.96633	-0.81538	-0.46796	-0.46586	-0.46447	0.04861	0.00123	-0.10499	-0.85704
69	60.05319	60.66532	-0.61212	-0.35131	-0.34991	-0.34875	0.04959	0.00071	-0.07966	-0.64406
70	53.0063	53.33154	-0.32524	-0.18666	-0.18609	-0.18541	0.05135	0.00021	-0.04314	-0.34285
71	47.72223	47.26913	0.45309	0.26004	0.25938	0.25846	0.05231	0.00041	0.06073	0.47811
72	42.27345	40.68332	1.59013	0.91261	0.91051	0.90992	0.05279	0.00513	0.21481	1.67875
73	37.25461	35.38306	1.87155	1.07412	1.07162	1.07223	0.05274	0.0071	0.253	1.97575
74	33.4101	31.52624	1.88386	1.08119	1.07852	1.0792	0.05247	0.00716	0.25397	1.98819
75	26.3679	23.78953	2.57837	1.47978	1.47532	1.48199	0.05143	0.01311	0.34508	2.71816
76	18.64284	15.69807	2.94476	1.69007	1.68348	1.69539	0.04976	0.01649	0.38795	3.09895
77	10.51744	7.5797	2.93774	1.68604	1.67768	1.68942	0.04773	0.01567	0.37821	3.08498
78	3.84685	1.19182	2.65503	1.52378	1.51492	1.52246	0.04608	0.01232	0.3346	2.78328
79	-2.06439	-4.19577	2.13137	1.22324	1.2153	1.21752	0.04478	0.00769	0.26361	2.23129
80	-9.32113	-10.40867	1.08755	0.62417	0.61971	0.61826	0.04354	0.00194	0.1319	1.13705
81	-14.8842	-15.60149	0.71729	0.41167	0.40858	0.40728	0.04282	0.00083	0.08614	0.74938
82	-21.30803	-22.25326	0.94523	0.54249	0.53833	0.53688	0.04251	0.00143	0.11312	0.9872
83	-27.08328	-27.25297	0.16969	0.09739	0.09666	0.09629	0.04285	0.00005	0.02037	0.17728
84	-36.05976	-34.99258	-1.06718	-0.61248	-0.60844	-0.60698	0.04459	0.00192	-0.13113	-1.11699
85	-44.17431	-43.09416	-1.08014	-0.61992	-0.61705	-0.61559	0.04835	0.00215	-0.13875	-1.13502
86	-50.86688	-49.55819	-1.30869	-0.75108	-0.74946	-0.74821	0.05305	0.0035	-0.1771	-1.382
87	-58.43632	-56.7072	-1.72911	-0.99238	-0.99404	-0.994	0.0603	0.00705	-0.2518	-1.84008
88	-69.09649	-67.71846	-1.37803	-0.79088	-0.79907	-0.79797	0.07636	0.00587	-0.22943	-1.49195
89	-76.4174	-75.11825	-1.29915	-0.74561	-0.75935	-0.75813	0.09096	0.00641	-0.23981	-1.42914
90	-84.2761	-83.3258	-0.95031	-0.5454	-0.56174	-0.56028	0.1112	0.00439	-0.19818	-1.0692
91	-92.48239	-91.97859	-0.5038	-0.28914	-0.30234	-0.30129	0.13764	0.00162	-0.12037	-0.58421
92	-99.5199	-99.18088	-0.33902	-0.19457	-0.20663	-0.20588	0.16401	0.00093	-0.09119	-0.40553
93	-104.52673	-105.42436	0.89764	0.51517	0.55593	0.55447	0.19033	0.00807	0.26883	1.10864
94	140.78753	137.69385	3.09368	1.77553	1.87033	1.88842	0.1503	0.06875	0.79421	3.64089
95	137.46792	134.84842	2.6195	1.50339	1.56543	1.57417	0.1304	0.04083	0.60958	3.0123
96	134.56475	132.62219	1.94256	1.11488	1.15194	1.15338	0.11683	0.0195	0.41949	2.19953
97	130.46147	129.24467	1.2168	0.69835	0.71446	0.71313	0.09918	0.00624	0.23663	1.35077
98	126.77493	126.07543	0.69949	0.40145	0.40762	0.40633	0.08547	0.00173	0.12422	0.76487
99	123.68684	123.59799	0.08885	0.05099	0.05152	0.05133	0.07643	0.00002	0.01476	0.0962
100	121.19778	121.208	-0.01022	-0.00587	-0.0059	-0.00588	0.06894	2.86713E-7	-0.0016	-0.01098
101	115.41227	116.48829	-1.07603	-0.61756	-0.61758	-0.61613	0.05723	0.00257	-0.1518	-1.14134
102	112.53284	113.56995	-1.03711	-0.59522	-0.59352	-0.59206	0.05173	0.00214	-0.13829	-1.09369
103	108.22353	109.80742	-1.58389	-0.90903	-0.90385	-0.90321	0.04629	0.00441	-0.19899	-1.66077
104	103.65953	105.66683	-2.0073	-1.15204	-1.14295	-1.14429	0.04209	0.00638	-0.23985	-2.0955
105	99.14243	101.18345	-2.04102	-1.17042	-1.16042	-1.16196	0.03923	0.00611	-0.23479	-2.12436
106	94.60158	96.91139	-2.30981	-1.32565	-1.31226	-1.31589	0.0378	0.00752	-0.2608	-2.40054
107	90.73011	93.00326	-2.27315	-1.30461	-1.29112	-1.29442	0.03734	0.00718	-0.25492	-2.36131
108	85.98383	87.90274	-1.91892	-1.10131	-1.09009	-1.09088	0.03764	0.00516	-0.21575	-1.99398
109	80.91399	83.08873	-2.17473	-1.24813	-1.23603	-1.23852	0.03859	0.00681	-0.24814	-2.26203
110	77.43553	79.41085	-1.97531	-1.13368	-1.12327	-1.1244	0.03959	0.00578	-0.2283	-2.05675
111	73.10072	74.87702	-1.77631	-1.01946	-1.01086	-1.01094	0.04102	0.00486	-0.20908	-1.85229
112	68.37758	69.61513	-1.23755	-0.71026	-0.7049	-0.70355	0.04277	0.00247	-0.14872	-1.29284
113	62.98302	64.05313	-1.07011	-0.61416	-0.6101	-0.60864	0.04456	0.00193	-0.13145	-1.12002
114	58.49142	58.92368	-0.43226	-0.24809	-0.24664	-0.24576	0.04604	0.00033	-0.05399	-0.45312
115	54.11	53.82468	0.28532	0.16375	0.1629	0.1623	0.04725	0.00015	0.03614	0.29947
116	48.11875	47.04416	1.0746	0.61389	0.61243	0.61243	0.04838	0.00213	0.1381	1.12923
117	42.97858	42.36904	0.60954	0.34983	0.3483	0.34713	0.04882	0.00069	0.07864	0.64083
118	37.2168	35.41656	1.80024	1.0332	1.02873	1.02896	0.04893	0.00605	0.23339	1.89286
119	32.05348	29.80254	2.25094	1.29186	1.28603	1.28925	0.04857	0.00938	0.29131	2.36586
120	25.90016	23.37682	2.52334	1.4482	1.44103	1.44698	0.04773	0.01156	0.32395	2.64982
121	20.75998	18.40638	2.3536	1.35078	1.34344	1.34759	0.04681	0.00985	0.29863	2.46918
122	14.51288	12.31358	2.1993	1.26223	1.25447	1.25722	0.04544	0.00832	0.2743	2.30399
123	9.44275	7.47041	1.97234	1.13197	1.12429	1.12543	0.04423	0.0065	0.24209	2.06361
124	6.35466	3.53553	2.81913	1.61796	1.60613	1.61591	0.04321	0.01294	0.34338	2.94643
125	0.01583	-2.1213	2.13713	1.22655	1.21666	1.21889	0.04176	0.00717	0.25444	2.23025
126	-6.92205	-7.89605	0.974	0.559	0.5541	0.55264	0.0404	0.00144	0.11339	1.01501
127	-13.35437	-13.51288	0.15851	0.09097	0.09012	0.08978	0.03931	0.00004	0.01816	0.16499
128	-18.51799	-18.9671	0.44911	0.25775	0.25526	0.25435	0.03859	0.00029	0.05096	0.46714
129	-26.14575	-26.69014	0.54439	0.31244	0.30937	0.30831	0.03835	0.00042	0.06157	0.5661
130	-33.753	-32.88063	-0.87237	-0.50067	-0.49593	-0.4945	0.03902	0.00111	-0.09964	-0.90778
131	-42.39888	-41.24407	-1.15482	-0.66278	-0.65734	-0.65592	0.04147	0.00208	-0.13644	-1.20478
132	-48.73772	-47.26912	-1.4686	-0.84286	-0.8373	-0.83635	0.04457	0.00363	-0.18064	-1.53711
133	-54.93793	-53.99191	-0.94603	-0.54295	-0.54078	-0.53932	0.04957	0.00169	-0.12317	-0.99537
134	-62.54518	-60.85657	-1.68861	-0.96913	-0.96885	-0.96862	0.0566	0.00626	-0.23725	-1.78992
135	-67.50101	-65.9894	-1.51161	-0.86755	-0.87038	-0.86957	0.06327	0.00568	-0.22598	-1.6137
136	-75.10796	-73.68173	-1.42623	-0.81855	-0.82675	-0.82576	0.07577	0.00623	-0.23644	-1.54316
137	-80.56905	-79.46302	-1.10602	-0.63477	-0.64519	-0.64376	0.08735	0.00443	-0.19916	-1.21188
138	-87.18366	-87.12701	-0.05666	-0.03252	-0.03339	-0.03326	0.10586	0.00001	-0.01145	-0.06336
139	-94.63148	-94.69575	0.06427	0.03689	0.03836	0.03821	0.128	0.00002	0.01464	0.0737
140	-99.12631	-99.58432	0.45801	0.26286	0.27596	0.27499	0.14449	0.00143	0.11301	0.53536
141	-104.65773	-105.47775	0.82002	0.47063	0.50064	0.49922	0.16681	0.00558	0.22337	0.98419

Minimum	-111.05459	-111.61868	-2.93216	-1.68283	-1.66526	-1.67664	0.03663	1.7079E-10	-0.35248	-3.04525
Maximum	145.21291	141.57615	3.85242	2.21099	2.20579	2.23907	0.19033	0.09053	0.91333	4.16278
Mean	31.5607	31.5607	0.	0.	0.00673	0.00875	0.06383	0.00801	0.02759	0.02532

Linear Regression

Regression Statistics

R	0.99889
R-square	0.99778
Adjusted R-square	0.99761
S	3.53059
N	119

Latent Heat in Watt = 227.89011 - 14.95202 * Temperature in degree C + 0.24884 * T^2 - 2.56734 * Met + 0.00715 * Met^2 + 0.132 * Temp*MET - 0.00017 * Temp*MET^2 - 0.00107 * MET*TEMP^2

ANOVA

	d.f.	SS	MS	F	p-level
Regression	8.	##########	76,861.	6,166.14172	0.
Residual	110.	1,371.15588	12.46505		
Total	118.	##########			

	Coefficient	Standard Error	LCL	UCL	t Stat	p-level	H0 (5%)
Intercept	227.89011	51.22701	126.3702	329.41002	4.44863	0.00002	rejected
Temperature in degree C	-14.95202	3.77904	-22.44119	-7.46285	-3.95657	0.00014	rejected
T^2	0.24884	0.06244	0.1251	0.37259	3.98521	0.00012	rejected
Met	-2.56734	0.82395	-4.20022	-0.93446	-3.11589	0.00234	rejected
Met^2	0.00715	0.00307	0.00108	0.01323	2.33346	0.02144	rejected
Temp*MET	0.132	0.06087	0.01137	0.25264	2.16849	0.03228	rejected
Temp*MET^2	-0.00017	0.00023	-0.00062	0.00028	-0.74993	0.4549	accepted
MET*TEMP^2	-0.00107	0.00101	-0.00307	0.00093	-1.06264	0.29027	accepted
Met^2*Temp^2	#N/A						

T (5%) 1.98177
LCL - Lower value of a reliable interval (LCL)
UCL - Upper value of a reliable interval (UCL)

Residuals

Observation	Latent Heat in Watt	Predicted Y	Residual	Standardized	Studentized	Deleted t	Leverage	Cook's D	DFIT	PRESS
1	31.29589	34.65291	-3.35703	-0.97617	-1.04651	-1.04697	0.12992	0.01724	-0.40457	-3.8583
2	33.5581	36.42587	-2.86777	-0.8339	-0.88841	-0.88755	0.11895	0.01123	-0.32612	-3.25494
3	36.07236	38.56842	-2.49606	-0.72581	-0.76663	-0.76807	0.10702	0.00745	-0.2654	-2.79521
4	38.77916	40.52975	-1.75058	-0.50904	-0.53576	-0.53402	0.09727	0.00326	-0.17529	-1.93921
5	40.98452	42.55059	-1.56607	-0.45539	-0.47693	-0.47525	0.08829	0.00232	-0.14789	-1.71773
6	43.88739	44.90468	-1.01729	-0.29581	-0.30825	-0.30698	0.07907	0.00086	-0.08995	-1.10464
7	48.13077	48.6456	-0.51483	-0.1497	-0.15498	-0.15429	0.06686	0.00018	-0.0413	-0.55172
8	53.91306	53.78921	0.12385	0.03601	0.03703	0.03686	0.05421	8.28614E-6	0.00883	0.13095
9	57.68313	56.68426	0.99886	0.29045	0.29782	0.29658	0.04884	0.00048	0.0672	1.05015
10	60.3618	59.21764	1.14416	0.3327	0.34045	0.33908	0.04501	0.00058	0.07362	1.19809
11	62.37461	61.11582	1.25879	0.36603	0.37409	0.37263	0.04262	0.00066	0.07863	1.31484
12	68.32161	66.4711	1.85051	0.5381	0.54855	0.5468	0.03775	0.00124	0.10831	1.92311
13	71.05684	69.33717	1.71967	0.50005	0.50933	0.50761	0.0361	0.00102	0.09823	1.78408
14	73.73844	72.23648	1.50196	0.43674	0.44459	0.44296	0.03498	0.00076	0.08433	1.5564
15	79.21213	77.22883	1.9833	0.57671	0.5868	0.58505	0.03411	0.00128	0.10995	2.05334
16	83.65098	81.80797	1.84301	0.53592	0.54533	0.54358	0.03423	0.00111	0.10234	1.90833
17	87.86593	85.49064	2.37529	0.69069	0.70303	0.70141	0.03479	0.00188	0.13317	2.46091
18	90.79693	89.1797	1.61723	0.47026	0.47888	0.47719	0.03566	0.00089	0.09176	1.67703
19	94.0087	92.5679	1.4408	0.41896	0.42685	0.42526	0.03664	0.00073	0.08294	1.49561
20	97.75034	96.86848	0.88186	0.25643	0.26145	0.26034	0.03806	0.00029	0.05179	0.91675
21	102.6625	102.21803	0.44448	0.12925	0.13191	0.13132	0.03995	0.00008	0.02679	0.46297
22	108.41695	108.34373	0.07322	0.02129	0.02175	0.02166	0.04209	2.19247E-6	0.00454	0.07644
23	112.18702	112.75054	-0.56352	-0.16386	-0.16755	-0.16681	0.04353	0.00013	-0.03558	-0.58916
24	115.61947	116.77759	-1.15812	-0.33676	-0.34455	-0.34317	0.04471	0.00059	-0.07424	-1.21233
25	118.55047	120.46275	-1.91228	-0.55606	-0.56921	-0.56745	0.04567	0.00163	-0.12414	-2.00379
26	123.27009	125.52261	-2.25252	-0.65499	-0.67087	-0.66918	0.04675	0.00233	-0.1482	-2.363
27	130.53239	133.29992	-2.76753	-0.80475	-0.82473	-0.82352	0.04786	0.0036	-0.18464	-2.90665
28	137.93068	141.22543	-3.29475	-0.95806	-0.98206	-0.9819	0.04828	0.00516	-0.22115	-3.46188
29	143.31937	146.15298	-2.83361	-0.82397	-0.84457	-0.84346	0.04819	0.00381	-0.18979	-2.97708
30	150.88207	152.86667	-1.9846	-0.57709	-0.59136	-0.58961	0.04769	0.00185	-0.13195	-2.084
31	158.75631	161.20586	-2.44956	-0.71229	-0.72792	-0.72792	0.04658	0.00274	-0.1609	-2.56924
32	162.94312	166.42749	-3.48437	-1.0132	-1.03716	-1.03752	0.04569	0.00543	-0.22701	-3.65118
33	168.83355	171.94822	-3.11467	-0.90569	-0.92661	-0.92601	0.04464	0.00423	-0.20017	-3.26021
34	174.41773	177.74088	-3.32315	-0.96631	-0.98805	-0.98794	0.04352	0.00468	-0.21073	-3.47434
35	178.63268	182.67893	-4.04625	-1.17658	-1.20247	-1.20494	0.0426	0.00678	-0.25417	-4.22629
36	185.86655	189.84595	-3.9794	-1.15714	-1.1819	-1.18406	0.04146	0.00637	-0.24626	-4.15153
37	195.24629	198.15933	-2.91304	-0.84706	-0.86482	-0.86382	0.04065	0.00334	-0.17782	-3.03648
38	205.24119	207.26863	-2.02744	-0.58954	-0.60193	-0.60018	0.04074	0.00162	-0.12369	-2.11355
39	210.65509	212.68109	-2.02601	-0.58913	-0.60173	-0.59998	0.04145	0.00165	-0.12476	-2.11361
40	217.86083	219.4946	-1.63378	-0.47507	-0.48568	-0.48398	0.04318	0.00112	-0.10282	-1.70751
41	229.36621	230.68965	-1.32344	-0.38483	-0.39453	-0.39301	0.04856	0.00084	-0.08879	-1.39098
42	238.94172	240.17217	-1.23045	-0.35779	-0.36827	-0.36682	0.05609	0.00085	-0.08941	-1.30356
43	246.28315	248.07903	-1.79587	-0.52221	-0.54001	-0.53826	0.06483	0.00213	-0.14172	-1.92037
44	259.18326	260.62101	-1.43774	-0.41807	-0.43683	-0.43522	0.08405	0.00185	-0.13184	-1.56968
45	267.47454	269.36713	-1.8926	-0.55033	-0.58071	-0.57895	0.10188	0.00403	-0.19499	-2.10729
46	273.61731	275.56566	-1.94836	-0.56655	-0.6029	-0.60115	0.11696	0.00508	-0.21878	-2.20643
47	279.50745	281.87055	-2.3631	-0.68715	-0.73863	-0.7371	0.13454	0.00894	-0.29063	-2.73047
48	283.88974	286.52384	-2.6341	-0.76595	-0.83033	-0.82915	0.14906	0.01273	-0.34702	-3.0955
49	286.56841	289.30406	-2.73565	-0.79548	-0.8671	-0.86612	0.15838	0.01492	-0.37572	-3.25044
50	23.04213	19.60441	3.43772	0.99963	1.16124	1.1631	0.25897	0.04968	0.68757	4.63908
51	23.7707	20.43701	3.33369	0.96938	1.09174	1.09271	0.2116	0.03372	0.56609	4.22843
52	25.30464	21.88617	3.41847	0.99403	1.08672	1.08762	0.16331	0.0243	0.48051	4.0857
53	25.74248	23.5012	2.24129	0.65173	0.69921	0.69757	0.1312	0.00778	0.27108	2.57974
54	27.22249	26.72892	0.49357	0.14352	0.15097	0.15029	0.09619	0.00026	0.04903	0.5461

55	28.45163	30.1121	-1.66047	-0.48284	-0.50302	-0.5013	0.07863	0.00228	-0.14644	-1.80217
56	30.63384	36.81891	-6.18507	-1.79851	-1.86182	-1.88325	0.06685	0.02618	-0.50407	-6.62817
57	34.39218	41.18524	-6.79306	-1.97531	-2.04408	-2.07455	0.06616	0.0312	-0.55217	-7.27431
58	39.19034	45.54268	-6.35234	-1.84715	-1.91296	-1.93673	0.06762	0.02798	-0.52158	-6.81305
59	46.36121	50.63969	-4.27849	-1.24411	-1.29036	-1.29431	0.0704	0.01329	-0.35618	-4.60249
60	52.58369	55.71321	-3.12952	-0.91001	-0.94532	-0.94485	0.0733	0.00745	-0.26574	-3.37706
61	62.03113	63.94551	-1.91438	-0.55667	-0.57944	-0.57768	0.07705	0.00295	-0.16691	-2.0742
62	72.33111	73.62657	-1.29546	-0.3767	-0.39252	-0.39101	0.07901	0.00139	-0.11453	-1.40659
63	79.84458	80.84624	-1.00167	-0.29127	-0.30345	-0.30219	0.07868	0.00083	-0.08831	-1.0872
64	87.06438	87.52499	-0.46061	-0.13394	-0.13943	-0.1388	0.07717	0.00017	-0.04014	-0.49913
65	97.0373	96.75575	0.28155	0.08187	0.08506	0.08468	0.07362	0.00006	0.02387	0.30393
66	109.54762	108.85291	0.69471	0.20201	0.20919	0.20827	0.06743	0.00033	0.056	0.74494
67	118.22692	116.69844	1.52848	0.44446	0.45919	0.45754	0.06316	0.0015	0.1188	1.63152
68	129.09546	125.80739	3.28807	0.95612	0.98542	0.98529	0.0586	0.00637	0.24581	3.49273
69	137.19595	133.66805	3.5279	1.02585	1.05555	1.0561	0.05547	0.0069	0.25594	3.7351
70	144.55877	141.65949	2.89928	0.84306	0.86656	0.86557	0.0535	0.00447	0.20579	3.06316
71	152.36355	148.86935	3.49419	1.01605	1.04414	1.04457	0.05308	0.00644	0.24732	3.69006
72	160.21785	157.58946	2.62839	0.76429	0.78609	0.78472	0.0547	0.00377	0.18877	2.78049
73	169.18641	166.53985	2.64656	0.76958	0.79344	0.79209	0.05925	0.00418	0.19878	2.81324
74	175.32713	173.62196	1.70517	0.49584	0.51284	0.51111	0.06521	0.00193	0.135	1.82413
75	181.68794	180.60603	1.08192	0.3146	0.32682	0.32549	0.07338	0.00089	0.0916	1.1676
76	190.09029	191.05762	-0.96733	-0.28128	-0.29491	-0.29369	0.09029	0.00091	-0.09252	-1.06334
77	198.77399	201.46597	-2.69198	-0.78278	-0.83128	-0.8301	0.11327	0.00931	-0.29668	-3.03585
78	206.08787	210.21663	-4.12877	-1.20057	-1.29293	-1.29693	0.13776	0.02815	-0.51839	-4.7884
79	213.91199	220.32436	-6.41237	-1.86461	-2.04962	-2.08039	0.17238	0.09224	-0.94946	-7.74799
80	221.37416	230.1006	-8.72644	-2.5375	-2.85993	-2.95904	0.21277	0.23305	-1.53836	-11.08502
81	23.19628	26.03755	-2.84127	-0.82619	-0.94084	-0.94035	0.22887	0.0277	-0.5123	-3.68456
82	23.20009	24.54654	-1.34645	-0.39152	-0.43351	-0.4319	0.18431	0.00448	-0.2053	-1.65068
83	24.21822	23.33225	0.88597	0.25763	0.27853	0.27736	0.14449	0.00138	0.11398	1.0356
84	24.82136	22.65755	2.16381	0.6292	0.66945	0.66776	0.11663	0.00624	0.24264	2.4495
85	25.24192	22.39094	2.85097	0.82901	0.87204	0.87109	0.09625	0.00854	0.28428	3.15461
86	26.25975	22.5129	3.74685	1.08952	1.13611	1.13763	0.08034	0.01189	0.33624	4.07417
87	26.91125	23.32816	3.58309	1.0419	1.07838	1.07919	0.06651	0.00873	0.28806	3.83839
88	27.92821	24.26532	3.66289	1.0651	1.09925	1.1003	0.06116	0.0083	0.28084	3.9015
89	28.53164	25.69219	2.83946	0.82566	0.85063	0.84956	0.05784	0.00468	0.2105	3.01378
90	29.13713	28.70331	0.43382	0.12615	0.12988	0.1293	0.05672	0.00011	0.03171	0.45991
91	30.80646	33.59268	-2.78622	-0.81019	-0.83524	-0.83408	0.05909	0.00462	-0.20901	-2.96118
92	32.0101	37.8741	-5.864	-1.70515	-1.76021	-1.7774	0.06158	0.02143	-0.45532	-6.24882
93	34.85143	44.04165	-9.19022	-2.67236	-2.76247	-2.85055	0.06418	0.05517	-0.7465	-9.82049
94	40.43677	49.16156	-8.72479	-2.53702	-2.62596	-2.6978	0.06517	0.0506	-0.7123	-9.33301
95	47.03791	54.80922	-7.77132	-2.25977	-2.33713	-2.38649	0.06511	0.0401	-0.6298	-8.31254
96	51.79328	59.02141	-7.22813	-2.10182	-2.17294	-2.21101	0.06439	0.03426	-0.58003	-7.72557
97	62.12902	66.50565	-4.37663	-1.27265	-1.31403	-1.31843	0.06199	0.01203	-0.33895	-4.66589
98	70.82971	73.01711	-2.1874	-0.63606	-0.65572	-0.65402	0.05908	0.00285	-0.16389	-2.32475
99	78.23532	79.06154	-0.82622	-0.24025	-0.24727	-0.24621	0.05598	0.00038	-0.05996	-0.87522
100	85.22595	84.3858	0.84014	0.2443	0.25106	0.24998	0.0531	0.00037	0.0592	0.88726
101	92.19371	90.67297	1.52074	0.4422	0.45363	0.45199	0.04974	0.00114	0.10341	1.60034
102	99.41352	96.1523	3.26122	0.94831	0.97141	0.97116	0.04699	0.00491	0.21566	3.42203
103	104.5827	101.38016	3.20255	0.93125	0.95276	0.95236	0.04466	0.00447	0.20591	3.35226
104	111.54959	107.24125	4.30834	1.25279	1.28029	1.28406	0.0425	0.00767	0.27053	4.49957
105	116.00163	111.42178	4.57985	1.33174	1.36014	1.36548	0.04133	0.00841	0.28351	4.77729
106	122.18455	117.58661	4.59795	1.337	1.36476	1.37019	0.04027	0.00824	0.28066	4.79085
107	126.03727	121.62819	4.40908	1.28208	1.30856	1.31286	0.04006	0.00753	0.26818	4.59306
108	129.96002	126.02054	3.93949	1.14553	1.16935	1.17133	0.04032	0.00606	0.24008	4.10499
109	135.47327	132.38826	3.08502	0.89707	0.91637	0.9157	0.04168	0.00385	0.19097	3.2192
110	140.5689	136.79028	3.77862	1.09876	1.12339	1.12474	0.04337	0.00603	0.23947	3.94991
111	147.60642	144.07773	3.52869	1.02608	1.05141	1.05192	0.0476	0.00582	0.23518	3.70506
112	154.18264	151.56035	2.62229	0.76252	0.78397	0.78259	0.05398	0.0037	0.18694	2.77192
113	160.75915	159.77797	0.98119	0.28531	0.29483	0.29361	0.06355	0.00062	0.07648	1.04777
114	167.23925	167.62683	-0.38759	-0.1127	-0.11721	-0.11668	0.07537	0.00012	-0.03331	-0.41918
115	172.70561	174.89394	-2.18833	-0.63633	-0.66661	-0.66492	0.08879	0.00457	-0.20757	-2.40158
116	179.9937	183.94525	-3.95155	-1.14904	-1.21733	-1.22003	0.10904	0.01912	-0.42682	-4.43517
117	185.32408	190.76458	-5.4405	-1.582	-1.69317	-1.70786	0.127	0.04397	-0.65141	-6.23197
118	190.42	196.74828	-6.32829	-1.84016	-1.9898	-2.01737	0.14475	0.07064	-0.82995	-7.39936
119	192.24231	200.30354	-8.06123	-2.34407	-2.55183	-2.6189	0.1562	0.12708	-1.1268	-9.55353
Minimum	23.04213	19.60441	-9.19022	-2.67236	-2.85993	-2.95904	0.03411	2.19247E-6	-1.53836	-11.08502
Maximum	286.56841	289.30406	4.59795	1.337	1.36476	1.37019	0.25897	0.23305	0.68757	4.79085
Mean	113.4789	114.24708	-0.76818	-0.22337	-0.23828	-0.24296	0.07563	0.01201	-0.09008	-0.87431

Appendix B: Dynamic model Fortran code

The following is the Fortran code of the two-nodes physiology model. For the detailed **multi-segment model** readers are referred to the ESP-r official release into the following directory:
Esp-r/src/ebld/segmentedocc.f90

```
C***********Dynamic occupant subroutine*******************************
      Subroutine DynamicOcc(ICOMP,METAo,CLOTHO)
      REAL TPA,TAIR,H2Oexp,HRexp,Mresp
      COMMON/ATPRES/PATMOS
      REAL TMRT,TOP,Tamb
      real PATMOS ! Ambient pressure
      integer ICOMP
      REAL  Tcr(2),Tsk(2)
      REAL  Cp_blood   ! Blood specific heat (J/Kg oC)
      parameter (Cp_blood=4190.0)
      real  ro_blood   ! Blood density (kg/l)
      parameter (ro_blood=1.29)
      real  Cp_body    ! Mean body specific heat (J/Kg oC)
      parameter (Cp_body=3500)
      real  hfg        ! Water heat of evaporation (J/Kg)
      parameter (hfg=2.43e6)
      real  cpair      ! Air specific heat (J/Kg oC)
      parameter (cpair=1005.7)
      real  mtotal     ! Total body mass (kg)
      parameter (mtotal=75.33)
      real  Ask        ! Total body area (m2)
      parameter (Ask=1.8518)
      real  Patm       ! Atmospheric pressure ! Ambiant relative humidity
      parameter (Patm=1.013e2)
      real   Psat_amb,Psatsk  ! Ambiant saturation pressure (kPa)/ skin saturation
pressure
      real  Pv_amb         ! Ambiant vapor pressure (kPa)
      real  HR_amb         ! Ambiant humidity ratio
      real  fs_thick                ! Fat skin thickness (mm)
      parameter (fs_thick=20)
C Heat exchange coefficients at skin surface
      real  hc,hr,he       ! Convection coefficient at still ambiant air (W/m2 oC)
                   ! Radiation coefficient (W/m2 oC)Evaporation coefficient (W/m2
kPa)
      real  Rcl,Rcle,fcl    !Clothing resistanve
      real  shiv,W,Qcrsk,K,PsatT,mswT,PskT,mshivT,Ccr
      real  resl,ress,sresT,lresT     ! latent and sensible heat loss from respiration
      real  Pskin,mblsk,Qboold,Csk,PVAMB,mbskT,ALFA
```

188

```
      real  sklat,skcon,skrad,expo  ! latent, convective, radiative heat loss
      real  METAo,CLOTHO,META
      real  SWEAT            ! Sweating weighting factor
      real  COLD             ! Shivering weighting factor
      INTEGER  t_scounter,time_step, prtime
      real  QTOT,COMF,MET,Qcomf,t_sB
      expo=1.5
      SWEAT=1.4
      COLD=1.0              ! Shivering weighting factor W is the mechanical work
      ALFA=0.1
      Tcr(1)=37.00          ! initial conditions
      Tsk(1)=33.00

C Clo = 1 - corresponds to the insulating value of a person wearing a business suit
C sitting in comfort at rest in a room at 21C with air movement of 0.1 m/s and
humidity less than 50%
      Rcl=0.155*CLOTHO   !m2k/w
      Rcle=0.02
      if (Rcl .LE. 0.078) then
        fcl = 1 + (1.29 * Rcl)
      else
        fcl = 1.05 + (0.645 * Rcl)
      endif
      t_sB=3600./float(NTSTEP)
      time_step=1
      t_scounter=1
      INDX=ICOMP*(-1)   ! negate the zone index for use in mzmixt.
      CALL MZMIXT(INDX,TMRT,TMIX)
      TAIR=TPA(ICOMP)
      TOP=0.5*TMRT+0.5*TAIR

10    if (t_scounter.LT. int(t_sB)) then
        if (TTcr(ICOMP).GT.5) then  ! if first time called for a zone TTcr(ICOMP)
          Tcr(1)=TTcr(ICOMP)! will be equal to zero if not it will be set to present core
temperature
          Tsk(1)=TTsk(ICOMP)
        end if

      META=METAo
      Tamb=TOP + 273.0
      RH=PCRH2(TPA(ICOMP),GFA(ICOMP),PATMOS)/100.0
      if (RH.lt.0.3)RH=0.3
      Psat_amb=PsatT(Tamb)
      Pv_amb=RH*psat_amb
      HR_amb=0.622*pv_amb/(Patm-Pv_amb)
      skT=Tsk(1)+273
      crT=Tcr(1)
      resl=lresT(META,(Tamb-273.0),HR_amb)
      ress=sresT(META,(Tamb-273.0),HR_amb)
```

```
C Calculation of the skin conductance from the correlations of Havenith.
    Kmuscle=(1.0/0.05)*Ask
    Kfatskin=Ask/((fs_thick-2.0)*0.0048+0.0044)
    K=1.0/(1.0/Kmuscle+1.0/Kfatskin)
    Psatsk=PsatT(skT)
    Qcrsk=K*(Tcr(1)-Tsk(1))    ! W=W/K*(K)

C heat transfer coeficients
    hr=0.7*4.0*5.67e-8*0.95*(273.0+(Tsk(1)+Tamb-273)/2)**3
    hc=7.5      ! could be modified to be calculated from de Dear hc=10.3V^0.6
W/(m2•ºC)
    he=16.5*hc

C functions called
    Pskin=PskT(Psatsk,he,Pv_amb,mswT(Tcr(1),Tsk(1),Ask,SWEAT))
    shiv=MshivT(Tcr(1),Tsk(1),cold)
    mblsk=mbskT(Tsk(1),Tcr(1))
    Qbld=(mblsk*ro_blood*Ask*Cp_blood*(Tcr(1)-Tsk(1)))/(3600.0)
    ALFA=0.0417737 + 0.7451832/(mblsk + 0.585417)
    Ccr=Cp_body*mtotal!*0.75!(1-ALFA)
    Csk=Cp_body*mtotal!*0.25!(ALFA)
    Mresp=1.43e-6*META              !kg or kg/s??
    HRexp=0.2*HR_amb+0.0277+6.5e-5*Tamb
    H2Oexp=Mresp*(HRexp-HR_amb)        !!kg/s?
    H2Oswt=mswT(Tcr(1),Tsk(1),Ask,SWEAT)*ASK !Kg/s
C Calculating the future skin and core temp
    QTOT=(Qcrsk-(Ask/expo)*((Tsk(1)-(Tamb-273)))/
    &  (Rcl+1/(fcl*(hc+hr)))+(Pskin-Pv_amb)/(Rcle+1/(fcl*he)))+Qbld)
    Tsk(2)=QTOT*time_step/Csk+Tsk(1)
    Tcr(2)=((META+shiv-resl-ress-Qcrsk-
    &     Qbld)*time_step/Ccr)+Tcr(1)
    sklat(ICOMP)=((Pskin-Pv_amb)/(Rcle+1/(fcl*he)))*(Ask/expo)+resl
    skcon(ICOMP)=((Tsk(1)-(Tamb-273))/(Rcl+1/(fcl*(hc+hr))))*
    &       (Ask/expo)+ress
    skrad(ICOMP)=((Tsk(1)-(Tamb-273))/(Rcl+1/(fcl*(hc+hr))))*
    &       (Ask/expo)*0.6
    COnflux=skcon(ICOMP)/Ask
    TTcr(ICOMP)=Tcr(2)
    TTSK(ICOMP)=Tsk(2)
    t_scounter=t_scounter+1

    if (t_scounter .eq. int(t_sB-1)) then
C    This code to calculate PMV CCCC test
    MET=META/Ask  !metabolic rate in w/m^2
    Pskin=PskT(Psatsk,he,Pv_amb,
    & mswT(TTcr(ICOMP),TTSK(ICOMP),Ask,SWEAT))
    Qcomf=(META-sklat(ICOMP)-skcon(ICOMP))/Ask
    COMF=(MET-58.2)*0.42
    if(COMF.LT.0)COMF=0
    PMV=(0.303*exp(-0.036*MET)+0.028)*(Qcomf+COMF)
```

```
PPD= 100.-95.*exp(-0.2179*((PMV)**2)-0.03353*((PMV)**4))

 open(221, file='Dynamic_results.csv', status='unknown',
& access='append')
 write(221,*) Tsk(2), ',' ,Tcr(2), ',' ,Qcomf, ',' ,
&    PMV, ',' ,PPD, ',' ,TOP, ',' ,RH, ',' ,CLOTHO,
&    ',' ,Rcl, ',' ,mblsk, ',' ,META, ',' ,shiv, ',' ,
&     resl, ',' ,ress, ',' ,sklat(ICOMP), ',' ,skcon(ICOMP)
 close(221)
 endif
 Go to 10

 endif

 END subroutine

 real function SresT(M,T,HR)
 implicit none
 real, intent(in):: M,T,HR
 real  Tex,mres
 real  cpair
 parameter (cpair=1005.7)
 mres=1.43e-6*M
 Tex=88.6+0.066*T+57.6*HR
 SresT=mres*(cpair*(Tex-T))
 return
 end function SresT

 real function LresT(M1,T1,HR1)
 implicit none
 real, intent(in):: M1,T1,HR1
 real  HRex,mres1
 real  hfg
 parameter (hfg=2.43e6)
 mres1=1.43e-6*M1
 HRex=0.2*HR1+0.0265+3.6e-5*T1
 LresT=mres1*(hfg*(HRex-HR1))
 return
 end function LresT

C Calculates the Control metabolic rate (shivering) (in Watts)
 real function MshivT(Tcr,Tsk,w)
 implicit none
 real, intent(in):: Tcr,Tsk,w
 real  Tshiver,Mshivmax
 if (Tcr.LE.35.8) then
  Tshiver=35.8
 else
  Tshiver=-1.0222e4+570.97*Tcr-7.9455*Tcr**2
 end if
```

```fortran
      if (Tcr.LT.37.0) then
        Mshivmax=-1.1861e9+6.552e7*Tcr-9.0418e5*Tcr**2
      else
        Mshivmax=0.0
      end if
      if (Mshivmax.LE.0) then
        Mshivmax=0.0
      end if
      if ((Tsk.GT.(40-Tshiver)).or.(Tsk.LT.Tshiver)) then
        MshivT=Mshivmax*(1.0-((Tsk-20.0)/(Tshiver-20.0))**2)
     &     *w/3600.0
        return
      else
        MshivT=0.0
        return
      end if
      if (MshivT.LE.0) then
        MshivT=0.0
      end if
      return
      end function MshivT

C Calculates the sudomotor response (sweat rate) (Kg/s/m2)
      real function mswT(Tcr,Tsk,A,w)
      implicit none
      real, intent(in):: Tcr,Tsk,w,A
      real  Tsweat

      if (Tsk.LT.33) then
        Tsweat=42.084-0.17833*Tsk
      else
        Tsweat=36.75
      end if

      if (Tcr.GT.Tsweat .or. Tsk.GT.33) then
        mswT=(45.8+739.4*(abs(Tcr-Tsweat)))*w/3600.0/1000.0/A
        return
      else
        mswT=0.0058e-3/A
        return
      end if
      end function mswT

C Calculates saturated vapor pressure for a given temperature (kPa)
      real function PsatT(T)
      real, intent(in)::  T

C Coefficients of saturation pressure correlation according to ASHRAE
      real  c8,c9,c10,c11,c12,c13
```

192

```fortran
      parameter (c8=-5800.2206,c9=1.3914993,c10=-0.04860239,
     & c11=0.41764768e-4,c12=-0.14452093e-7,c13=6.549673)

      PsatT=(exp(c8/T+c9+c10*T+c11*T**2+c12*T**3+c13*log(T)))/1000.0    !
Saturation pressure correlation according to ASHRAE
      return
      end function PsatT


C Calculates the vapor pressure at skin (kPa)
      real function PskT(Psatsk,he,Pa,mswT)
      real, intent(in)::  Psatsk,he,Pa,mswT
       PskT=(Psatsk/he+Pa*0.3+mswT*0.3*2.43e6/he)/(1/he+0.3)
      if (PskT>=Psatsk) then
       PskT=Psatsk
      endif
      return
      end function PskT


C Calculates skin blood flow in (L/m2hr)
      real function mbskT(Tsk,Tcr)
      real, intent(in)::  Tsk,Tcr
      real Con,Dil,mbbsk
      Con=0.5*(34-Tsk)
      if(Con.LT.0) then
      Con=0
      endif
      Dil=50*(Tcr-37)
      if(Dil.LT.0) then
      Dil=0
      endif
      mbbsk=(6.3+Dil)/(1+Con)
      if ( mbbsk.LT.0.5) then
        mbskT=0.5
      else if( mbbsk .GT.90)then
        mbskT=90
      else
        mbskT=mbbsk
      end if
      return
      end function mbskT
```

References

Al-Othmani, M., Ghaddar, N., & Ghali, K. (2008). A multi-segmented human bioheat model for transient and asymmetric radiative environments. *International Journal of Heat and Mass Transfer*, 51(23-24), 5522-5533.

Andrews CJ, Chandra Putra H, Brennan CB (2013). Simulation Modeling of Occupant Behavior in Commercial Buildings. *Prepared by the Center for Green Building at Rutgers University for the Energy Efficient Buildings Hub*, Philadelphia, PA.

Angelova, R. A., Pichurov, G., Simova, I., Stankov, P., & Rodrigo, I. (2015). CFD based study of thermal sensation of occupants using thermophysiological model. Part II. *International Journal of Clothing Science and Technology*.

Arens, E. A., & Zhang, H. (2006). The skin's role in human thermoregulation and comfort. in: N. Pan, P. Gibson (Eds.), Thermal and Moisture Transport in Fibrous Materials, *Woodhead Publishing Ltd*, 2006, pp. 560e602.

ASHRAE Handbook-Fundamentals, A. S. H. R. A. E. (2017). ASHRAE-American Society of Heating *Ventilating and Air-Conditioning Engineers*.

Avolio, A. P. (1980). Multi-branched model of the human arterial system. *Medical and Biological Engineering and Computing*, *18*(6), 709-718.

Awbi, H.B., 1991. Ventilation of buildings. Baker, NY Chapman & Hall.

Bartak, M., Beausoleil-Morrison, I., Clarke, J. A., Denev, J., Drkal, F., Lain, M., ... & Stankov, P. (2002). Integrating CFD and building simulation. *Building and Environment*, *37*(8-9), 865-871.

Beausoleil-Morrison, I. (2000). *The adaptive coupling of heat and air flow modelling within dynamic whole-building simulation* (Doctoral dissertation, University of Strathclyde).

Beausoleil-Morrison, I., 2002. The adaptive conflation of computational fluid dynamics with whole-building thermal simulation. Energy and Buildings, 34 (9), 857–871.

Blazejczyk, K., Nilsson, H., & Holmér, I. (1993). Solar heat load on man. *International journal of biometeorology*, *37*(3), 125-132.

Blocken, B., Stathopoulos, T., Carmeliet, J., & Hensen, J. L. (2011). Application of computational fluid dynamics in building performance simulation for the outdoor environment: an overview. *Journal of Building Performance Simulation*, *4*(2), 157-184.

Boudier, K.; Fiorentini, M.; Hoffmann, S.; Kalyanam, R.; Kokogiannakis, G. (2016): Coupling a thermal comfort model with building simulation for user comfort and energy efficiency. In: Proceedings of the Central European

Symposium on Building Physics (CESBP) and BauSIM, Dresden, Germany, p. 481–487.

Carrier Corporation. Carrier Air Conditioning Company. (1965). *Handbook of air conditioning system design* (Vol. 1). McGraw-Hill Companies.

Chartered Institution of Building Services Engineers (CIBSE). (2008). CIBSE Concise Handbook. The Chartered Institution of Building Services Engineers London. ISBN 978 – 1 – 903287 – 94 – 1.

Chai, T., & Draxler, R. R. (2014). Root mean square error (RMSE) or mean absolute error (MAE)?–Arguments against avoiding RMSE in the literature. Geoscientific model development, 7(3), 1247-1250.

Chen, Q., Peng, X., and van Paassen, A.H.C., 1995. Prediction of room thermal response by CFD technique with conjugate heat transfer and radiation models. ASHRAE Transactions, 101 (2), 50–60.

Chen, Q.Y., 2009. Ventilation performance prediction for buildings: a method overview and recent applications. Building and Environment, 44 (4), 848–858.

Cheng, Y., Niu, J., & Gao, N. (2012). Thermal comfort models: A review and numerical investigation. Building and Environment, 47, 13-22.

Choudhury, A. R., Majumdar, P. K., & Datta, C. (2011). Factors affecting comfort: human physiology and the role of clothing. In *Improving comfort in clothing* (pp. 3-60). Woodhead Publishing.

CIBSE Guide, A. (2018). Environmental design. Chartered Institute of Building Services Engineers. London (CIBSE).

Clarke, J. A., & Hensen, J. L. M. (2015). Integrated building performance simulation: Progress, prospects and requirements. *Building and Environment*, *91*, 294-306.

Clarke, J. A. 2001. *Energy simulation in building design*, 2nd ed., Oxford: Heineman. ISBN 0750650826

Clarke, J. A., Kelly, N. J., & Tang, D. (2007). A review of ESP-r's flexible solution approach and its application to prospective technical domain developments. *Advances in building energy research*, *1*(1), 227-247.

Coakley, D., Raftery, P., & Keane, M. (2014). A review of methods to match building energy simulation models to measured data. *Renewable and sustainable energy reviews*, *37*, 123-141.

Conceição, E. Z. (2003, August). Numerical simulation of buildings thermal behaviour and human thermal comfort multi-node models. In Proceedings of the 8th International IBPSA Conference-Building Simulation 2003 (pp. 227-234).

Cook, M. J. (1998). An Evaluation of Computational Fluid Dynamics for Modelling Buoyancy-Driven Displacement Ventilation. PhD Thesis, De Montfort University.

Cowie, A. R. (2017). *Numerical Optimisation of Building Thermal and Energy Performance in Hospitals* (Doctoral dissertation, University of Leeds).

Crawley, D. B., Hand, J. W., Kummert, M., & Griffith, B. T. (2008). Contrasting the capabilities of building energy performance simulation programs. *Building and environment*, *43*(4), 661-673.

Crawley, D. B., Lawrie, L. K., Winkelmann, F. C., Buhl, W. F., Huang, Y. J., Pedersen, C. O., ... & Glazer, J. (2001). EnergyPlus: creating a new-generation building energy simulation program. *Energy and buildings*, *33*(4), 319-331.

Crawley D. B. (2008). *Building performance simulation: a tool for policymaking* (Doctoral dissertation, University of Strathclyde).

Cropper, P. C., Yang, T., Cook, M., Fiala, D., & Yousaf, R. (2010). Coupling a model of human thermoregulation with computational fluid dynamics for predicting human–environment interaction. *Journal of Building Performance Simulation*, *3*(3), 233-243.

Daanen, H. (1991). Arterio-venous anastomoses and thermoregulation.TNO Institute for Perception Group: Thermophysiology, Soesterberg, Netherland, 1991.

Daly, D., Cooper, P., & Ma, Z. (2014). Understanding the risks and uncertainties introduced by common assumptions in energy simulations for Australian commercial buildings. *Energy and Buildings*, *75*, 382-393.

Daniels, R., & Bodkin, A. (2017). Guidelines on ventilation, thermal comfort and indoor air quality in schools.

De Dear, R. J., & Brager, G. S. (2002). Thermal comfort in naturally ventilated buildings: revisions to ASHRAE Standard 55. *Energy and buildings*, *34*(6), 549-561.

De Dear, R. J., Arens, E., Hui, Z., & Oguro, M. (1997). Convective and radiative heat transfer coefficients for individual human body segments. *International Journal of Biometeorology*, *40*(3), 141-156.

De Dear, R., & Brager, G. (1998). Developing an adaptive model of thermal comfort and preference. *UC Berkeley: Center for the Built Environment*.

De Dear, R., & Brager, G. S. (2001). The adaptive model of thermal comfort and energy conservation in the built environment. *International journal of biometeorology*, *45*(2), 100-108.

De Wilde, P. (2014). The gap between predicted and measured energy performance of buildings: A framework for investigation. *Automation in Construction*, *41*, 40-49.

De Wilde, P. (2018). *Building performance analysis*. John Wiley & Sons.

Deevy, M., Sinai, Y., Everitt, P., Voigt, L., & Gobeau, N. (2008). Modelling the effect of an occupant on displacement ventilation with computational fluid dynamics. *Energy and Buildings*, *40*(3), 255-264.

Dixit, A., & Gade, U. (2015). A case study on human bio-heat transfer and thermal comfort within CFD. *Building and Environment*, *94*, 122-130.

Djongyang, N., Tchinda, R., & Njomo, D. (2010). Thermal comfort: A review paper. *Renewable and sustainable energy reviews*, *14*(9), 2626-2640.

Djunaedy, E., Hensen, J.L.M., and Loomans, M., 2005. External coupling between CFD and energy simulation: implementation and validation. ASHRAE Transactions, 109, 612–624.

Dodoo, A., Tettey, U. Y. A., & Gustavsson, L. (2017). On input parameters, methods and assumptions for energy balance and retrofit analyses for residential buildings. *Energy and Buildings*, *137*, 76-89.

DoE, U. S. (2020). Energyplus engineering reference. *The reference to energyplus calculations*.Retrieved from: https://energyplus.net/sites/all/modules/custom/nrel_custom/pdfs/pdfs_v9.3.0/EngineeringReference.pdf

Du Bois, E. F. (1939). Heat loss from the human body: Harvey Lecture, December 15, 1938. *Bulletin of the New York Academy of Medicine*, *15*(3), 143.

ESRU. 2002. *The ESP-r System for Building Energy Simulation, User Guide Version 10 Series*, Glasgow: University of Strathclyde. ESRU Manual No. U02/1

Fanger, P. O. (1970). Thermal comfort. Analysis and applications in environmental engineering. *Thermal comfort. Analysis and applications in environmental engineering.*

Fanger, P. O. (1973). Assessment of man's thermal comfort in practice. *Occupational and Environmental Medicine*, *30*(4), 313-324.

Fiala, D. (1998). Dynamic simulation of human heat transfer and thermal comfort (Doctoral dissertation, De Montfort University).

Fiala, D., Havenith, G., Bröde, P., Kampmann, B., & Jendritzky, G. (2012). UTCI-Fiala multi-node model of human heat transfer and temperature regulation. International journal of biometeorology, 56(3), 429-441.

Fiala, D., Lomas, K. J., & Stohrer, M. (2001). Computer prediction of human thermoregulatory and temperature responses to a wide range of environmental conditions. International Journal of Biometeorology, 45(3), 143-159.

Flett, G. H., & Kelly, N. (2014, September). Towards detailed occupancy and demand modelling of low-carbon communities. In *1st International Conference on Zero Carbon Buildings Today and in the Future, ZCB2014,*.

Foda, E., & Sirén, K. (2011 a). A new approach using the Pierce two-node model for different body parts. *International journal of biometeorology*, *55*(4), 519-532.

Foda, E., Almesri, I., Awbi, H. B., & Sirén, K. (2011 b). Models of human thermoregulation and the prediction of local and overall thermal sensations. Building and Environment, 46(10), 2023-2032.

Fountain, M., BRAGER, G. & DE DEAR, R. 1996. Expectations of indoor climate control. Energy and Buildings, 24, 179-182.

Fu, G. (1995). A transient, 3-D mathematical thermal model for the clothed human. KSU, Dissertation.

Gagge, A. P., Fobelets, A. P., & Berglund, L. (1986). A standard predictive index of human response to the thermal environment. *ASHRAE trans*, *92*(2), 709-731.

Gagge, A. P., Stolwijk, J. A. J., & Hardy, J. D. (1967). Comfort and thermal sensations and associated physiological responses at various ambient temperatures. *Environmental research*, *1*(1), 1-20.

Gagge, A.P., Nishi, Y. and Gonzalez, R.R., (1972). Standard effective temperature index of temperature sensation and thermal discomfort, Proceedings of the CIB Commission W45 (Human requirements) Symposium, Building Research Station, UK.

Gagge, A.P., Stolwijk, J.A.J. and Nishi, Y., (1971). An effective temperature scale based on a single model of human physiological temperature response, ASHRAE Transactions, 77, 247–262.

Gan, G. (1995). Evaluation of room air distribution systems using computational fluid dynamics. Energy and buildings, 23(2), 83-93.

Gao, N. P., & Niu, J. L. (2005). CFD study of the thermal environment around a human body: a review. Indoor and built environment, 14(1), 5-16.

Gao, N., & Niu, J. (2004). CFD study on micro-environment around human body and personalized ventilation. *Building and Environment*, *39*(7), 795-805.

Haldi, F., & Robinson, D. (2008). On the behaviour and adaptation of office occupants. *Building and environment*, *43*(12), 2163-2177.

Hammel, H. T., Jackson, D. C., Stolwijk, J. A. J., Hardy, J. D., & Stromme, S. B. (1963). Temperature regulation by hypothalamic proportional control with an adjustable set point. *Journal of Applied Physiology*, *18*(6), 1146-1154.

Hand J.W. (2018). Strategies for deploying virtual representations of the built environment (The ESP-r cookbook). *Energy Systems Research Unit. Department of Mechanical and Aerospace Engineering. University of Strathclyde. Glasgow. UK.*

Hardy, J. D., & Stolwijk, J. A. (1966). Partitional calorimetric studies of man during exposures to thermal transients. *Journal of Applied Physiology*, *21*(6), 1799-1806.

Havenith, G. (2001). Individualized model of human thermoregulation for the simulation of heat stress response. *Journal of Applied Physiology*, *90*(5), 1943-1954.

Havenith, G. (2002). Interaction of clothing and thermoregulation. *Exogenous Dermatology*, *1*(5), 221-230.

Havenith, G., & Fiala, D. (2011). Thermal indices and thermophysiological modeling for heat stress. *Comprehensive Physiology*, *6*(1), 255-302.

Heiselberg, P., 1996. Room air and contaminant distribution in mixed ventilation. ASHRAE Transactions, 102 (2), 332–339.

Hensen, J. L. (1990). Literature review on thermal comfort in transient conditions. *Building and Environment*, *25*(4), 309-316.

Hensen, J. L., & Lamberts, R. (Eds.). (2012). *Building performance simulation for design and operation*. Routledge.

Hoes, P., Hensen, J. L., Loomans, M. G., de Vries, B., & Bourgeois, D. (2009). User behavior in whole building simulation. *Energy and buildings*, *41*(3), 295-302.

Holopainen, R. (2012). A human thermal model for improved thermal comfort. VTT Technical Research Centre of Finland.

Holopainen, R., & Tuomaala, P. (2010). New human thermal model integrated in a building simulation environment for a more accurate estimation of thermal comfort in transient conditions. In *SB10 Finland: Sustainable Community-buildingSMART*. Suomen Rakennusinsinöörien Liitto RIL.

Hong, T., Chou, S. K., & Bong, T. Y. (2000). Building simulation: an overview of developments and information sources. *Building and environment*, *35*(4), 347-361.

Höppe, P. (1999). The physiological equivalent temperature–a universal index for the biometeorological assessment of the thermal environment. *International journal of Biometeorology*, *43*(2), 71-75.

Höppe, P. R. (1993). Heat balance modelling. *Experientia*, *49*(9), 741-746.

Huizenga, C., Hui, Z., & Arens, E. (2001). A model of human physiology and comfort for assessing complex thermal environments. Building and Environment, 36(6), 691-699.

Huizenga, C., Zhang, H., Arens, E., & Wang, D. (2004). Skin and core temperature response to partial-and whole-body heating and cooling. Journal of Thermal Biology, 29(7-8), 549-558.

Humphreys, C. M., Henschel, A., & Lee, D. H. (1966). *Sensible and latent heat losses from occupants of survival shelters*. OCCUPATIONAL HEALTH RESEARCH AND TRAINING FACILITY CINCINNATI OH.

IEA (2019, a), Heating and Cooling Strategies in the Clean Energy Transition, IEA, Paris https://www.iea.org/reports/heating-and-cooling-strategies-in-the-clean-energy-transition

IEA (2019, b), The Critical Role of Buildings, IEA, Paris https://www.iea.org/reports/the-critical-role-of-buildings

IEA and UNEP (United Nations Environment Programme) (2019), 2018 Global Status Report: Towards a Zero-Emission, Efficient and Resilient Buildings and Construction Sector, UNEP, http://wedocs.unep.org/bitstream/handle/20.500.11822/30950/2019GSR.pdf?sequence=1&isAllowed=y

IEA. Energy technology perspectives. Technical report, IEA/OECD, Paris, 2016.

ISO 9920, (2009). *Ergonomics of the Thermal Environment - Estimation of the Thermal Insulation and Water Vapour Resistance of a Clothing Ensemble.* International Standard, International Organization for Standardization (ISO), Geneva.

ISO 8996, (2004). Ergonomics of the thermal environment—determination of metabolic rate. *BSI, London*.

ISO 7730, (2005). *Ergonomics of the thermal environment-Analytical determination and interpretation of thermal comfort using calculation of the PMV and PPD indices and local thermal comfort criteria*.

Jones, B. W. (1992). Transient interaction between the human and the thermal environment. ASHRAE Trans., 98(1), 189-195.

Jones, B. W. (2002). Capabilities and limitations of thermal models for use in thermal comfort standards. *Energy and Buildings*, *34*(6), 653-659.

Karaki, W., Ghaddar, N., Ghali, K., Kuklane, K., Holmér, I., & Vanggaard, L. (2013). Human thermal response with improved AVA modeling of the digits. International Journal of Thermal Sciences, 67, 41-52.

Karmann, C., Schiavon, S., & Bauman, F. (2017). Thermal comfort in buildings using radiant vs. all-air systems: A critical literature review. *Building and Environment*, *111*, 123-131.

Katić, K., Li, R., & Zeiler, W. (2016). Thermophysiological models and their applications: A review. *Building and Environment*, *106*, 286-300.

Kato, S.,Yang, J.H. (2006) Benchmark Tests of CFD of Airflow around Human Body in a Room with Displacement Ventilation. retrived from: https://www.cfd-benchmarks.com/air+quality/

Kelly, N. J. (1998). Towards a design environment for building integrated energy systems: the integration of electrical power flow modelling with building simulation.

Kerslake, D. M., & Waddell, J. L. (1958). The heat exchanges of wet skin. *The Journal of physiology*, *141*(1), 156.

Klepeis, N. E., Nelson, W. C., Ott, W. R., Robinson, J. P., Tsang, A. M., Switzer, P., ... & Engelmann, W. H. (2001). The National Human Activity Pattern Survey (NHAPS): a resource for assessing exposure to environmental pollutants. *Journal of Exposure Science & Environmental Epidemiology*, *11*(3), 231-252.

Kobayashi, Yutaka, and Shin-ichi Tanabe (2013). Development of JOS-2 human thermoregulation model with detailed vascular system. *Building and Environment.* 66, 2013: 1-10.

Lee, K. H., & Schiavon, S. (2014). Influence of three dynamic predictive clothing insulation models on building energy use, HVAC sizing and thermal comfort. *Energies*, *7*(4), 1917-1934.

Machle, W., & Hatch, T. F. (1947). Heat: man's exchanges and physiological responses. *Physiological reviews*, *27*(2), 200-227.

Mahdavi, A. (2011). The human dimension of building performance simulation. In *Proceedings of Building Simulation* (pp. K16-K33).

Murakami, S., Kato, S., & Zeng, J. (2000). Combined simulation of airflow, radiation and moisture transport for heat release from a human body. Building and environment, 35(6), 489-500.

Negrao, C. O. (1995). *Conflation of computational fluid dynamics and building thermal simulation* (Doctoral dissertation, University of Strathclyde).

Nicol, J. F., & Humphreys, M. A. (2002). Adaptive thermal comfort and sustainable thermal standards for buildings. *Energy and buildings*, *34*(6), 563-572.

Nielsen, P.V. (1974). Flow in Air Conditioned Rooms: Model experiments and numerical solution of the flow equations. Ph.D. Thesis, Technical University of Denmark, Copenhagen.

Nielsen, P. V., Allard, F., Awbi, H. B., Davidson, L., & Schälin, A. (2007). Computational fluid dynamics in ventilation design REHVA guidebook No 10. (Brussels: Federation of European Heating and Air Conditioning Associations)

Nielsen, P.V., (2004). Computational fluid dynamics and room air movement. Indoor Air, 14 (Suppl. 7), 134–143.

Nielsen, P. V., Murakami, S., Kato, S., Topp, C., & Yang, J. H. (2003). Benchmark tests for a computer simulated person. *Aalborg University, Indoor Environmental Engineering*.

Niemeyer, D. C. (2003). *Hard facts on smart classroom design: Ideas, guidelines, and layouts*. Rowman & Littlefield.

Parsons, K. (2014). *Human thermal environments: the effects of hot, moderate, and cold environments on human health, comfort, and performance*. CRC press.

Pennes, H. H. (1948). Analysis of tissue and arterial blood temperatures in the resting human forearm. *Journal of applied physiology*, *1*(2), 93-122.

Pichurov, G., Angelova, R., Simova, I., Rodrigo, I., & Stankov, P. (2014). CFD based study of thermal sensation of occupants using thermophysiological model. Part I. *International Journal of Clothing Science and Technology*. Vol. 26 No. 6, 2014 pp. 442-455

Rida M., Hoffmann S., "Using a Dynamic Clothing Insulation Model in Building Simulation – Impact on Thermal Comfort and Energy Consumption," in *IBPSA*, Rome, 2019.

Rida, M., Ghaddar, N., Ghali, K., & Hoballah, J. (2014, b). Elderly bioheat modeling: changes in physiology, thermoregulation, and blood flow circulation. International journal of biometeorology, 58(9), 1825-1843.

Rida, M., Karaki, W., Ghaddar, N., Ghali, K., & Hoballah, J. (2014, a). A new mathematical model to simulate AVA cold-induced vasodilation reaction to local cooling. International journal of biometeorology, 58(9), 1905-1918.

Rupp, R. F., Vásquez, N. G., & Lamberts, R. (2015). A review of human thermal comfort in the built environment. *Energy and Buildings*, *105*, 178-205.

Salloum, M. D. (2005). *A new transient bio-heat model of the human body and its integration to clothing models-by Maher Douraid Salloum.* Master's thesis, American University of Beirut, 2005.

Salloum, M., Ghaddar, N., & Ghali, K. (2007). A new transient bioheat model of the human body and its integration to clothing models. International journal of thermal sciences, 46(4), 371-384.

Schellen, L., Loomans, M. G. L. C., Kingma, B. R. M., De Wit, M. H., Frijns, A. J. H., & van Marken Lichtenbelt, W. D. (2013). The use of a thermophysiological model in the built environment to predict thermal sensation: coupling with the indoor environment and thermal sensation. Building and Environment, 59, 10-22.

Severens, N. M., van Marken Lichtenbelt, W. D., Frijns, A. J., Kingma, B. R., de Mol, B. A., & van Steenhoven, A. A. (2009). Measurement of model coefficients of skin sympathetic vasoconstriction. *Physiological measurement*, *31*(1), 77.

Shih, T. C., Yuan, P., Lin, W. L., & Kou, H. S. (2007). Analytical analysis of the Pennes bioheat transfer equation with sinusoidal heat flux condition on skin surface. *Medical Engineering & Physics*, *29*(9), 946-953.

Smith, C. E. (1993). A transient, three-dimensional model of the human thermal system. KSU, Dissertation.

Sørensen, D. N., & Voigt, L. K. (2003). Modelling flow and heat transfer around a seated human body by computational fluid dynamics. *Building and environment*, *38*(6), 753-762.

Sorensen, D.N. and Nielsen, P.V., (2003). Quality control of computational fluid dynamics in indoor environments. Indoor Air, 13 (1), 2–17.

Srebric, J. and Chen, Q. (2002). An example of verification, validation, and reporting of indoor environment CFD analyses. ASHRAE Transactions, 108(2), 185-194.

Srebric, J., Vukovic, V., He, G., & Yang, X. (2008). CFD boundary conditions for contaminant dispersion, heat transfer and airflow simulations around human occupants in indoor environments. *Building and Environment*, *43*(3), 294-303.

Standard, A. S. H. R. A. E. (2013). Standard 55-2013, Thermal environmental conditions for human occupancy. *American Society of Heating, Refrigerating and Air Conditioning Engineers*.

Stolwijk, J. A. (1971). A mathematical model of physiological temperature regulation in man. Technical report, John B. Pierce Foundation Laboratory and Department of Epidemiology and Public Health, Yale University School of Medicine, 1971.

Stolwijk, J. A. J., & Hardy, J. D. (1966). Temperature regulation in man—a theoretical study. *Pflüger's Archiv für die gesamte Physiologie des Menschen und der Tiere*, *291*(2), 129-162.

Stolwijk, J.A. J. and Hardy, J.D., 1977, Control of body temperature, in Handbook of Physiology, section 9: reaction to environmental agents, Bethesda, Maryland: American Physiological Society, pp. 45–68.

Takada, S., Sasaki, A., & Kimura, R. (2016). Fundamental study of ventilation in air layer in clothing considering real shape of the human body based on CFD analysis. *Building and Environment*, *99*, 210-220.

Takemori, T., Nakajima, T., & Shoji, Y. (1996). A fundamental model of the human thermal system for prediction of thermal comfort. *Heat Transfer-Japanese Research*, *24*(2).

Tanabe, S. I., Kobayashi, K., Nakano, J., Ozeki, Y., & Konishi, M. (2002). Evaluation of thermal comfort using combined multi-node thermoregulation (65MN) and radiation models and computational fluid dynamics (CFD). Energy and Buildings, 34(6), 637-646.

van Hoof J. (2008). Forty years of Fangers model of thermal comfort: comfort for all?. Indoor Air;18(3):182–201.

van Hoof, J., & Hensen, J. L. (2006). Thermal comfort and older adults. *Gerontechnology*, *4*(4), 223-228.

van Marken Lichtenbelt, W. D., Frijns, A. J. H., Fiala, D., Janssen, F. E. M., Van Ooijen, A. M. J., & Van Steenhoven, A. A. (2004). Effect of individual characteristics on a mathematical model of human thermoregulation. Journal of Thermal Biology, 29(7-8), 577-581.

van Treeck, C., Frisch, J., Pfaffinger, M., Rank, E., Paulke, S., Schweinfurth, I., & Holm, A. (2009). Integrated thermal comfort analysis using a parametric manikin model for interactive real-time simulation. *Journal of Building Performance Simulation*, *2*(4), 233-250.

Versteeg, H. K., & Malalasekera, W. (2007). *An introduction to computational fluid dynamics: the finite volume method*. Pearson education.

Viessman W. (1966) Man and His Thermal Environment. In: Jennings B.H., Murphy J.E. (eds) Interactions of Man and His Environment. Springer, Boston, MA

Villi, G., & De Carli, M. (2014, February). Detailing the effects of geometry approximation and grid simplification on the capability of a CFD model to address the benchmark test case for flow around a computer simulated person. In *Building Simulation* (Vol. 7, No. 1, pp. 35-55). Springer Berlin Heidelberg.

Wang, Z., de Dear, R., Luo, M., Lin, B., He, Y., Ghahramani, A., & Zhu, Y. (2018). Individual difference in thermal comfort: A literature review. *Building and Environment*, *138*, 181-193.

Wissler, E. H. (1985). Mathematical simulation of human thermal behavior using whole body models. *Heat transfer in medicine and biology*, *1*(13), 325-373.

Wyndham, C. H., & Atkins, A. R. (1968). A physiological scheme and mathematical model of temperature regulation in man. *Pflügers Archiv*, *303*(1), 14-30.

Wyon, D. P. Enhancing productivity while reducing energy use in buildings. Proceedings of the E-Vision 2000 Conference, 2000. 11-13.

Yamane, Y & Ito, T & Sakai, Koji & Ono, H. (2013). Evaluation of the thermal environment around the human body in a solar radiation environment - study of coupled analysis of cfd and thermoregulation models. In *13th Conference of International Building Performance Simulation Association*, pages 1985–1990, 08 2013.

Yan, D., Hong, T., Dong, B., Mahdavi, A., D'Oca, S., Gaetani, I., & Feng, X. (2017). IEA EBC Annex 66: Definition and simulation of occupant behavior in buildings. *Energy and Buildings*, *156*, 258-270.

Yan, D., O'Brien, W., Hong, T., Feng, X., Gunay, H. B., Tahmasebi, F., & Mahdavi, A. (2015). Occupant behavior modeling for building performance simulation: Current state and future challenges. *Energy and Buildings*, *107*, 264-278.

Yang, T., Cropper, P. C., Cook, M. J., Yousaf, R., & Fiala, D. (2007, September). A new simulation system to predict human-environment thermal interactions in naturally ventilated buildings. In *Proc. 10th International Building Performance Simulation Association Conference and Exhibition (BS2007), Beijing, China* (pp. 751-756).

Zelenský, P., Barták, M., & Hensen, J. L. (2013). Simplified representation of indoor heat sources in CFD simulations. In *Proceeding of the 13th International Conference of the International Building Performance Simulation Association* (pp. 3-29).

Zhang, H., Arens, E., Huizenga, C., & Han, T. (2010 a). Thermal sensation and comfort models for non-uniform and transient environments: Part I: Local sensation of individual body parts. *Building and Environment*, *45*(2), 380-388.

Zhang, H., Arens, E., Huizenga, C., & Han, T. (2010 b). Thermal sensation and comfort models for non-uniform and transient environments, part II: Local comfort of individual body parts. *Building and Environment*, *45*(2), 389-398.

Zhang, H., Arens, E., Huizenga, C., & Han, T. (2010 c). Thermal sensation and comfort models for non-uniform and transient environments, part III: Whole-body sensation and comfort. *Building and Environment*, *45*(2), 399-410.

Zhang, H., Huizenga, C., Arens, E., & Yu, T. (2001). Considering individual physiological differences in a human thermal model. *Journal of thermal biology*, *26*(4-5), 401-408.

Zolfaghari, A., & Maerefat, M. (2010 a). A new simplified thermoregulatory bioheat model for evaluating thermal response of the human body to transient environments. *Building and Environment*, *45*(10), 2068-2076.

Zolfaghari, A., & Maerefat, M. (2010 b). A new simplified model for evaluating non-uniform thermal sensation caused by wearing clothing. *Building and Environment*, *45*(3), 776-783.

Zmeureanu, R., & Doramajian, A. (1992). Thermally acceptable temperature drifts can reduce the energy consumption for cooling in office buildings. *Building and Environment*, *27*(4), 469-481.